UNIVERSITY OF HULL

Dynamics of microplastics particles in rivers: experimental settling processes and numerical models of the transport and deposition

being a thesis submitted in fulfilment of the
requirements for the degree of
Doctor of

Earth Science

in the University of Hull

by

M.S.c. Lucrecia Alvarez Barrantes

April 2023

Dedication

Dr. Laura Elena Segura Mena (†) (1983-2020)

Rest in peace

Acknowledgements

I would like to express my sincere gratitude to my supervisors: Robert Dorrell, Anne Baar, Roberto Fernandez, Christopher Hackney and Daniel Parsons. Thanks for being my mentors and teaching me different skills, helping me to achieve my goal of completing my research. I want to give a special thanks to my first supervisor, Rob, for his great dedication and time throughout this process and for guiding me to develop quality experimental conditions. I thank Anne, for transmitting her knowledge, dedication and help in the numerical model chapter. I thank Roberto, for his guidance and encouragement to learn to program codes, as well as for teaching me to focus on details. Chris, thanks for your appropriate contributions throughout the investigation and for helping me organize my ideas. Dan, thank you also for your contributions and assistance at every stage of the research project.

I would like to extend my sincere thanks to the Energy and Environment Institute for allowing me to be part of the student committee and get involved in the organization of social and academic events. Thanks to Johanna Arnett and Joanne Dewey for all the administrative support they gave me. Thanks to the laboratory technician Emma Chapman.

I am very grateful to my family, my mother Isabel, my father Edgardo, my sisters Lizi and Ileana, and my niece Valeria, who, despite the distance, accompanied me throughout this process.

My special thanks to my boyfriend David, whom I met during this process, giving me the motivation and joy that I needed to finish this investigation. Thanks for now be part of my adventures.

I thank my Hull friends, Hull squad: Fee, Fiona, Jess, Vic, Rick, Julian, Hanna, Amber and Clare; Paulo, Goska, Flavia, Jana, Marijke, Serena, Wool, Lulu, Eva, Peter, Roheel, Soheel. Thank you, for being part of my life, and accompanying me on all the adventures: camping, hiking, pub nights, BBQ, fires, dinners, millions of coffee breaks, and trips. My friends from Costa Rica, thank you for the support from a distance and for dedicating time during my visits: La nena Raquel, El Jo Sebas-Chinchi, Las Lagartas: Mari Cruz y Lau, Amigos del corazon: Laura (†), Olman, Carito, Mariana, Javi y Elena.

Publications and Conferences

River fluxes of microplastics (Poster), Hull Postgraduate Day, January 2020, Hull.

Controls on microplastic deposits in non-cohesive sediments (Poster) Plastics in the Environment 2020, September 2021, online.

Sediment and high-density microplastic particles settling process in freshwater: experimental settling tubes (Oral presentation, Won the runner-up presentation), April 2022UK, Young Coastal Scientist and Engineers Conference, Bournemouth.

Sediment and high-density microplastic particles settling process in freshwater: experimental settling tubes (Oral presentation), Hull Postgraduate Day, May 2022, Hull.

Abstract

Microplastic pollution is an environmental problem facing rivers, oceans, and coastlines. Estimations suggest that around 1.15 to 12.7 million tonnes of plastic waste enter the ocean every year from the global riverine system. In the environment, organisms ingest plastic they cannot distinguish from food, causing them harmful and lethal effects. Observations from rivers show that suspensions of microplastic are composed of particles, formed from different plastic polymers, with densities buoyant, non-buoyant or neutrally-buoyant in water. The microplastic particles are found transported in the river flow and deposited in the sediments.

The vertical distribution of microplastic particles trapped in sedimentary deposits shows that the amount of plastic deposits decreases in deeper layers. However, all the types of plastics are found in similar percentages all over the layers, lacking current physical explanation. To understand the physical parameters that control the trapping of microplastic pollution within sedimentary deposits, a series of sedimentation experiments were designed using different mixtures of microplastic particles and sediment. The results highlight the relative importance of microplastic-sediment concentrations controlling plastic material distribution within the deposits.

The sediment-microplastic deposits have become an active component of river systems generating changes in the bedforms; the presence of the plastics is increasing the average diameter of the materials in the bed, and therefore there is a need for a higher critical shear stress for erosion. A numerical model of a braided river with plastics was created to predict the physical changes in the bedforms due to the interaction of the plastics and sediment in the river bed. The model describes how a higher amount of plastic can be deposited in the bars and river banks near the sources, decreasing the erosion capacity of the river flow in these areas and promoting the formation of more extensive sediment bars and deeper or wide channels. The model allowed studying the deposition, resuspension, and transport patterns of microplastic loads, identifying key processes such as high concentrations of plastic (hotspots).

Contents

List of Figures

List of Tables

Abbreviations

A_{Mp}, microplastic pellets rounded side.

ABS, Acrylonitrile Butadiene Styrene

a, particle longest axis

b, particle intermediate axis

c, particle shortest axis

C1, diameter cylinder coefficient, equation 1-1

C_1, empirical parameter Ferguson and Church equation (2004), 2-1

C2, diameter cylinder coefficient, equation 1-1

C_2, empirical parameter Ferguson and Church equation (2004), 2-1

COP, Chemical organic pollutants

CoPA, Polyamide block copolymers

D_*, equivalent diameter equation 1-3

D_d, dimensional grain size equation 5-11

D_{Mp}, microplastic equivalent diameter

D_S, sediment equivalent diameter

Dc, diameter of the cylinder equation 1-1

F_d, drag force.

F_g, gravity force

F_f, fluid forces

g, gravity force

EPS, expanded polyester spheres.

ESD, particle size defined by Kaiser et al. (2019)

h, slices thickness

H_{MP} , microplastic substrate height

H_S, sediment substrate height

H_T, total substrate height

HMP-S, mixture of high content of microplastic and sediment substrate

h_{Mp}, the microplastic height of the rectangular side

LMP-S, Mixture of low content of microplastic and sediment substrate

L_c, length of the cylinder equation 1-1

M, mass

MP, microplastic

PA, Nylon

PC, Polycarbonate

PE, polyethylene

PET, polyethylene Terephthalate

PHM, Propylene Glycol Monooleate

PLA, Polylactic Acid

POM, Acetal

PP, Polypropylene

PPMA, acrylic

PS, Polystyrene

PVC, Polyvinyl Chloride

Re, Reynolds number

S, Sediment dominated.

T_T = total transport sediment predictor

V, volume

$V_{f,}$ fluid volume

V_{MP}, microplastic volume

V_S, sediment volume

V_{ST}, total volume of the suspension in the settling tube (V_{ST} $=V_{MP}+V_S+V_f$)

v, kinematic viscosity of the fluid

W_{sMp}, microplastic hindered fall velocity.

W_{sS}, sediment hindered fall velocity.

w_s, particle fall velocity.

w_{sMp}, microplastic fall velocity.

w_{sS}, sediment fall velocity.

z, unitary heights expressed as the relation of the thickness of a deposit divided by H_T, z=1 is the top of the deposit and z=0 is the bottom.

ρ, density

ρ_{sus}, suspension density $(\rho_{sus} = \rho_s\Phi_s + \rho_{MP}\Phi_{MP} + \rho_f(1 - \Phi_{MP} - \Phi_S))$

ρ_{MP}, microplastic density

ρ_f, fluid density

ρ_s, sediment density

Φ_T, Total volumetric concentration ($\Phi_{Mp}+\Phi_S+\Phi_f$)

Φ_f, fluid volumetric concentration

Φ_{Mp}, microplastic volumetric concentration

Φ_S, sediment volumetric concentration

Φ_{S+Mp}, sediment and microplastic volumetric concentration

Chapter 1 . Introduction

1.1. Thesis structure

The thesis comprises six chapters, an introduction, methodological chapter, three main data chapters and a conclusion (Figure 1-1). Chapter 1 introduces microplastic pollution in rivers describing the microplastics physical characteristics (size, density and shape), pollutant sources, spatial distribution characteristic and its dynamics of transport and deposition. The chapter ends with the research proposal, divided into two objectives: microplastic-sediment depositional structure (objective 1) and microplastic–sediment transport and deposition dynamic (objective 2).

The experimental conditions to develop objective one are explained in chapters 2, 3 and 4. Chapter 2 includes the theoretical concepts, methods and scenarios. Given the extensive scenarios to solve objective 1, the results were divided into two chapters. Chapter 3 includes the results and discussion of the experimental work for the first set of scenarios: Negatively buoyant microplastic-sediment and baseline (only sediment and only microplastic). Chapter 4 presents the results and discussion for the second set of scenarios: Neutral buoyant-sediment, positively buoyant-sediment and extended concentrations.

Chapter 5 includes the theoretical concepts, methods, results and discussion of the microplastic–sediment transport deposition dynamic (objective 2). Finally, the thesis ends with a conclusion chapter that integrates all the results and discusses the two objectives.

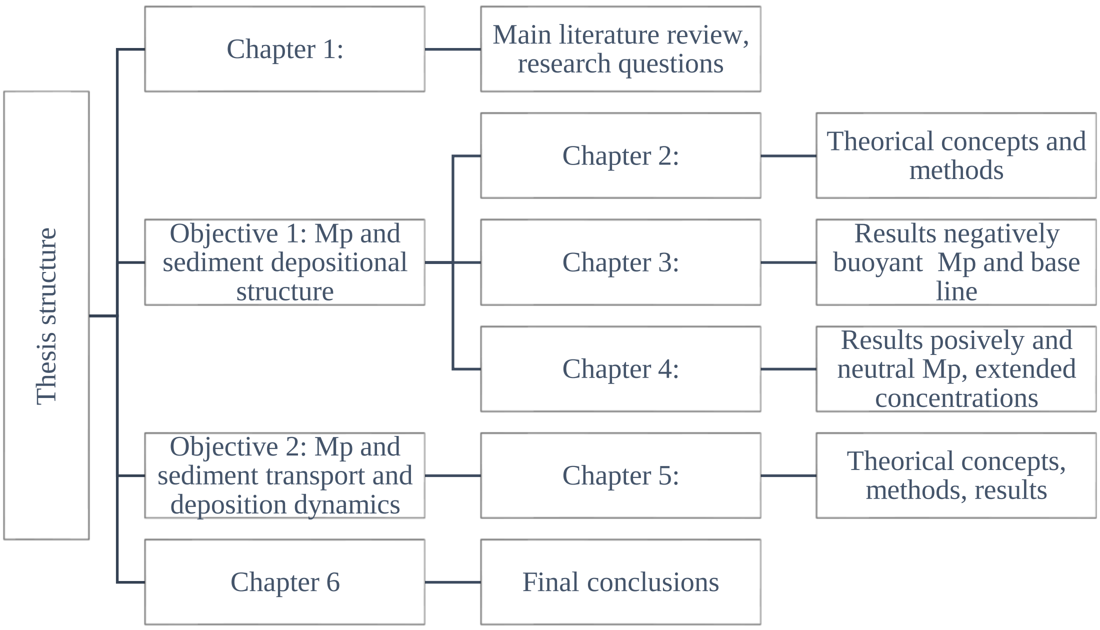

Figure 1-1. Thesis chapter's structure.

1.2. Authors contributions

Lucrecia Alvarez contributed to the conception and design of the methods, performed all the experimental settling tubes, hydromorphological numerical braided rivers scenarios, data analysis, discussion, conclusions, and write the original draft. The supervisors Robert Dorrell, Anne Baar, Roberto Fernandez, Christopher Hackney and Daniel Parsons contributed to the conception and design of the research; with a greater emphasis of Robert Dorrell in the methods and results analysis of the experimental settling tubes (Chapter 2,3 and 4) and Anne Baar in the software methods, and model setup of the braided river hydromorphological numerical (Chapter 5). Robert Dorrell, Anne Baar and Roberto Fernandez, collaborated with base codes to analyse the results, which were modified by myself to adapted to the experimental and numerical model conditions. The code in the Appendix 3, was developed by Roberto Fernandez. All the supervisors reviewed the original draft.

1.3. Microplastic pollution in rivers

Microplastic pollution (plastic particles smaller than 5000 µm) is a problem facing rivers, oceans, coastlines, and deep sea environments (Browne et al., 2011; Erni-Cassola et al., 2019; The Royal Society, 2019). Estimations suggest that around 1.15 to 12.7 million tonnes of plastic waste enter oceans annually from fluvial systems (Jambeck et al., 2014; Lebreton et al., 2017). The plastic load is estimated to represent 80% of the plastic in the oceans, converting rivers into the main source of plastic pollution (Jambeck et al., 2014; Lebreton et al., 2017, Meijer et al., 2021). Microplastics can contain chemicals associated with human diseases and can cause harmful effects to organisms (Wright et al., 2013; Rochman et al., 2016; Prokic et al., 2021). It is essential to comprehend the transport and deposition behaviour of microplastic particles to understand better the amount of plastics stored and transported in the river system to mitigate the impacts. For this reason, this research is focused on studying the transport, deposition and storage process of the microplastic suspended fluxes in rivers.

Microplastic particles are defined as plastics with a size between 0.1 µm a 1000 µm -5000 µm, Figure 1-2 (Blair and Quinn, 2017; Hartmann et al., 2019; The Royal Society, 2019). A 5000 µm upper limit is proposed by National Oceanic and Atmospheric Administration as a biological criterion as larger items were considered more unlikely to be ingested (Hartmann et al., 2019). A 1000 µm upper limit is a suggestion that plastic should be classified from a nomenclature point of view based on the International System of Units (SI) prefixes for length (Hartmann et al., 2019).

Figure 1-2 compares the sediment size distribution of plastic pollution and natural sediment. Plastic pollution can be classified into 3 or 4 categories. Nanoplastics are plastic smaller than microplastic (less than 0.01-0.001μm), and mesoplastic-macroplastic is bigger than microplastic (higher than 1-5 mm). According to the International Organization for Standardization (ISO 14688-1, 2017), sedimentary particles are classified into: fine particles, including clay and silt, with sizes less than 0.002 mm to 0.063 mm; coarse particles, including sand and gravel, are between 0.0633 mm to 63 mm, and very coarse particles, including cobbles and boulders, are from 63 mm and higher than 630 mm. Therefore, microplastic particles have similar clay to gravel sizes.

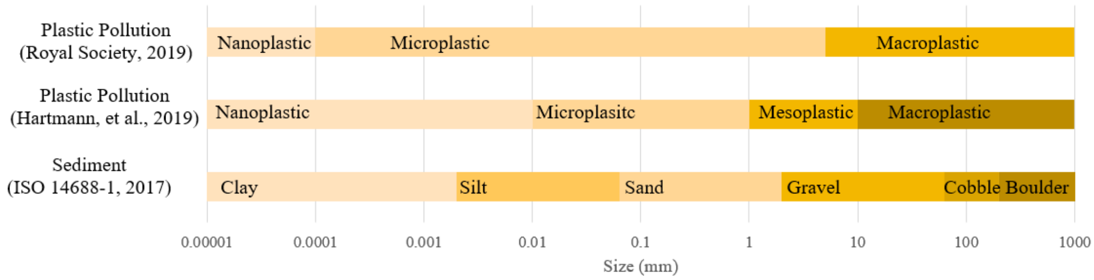

Figure 1-2. Size distribution of sediment and plastic pollution (ISO 14688-1, 2017; Hartmann et al., 2019; The Royal Society, 2019)

Plastic is a diverse material, with over 94 different polymers whose uses vary depending on the market's needs (Blair and Quinn, 2017). Plastic is typically composed of polymers with densities ranging from 0.88 to 1.7 g/cm^3 (Shim et al., 2018); however, these limits may vary according to the necessities of the plastic industry. Table 1.1 highlights 11 common plastic types from positively to negatively buoyant in water, their respective density, common uses, and abbreviated prefix (Blair and Quinn, 2017). Polyethylene (PE), polypropylene (PP), polystyrene (PS) and acrylic (PMMA), are recognized as the most abundant common types of plastic found in the aquatic environment (Erni-Cassola et al., 2019). The plastic density range classified microplastics into three categories (Figure 1-3):

- Negatively-buoyant microplastic, plastics with a density higher than freshwater (998 kg/cm^3 at 20°C, Fierro and Nyler, 2007)
- Positively buoyant microplastic, plastic with a density lower than freshwater.
- Neutral buoyant microplastics, plastic with a density equal to or similar to freshwater.

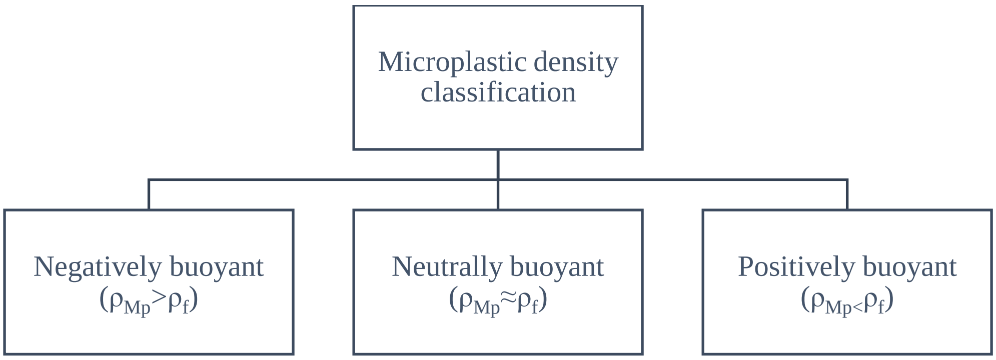

Figure 1-3. Microplastic categorisation according to the plastic density. Where ρ_{Mp} is the density of the plastic and ρ_f is the density of the fluid.

Therefore, the microplastics polluting rivers can sink, float, or rise in the flow, in contrast with the sediment particles, classified as negatively-buoyant particles with a commonly recognised density of 2650 kg/m^3 (Dingman, 2008).

Table 1.1. The industry of plastic characteristics (Blair and Quinn, 2017).

Name	**Symbol**	**Common uses**	**Common densities (Kg/m^3)**
Polyethene	PE	Plastic bags - packaging laundry detergent	920-970
Polystyrene	PS	Foam applications	960-1050
Polypropylene	PP	Living hinges - textiles	880-1230
Acrylonitrile Butadiene Styrene	ABS	3D printing	1040-1120
Acrylic	PMMA	Optical devices	1160-1040
Nylon	PA	Rope or thread	1130-1380
Acetal	POM	Gears	1170-1420
Polylactic Acid	PLA	Food packaging	1200-1430
Polycarbonate	PC	Used in greenhouses	1150-1520
Polyethylene Terephthalate	PETE-PET	Plastic bottle, fibres polyester	1300-1500
Polyvinyl Chloride	PVC	Insulation of electrical water and sewer pipes	1150-1700

Particles can be classified according to the relation between the three axes sizes: *a* is the longest axis, *b* is the intermediate axis, and *c* is the shortest axis. The Zingg classification (Lewis and McConchie, 1994) is a standard method to categorise the particle shape into four types: discs, blades, rods, and spheres (Figure 1-4). Microplastic is produced from the fragmentation of meso-macroplastic (secondary microplastic) or directly from the industry (primary microplastic) (Hartmann et al., 2019), creating eight common microplastic categories based on the shape and polymer (Table 1.2): fragments, fibres, microbeads, film, foam, pellets, spherules, and sheets(Blair and Quinn, 2017; The Royal Society, 2019).

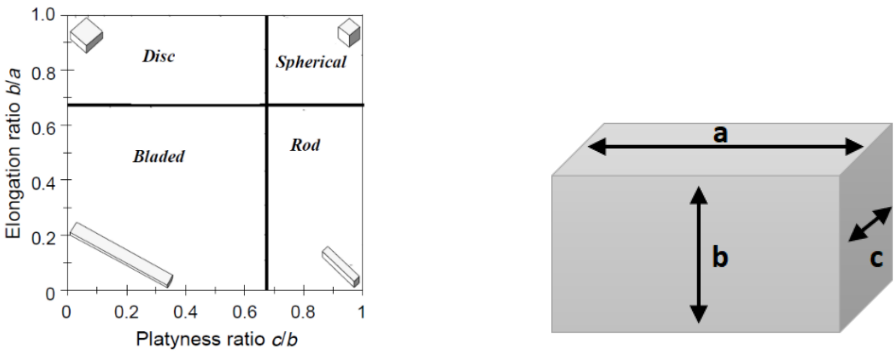

Figure 1-4. Zingg classification of shapes of particles; 'a' is the longest axis, 'b' is the intermediate axis, and 'c' is the shortest axis. (Lewis and McConchie, 1994).

Table 1.2 describes the categories of microplastic pollution and its typical shape based on the Zingg classification (Lewis and McConchie, 1994). Sheets and films are thin, flexible, and irregularly microplastic particles. Fibres are mostly sticks from synthetic textiles and ropes. Fragments can be irregular and rigid particles. Foam is a specific name for polystyrene spheres; microbeads are related to tiny spheres of health and beauty products, and pellets and spheres have spherical and cylinder shapes, respectively (Blair and Quinn, 2017; The Royal Society, 2019). Some of these categories are associated with the type of polymer due to a determined plastic product always forms a specific shape; for example, spheres of polystyrene and microbeads. Consequently, plastic products entering the environment comprise particles of many different shapes, colours, polymers, and sizes.

Table 1.2. Common categories of microplastic pollution (Lewis and McConchie, 1994; Blair and Quinn, 2017; The Royal Society, 2019).

Name	Description	Common shape (Zingg classification)	Example
Fragment/Sheets	Irregular and rigid plastic fragments. This type of particle is related to the defragmentation of macroplastic, for example, plastic bottles.	Disc-shaped	
Films	Thickness, flexible and irregular plastic particles, such as plastic bag fragments.	Disc-shaped	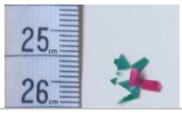
Fibres	Sticks from synthetic textiles and ropes	Bladed-Rod-like	
Foam	Spheres of expanded polystyrene (EPS)	Spherical	
Spheres / Pellet	Spherical and cylinder pieces of plastic.	Spherical	
Microbeads	Tiny spheres of health and beauty products.	Spherical	

1.3.1. Sources

Direct littering, the effluent of sewage treatment plants, and industrial production are some of the many sources of microplastic pollution to the river system. Wind and rain are natural processes that cause plastic debris accumulation in urban areas (Bauer-Civiello et al., 2019), agriculture and soils (Lwanga et al., 2023; Zhou et al., 2023). Effluents of sewage treatment plants and plastic industry contain microplastic particles , becoming direct pollution to rivers (Browne et al., 2011; Kim et al., 2015; Blair et al., 2019). Investigations measuring microplastic concentrations in the dry season, at the beginning of the rainy season, and debris post-wet season (Moore et al., 2011; Bauer-Civiello et al., 2019; Emmerik et al., 2019; Wagner et al., 2019), as a result, have shown that these sources are constantly polluting the rivers.

1.3.2. Microplastic particles transported in the river flow

Microplastic suspended concentrations are the number of particles in a given flow volume. The suspended concentrations can be formed by different volumes of negative, positive and neutrally plastic particles (Scherer et al., 2020; Sulistyowati et al., 2022; Kieu-Le et al., 2023; Apetogbor et al., 2023). Figure 1-5 presents the results of the plastic abundance in four rivers illustrating the typical heterogeneous microplastics pollution in the river environment. The four rivers contain plastic, such as PE, characterised to be positively buoyant, PET is a negatively buoyant plastic and PP and PS can have a diferents densities between 880 kg/m^3 to 1230 kg/ m^3 (Shim et al., 2018).

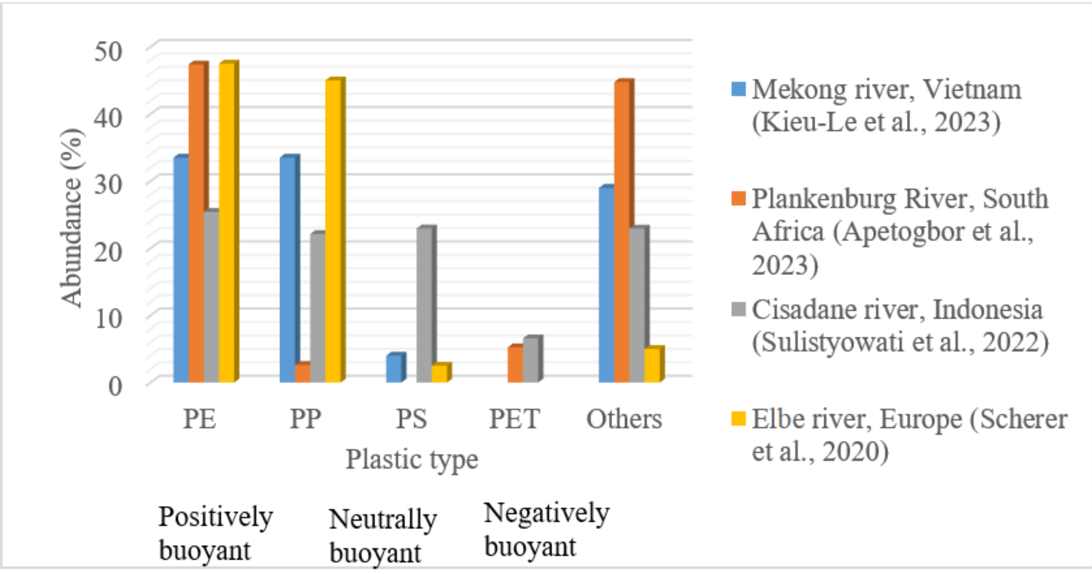

Figure 1-5. Distribution of the plastic type of microplastic pollution in water found in the Mekong river (Kieu-Le et al., 2023), Plankenburg river (Apetogbor et al., 2023), Cisadane river (Sulistyowati et al., 2022) and Elbe river (Scherer et al., 2020).

The microplastic bedload transport has been measured in flume experiments by Born et al. (2023), using microplastic particles between a size of 1000-3000 µm, with densities 910-1130 kg/m3. Microplastics concentrations were measured near the bed in uniform flows' conditions. However, there is need in the definition of the physics characteristics (shape, density, size) and hydraulics conditions (shear stress-velocities) where the plastic particle is transported as suspended or bed load.

The horizontal spatial distribution of the microplastic pollution in the river flow is characterised to be composed of variable concentrations. Waldschläger et al. (2020) compiled publications of plastic pollution in fluvial systems from 34 rivers, reporting maximum concentrations in water samples of 8925 ±1591 microplastics per square cubic meter (Mp/m^3) in China and 12 932 Mp/m^3 in United States, and a minimum of 1 Mp/m^3 in the Ottawa River in Canada.

1.3.3. Microplastic deposition in sediments

Microplastic particles entering river systems are transported, deposited, and stored in the main channel and riverbanks, which suggests that sediments may act as a reservoir for microplastic pollutants. (Hurley et al., 2018; Dikareva and Simon, 2019; Fan et al., 2019; Jiang et al., 2019; He et al. 2021; Scopetani et al., 2020; Waldschläger et al., 2020). The microplastic and sediment mixtures are formed by the deposition of suspended concentrations. Observation of sediment samples shows that the sediment bed contains roughly equal mixes of positively, neutrally and negative buoyant plastic particles (Hurley et al., 2018; Dikareva and Simon, 2019; Fan et al., 2019; Jiang et al., 2019; Chouchene et al., 2021; Lin et al., 2021; Saarni et al., 2021).

Figure 1-6 shows the types of plastics founds in sediment samples of four rivers. It is critical to note that all samples contained roughly equal mixes of positively, neutral and negatively buoyant particles. Between 38% to 70% of microplastic was positively buoyant plastic, including expanded polyester spheres (EPS), with a density estimated between 0.015-0.035 g/cm^{3,} and around 30%-42% are negatively buoyant plastic (Klein et al., 2015; Fan et al., 2019; Jiang et al., 2019; Simon-Sanchez et al., 2019).

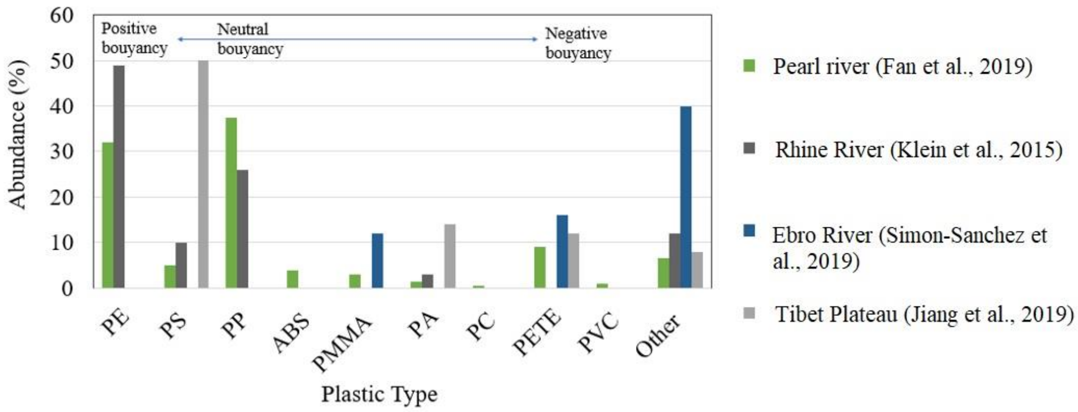

Figure 1-6. Plastic types deposited in the sediment bed of the Rhine (Klein et al., 2015), Pear (Fan et al., 2019), Ebro (Simon-Sánchez et al., 2019), and Tibet Plateau (Jian et al., 2019) rivers.

The horizontal spatial distribution of the microplastic pollution in the river bed is characterised to be composed of heterogeneous concentrations. Hurley et al. (2018) studied microplastic pollution in a catchment and found concentrations of microplastics between N=500 to 75000 microplastic particles per kilogram of sediment. Klein et al. (2015) studied microplastic pollution in an urban river and found microplastic concentrations from N=300 to 10000 microplastic particles per kilogram of sediment. Higher amounts have been reported in Canada N=210883 to 42989 particles per kilogram of sediment (Castañeda et al., 2014). The high amounts of particles deposited in the river are so common in the literature that they are referred as hotspots (Hurley et al., 2018; Klein et al., 2015).

The vertical distribution of microplastic particles in sedimentary deposits shows that plastic deposits generally decrease in deeper layers (Mao et al., 2021; Zhou et al., 2021). The different types of plastics are found in similar percentages in all the layers without any physics explanation related to their expected deposition. For example Zhou et al. (2021) measured the microplastic pollution in 15 different sites of the Fuhe river (China) in depths up to 50 cm below the river bed, describing an heterogeneous vertical microplastic distribution in sediments. The author found negative buoyant plastics such as polyethylene terephthalate (PET) and buoyant plastic polyethene (PE) deposited all over the sediment depth.

Researchers have measured the fall velocity for different categories and plastic types to understand the deposition process of microplastics. However, it is proven challenging to cover the range of plastics and shapes (Khatmullina and Isachenko, 2017; Kaiser et al., 2019; [a]Waldschläger and Schüttrumpf, 2019).

Khatmullina and Isachenko (2019) developed an equation for cylinders tested with microplastic fibres made of fishing lines found at the coastline, with diameters between 0.15 mm-0.71 mm and densities 1130-1168 kg/m^3. The equation is defined as

$$w_s = \frac{\pi}{2 * v} g \frac{(\rho_s - \rho_w)}{\rho_w} \frac{Dc * Lc}{C1 * Lc + C2} (mm/s) \tag{1-1}$$

Where Dc is the cylinder diameter, and Lc is the cylinder. The coefficient C1 and C2 refers to the particle diameter described in Figure 1-7. The relative errors vary between 3.7%-1.1%, which can be considered a correct approximation for plastic with a cylinder geometry. The authors suggest an averages C1= 55.238 mm-1 and C2=12.691.

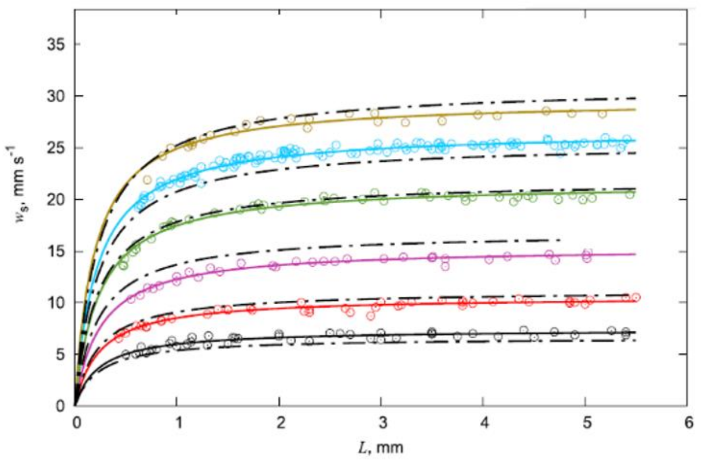

Diameter of cylinder (mm)	C1 (mm-1)	C2
0.15	49.283	11.737
0.22	58.282	14.179
0.34	60.552	15.230
0.46	55.985	13.334
0.6	52.749	11.442
0.71	57.726	11.058
—·—	55.238	12.691

Figure 1-7. Khatmallina and Isachenko (2017) diagram for plastic settle velocity. Circles represent experimental data, coloured solid and dash-dot black curves represent settling velocity predicted for C1 and C2 as is shown in the symbology, w_s is the fall velocity, and L is the cylinder length (Modified Khatmullina and Isachenko., 2017).

Kaiser et al. (2019) also try to represent the microplastic settlement process by conducting experiments with various types, shapes, and sizes. The author evaluated irregularly shaped PA, PMMA, and PET, with densities of 1140, 1190, and 1390 kg m^{-3}, respectively, and particles sized from 6 µm to 251 µm. According to the results, the author proposes a multiple quadratic regression that predicts the terminal sinking velocity as a function of particle size, density of the fluid, and plastic, with an R^2= 0.58 defined as:

$$w_s = 11.68 + 0.1991 \text{ ESD} + 0.0004 * \text{ESD } 2 - 0.0993\ \Delta\rho + 0.0002\ \Delta\rho \qquad (1\text{-}2)$$

$$ESD = (\text{ac}^2)^{1/3} \qquad (1\text{-}2a)$$

Where ESD is the particle size, Δρ is particle density minus fluid density, A and C are the measured major (i.e. longest) and minor (i.e. shortest) axes of the particle.

[a]Waldschläger and Schüttrumpf (2019) presented an interesting study for pellets, fibers, foams and fragments of 7 plastic: PP, PE, PS, EPS, PVC, PET, CoPA (Polyamide block copolymers)

(Figure 1-8.). The experiment reproduces the natural settlement process of microplastic fluxes in a river (Figure 1-8). As has been described, field studies show that river pollution is composed of multiple different plastic types (Figure 1-5 , *Figure 1-6*). For example, in the Pearl River, China (Fan et al., 2019) found 18 different plastics.

Plastic is known to transport contaminants, organic matter, and organisms in the water environment; as a results from the adsorption and absorption phenomenon, which can be chemical, physical, or organic (Blair and Quinn, 2017; Leiser et al., 2020). The adsorption and absorption phenomena increases the size and weight of the microplastic particles in the environment, increasing their fall velocity and impacting the settlement processes of positively, neutrally and negatively buoyant plastics.

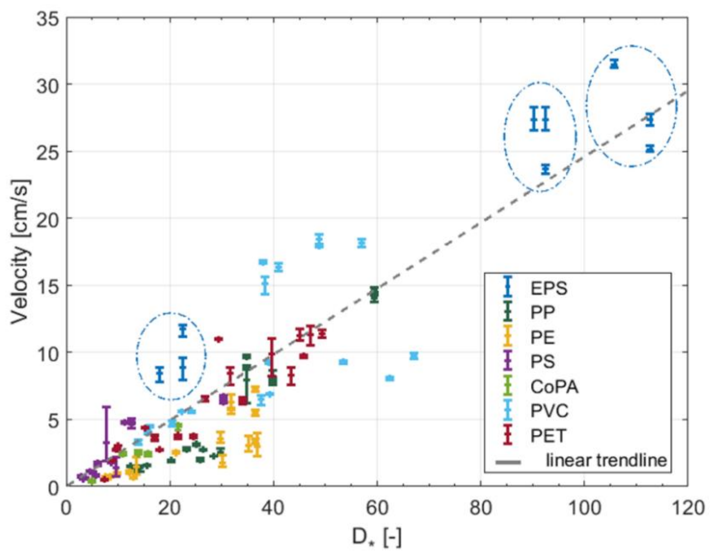

Polymer type	Shape	Density (kg/m^3)
PP	Sphere, pellet, fiber, fragment	826-870
PE	Sphere, pellet, fiber, fragment	894-936
PS	Sphere, pellet, fiber, fragment	1008-1021
EPS	sphere (foam)	22
PVC	pellet, fragment	1307
PET	pellet, fiber, fragment	1368
CoPA	fiber	1101-1107

Figure 1-8. ᵃWaldschläger and Schüttrumpf (2019) fall velocity experiment. The diagram shows that particle velocities depend on the dimensionless diameter D_*, shape categories and density of plastics. (Modified from ᵃWaldschläger and Schüttrumpf , 2019).

Microplastic aggregation process has been observed in the natural environment as lakes and seas, combined with other processes such as biofilm and marine organic matter (Hann et al., 2019; Leiser et al., 2020). Plastic is a material that has the properties of intermolecular interactions and electrostatic forces responsible for aggregations (Gingell and Parsegian, 1973; Silveira et al., 2018; Li and Xu, 2019) and can form flocs with microplastic and nano plastic particles by adding chemicals (flocculants) (Lu et al., 2018; Skaf et al., 2020). Hoellein (2018) studied the effect of biofilm on the fall velocity in microplastic (pellets, fragments, and fibres) and found that the biofilm increased the fall velocity by 43% to 50%.

The microplastic fall velocities are defined by the range of plastic types, sizes, shapes, densities, and aggregation processes. From this analysis, denser particles or aggregations are expected to fall first, and positively buoyant plastic tends to rise or float. However, is unclear why sediment samples show equal amounts of negatively, positively and neutrally plastic deposits in different riverbanks and beds layers. For this reason, the first subject to be developed in this research is: microplastic-sediment depositional structure. To understand the vertical distribution of the microplastics pollution in the river bed (Figure 1-9).

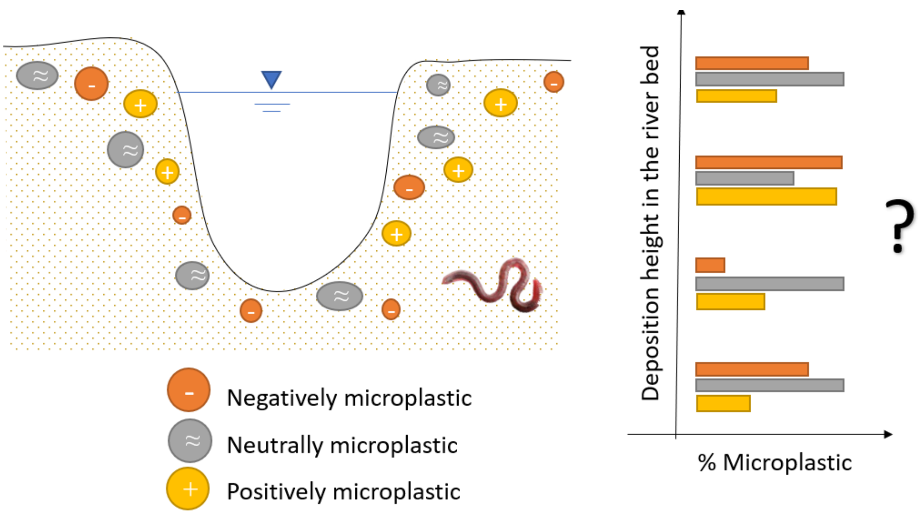

Figure 1-9. Sediment deposits are characterized to storages equal amounts of negatively, positively and neutrally microplastic all over the river channel.

1.3.4. Transport and deposition dynamics of microplastic pollution

The dynamics of plastic debris in rivers have been studied in the field (Kim et al., 2015; Liedermann et al., 2018; Eo et al., 2019; Emmerik et al., 2019; Rowley et al., 2020; He et al.,2021; Liro et al., 2020; Rolf et al.,2022), laboratory experiments (Russell et al., 2022) and numerical models (Critchell and Lambrechts, 2016; Besseling et al., 2017; Ding et al., 2019; Cook et al., 2020) in the last years. Each study has helped recreate the transport and deposition of plastic debris in rivers, process described as highly heterogeneous, depending on the river hydraulics and hydrology (Kumar et al., 2021).

Field observations have measured the spatial distribution of the microplastic pollution, showing a clear relation with hydraulics characteristics of the river flow and the location of the sources (Kim et al., 2015; Liedermann et al., 2018; Eo et al., 2019; Emmerik et al., 2019; Rowley et al. 2020). For example Liedermann et al. (2018) detected high microplastic concentrations accumulate in the low-velocity of the Danube river (Austria). It has been measured that wind, tides, and velocity vectors can influence its spatial distribution (Kim et al., 2015; Liedermann et al., 2018; Eo et al., 2019; Emmerik et al., 2019). Rowley et al. (2020) studied the microplastic water pollution in the Thames river (England) and measured more microplastics near the outflow point of a sewage treatment and during the greatest rainfall months.

More recently, the accumulation and migration of plastics have been related to morphology parameters such as topography, bedforms, flood areas, and vegetation (He et al.,2021; Russell et al., 2022; Liro et al., 2020; Rolf et al.,2022). Rolf et al. (2022) found that the local topography, soils, and vegetation influence the accumulation and migration of microplastic particles in flooding areas. Liro et al. (2020) demonstrated that the retention of microplastic debris in mountain rivers is controlled by morphology; a linear channel accumulates less plastic than a braided river, influenced by the area of vegetation and wood that promote the accumulation of plastics. Russell et al. (2022) study the influences of negatively buoyant microplastics (1050 to 1600 kg/m^3) in the form of bedforms in a flume. Plastic interrupts the bedload sand movement leading to reduced dunes with several sizes and forms, ending in non-heterogeneous deposits. The key finding of all these studies is that plastic is an active constituent of rivers, changing the natural river conditions.

Numerical models have been advanced, incorporating hydrodynamics, mass balance, and statistical theories to study the transport and deposition of this pollutant in aquatic environments (Uzum et al. 2021). Depending on the study case, models include the influences of tides, wind flows, bathymetry, sources, and/or aggregation processes.

Numerical models describe that the plastic physical characteristic, source location and quantities of debris had an important effect on the transport, sedimentation, and resuspension areas (Critchell and Lambrechts, 2016; Besseling et al., 2017; Ding et al., 2019; Cook et al., 2020). In these models, positive buoyant microplastics have higher mobility and are transported long distances in the upper layers (Enders et al., 2014; He et al., 2021). Negative buoyant microplastics accumulate close to the source points, and high velocity promotes the transport of the sinking microplastics in the bed (Ding et al., 2019; He et al., 2021). Neutrally buoyant microplastic particles behaved similarly to solutes following open channel flow theoretical dispersion theories (Cook et al., 2020). Flow conditions define the accumulation of microplastic in the water column and sediment (Quik et al., 2015; He et al., 2021). High flows transport more microplastics (Wagner et al, 2019), and converge zones accumulate plastic (Frére et al., 2017; Alosairi et al., 2020)

The variety of numerical models has covered an important range of plastics types and hydrodynamics. However, it is highlighted that few models integrate the study of sediment and microplastic particles interacting in the river bed (Drummond et al., 2022; Shiravania et al., 2023). As it was described in previous sections, suspended microplastic concentrations (Section 1.2.2.) can be stored in the sediment (Section 1.2.1.), influencing the plastic accumulation and migration in the river bed (Section 1.2.3.). Numerical models include the dynamic of the microplastics with a static river bed without considering the plastic storage in the river bed. Studying the dynamics of the interactions between the microplastic and sediment enables an understanding of more realistic spatial and temporal distribution patterns, morphology changes, and load balances of plastic debris, with more accurate estimations of the dynamics of microplastic fluxes to interpret its environmental impacts. Therefore, this research's second objective focuses on developing a numerical model to simulate microplastic–sediment transport, deposition and remobilization dynamic of microplastic (Figure 1-10).

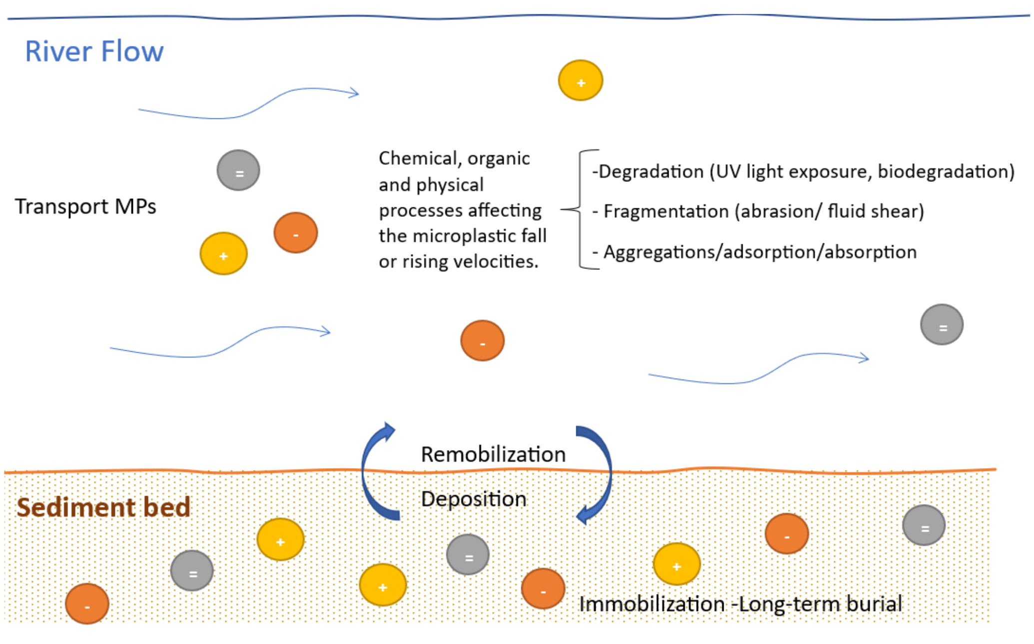

Figure 1-10. Transport and deposition dynamics of the microplastics in river. The microplastics particles entering in the river system are transported by the river flow. Chemical, organic and physical processes affect the microplastic fall or rising velocities. In the sediment bed the microplastic is deposited, immobilization, long term burial or can be remobilized. (Adapted from: Blair and Quinn, 2017; Leiser et al., 2020;Alimi et al., 2022; Drummond et al., 2022).

1.4. Research proposal

As highlighted by this literature review, microplastic pollution is an environmental problem affecting rivers, oceans, and coastlines (Browne et al., 2011; The Royal Society, 2019). The microplastic contamination is increasing yearly, and rivers are the key vector for waste to oceans (Lebreton et al., 2017). The research aims to understand the physical parameters that govern the transport, deposition and storage of these plastic particles in fluvial systems. The research proposal is divided into two objectives.

Objectives 1:

The first objective is to create settling experiments, to understand the depositional processes of microplastic pollution trapped in sedimentary deposits.

From studies of natural sediment mixtures, it is hypothesised that particle interaction in the suspension governs the settling and deposition process of microplastic particles. Two separate experiments were designed with positively, neutrally and negatively buoyant suspended microplastic-sediment mixtures to recreate scenarios that represent the range of plastic densities that pollute real-world rivers:

- Experimental settling process of microplastic and sediment mixtures: baseline and negatively buoyant.
- Experimental settling process of microplastic and sediment mixtures: positively - neutrally buoyant and constant suspension density.

Objective 2:

The second objective is to create a numerical model to simulate microplastic–sediment transport and deposition dynamics, to understand the spatial and temporal distribution patterns, morpholicaly changes, and load balances of plastic debris in rivers.

From field sampling and flume experiments, it is hypothesised that hydraulics parameters determined by channel geometry control transport, sedimentation, erosion and resuspension of the microplastics-sediment particles. A hydro-morphodynamical numerical model was run to identify the influences of the flow forces in distributing the microplastic concentration and the interactions between the sediment bed. The objectives and research question of this chapter are:

- Study the effects of plastic in the formation of bedforms. What are the morphological changes in a riverbed with microplastic?

- Study the microplastic fluxes load balance in a river. How much plastic gets in and out of the river system?
- Study the patterns of the transport and deposition of the microplastic fluxes in a braided river.: How does the interaction between the sediment and microplastics influence plastic fluxes' transport and deposition patterns?

Chapter 2 . Experimental settling process of microplastic and sediment mixtures in rivers: introduction, materials, scenarios and methods

Chapter 2 introduces the literature review and methods of the settling experiments designed to understand the depositional processes of microplastic pollution trapped in sedimentary deposits in fluvial system. The chapter starts with an introduction to microplastic pollution, followed by a description of the resultant deposits due to the interactions between the particles in suspension. The methods describe the materials, scenarios and procedures. The materials used are microplastics, sediments and saline solutions. There are three scenarios: baseline, variable suspension density with bimodal particle density and fixed suspension density. The procedures include seven steps, which go from the preparation of the materials to the determination of the volumetric contents and size distribution of the resultant deposits.

2.1. Introduction

Microplastic particles entering rivers systems can be deposited and stored in the main channel and riverbanks, forming mixtures of sediments with positively, neutrally and negatively buoyant plastic particles (Hurley et al., 2018; Dikareva and Simon, 2019; Fan et al., 2019; Jiang et al., 2019; Scopetani et al., 2020). The vertical distribution of microplastic particles samples in sedimentary deposits registered a mixed stratigraphy, where the amount of plastic deposited decreases with depth, and different types of plastics are found in similar percentages in different depths(Mao et al., 2021; Zhou et al., 2021).

Microplastic is commonly defined as plastic particles with a size between 0.1 µm to 5000 µm (The Royal Society, 2019). Microplastic particles can be formed of positively, negatively or neutraly buoyant plastics with respect to water, typical densities ranging from 880 up to 1700 kg/m^3 (Shim et al.,2018). Microplastic particles are classified into eight common shape categories based on their geometry and polymer type. The shapes categories include disc-shaped (film, fragments/sheets), bladded-rod (fibres), and spherical (foam, pellets, microbeads) particles (Lewis and McConchie, 1994; Shim et al.2018; The Royal Society, 2019).

Siliciclastic sedimentary particles (henceforth referred to as sediment particles) are typically classified by their grainsize, according to the International Organization for Standardization (International Organization for Standardization, 2017). Fine particles, including clay, have grainsizes less than 2 µm, silt is defined as having grainsizes between 2 µm to 63 µm; coarse particles, including sand, have grainsizes between 63 µm to 200 µm, gravels have grain sizes between 200 µm to 63 000 µm, and very coarse particles, including cobbles and boulders, have grainsizes between 63 000 µm and higher. The density of these particles is commonly recognised as 2650 kg/m^3 (Dingman, 2008).

The rates at which microplastic and sediment particles settle out of suspension depends on the interaction between fluid forces and particle properties. Particles in a quiescent fluid start to settle with a vertical speed that depends on the balance between the forces exerted by gravity (F_g) and drag (F_d) (Lick, 2009). The drag force is described as the fluid resistance acting opposite to the relative motion, whilst the gravity force is the natural phenomenon by which all objects with mass or energy are attracted to one another (Lick, 2009). The values of gravity and drag depend on the particle weight and the fluid viscosity. The fall velocity of a particle is thus a result of the balance between gravitational and drag forces. Here, the fall velocity is defined using an empirical formula for particles, given by Ferguson and Church (2004):

$$w_s = \left|\frac{\Delta g D^2}{c_1 v + (0.75\ c_2 \Delta g D^3)^{0.5}}\right| \tag{2-1}$$

Where v (m^2/s) is the kinematic viscosity of the fluid, $g(m/s^2)$ is the gravitational acceleration, D is the diameter of the equivalent particle, c_1 and c_2 are empirical parameters that take values of 18 and 0.4 for smooth spheres, and 24 and 1.2 for very angular grains (Ferguson and Church, 2004). The empirical parameters values where suggested based in experimental data sets for natural sands of no spherical shape.

Δ describes the submerged specific gravity of a particle given by:

$$\Delta = \frac{\rho - \rho_f}{\rho_f} \tag{2-2}$$

Where ρ_f (kg/m^3) denotes the density of the fluid, and ρ (kg/m^3) the particle density.

The shape of the particle is known to influence the fall velocity (w_s); irregular particles are expected to fall at different rates than perfect spheres (Ferguson and Church, 2004; Camenen, 2007). The irregularity of a particle can be compared to idealised spherical particles through a term known as the equivalent diameter (D_{equi}). The equivalent diameter is a physical property used to represent a three-dimensional shape by one dimension. The particle texture and geometry influence this dimension. Only perfect spheres can effectively be described by one dimension, such as a radius or diameter (Valsangkar, 1992; Malvern Instruments Limited, 2015). Yet numerical expressions such as Eq. 2-1 require the characterisation of irregular particles using a single dimension value. To calculate a representative effective diameter for irregular particles, different methodologies, such as weight, volume, area and sieves, have been employed (Malvern Instruments Limited, 2015). Volumetric and area analysis are used herein to estimate the equivalent diameter sphere. The volumetric analysis of particles enables the estimation of an equivalent diameter of an imaginary sphere with equivalent volume to the observed irregular particle (Malvern Instruments Limited, 2013). The area analysis measures the particle surface area, which can be mapped to spherical volume.

The representative equivalent diameters for the volumetric analysis, were detailed in section 2.4.2, estimated using a granulometric curve. The curve can describe the particle grain size distributions and is created with the accumulated volumes plotted against varying bins of grainsize (Diplas et al., 2008). From the granulometric curve, the statistical percentiles 10 % (D_{10}), 50% (D_{50}), and 90% (D_{90}) can be used to represent the finer, medium, and larger grain size in the sample (Diplas et al., 2008).

Particle interaction in a suspended concentration

Sedimentary and microplastic deposits are formed when the fluid forces responsible for maintaining particles in suspensions decrease causing particles to settle and subsequently form substrates with textural characteristics (known as stratigraphy) (Druit, 1995; Amy et al., 2006; Guo et al., 2015; Dorrell, et al., 2011). The stratigraphy textural characteristics depends on particle properties, density, size, and shape, and the number of particles present in the suspension, concentration (Druit, 1995; Amy et al., 2006; Dorrell et al., 2011; Guo et al., 2015). Experimental settling research on particles in suspension recognises regimes based on the concentration of suspended particles (Figure 2-1).

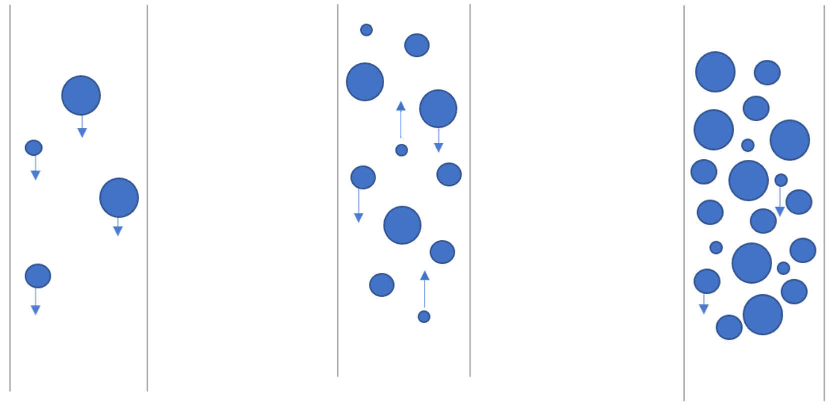

Figure 2-1. Schematic settling particle process in low high concentrations and particle matrix compression (settlings stages). At low concentrations, particles settle at their fall velocity. At high concentrations, particles are more near to each other, and the interflows influence the particle's buoyant state (positive, neutral, or negative). Particle compression, particles are so near each other that the matrix of particles slowly compresses under its own weight (Adapted from Druitt,1995).

Depending on the objectives and results of these studies, the settling stages can be named and classified differently. Gou et al. (2015) described their settling regimes as initial free settlement, hindered settlement, and self-weight consolidation settlement. Amy et al. (2006) defines five regimes groups as a function of the grain size distribution and sediment type (cohesive or non-cohesive). Druitt (1995) divided the regimes into low, intermediate, and high concentrations. Dorrell and Hogg (2010) proposed numerical methods that are able to recreate observed changes in the grain size profiles during the sedimentation process, classifying the settling behaviour into regimes, that depends on the initial volume proportions and settling velocities. Despite the regimes' names or categories assigned, all these studies conclude that sediment concentration governs the stratigraphy of the resulting deposits as concentration directly controls the particles fall velocity.

The definition regime varies depending on the materials size distribution, shape and density, used in the laboratory settling tube. Particles matrix compression have been reported between volumetric concentrations 30%-65%, high concentration between 20%-44%, and low concentrations less than 10% (Druitt, 1995). Relating the results of each research to real concentrations is complex. For example, river catchments have reported suspended sediment concentrations with volumetric content less than 1% (Horowitz, A.J., 2003); however, the measurements are typically made in more low flow events than high events. Amy et al. (2006)

settling tubes were related to the depositional sediment gravity flows to understand the bimodality in sediment texture found in some turbidite systems. The effect of the particle interaction processes operating in microplastic and sediment mixtures remains uncertain, particularly with respect to the effect of plastic density and concentration. For this reason, this research aims to understand the physical parameters that control the vertical distribution of microplastics in sedimentary deposits. For this, a set of experimental settling tubes were designed based on theories of particle interactions. In this research, it is decided to define the settling regimes in the function of the concentrations (low-medium-high), incorporating the main concepts of the different studies, described as:

In low concentration solutions, particles tend to fall individually without influences from other particles (Pane and Schiffman, 1985; Druit, 1995; Abu-Hejleh et al., 1996). Faster particles (larger or denser) settle first, followed by the medium and smallest, generating vertical gradient size distributions (Druit, 1995) in a free settling stage (Guo et al., 2015).

As the number of particles increases (higher concentrations), the particles are closer to each other. The distance between them is reduced, and the viscosity enhanced (Richardson and Zaki, 1954). The fluid surrounding the particles creates a displacement flow (interflows) as the grains settle (Amy et al., 2006), which inhibits the fall velocity (Druit, 1995; Amy et al., 2006; Guo et al., 2015), a phenomenon described as a hindered settling regime (Kynch, 1952; Richardson and Zaki, 1954; Dorrell and Hogg, 2010; Guo et al., 2015). The range that inhibits the particles fall velocities depends on the concentration of the suspensions and the particle densities (Phillips and Smith, 1971). Particles may be resuspended and rise as a result of the counterflows, intermediate density particles may remain with small terminal settling velocities in comparison to the counterflow, and higher density particles may settle (Druit, 1995, Dorrell and Hogg, 2010).

In particle compression, the network of the interflows is stronger (Druit, 1995; Amy et al., 2006; Guo et al., 2015), and the contributions from effective viscosity are stronger (Richardson and Zaki, 1954). Particles are so near each other that the matrix of particles slowly compresses under its own weight (self-weight load), a process controlled by the rate at which the interflows escape from the particle matrix (Mehta and Mcanally, 2008; Guo et al., 2015).

It is the concentration of suspended particles that exerts a strong control on determines the stratigraphy formed after the settling process. In lower concentration suspensions, larger or denser grains settle first, followed by the medium and smallest grainsizes, generating a vertical in gradient size distributions within the deposit (Druit, 1995). In particle compression, the particle matrix descend at a similar fall velocity to each other, there is slight particle segregation, forming an ungraded deposit (Druit, 1995; Dorrell and Hogg, 2010). In higher concentrations, a mixture of graded and ungraded deposits is formed (Druit, 1995; Amy et al., 2006; Guo et al., 2015).

The reductions in the particle fall velocity the different concentrations can be estimated by the modified Davis and Gecol (1994) equation, described as the hindered fall velocity (W_S). The equation includes all effects produced by particles during particle-to-particle interactions, such as return flow, increased viscosity, and the buoyancy of a bimodal mixture (Cuthbertson et al., 2008). The Davis and Gecol (1994) model is based on the work developed by Batchelor (1982), Batchelor and Wen (1982), and Richardson-Zaki (1954). The equation can be defined for a bimodal mixture of microplastics and sediment as:

$\mathrm{W_{sMpP}} = \mathrm{w_{sMp}}(1-\Phi)^{-(\mathrm{S_{MpMp}})}\left(1+\left(\mathrm{S_{MpS}}-\mathrm{S_{MpMp}}\right)\Phi_{\mathrm{S}}\right)$ (Microplastic hindered fall velocity) (2-3)

$\mathrm{W_{sS}} = \mathrm{w_{sS}}(1-\Phi)^{-(\mathrm{S_{ss}})}\left(1+\left(\mathrm{S_{SMp}}-\mathrm{S_{SS}}\right)\Phi_{\mathrm{Mp}}\right)$ (Sediment hindered fall velocity) (2-4)

Where

$\mathrm{S_{MpS}} = -2.5-\left(\left(\frac{\mathrm{D_S}}{\mathrm{D_{Mp}}}\right)^2+3\left(\frac{\mathrm{D_S}}{\mathrm{D_{Mp}}}\right)+1-\frac{1.87\left(\mathrm{D_S}/\mathrm{D_{Mp}}\right)}{1+0.0024\left(\mathrm{D_S}/\mathrm{D_{Mp}}\right)^2}\right)\left(\frac{\rho_{\mathrm{S}}-\rho_{\mathrm{f}}}{\rho_{\mathrm{Mp}}-\rho_{\mathrm{f}}}\right)$ (Empirical parameter for Microplastic hindered fall velocity) (2-5)

$\mathrm{S_{SMp}} = -2.5-\left(\left(\frac{\mathrm{D_{Mp}}}{\mathrm{D_S}}\right)^2+3\left(\frac{\mathrm{D_{Mp}}}{\mathrm{D_S}}\right)+1-\frac{1.87\left(\mathrm{D_{Mp}}/\mathrm{D_S}\right)}{1+0.0024\left(\mathrm{D_{Mp}}/\mathrm{D_S}\right)^2}\right)\left(\frac{\rho_{\mathrm{Mp}}-\rho_{\mathrm{f}}}{\rho_{\mathrm{S}}-\rho_{\mathrm{f}}}\right)$ (Empirical parameter for sediment hindered fall velocity) (2-6)

Where W_{sMP} (m/s)and W_{sS} (m/s) are the microplastics and sediment hindered fall velocity and, w_{sMp} and $w_{sS,}$ is the free settling fall velocity (m/s), Φ the volumetric concentration of particles (m^3/m^3), D_{MP} and D_S are the particle size (m), S_{MpMp} and S_{SS} are empirical parameters, with a value of -5.63 for bidisperse suspensions (Cuthbertson et al., 2008). The empirical parameter value of -5.63 approximations come from the application of the Batchelor and Wen (1982) equation to particulates of the same type of material. When applied to only sediment or plastic; equations 2-5 or 2-6 yield parameters $\frac{D_{Mp}}{D_{Mp}}$ or $\frac{D_S}{D_S}$ and $\frac{\rho_{Mp}-\rho_f}{\rho_{Mp}-\rho_f}$ or $\frac{\rho_S-\rho_f}{\rho_S-\rho_f}$, which becomes 1.

Given these points, the definition of a suspension in a low or high concentration depends on the size, density, and shape of materials interacting with the fluid. When considering microplastics, the size, shape, and density of microplastic particles are well known. However, it is unclear how the particle interaction between sediments and microplastic particles affects the resulting deposition patterns. In this present study research 52 settling tubes experiments are designed consisting of comparatively low and high microplastic-sediment concentrations. The range of microplastic-sediment concentrations in the 52 settling tubes simulated the settling process of negatively, positively, and neutrally buoyant microplastics; using one type of plastic and saline solutions to recreate the buoyant scenarios, representing the range of plastics that are observed in natural river systems.

In this research, the delimitation of the settling regimes (low, intermediate and high concentration) is defined by the suspension density; a physical parameter that describes the microplastic, fluid, and sediment mixture composition in each experimental tube (suspension concentration). The suspension density is the result of the summation of each material volume (percentage) multiplied by its density defined as:

$$\text{Suspension density}: \ \rho_{sus} = \rho_s \Phi_s + \rho_{MP}\Phi_{MP} + \rho_f(1 - \Phi_{MP} - \Phi_S) \qquad (2\text{-}7)$$

Where ρ_f, ρ_s and ρ_{MP} are the fluid, sediment, and microplastic density in kg/m^3. Φ_s and Φ_{MP} are the volumetric concentration (m^3/m^3) of the sediment and microplastic.

2.2. Materials

The experimental work conducted here uses negatively buoyant (sinking) microplastic particles (semi-cuboid nylon fragments), non-cohesive sediment (glass spheres), with respective water or saline solutions. The glass spheres and microplastic materials were purchased from Guyson International Ltd (www.guyson.co.uk) and are commonly used in industrial settings as abrasives to remove paint or clean corroded surfaces. Table 2.1 shows a summary of the materials properties.

The microplastics used herein are polyamide nylon semi-cuboid particles, an industrial particle abrasive sold as Guyson Thermoflash plastic with a side dimension of 500 µm. They are orange in colour and have a density of 1150 kg/m^3 (ρ_{MP}) (Guyson International-a, 2021). The Thermoflash plastic material was chosen based on its size, type and density.

The Thermoflash particle size is smaller than 5000 µm and is thus can considered a microplastic (Hartmann et al., 2019). Further, the microplastic size was such that it was larger than the largest glass spheres to aid the classification of materials based on the grain size distribution. The density had to be greater than the density of freshwater (negative buoyant microplastic) but less than the maximum density of a saline solution at room temperature (20°C- 1197.17 kg/ m^3, Ionut et al., 2015); to create neutral and positive buoyant plastic with saline solutions. Finally, the Nylon is considered a type of plastic that can be found in the river environment (Klein et al., 2015; Simon-Sanchez et al., 2019). Henceforth, the Thermoflash plastic particles are referred to as microplastics.

Table 2.1. Properties of the materials used in the experiment. Properties listed of the microplastic, and sediment corresponded to the supplier specifications.

Materials	**Description**	
Microplastic	Oranges semi-cuboid nylon particles, 500 µm, ρ_{MP} = 1150 kg/m^3	
Sediment	White glass spheres, ρ_S = 2400-2600 kg/m^3 Guyson International Limited, 2021	
	Size (µm)	**Volume Distribution (%)**
	45-90 µm (Honite 18)	20
	53-106 µm (Honite 16)	20
	75-150 µm (Honite 14)	20
	106-212 µm (Honite 13)	20
	150-250 µm (Honite 12)	20
Cylindrical setting tube	Waterproof carton tube, 7.2 cm diameter, 25 cm height.	
Fluid	Filtered water (18-20°C) or salinity solution	

Glass spheres were selected as representative of fine-grained sediment with a graded size distribution, following standard practices in sedimentological research (Amy et al., 2006). Glass spheres are advantageous because they are clean (without pollutants or organic matter, which might cause aggregations), and are produced with controlled size distributions, useful in laboratory experiments. The glass sphere sizes for this study were chosen based on a previous study where similar experiments were conducted to determine the characteristics of sediment deposits in mixtures of cohesive and non-cohesive sediment (Amy et al., 2006). The glass spheres were purchased commercially as Honite 18 (sizes ranging between 45-90 µm), Honite 16 (53-106 µm), Honite 14 (75-150 µm), Honite 13 (106-212 µm), and Honite 12 (150-250 µm) with a density between 2400-2600 kg/m^3 (Guyson International-b, 2021). Henceforth, the Honite glass beads are referred as sediment or sedimentary particles.

A waterproof 'Pringles' carton was used as a settling tube, selected as an easily accessible, economical waterproof container without plastic and easy to cut. The carton container tube has already been tested as settling tubes in experiments similar to these (Amy et al., 2006). The size of the cylinder settling tube was measured with a Vernier Caliper, and have a diameter of 0.072 m and a height of 0.25 m. Thus, the total tube volume is 1.018 x 10^{-6}m^3.

Settling tubes were filled with filtered tap water or a saline solution to create negatively, positively, and neutrally buoyant plastics suspensions, with fluid densities ranging from 998 kg/m^3 to 1195.6 kg/m^3. The saline solutions are included to create buoyant conditions for neutrally and positively buoyant microplastic using a negative buoyant plastic density. The experiments' design focused on representing river environments; the saline solutions are not included to represent coastal/marine environments.

2.3. Scenarios

The set of experiments is made up of 52 settling tubes. The experiments consisted of adding different volumes of microplastic, sediments, and fluid in a tube to study the stratigraphy formed after being mixed and allowed to settle. The scenarios were designed to cover the three settling regimes described in section 2.1 (low, high). The parameter selected to describe the scenario conditions is the suspension density (equation 2-7), as it describes the volumetric concentration and density mixtures composition and can be related to the different settling regimes. *Figure 2-2* shows a diagram with the scenarios described:

A) Baseline: Included as a comparable scenario to analyse the changes in the pure samples of sediment and microplastic; and the results of previous studies investigating formed from uniform sediment with the same methodology of carton containers(e.g. Amy et al. 2006). The baseline scenario has seven settling tubes:

- 3 with only negatively buoyant microplastic.
- 4 with only sediments.

B) Scenario 1: Variable suspension density with bimodal particle density. Designed to study the settling process in the settling regimes of positively, negatively, and neutrally buoyant microplastics suspension densities between 1092 kg/m^3 to 1659 kg/m^3. The variable suspension density scenario is composed of 27 settling tubes:

- 19 tubes with negatively buoyant microplastic and sediment, compared to initial suspension.
- Three tubes with neutrally buoyant microplastic and sediment, compared to initial suspension.
- Five tubes with positively buoyant microplastic and sediment, compared to initial suspension.

C) Scenario 2: Fixed suspension density. Designed to study the settling process of three plastics densities (positively, negatively, and neutrally buoyant) in a free settling regime. Designed to consider solely the free settling regime, expanding the results to different plastic densities and concentrations more representative of riverine environments. The fixed suspension density scenario has three target suspension densities: 1052 kg/m^3, 1152 kg/m^{3}and 1227 kg/m^3, and is composed of 18 settling tubes.

- Six tubes with negatively buoyant microplastic, compared to initial suspension density.
- Six tubes with neutrally buoyant microplastic, compared to initial suspension density.
- Six tubes with positively buoyant microplastic, compared to initial suspension density.

The methodology to develop this experimental work is explained in this thesis chapter. The results and discussion for the baseline, negatively buoyant microplastics with variable suspension density are described in chapter three. The results of positively and neutrally microplastics variable suspension density, and constant suspension density are described in chapter four.

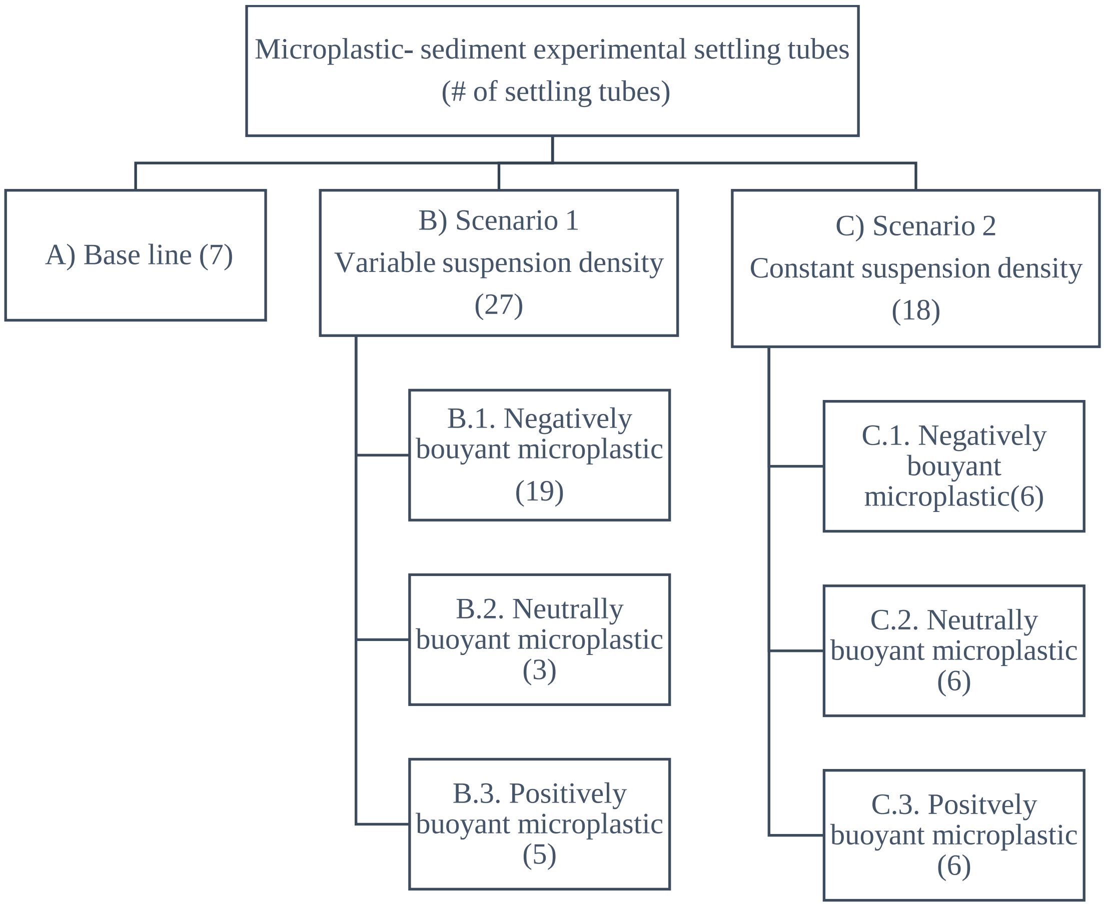

Figure 2-2. Set of experiments to study the positively, negatively, and neutrally buoyant microplastic particle settling process in different suspended concentrations.

The different volumes of microplastic (Φ_{MP}), sediment (Φ_S), and fluid (Φ_f) that were added to each settling tube are presented in Table 2.2 and Figure 2-3. The settling tubes are called "$MP_{number}S_{number}$", where MP refers to microplastic and S to sediment, and the subscript number specifies the percentage of the total volume composed of each material, respectively. The following symbols refer to the microplastics: "+" positively buoyant; and "≈" approximately to neutrally buoyant.

Table 2.2 shows the scenarios, names assigned, and the volumes of materials. More details of the planning and estimations of the quantities of the materials are given below.

Table 2.2. Name, volume and mass of the microplastic, sediment and water added to each experimental tube.

#	Name	Microplastic			Sediment			Fluid		Suspension density (kg/m³)
		Volume		Mass, M_{Mp} x10⁻³kg±1x10⁻⁵kg	Volume		Mass, M_S x10⁻³kg±1x10⁻⁵kg	Volume, Vf x10⁻⁶m³±1x10⁻⁶m³	Density (kg/m³)	
		Φ_{Mp} (-)	V_{MP} x10⁻⁶m³		Φ_S (-) ±4%	V_S x10⁻⁶m³±4%				
Scenario: Baseline										
1	MP_5S_0	0.05	50.00	57.5	0.00	0.00	0.00	950.00	998.00	1006.60
2	$MP_{10}S_0$	0.10	100.00	115.0	0.00	0.00	0.00	900.00	998.00	1013.20
3	$MP_{15}S_0$	0.15	150.00	172.5	0.00	0.00	0.00	850.00	998.00	1020.80
4	MP_0S_9	0.00	0.00	0.00	0.09	94.57	235.00	900.00	998.00	1140.04
5	MP_0S_{19}	0.00	0.00	0.00	0.19	190.28	470.00	800.00	998.00	1283.81
6	MP_0S_{29}	0.00	0.00	0.00	0.29	287.17	705.00	700.00	998.00	1429.33
7	MP_0S_{39}	0.00	0.00	0.00	0.39	385.25	940.00	600.00	998.00	1576.64
Scenario 1: Negatively buoyant microplastic										
8	MP_5S_{14}	0.05	50.45	57.50	0.14	142.28	352.50	800.00	998.00	1219.37
9	MP_5S_{24}	0.05	51.76	57.50	0.24	239.58	587.50	700.00	998.00	1364.06
10	MP_5S_{33}	0.05	51.07	57.50	0.34	336.06	822.50	600.00	998.00	1510.52
11	MP_5S_{43}	0.05	51.39	57.50	0.43	434.74	1057.50	500.00	998.00	1658.79
12	MP_5S_5	0.05	50.15	57.50	0.05	47.14	117.50	900.00	998.00	1076.43
13	MP_7S_{12}	0.07	70.55	80.50	0.12	123.16	305.50	800.00	998.00	1193.71
14	$MP_{10}S_9$	0.10	101.60	115.00	0.09	94.57	235.00	800.00	998.00	1155.33
15	$MP_{10}S_{19}$	0.10	101.21	115.00	0.19	190.28	470.00	700.00	998.00	1299.19
16	$MP_{10}S_{29}$	0.10	101.83	115.00	0.29	287.17	705.00	600.00	998.00	1444.81
17	$MP_{13}S_7$	0.13	131.34	149.50	0.07	66.08	164.50	800.00	998.00	1117.09
18	$MP_{13}S_{16}$	0.13	130.55	149.50	0.16	161.45	399.50	700.00	998.00	1260.46
**Table continues on next page*										

19	MP_7S_{32}	0.07	71.41	80.50	0.32	316.47	775.50	600.00	998.00	1484.19
20	MP_5S_9	0.05	50.30	57.50	0.09	94.57	235.00	850.00	998.00	1147.69
21	MP_8S_7	0.08	75.34	86.30	0.07	71.82	176.30	850.00	998.00	1115.82
22	$MP_{10}S_5$	0.10	100.30	115.00	0.05	47.14	117.50	850.00	998.00	1084.19
23	$MP_{10}S_{14}$	0.10	101.91	115.00	0.14	142.28	352.50	750.00	998.00	1227.04
24	$MP_{15}S_{14}$	0.15	151.36	172.50	0.14	142.28	352.50	700.00	998.00	1234.71
25	$MP_{15}S_5$	0.15	150.45	172.50	0.05	47.14	117.50	800.00	998.00	1091.68
26	MP_5S_{29}	0.05	50.92	57.50	0.29	287.17	705.00	650.00	998.00	1437.07
Scenario 1: Positively buoyant microplastic										
27	$+MP_5S_{24}$	0.05	50.76	57.50	0.24	238.58	587.50	700.00	1195.60	1504.49
28	$+MP_5S_{43}$	0.05	50.76	57.50	0.43	429.44	1057.50	500.00	1195.60	1738.88
29	$+MP_5S_5$	0.05	50.76	57.50	0.05	47.72	117.50	900.00	1195.60	1270.09
30	$+MP_{13}S_7$	0.13	131.98	149.50	0.07	66.8	164.50	800.00	1195.60	1289.93
31	$+MP_{13}S_{16}$	0.13	131.98	149.50	0.16	162.23	399.50	700.00	1195.60	1407.03
Scenario 1: Neutrally buoyant microplastic										
32	$\approx MP_5S_{24}$	0.05	50.76	57.50	0.24	238.58	587.50	700.00	1120.20	1450.90
33	$\approx MP_5S_{43}$	0.05	50.76	57.50	0.43	429.44	1057.50	500.00	1120.20	1700.61
34	$\approx MP_5S_5$	0.05	50.76	57.50	0.05	47.72	117.50	900.00	1120.20	1201.20
Scenario 2: Negatively buoyant microplastics										
35	$MP_{2.0}S_{2.4}$	0.02	20.00	23.00	0.024	2.40	61.10	954.00	1012.50	1052.00
36	$MP_{2.0}S_{2.8}$	0.02	20.00	23.00	0.028	2.80	70.50	950.00	1006.80	1052.00
37	$MP_{2.0}S_{3.1}$	0.02	20.00	23.00	0.031	3.10	77.60	947.00	1002.60	1052.00
38	$MP_{0.5}S_{2.4}$	0.005	5.00	5.80	0.024	2.40	61.10	969.00	1014.60	1052.00
39	$MP_{0.5}S_{2.8}$	0.005	5.00	5.80	0.028	2.80	70.50	965.00	1009.10	1052.00
40	$MP_{0.5}S_{3.1}$	0.005	5.00	5.80	0.031	3.10	77.60	962.00	1004.90	1052.00
Scenario 2: Neutrally buoyant microplastics										
41	$\approx MP_{2.0}S_{2.4}$	0.02	20.00	23.00	0.024	24.00	61.10	954.00	1117.30	1152.00
42	$\approx MP_{2.0}S_{2.8}$	0.02	20.00	23.00	0.028	28.00	70.50	950.00	1112.10	1152.00
Table continues on next page										

43	$\approx MP_{2.0}S_{3.1}$	0.02	20.00	23.00	0.031	31.00	77.60	947.00	1108.20	1152.00
44	$\approx MP_{0.5}S_{2.4}$	0.005	5.00	5.80	0.024	24.00	61.10	969.00	1117.80	1152.00
45	$\approx MP_{0.5}S_{2.8}$	0.005	5.00	5.80	0.028	28.00	70.50	965.00	1112.70	1152.00
46	$\approx MP_{0.5}S_{3.1}$	0.005	5.00	5.80	0.031	31.00	77.60	962.00	1108.80	1152.00
Scenario 2: Positively buoyant microplastics										
47	$+MP_{2.0}S_{2.4}$	0.02	20.00	23.00	0.024	24.00	61.10	954.00	1195.90	1227.00
48	$+MP_{2.0}S_{2.8}$	0.02	20.00	23.00	0.028	28.00	70.50	950.00	1191.10	1227.00
49	$+MP_{2.0}S_{3.1}$	0.02	20.00	23.00	0.031	31.00	77.55	947.00	1187.40	1227.00
50	$+MP_{0.5}S_{2.4}$	0.005	5.00	5.80	0.024	24.00	61.10	969.00	1195.20	1227.00
51	$+MP_{0.5}S_{2.8}$	0.005	5.00	5.80	0.028	28.00	70.50	965.00	1190.40	1227.00
52	$+MP_{0.5}S_{3.1}$	0.005	5.00	5.80	0.031	31.00	77.55	962.00	1186.80	1227.00

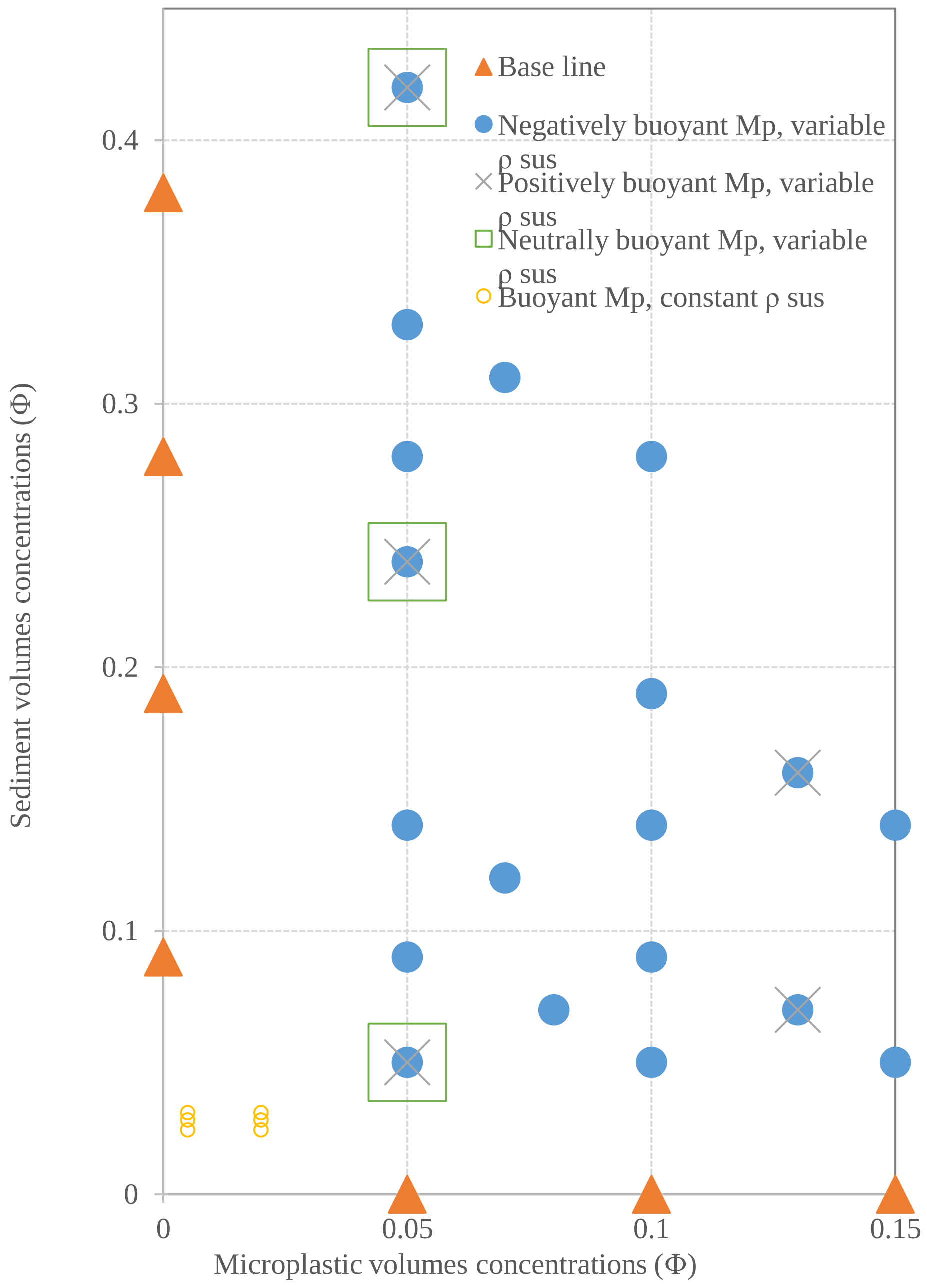

Figure 2-3. Microplastic and sediment concentrations added to each settling tube. Orange triangles correspond to the baseline. Blue circles are the nineteen settling negatively buoyant, green squares are the neutrally buoyant and grey "X" positively buoyant microplastics, all from scenario 1. The yellow circles at the bottom left correspond to scenario 2.

The volumes used for the experiments are 1,000 cm^3 due to the total volume of the cylinder being 1018 cm^3 and the necessity to leave a space gap for the mixing process.

The sum of $V_{MP,}$ V_S and V_f corresponds to the total volume (V_{ST}) inside the experimental tube, and the volumetric concentration (Φ) is the unitary percentage of each material divided by the total volume ($\Phi_{Mp=}V_{Mp}/V_{ST}$, $\Phi s = V_S / V_{ST}$ or $\Phi_f = V_f/V_{ST}$).

The mass of microplastic and sediment (dry materials) is estimated using their density and equation 2-3, where *M* is the mass, *V* is the volume, and ρ is the density of materials.

$$\rho = \frac{M}{V} \tag{2-8}$$

The microplastic density is 1150 kg/m^3, and glass spheres are 2400-2600 kg/m^3, based on the specifications given by the supplier.

When estimating the sediment volumes, an intermediate density value (2500 kg/m^3) is used for all the calculations. The range in values (2400 and 2600 kg/m^3) are considered to inform the uncertainty of calculating the volumes, a difference of – 4.2% and + 3.8% in the volumes. The uncertainty of the volumes is considered as ± 4% in all the sediments volume estimations.

The 52 settling tubes contain microplastic concentrations (Φ_{MP}) in the range of 0.005 to 0.15 and sediment fractions (Φ_S) in the range of 0.024 to 0.42.

The baseline concentrations (Figure 2-3, orange triangles) correspond to total fractions, Φ_S = 0.9, 0.19, 0.29, and 0.39, for sediment and Φ_{MP} = 0.05, 0.10, and 0.15, for microplastic.

For scenario one, negatively buoyant microplastics experiments 8 to 20 of Table 2.2 were conducted first to cover a broad range of total fractions of microplastic and sediment materials (Φ_{MP}+ Φ_S): 0.10, 0.19, 0.29, 0.39 and 0.49. After analysing the settling tubes with total fractions between 0.1 to 0.49, the volumetric concentrations of tubes MP_5S_9 to MP_5S_{28} were chosen to add finer detail in fractions lower than 0.3. The range between a total fraction of 0.14 to 0.30 was identified as the threshold between free settling and hindered effects after analysing the stratigraphy formed in the first twelve tubes.

The microplastic and sediment volumes for the positively and neutrally buoyant runs in scenario one (Figure 2-3, squares and "X" symbols) have similar mixtures to the negatively buoyant runs. The settling tubes have the same microplastic volumes (Φ_{MP} =0.05-0.010), and a low (Φ_S =0.05), medium (Φ_S =0.024), and high (Φ_S =0.043) sediment concentration. The selection of the fluid density to recreate the required buoyant conditions (column 10, Table 2.2) is explained in detail in section 2.4.1.

2.4. Methods

The experiment's first step (Figure 2-4) consisted of adding the requisite volumes of the three materials (microplastic, sediment, and fluid) to each settling tube as detailed in Table 2-2. The mass of microplastic and sediment was weighed on a scale (Ohaus, Scout Precision Balance) with a precision of ±0.01g. An equal fraction of each sediment size (Table 2-1) was weighed separately to promote the same size distribution of glass spheres in each settling tube. The mass of each sediment fraction was estimated as the total sediment weight divided by five. The total mass of the materials was mixed manually for at least 30s in a separate container to guarantee a uniform mixture of the 6 fractions (5 sediments - 1 microplastic).

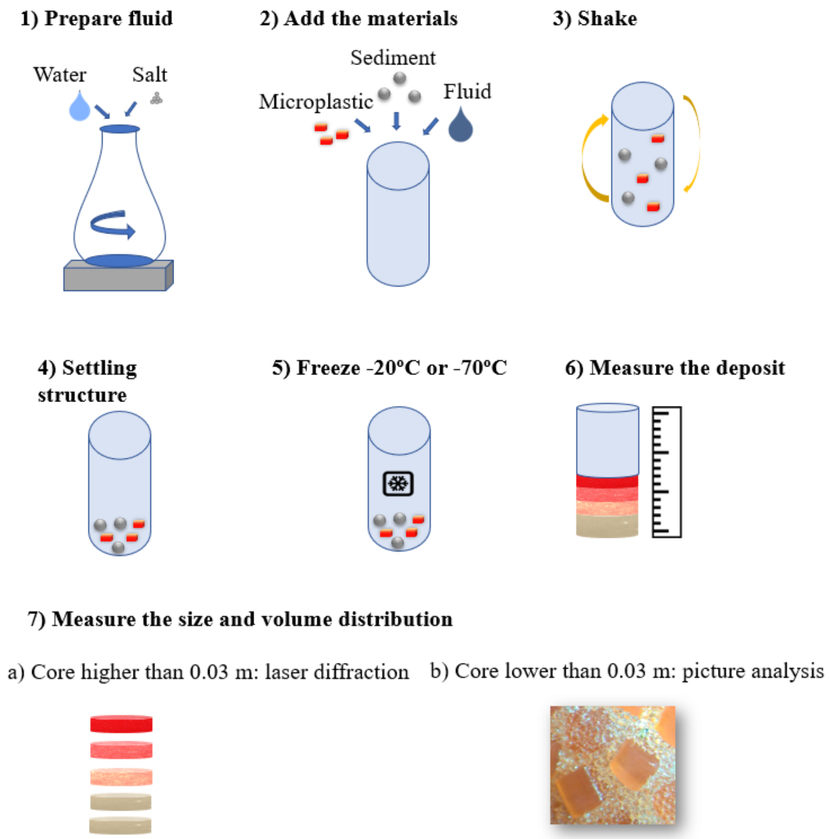

Figure 2-4. Diagram summarising the seven basic steps of this experiment. 1) Preparation of fluid. 2) Premeasured microplastic, sediment, and fluid samples were added to the settling tube. 3) Mix the materials until thoroughly mixed. 4) Leave the material inside the tube to settle for 24 hours. 5) Move the settling tube to the freezer-20 ºC (water) or -70ºC (saline solutions) for 24 hours. 6) Measure the height of the substrates identified in the frozen tube. 7) Measure the size and volume distribution.

The second step consisted of preparing the salinity solution for the required scenarios. For this, the defined mass of salt (Table 2.3) for 1 litre of filtered water was mixed in a beaker of 1.5 L capacity with a magnetic stirrer until all the salt particles were diluted. The fluid density was checked with an Anton Paar density meter (precision ± 0.1 kg/m^3). Three measurements were taken to ensure consistency of reading. If the fluid density was not as required, an extra small amount of salt or water was added until the desired fluid density was obtained. Subsequently, the fluid volume was added first to settling tube, and then the microplastic and sediment volumes, thus ensuring that the dry materials were completely submerged in the fluid volume (V_f). The fluid volume was measured with a glass cylinder scale of 250 ml with a precision of ±1x10^{-6} m^3.

Once all three materials were combined in the tube, the tube was shaken until the suspension was thoroughly mixed. For this, the tube was moved horizontally for 30 s with rotations of 90°every 5 s, vertically for 30 s with rotations of 180° every 5 s and finally rotated 60 times from side to side (vertically 180° clockwise and anticlockwise). All the movements were made sequentially, taking 1 minute and 30 seconds (Figure 2-5). After this mixing, the tube and its contents were left to settle for 24 hours and then moved to a freezer for a further 24 hours. A -20 °C freezer was used for the settling tubes with fresh water only, and a -70°C freezer for those containing saline solutions because its freezing point is lower than freshwater.

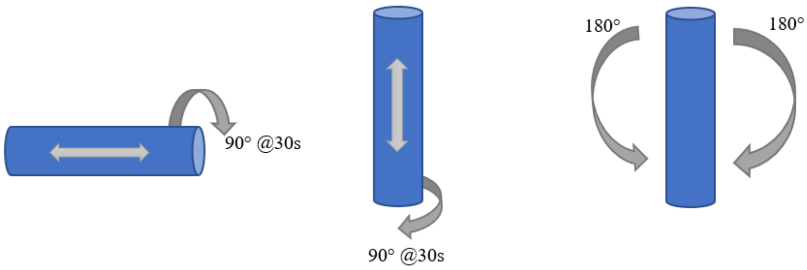

Figure 2-5. Three steps diagrams for the shaking process, the first movement is horizontal for 30 s with rotations 90°every 5 s, the second movement is vertical for 30 s with rotations 180° every 5 s, and the third movement is rotation 60 times side to side (verticals 180° clockwise- un clock). All the movements were made sequentially, taking 1 minute and 30 seconds.

The frozen tubes were carefully withdrawn from the tube and photographed. The depositional structures were identified by visual analysis, including the occurrence of layers within the deposit and each identified layer's height. The heights of the different layers were measured at four points around the tube's circumference (at 90° intervals) with a digital Vernier caliper with a ± $0.1x10^{-4}$ m precision. The averages of these measurements were used for the analysis of the results.

The settling core was then prepared for particle and volume distribution analysis. Two different methodologies were applied depending on the size of the core. A Malvern Mastersizer (a laser diffraction particle size analyser) was used for a core of height greater than 0.03 m. When core heights were smaller than 0.03 m, the sample size limited the use of the Malvern Mastersizer and a picture analysis method was employed. Further details of both these methods are described in points iii) and iv) of this section.

Finally, to help understand the regimes of the settling process in the experimental tubes, four settling tubes (MP_5S_{14}, MP_5S_{42}, MP_5S_5, MP_5S_9) were repeated in transparent bottles of 0.9 m diameter, 0.20 m height, and a capacity of $1x10^{-6}$ m^3. The same materials corresponding to the run ID as described in Table 2.2 were added to these bottles. The four settling tubes in transparent bottle were selected because they have the same microplastic fraction (0.05) yet represent the full spectrum of sediment concentrations (low, medium, and high;0.05, 0.10, 0.13, 0.40, respectively). To capture the settling processes operating in each of these runs in detail, the bottles were shaken and a video of the settling process was recorder from a 30 cm distances, with a camera with a 13 MP (wide) AF + 5 MP (ultrawide) lenses. The settling process in the four tubes was recorded for 1.5 minutes, adequate time to capture all the settling processes operating. From the video 22 frames were extracted every 5 -10 seconds (Appendix 1). A reference distance from the top of the suspended microplastic to the bottom of the bottle was measured. The measured distances were plotted versus frame time, and the suspension's settling velocity corresponds to the slope of the fitted curve.

2.4.1. Saline solutions preparations

i. Variable suspension density

To recreate fluid densities that simulated the effect of having positively and neutrally buoyant microplastic particles, given that the polymer used was a negatively buoyant plastic with respect to water (nylon pellets, ρ_{MP}=1150 kg/m^3), tests were run in the laboratory to define the amount of salt required to be added to freshwater to recreate the necessary buoyant stages. To assess whether fluid density was greater/equal to microplastic density the behaviour of microplastic particles within these fluids was assessed. To define a neutrally buoyant stage, it was expected that microplastic particles would remain in suspension within the water column. In the positively buoyant stage, all the microplastic would be expected to remain in suspension in the water surface.

To achieve this, a measured amount of salt was added to 100 ml of filtered water. The solution was mixed for 5 min until all the salt was dissolved. Around 10 g of microplastic was added to the fluid. The particle behaviour was observed to decide the solute density matching the mean particle density.

For the neutral condition, 6 solutions were tested, with amounts of salt between 19 g to 20 g, increasing with steps between 0.125 g to 0.250 g. It was observed that the neutral condition can be achieved by adding 19.5 g of salt in 100 ml of water. On average, an equal amount of particles sink, remain in suspension and stay neutrally in the salinity solution (Figure 2-6). The fluid density was measured with an Anton Paar density meter (precision 0.1 kg/m^3) and was found to be 1120 kg/m^3 (18.7°C). Figure 2-6 shows a picture of the 6 salinity solutions and the buoyant conditions of the microplastic particles.

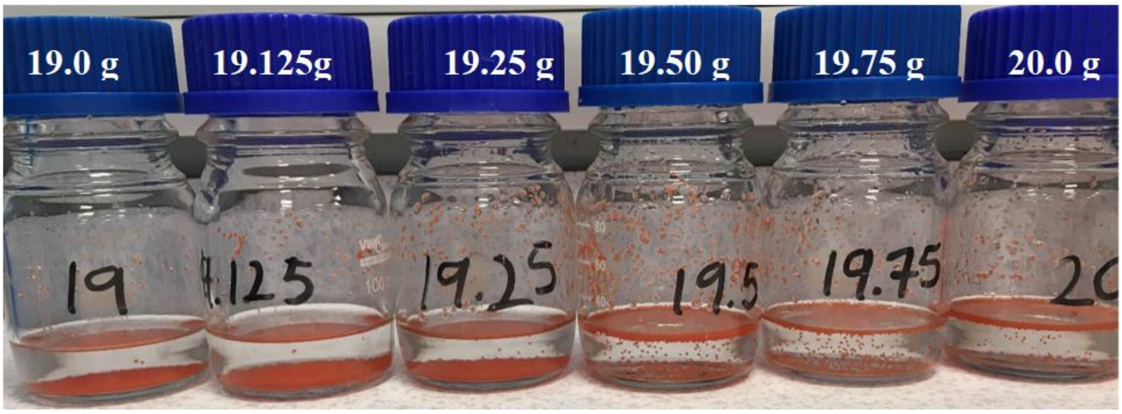

Figure 2-6. Saline solutions test to define the neutral buoyant microplastic particles condition. The numbers represent the amount of salt in grams added to 100 ml of water. The neutral condition selected is 19.5 g/100 ml water.

For the positively buoyant condition, the amount of salt selected was 34 g salt added to every 100 ml, with a resulting fluid density of 1196 kg/m^3 (18.7°C). In this scenario all the microplastic particles were observed to rise and remain on the surface of the solution.

ii. **Constant suspension density**

The constant suspension density set of experimental runs were designed to recreate a set of positively, negatively, and neutrally buoyant plastics within a target suspension density. Each tube has different volumes of microplastic, sediment, and salinity solution, always resulting in the exact value of the suspension density. The target suspension density was selected so that the fluid represented the microplastic buoyant stage (negatively positively and neutral). The constant suspension density set resulted in a range of 18 different fluid densities that are created by adding an amount of salt to recreate six settling tubes with negatively buoyant microplastic, six tubes with neutrally buoyant microplastic, and six tubes with positively buoyant microplastic.

The volumetric concentrations of microplastic used in these runs are 0.02 and 0.005 (m^3/m^3), with sediment volumes of 0.026, 0.030, and 0.033 (m^3/m^3). The following conditions were fulfilled when selecting these concentrations:

- Six settling tubes for each type of buoyancy (positively, negatively and neutrally) with different volumes of V_{MP} and V_S. The set of volumes for each buoyancy should have the same values between the positively, negatively and neutrally microplastic scenarios.
- The summation of the sediment and microplastic volumes should be lower than 5% ($V_{MP}+V_S<1\%$) to represent a lower suspended concentration.

Fluid density was estimated using the target suspension density and equations 2-7 described as:

$$\text{fluid density}: \ \rho_f = \frac{\rho_{sus} - \rho_s C\Phi_s - \rho_{MP}\Phi_{Mp}}{(1 - C_{Mp} - V_S)} \qquad (2\text{-}9)$$

Where ρ_{sus}, ρ_f, ρ_s and ρ_{Mp} are the suspension, fluid (salinity solution), sediment, and microplastic density in kg/m^3, respectively, and Φ_s and Φ_{MP} are the volumetric concentrations of the sediment and microplastic, respectively.

Based on the last requirement the following target suspension density was selected:

- Negatively buoyant microplastics, suspension density: 1052 kg/m^3.
- Neutrally buoyant microplastics, suspension density: 1152 kg/m^3
- Positively buoyant microplastics, suspension density: 1227 kg/m^3

The amount of salt required to obtain the fluid density was obtained from a typical table of mass of sodium chloride (NaCl) versus temperature (Ionut et al., 2015). The estimations are shown in Table 2.3, and were made with linear interpolations between the concentration of salt in $0.001m^3$ litre of water at 20°C. The value was used as the first approximation to create the saline solution. Therefore, it was necessary to add an extra small amount of salt or water until the desired fluid density was obtained due to the water temperature in the laboratory was not exactly 20°C. The desired fluid density and temperature were recorded measured with the Anton Paar density meter three times.

Table 2.3. Amount of salt needed per 1 litre of water for each experimental tube.

Name	**Density ρ_f (kg/m^3)**	**Mass salt 0.001 m^3 water (20 C) (kg)**
Scenario 1: Positively buoyant microplastic		
$+MP_5S_{25}$, $+MP_5S_{42}$, $+MP_5S_5$, $+MP_{13}S_7$, $+MP_{13}S_{16}$	1196	0.3400
Scenario 1: Neutral microplastic		
$\approx MP_5S_{24}$, $\approx MP_5S_{42}$, $\approx MP_5S_5$	1120	0.1950
Scenario 2: Negatively buoyant microplastics		
$MP_{2.0}S_{2.4}$	1012.5	0.0123
$MP_{2.0}S_{2.8}$	1006.8	0.0050
$MP_{2.0}S_{3.1}$	1002.6	0.0236
$MP_{0.5}S_{2.4}$	1014.6	0.0181
$MP_{0.5}S_{2.8}$	1009.1	0.0036
$MP_{0.5}S_{3.1}$	1004.9	0.0122
Scenario 2: Neutral microplastics		
$\approx MP_{2.0}S_{2.4}$	1117.3	0.1921
$\approx MP_{2.0}S_{2.8}$	1112.1	0.1826
$\approx MP_{2.0}S_{3.1}$	1108.2	0.1756
$\approx MP_{0.5}S_{2.4}$	1117.8	0.1925
$\approx MP_{0.5}S_{2.8}$	1112.7	0.1902
$\approx MP_{0.5}S_{3.1}$	1108.8	0.1846
Scenario 2: Positively buoyant microplastics		
$+MP_{2.0}S_{2.4}$	1195.9	0.3480
$+MP_{2.0}S_{2.8}$	1191.1	0.3376
$+MP_{2.0}S_{3.1}$	1187.4	0.3298
$+MP_{0.5}S_{2.4}$	1195.2	0.3464
$+MP_{0.5}S_{2.8}$	1190.4	0.3362
$+MP_{0.5}S_{3.1}$	1186.8	0.3285

iii. The saline solution control tube

A control tube was made to measure the salinity solutions' temperature and density fluctuations during the settling process. The control tube has the same salinity solution created for $+MP_{2.0}S_{3.1}$ ($\rho_f = 1187.8$ kg/m^3). The temperature and density inside the tubes were measured every 10-15 minutes for 2.5 hours. It is expected that the substrates were formed during this period. A second round of four measurements was made 20 hours later; one before the tube was moved to the -70 C freezer and the remaining three after the frozen process. The standard deviation of the fluid density variation during the control tube is estimated at ±0.26 kg/m3 (Table 2.4), demonstrating that density fluctuations are not negligible enough to change the plastic's buoyancy during the run of the experiment.

Table 2.4. Measurements data of the fluid density and temperature inside the control tube.

Day	**Time**	**Temperature (C)**	**Density (kg/m^3)**	**Comments**
27/04/2021	15:45	21.1	1187.8	Final measurement before the shaking
27/04/2021	16:12	21.3	1187.7	Initial measurement after the shaking
27/04/2021	16:29	21.3	1187.8	
27/04/2021	16:40	21.2	1187.9	
27/04/2021	16:50	21.2	1188.0	
27/04/2021	17:02	20.9	1188.0	
27/04/2021	17:24	20.8	1188.0	
27/04/2021	18:04	20.6	1188.3	
28/04/2021	13:23	20.2	1188.5	Before the frozen process
28/04/2021	14:05	-5.6	1200.1	After the frozen process
28/04/2021	14:35	-11.5	1204.3	
28/04/2021	15:15	-16.4	1217.0	The density equipment starts to fluctuate in the measurements. Ice is formed on the surface of the tube.

2.4.2. Particle size and volume distribution cores higher than 0.03 m

To study the detailed particle size and volume distribution within the frozen deposits for cores with a size larger than 0.03 m, approximately 0.01 m thick slices were cut with a Metkon Geoform machine using the "thin sectioning system". The cut deposit only includes the substrates that contain microplastic and sediment. The thickness of each slice was measured with a Vernier caliper to quantify losses arising from the machine blade. The slice was submerged for 2-3 seconds in water to remove all possible contamination on the surface due to the cutting process. The face of each clean slice was photographed and stored in a $1x10^{-4}$ m^3 glass jar and allowed to thaw. The grain size distribution of the mixtures was measured using laser diffraction machine used by Malvern, Mastersizer 2000, which is used to quantify the microplastic and sediment volumes within each slice (deposit layer).

The Malvern Mastersizer machine measured individual particles' volume and size distribution using an optical laser. The particle size distribution reported by the instrument is estimated depending on the particle's geometry, using a summation of the contributions of the different derived diameters. The final diameter reported is an imaginary sphere equivalent to this estimated volume, Equation 2-10. (Malvern Instruments Limited, 2013).

$$D_{equi} = \sqrt[3]{\frac{6V}{\pi}} \tag{2-10}$$

Where D_{equi} is the equivalent particle diameter, and V is the volume of the particle.

The settings of the Malvern Mastersizer machine used in the analysis were: 2500 revolutions per minute for the pump speed, refraction of 1.55, obscuration average between 10-20%, and adsorption of 0.01. Refraction defines the speed of the light within the material. The absorption value is the amount of light absorbed by the particles. The goal of the speed pump is that the particles do not sink. The obscuration is used to control the optimum quantity that should be added to the machine, the manual recommends 10-20% for wet samples. For more details on these parameters, see Table 2.5.

Table 2.5. Settings of the Malvern Mastersizer machine selected for the particle size and volume analysis. The definition provided for each index is presented as it appears in the user's manual (Malvern Instruments Limited, 2013).

Index	**Meaning**	**Value for this research**
Refraction	Value of between 0 and 5. The value relates to the speed of light within the material, which in turn allows the degree of refraction (light bending) to be predicted when light passes from one medium to another.	1.55
Absorption	A value between 0 and 10. The value measures the quantity of light absorbed by the particles. Generally, transparent samples will have a low or zero absorption, while coloured or black samples will have a higher value.	0.01
Pump speed	The value ensures the sample does not sink to the bottom.	2500
Obscuration	The optimal obscuration settings for measurement are both sample and dispersion unit dependent. As a rough guide, use a range of 10-20% for a wet dispersion unit and 1-10% for a dry dispersion unit.	All were wet samples; the obscuration was always in a range between 10% to 20%.

To corroborate that the settings for a transparent material (absorption=0.01) are not influenced by the plastic colour (orange), a different measurement of the pure microplastic was made using two different absorption settings: 1 and 6. The average of the repetitions measurements is

D_{50}=698.0 ±1.6 µm for refraction 1.55 and absorption 1 and D_{50}=698.36 ±1.48 µm for refraction 1.55 and absorption 6. A third measurement was made with a refraction value of 3 and absorption of 0.01, ending in a similar average D_{50}=700.8±1.4 µm. The results of these three sets are shown in Table 2.6, from which it is concluded that the absorption and refraction value selected does not affect the microplastic measurements.

Table 2.6. Results of the refraction and absorption test.

Test	Diameter (D_{50})		
	Refraction 1.55 Absorption 1	**Refraction 1.55 Absorption 6**	**Refraction 3 Absorption 0.01**
Measurement 1 (µm)	696.31	697.06	699.44
Measurement 2 (µm)	698.13	699.97	700.82
Measurement 3 (µm)	699.57	698.04	702.07
Average (µm)	**698.00**	**698.36**	**700.77**
Standard Deviation (µm)	**1.64**	**1.48**	**1.32**

When the settings were finalised, each sample was prepared to be added to the machine. The materials were mixed with a spoon to guarantee a homogeneous mixture of the microplastic and sediment particles. Typically, when running samples through a Mastersizer, it is often necessary to add water to hydrate the sample. However, this step was unnecessary here as the sample had enough water from the thawing process. The sample was added to the machine, and measurements were repeated from the same sample three times. A quick plot from the measured volume versus the size distribution was done using the tools inside the software as a quality control step to verify if one of the measurements differed from the others. The sample was measured again if a significant difference (1%-2%) between the three measured curves was detected. The significant differences were detected in 8% of the samples. The three measurements of the sample were used to estimate the equivalent diameters.

i. Equivalent diameter

The percentiles 10 % (D_{10}), 50% (D_{50}) and 90% (D_{90}) were selected as the equivalent diameters that represent the size of the deposit distribution. For the characteristic diameters estimation, the volume percentages were extracted from the Malvern Mastersizer software specifying size classes (bins) every 10 micrometres, starting from 0.001 µm and ending in 2000 µm, for a total of 200 bins. The value of 0.001 µm is the minimum that the software settings allow.

The raw probability distribution was extracted and post-processed to estimate the characteristic diameters of each material. Post-processing was done to estimate the separate diameters of the microplastic and sediment in the mixture samples, values that the Malvern Mastersizer did not give directly. A permanent division between the materials was defined between 330 µm to 380 µm to facilitate the estimations (Figure 2-7). Although both materials share this range, the shared volume of each material in this range was below 0.570% suggesting a limited impact on the overall volumes defined by using this separator value. Sediment was defined as the material between 0.001 µm to 350 µm and microplastic from 350 µm to 2000 µm (based on the input grainsizes defined in Table 2-1). Any sediment volumes above 350 µm were reclassed as zero, and any microplastic volumes below 350 µm were reclassed as zero. For the mixture samples, all material below 350 µm was treated as sediment and all material above 350 µm as microplastic. Appendix 2 includes a table with the detail of this estimation.

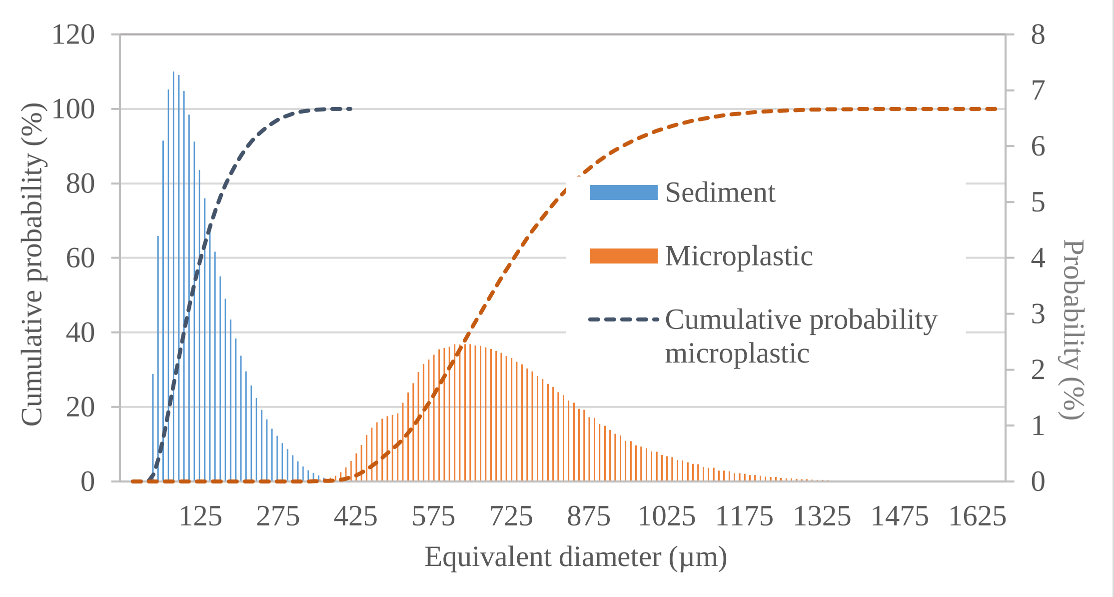

Figure 2-7. Cumulative probability distribution of the pure sediment and microplastic samples used in the experiments.

To separates the sediment and microplastic fractions based on the permanent division value, the characteristic grain sizes were directly compared to Malvern Mastersizer output average characteristic diameters (D_{10}, D_{50}, D_{90}). The percentiles between the bins were made using linear interpolation and Matlab^{TM}'s piecewise cubic Hermite interpolating polynomial 'Pchip'. Figure 2-8 compares the estimated values and those output by the Malvern Mastersizer. The estimated values show excellent correlation, with $R^2 = 0.999$ with differences of 6.3µm between the post-processed and the Malvern Mastersizer. After the validation, it was decided to use the results of the Pchip interpolation since it shows smaller differences between the estimated values and Malvern Mastersizer (6.3036 <6.3438).

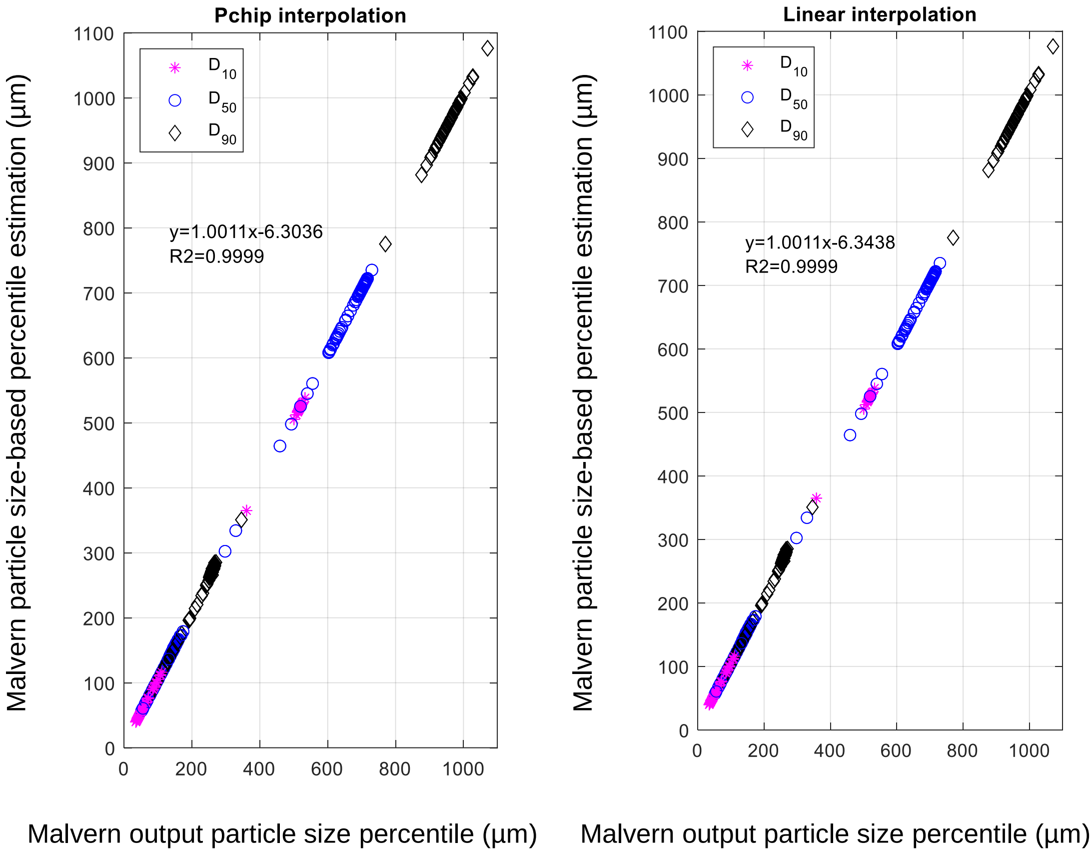

Figure 2-8. Comparison of size distribution estimated and the direct outputs of the Malvern Mastersizer particle size percentiles with two interpolation methods: linear and p-chip.

The process described above was programmed in the software Matlab™ R2020a, the programmed code was developed with the supervisors and is included in Appendix 3. The programmed code uses the raw Malvern Mastersizer results as inputs. The main matrix includes the measurement volumes of the three repetitions of each substrate slice, an identifier for the experimental tube, and the total volume of microplastics. The code separates the sediment and microplastic fractions based on the permanent division value defined above. The code estimates the characteristic diameters resulting from the interpolation function (Pchip) with the cumulative volumes and creates separated plots of each experimental tube's total, sediment, and microplastic size and volume distributions (Figure 3-4, Figure 3-5, Figure 3-6, Figure 4-4, Figure 4-6).

From the Malvern Mastersizer and post-processed analysis of the pure samples, a D_{10}=73±0.05 µm, D_{50}=105±0.2µm, D_{90}=211±0.5µm was obtained for the sediment, and D_{10}=507±1.4 µm, D_{50}=686±2.4µm and D_{90} = 940±4.4µm for the microplastic. However, it is noted that the supplier defined the size of the microplastic particles as 500 µm (Table 2-1). The discrepancy between the Malvern Mastersizer data and the vendor data required further analysis to determine the most accurate or appropriate methodology to estimate the equivalent diameter (Tinke et al., 2008; Sijs et al., 2021). Microscope images showed that the microplastic particles had an irregular cubic/cylinder shape with four rectangular sides and two rounded sides (Figure 2-9). Microplastic researchers describe this geometry as 'pellets', defined as spherical or cylinder pieces of plastic (Hartmann et al., 2019; The Royal Society, 2019). Subsequently, three further methodologies were tested to evaluate the suitability of the equivalent diameters produced by the Malvern Mastersizer: microscopy, sieves, and image analysis. The methods and results of these particle size tests are included in this section to justify the final methodology selected for processing the results.

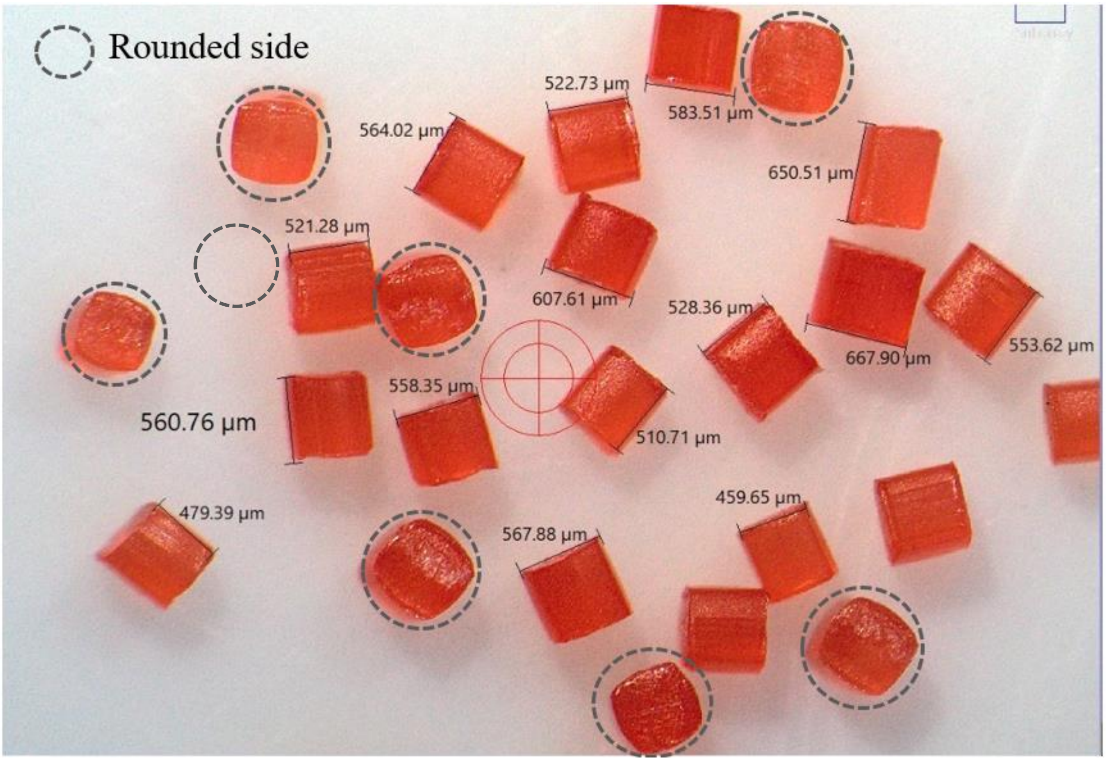

Figure 2-9. Microplastic particles geometry seen in the microscope showing the cubes irregularities forms, 4 sides are rectangular, and 2 two sides are rounded (dash grey circles)

The volume of 22 individual microplastic particles was estimated using a microscope by multiplying the area of the rounded side (A_{Mp}) and the height of the rectangular side (h_{Mp}). The equivalent diameter (D_{equi}) was estimated using equations 2-10, and the microscope derived volume was thus estimated. From these measurements, it is estimated that the microplastic rounded side has an average area of 258605 ±26762 μm^2, the rectangular side has an average height of 513.17±41µm, and the average equivalent diameter is 631 µm ±26µm. The second step for this test was to measure the biggest particles (<650 µm) in a sample of around 550 particles. Nine particles were detected to have heights between 650 µm to 1267 µm, representing 2% of the sample, with an estimated equivalent diameter of D=886 µm. From this, it is apparent that the average microscope diameter (631±26µm) is coherent with the Malvern Mastersizer D_{50}=686µm ±2.4µm. However, it is noted that these measurements inferred that the D_{90} of the Malvern Mastersizer seems to be overestimated and as such does not robustly represent the higher percentile of 90%.

A second analysis was undertaken using a conventional set of five mesh sieves (710 µm, 600 µm, 500 µm, 400 µm, and 300 µm) with a microplastic sample of 100 g. Higher and lower mesh sizes were not used because all the particles cross the 710 µm sieve, whilst the smallest particles never cross the 300 µm. The sieving was repeated two times, obtaining the following results: 25% have a sieve size of 600-710 µm, 74 % of 500-600 µm, and 1% of 400-600µm. The diameters were transformed into a perfect sphere to compare the results with the Malvern Mastersizer. With an estimation of the D_{10}=635 µm, D_{50}= 702 µm, and D_{90}= 825 µm. The D_{50} sieve diameter has consistent results with the Malvern Mastersizer, they differ by 2%, the D_{10} differs by 25%, and the D_{90} by 12%.

Finally, analysis was conducted using particle image size analysis. Here, a picture of around 300 particles was taken with a camera, a light, and a millimetric ruler for the reference scale. With the help of a Matlab™ R2020a code (Fernandez, 2021), the image was converted into black and white colours to estimate the projected area captured in the pictured. The average particle side was estimated as the square cubic area. It is noted that if two particles were located near each other, the current methodology measured them as one larger particle. Diameters up to 1.4 µm were reported, showing a possible reason behind the resulting overestimation of the D_{90} value. The equivalent diameters derived from the image analysis were translated to a perfect sphere to compare the results with the Malvern Mastersizer. The estimated equivalent spheres are D_{10}=546 µm, D_{50}= 669µm, and D_{90}= 930 µm, with differences of 1%-8% between the Malvern Mastersizer. To remove the effect of particles coalescing in the image, a second sample of 50 particle well spaced was measured with the imaging methodology, to avoids the creation of false larger particles. The estimated characteristics diameter D_{10}=572 µm, D_{50}= 666µm, and D_{90}= 724 µm, with differences of 3%-23% between the Malvern Mastersizer. Appendix 4 detail the outputs of this picture analysis.

Figure 2-10 shows a diagram describing how the four methods (sieves, two image analyses, and Malvern Mastersizer) measured the equivalent diameter, resulting in four cumulative curves highlighting the differences between each approach. From the microscope analysis, the sieves, and the image estimation, it was clear that the Malvern Mastersizer is generating results in the D_{90}, that do not truly represent the sample. Subsequently, it was decided that the equivalent diameter representing the microplastic is the D_{50} of the Malvern Mastersizer. An accurate representation of the real mass of the particle geometry, consistent with the microscopy and image analysis methods.

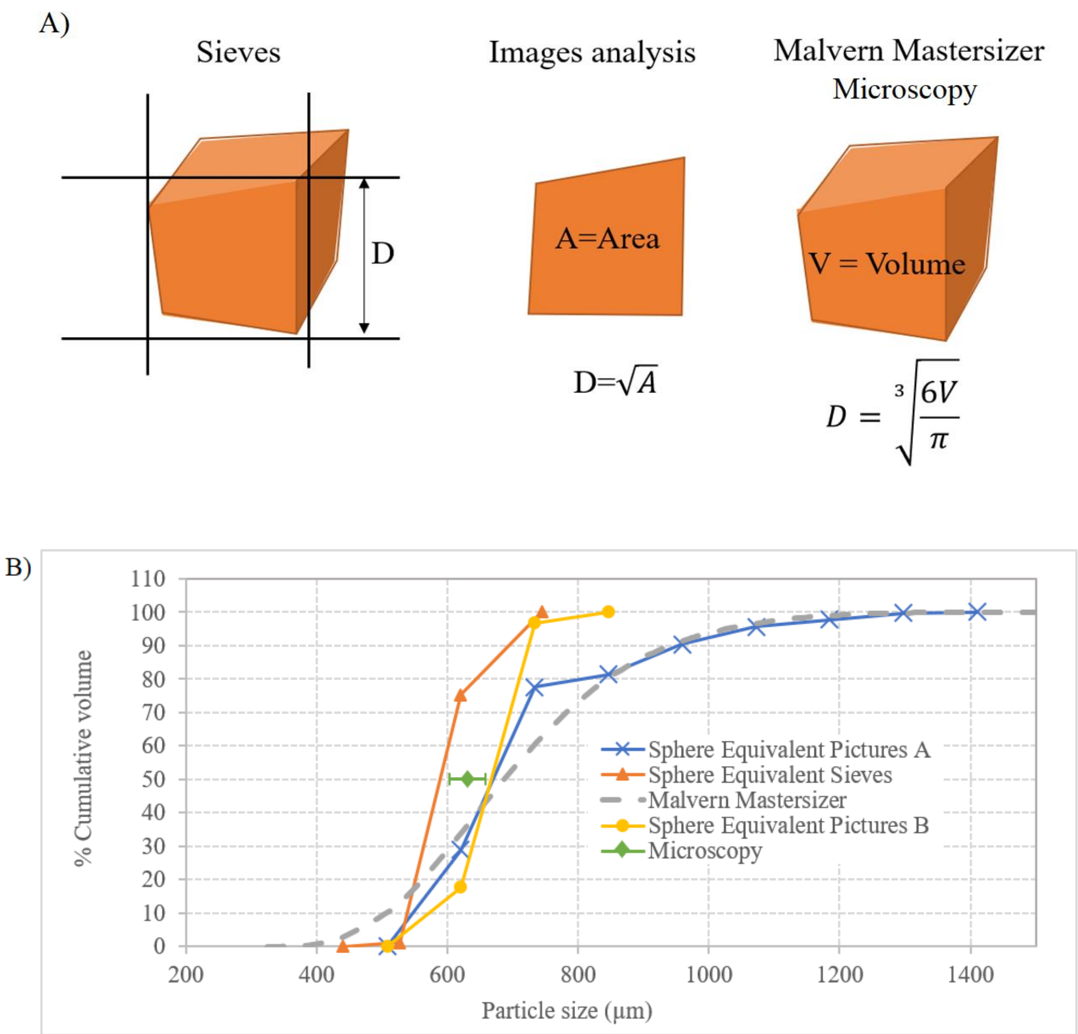

Figure 2-10. A) Diagram to reference the measurement equivalent diameter using four different methodologies: sieves, image analysis, microscopy, and Malvern Mastersizer. B) Comparison of sieves, images analysis, microscopy, and Malvern Mastersizer techniques to obtain the grain size distribution of the microplastic particles used in the experiments.

It is noted here that in three substrate slices with low microplastic content, the Malvern Mastersizer machine could not recognise the microplastic volume and size. In this case, a separate analysis was done to determine the volume and size distribution. The sample was submerged twice in 1 litre of water to dilute all the salt of the salinity solution and mixed for 2 minutes. The cleaned materials were moved to dry in an oven for 24 hours at 60º C. The microplastic was separated from the sediment using a 420 µm sieve and weighted in a precision scale, Ohaus adventurer analytical balance (±0.1mg). The estimation of the microplastic volume was made with the dry weights of the sample. The microplastic size distribution was measured using image analysis (see above for details of the methodology). The particles were separated from each other, and a picture was taken with a scale. The results of the image analysis were combined with the sediment particle size distribution obtained from the Malvern Mastersizer to create the stratigraphy plots.

ii. Volume errors laser diffraction methods

To measure the difference between mixed samples of microplastic and sediment in the Malvern Mastersizer, four samples with defined volumes were prepared in the laboratory (Table 2.7). The volume estimation was based on Equation 2-10, with the average density given by the supplier. The samples cover 90% of the volume ranges used in these experiments. Dry materials were wetted and mixed with a spoon to guarantee a homogeneous mixture of the microplastic and sediment particles, and the sample was repeated three times. The volume estimation was based on the division of 350 µm between microplastic and sediment, already explained above. A linear equation was used to correct volume measurements by the Malvern Mastersizer, with errors estimated at 4%-13% (Figure 2-11).

Table 2.7. Volumes measured in the laboratory and by the Malvern Mastersizer in four samples

Name of the samples	**Volumes measured in the laboratory**		**Volumes measured in the Malvern Mastersizer**	
	Volume Sediment Vs (cm^3)	**Volume Microplastic V_{MP} (cm^3)**	**Volume Sediment (cm^3)**	**Volume Microplastic (cm^3)**
Sample 1,	80.55±0.63	19.13	77.21±0.10	22.79±0.10
Sample 2,	57.99±0.97	41.51	50.85±0.77	49.15±0.77
Sample 3,	31.52±0.86	68.04	19.25±0.26	80.74±0.26
Sample 4,	13.31±0.46	86.41	11.1±1.01	88.90±1.01

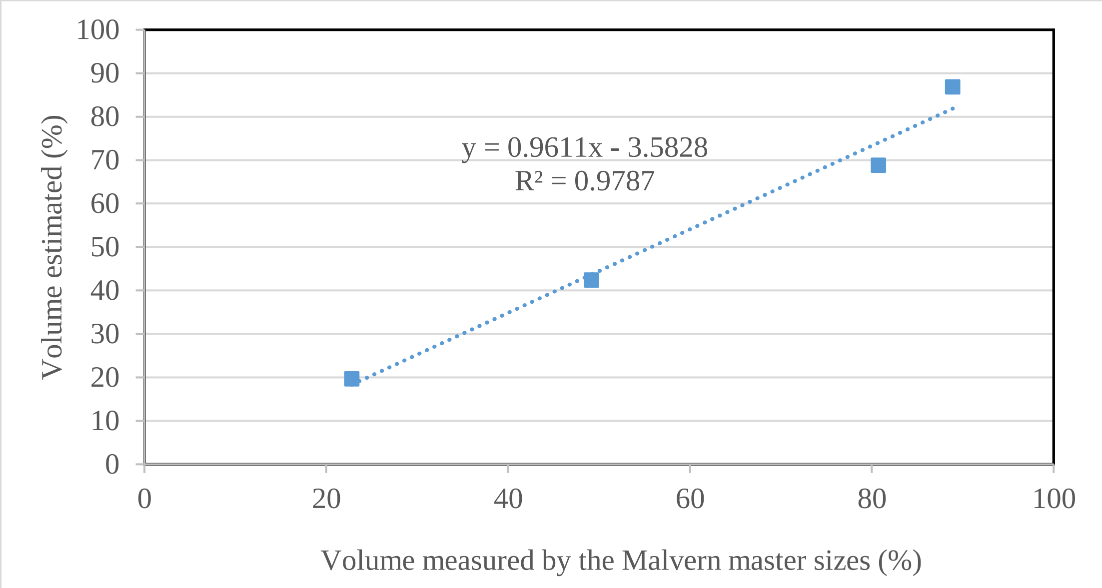

Figure 2-11. Volumes measured of the control weighted samples versus the Malvern Mastersizer.

Seven slices from the experimental tubes $M_{10}S_9$ and MP_7S_{12} were repeated three times to evaluate the differences between a measurement of the same slice in the Malvern Mastersizer. The sample was measured three times during each repetition, with nine data points for each sample. Figure 2-12 shows the results of the D_{50} size distribution variations of the microplastics, mixtures, and sediments. The main variations are identified in the samples that contain microplastic: ±10 μm for pure microplastic and ±7.4 μm for mixtures. The sediment differences are ±2.2 μm. The size distribution estimation is based on diameter characteristics given by the Malvern Mastersizer. The small differences between the repeated samples (less than ±10 μm) corroborate that the materials are well mixed before the measurement.

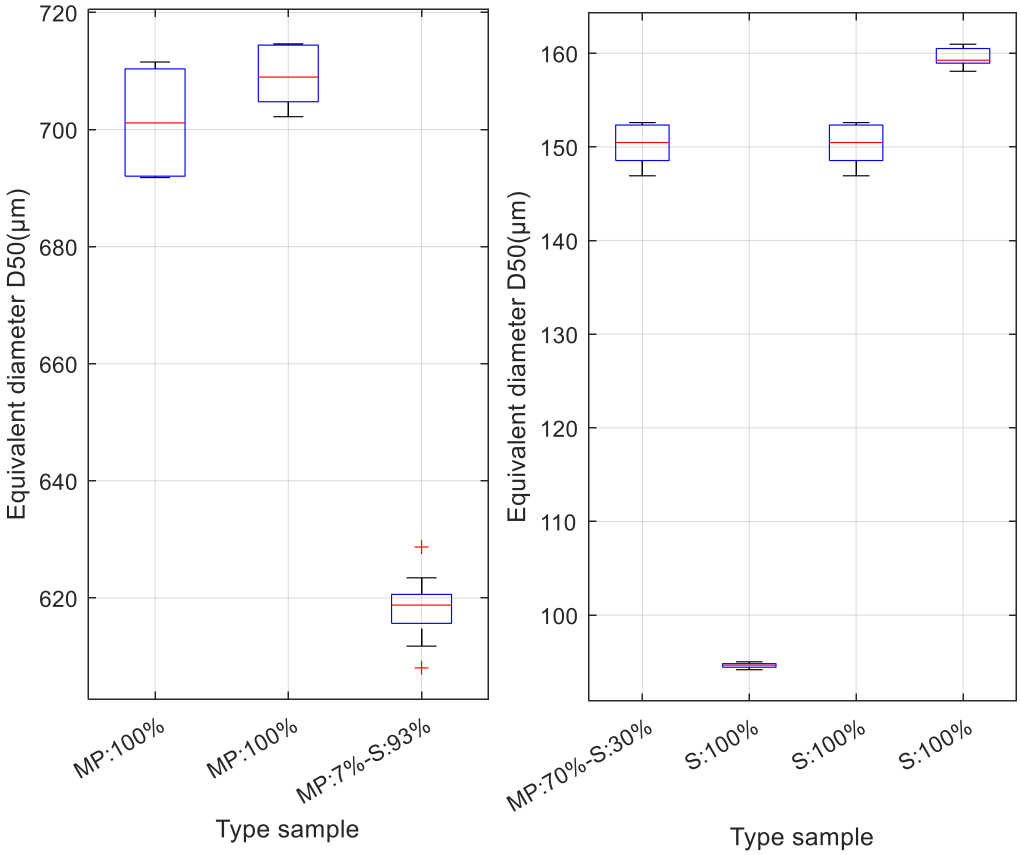

Figure 2-12. Experimental errors in the repetition of three samples of the seven slices. Results are shown based on the diameters characteristics of the Malvern Mastersizer outputs. The variations are summarised in ±10µm for the pure microplastic, ±7.4 µm for the mixtures, and ±2.2 µm for sediment.

2.4.3. Volume distribution in cores lower than 0.03 m

The settling tubes with a core height of less than 3 cm were too small to cut into two or more slices, limiting the use of the laser diffraction methodology. Instead, the volume and size distributions were made using image analysis of the frozen core. For this, the frozen cores were cut with a Metkon Geoform machine along the vertical axis. The inside area of the semi-circular cores was submerged in water for 1-2 seconds to clean all possible contamination and they were then photographed under a microscope (Olympus SZX10, DFPLAPO1X-4). Three photographs of the core in different areas were taken to identify the substrate types, volumes distribution, and heights.

The substrates types (sediment, microplastic, or mixtures) and heights for each settling tube were identified using one of the photographs of the core. The classification of the substrates was carried out by observing the type of materials in the microscope image. The heights of substrates were measured based on the picture scale. An image analysis code was developed to identify the number of microplastics present in the mixed substrates, using three different pictures of each settling tube. The volume distribution was estimated by the relation of the total surface area of the microplastic or sediment divided by the total area of the sample.

i. Volume errors of the image analysis

A calibration curve was made to estimate the differences between the real volume and the image analysis. Thirteen premeasured mixtures of microplastic and sediment were prepared in the laboratory, with the following microplastic volumetric concentrations: 0.7%, 3.5%, 8.0%, 17.9%, 22.5%, 30.3%, 33.6%, 36.7%, 42.0%, 46.0%, 50.3%, and 59.4*%* (Table 2.8). The prepared mixtures were photographed in the microscope in three different areas to obtain an average value using the image code. Three calibration curves were defined as the trendline between the real volume and the average image analysis (Figure 2-13). The first calibration curve is estimated for microplastic volume values of 30.3%, the second for volumes between 8.0% to 30.3% and the last for less than 8.0%.

Once the distribution of the average volume was processed, the calibration curve was used to correct the results of the image analysis code. The image analysis code, calibration curve pictures analysis, substrates identification, and microplastic volumes are included in Appendix 5.

Table 2.8. Calibration curve microplastic volumes.

Sample number	**Volumetric concentration of microplastic**	
	Real	**Image analysis**
1	0.72% ±0.03	2.56%±0.45
2	3.50% ±0.14	3.42%±0.49
3	8.00%±0.30	5.10%±0.59
4	12.7% ±0.44	8.66%±1.39
5	17.9%±0.59	13.6%±0.67
6	22.5%± 0.70	15.3%±1.05
7	30.3% ±0.86	19.1%±0.06
8	33.6% ±0.91	25.8%±0.22
9	36.7% ±0.94	28.5%±1.03
10	42% ±0.99	32.5%±0.96
11	46.5%±1.01	36.8%±2.00
12	50.3% ±1.02	42.4%±0.98
13	59.2% ±0.99	50.7%±0.30

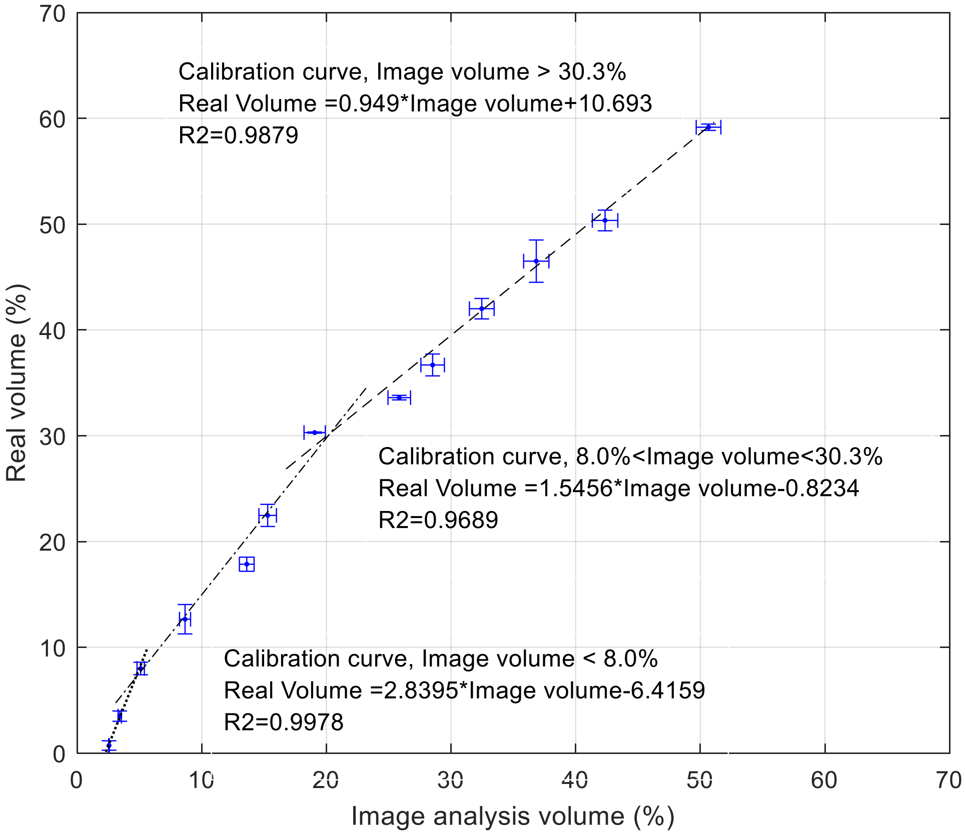

Figure 2-13. Calibration curve between the microplastic real volume and the measured in the image analysis.

Chapter 3 . Experimental settling process of microplastic and sediment mixtures: baseline and negatively buoyant results

The following chapter includes the results, discussion, and conclusions of the experimental work described in Chapter 2 for the seven baselines (Scenario A, *Figure 2-2*) and 19 negatively buoyant microplastic settling tubes (Scenario B-1, *Figure 2-2*) variable suspension density. At is was described in Chapter 2, the experimental settling tubes consisted in adding different volumes of negatively buoyant microplastic, sediment and water. To study the depositional patterns of a mixture of microplastic and sediment particles in the river beds in low and high concentrations. The chapter starts with a brief introduction to the main objective of the research, the methodology, and the initial volumetric contents of the experiments. The results describe the heights, final volumetric content, and particle size distribution of the substrates formed after the settling process. An analysis of particles' fall velocity is included to help understand the formation of the substrates. Following the results and the particle interaction theories, the settling tubes are classified in low and high concentrations; and the outcomes are related to the samples of microplastics in the riverbed. Concluding that the negatively buoyant microplastics and sediment substrates formation in calm waters depends on the plastic-sediment properties (density, size, geometry) and the number of particles in the suspension.

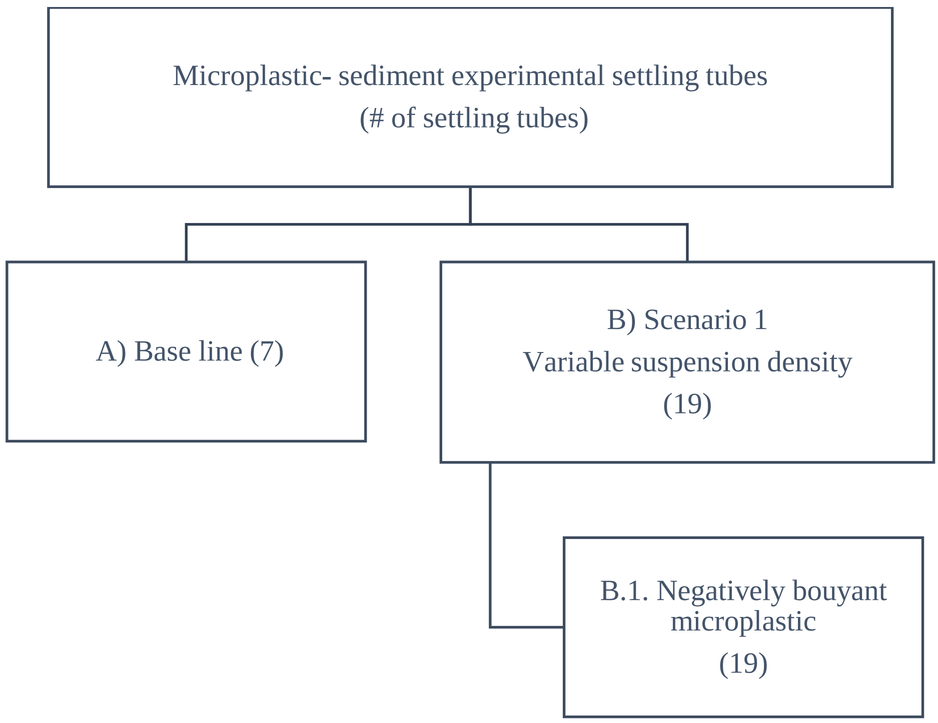

Figure 3-1. Set of experimental settling tubes included in this chapter thesis.

3.1. Introduction

Plastic pollution measurements in rivers have shown that a significant volume of primary (industry production) and secondary (fragmentation) microplastics (Hartmann et al., 2019) are formed from high-density plastic, such as Polyethylene Terephthalate (PET), Nylon (PA), and Polyvinyl Chloride (PVC). The negatively buoyant plastic particles have been found deposited and stored in riverbeds and banks (Hurley et al., 2018; Dikareva and Simon, 2019; Fan et al., 2019; Jiang et al., 2019; Chouchene et al., 2021; Lin et al., 2021; Saarni et al., 2021). In the marine environment, these high-density plastics pollute coastlines and are found deposited in the deep sea (Erni-Cassola et al., 2019), resulting in harmful effects on animals (Wright et al., 2013, Rochman et al., 2016). The vertical distribution of microplastic particles in sedimentary deposits shows that in general the amount of plastic decreases with depth of the deposit, without specific patterns of deposition related to the polymer's density. Researchers found in the sediment samples different plastics types in similar percentages throughout the deposit without any physical explanation (Mao et al., 2021; Zhou et al., 2021).

Therefore, to investigate this phenomenon, a set of experimental settling tube experiments has been designed with different concentrations of sediment and plastic to study the influences of the interactions between particles in a suspension. Studies have found that the particles interactions in a suspension are responsible for observed sediment stratigraphy depositional patterns (Kynch, 1952; Richardson and Zaki, 1954; Phillips and Smith, 1971; Pane and Schiffman, 1985; Druit, 1995; Abu-Hejleh et al., 1996; Guo et al., 2015; Amy et al., 2006, Mehta and Mcanally, 2008, Dorrell et al., 2013).

In these experiments varying volumes of three materials (microplastic, sediment, and water) are added to each settling tube. Once all three materials were incorporated, the tube was shaken until the suspension was thoroughly mixed. The tube was left to settle for 24 hours and then carefully moved to a freezer at -20 °C for 24 hours. The frozen tubes were carefully withdrawn, and the depositional structure was analysed to study the detailed particle size and volume distribution within the frozen deposits.

Table 3-1 shows the ID, volumetric concentrations, and suspension density of the experimental tubes included in this chapter. Figure 2-3, shows a diagram of the volumetric concentrations of the experimental work.

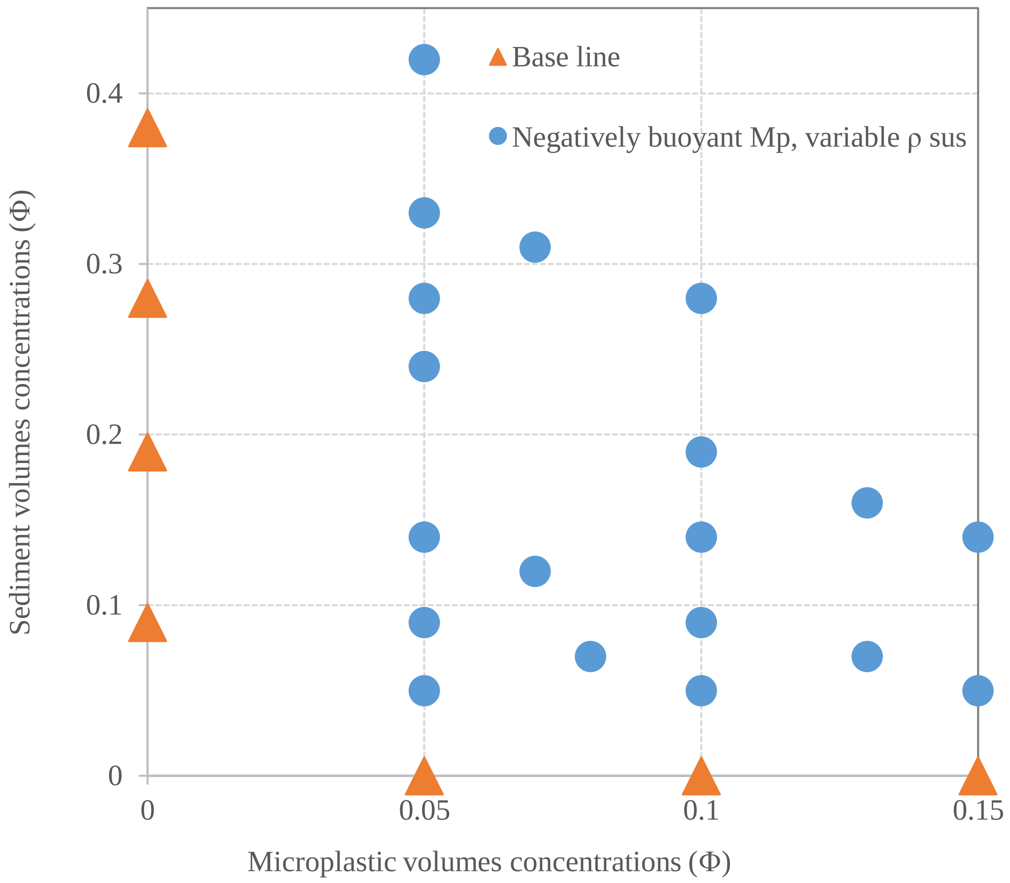

Figure 3-2. Volumetric concentrations of microplastic and sediment added in each settling tube. Blue circles are the nineteen settling tubes of negatively buoyant microplastic variable suspension density, and orange triangles correspond to the baseline settling tubes.

Table 3.1. Name, volumetric concentrations of microplastic, sediment and fluid added to each experimental tube, order in the function of the suspension density.

#	Name	Volumetric concentration (-)			Suspension density (kg/m^3)
		Microplastic	Sediment	Fluid	
1	MP_5S_0	0.05	0	0.95	1006 (baseline)
2	$MP_{10}S_0$	0.1	0	0.9	1013 (baseline)
3	$MP_{15}S_0$	0.15	0	0.85	1021 (baseline)
4	MP_5S_5	0.05	0.05	0.9	1076
5	$MP_{10}S_5$	0.1	0.05	0.85	1084
6	$MP_{15}S_5$	0.15	0.05	0.8	1092
7	MP_8S_7	0.08	0.07	0.85	1116
8	$MP_{13}S_7$	0.13	0.07	0.8	1117
9	MP_0S_9	0	0.09	0.91	1140 (baseline)
10	MP_5S_9	0.05	0.09	0.86	1148
11	$M_{10}S_9$	0.1	0.09	0.8	1155
12	MP_7S_{12}	0.07	0.12	0.81	1194
13	MP_5S_{14}	0.05	0.14	0.81	1219
14	$MP_{10}S_{14}$	0.1	0.14	0.76	1227
15	$MP_{15}S_{14}$	0.15	0.14	0.71	1235
16	$MP_{13}S_{16}$	0.13	0.16	0.71	1260
17	MP_0S_{19}	0	0.19	0.81	1284 (baseline)
18	$MP_{10}S_{19}$	0.1	0.19	0.71	1299
19	MP_5S_{24}	0.05	0.24	0.71	1364
20	MP_0S_{29}	0	0.29	0.71	1429 (baseline)
21	MP_5S_{29}	0.05	0.29	0.66	1437
22	$MP_{10}S_{29}$	0.1	0.29	0.61	1445
23	MP_7S_{32}	0.07	0.32	0.61	1484
24	MP_5S_{34}	0.05	0.34	0.61	1511
25	MP_0S_{39}	0	0.39	0.61	1577 (baseline)
26	MP_5S_{43}	0.05	0.43	0.51	1659

3.2. Results

Figure 3-3 depicts the 26 frozen settling tubes and the resultant substrates, in which the orange layer represents deposits of microplastics, and the white layer represents sediment. The thickness of each individual substrate layer within each tube varies as a function of the input amounts of microplastic and sedimentsTable 3.2 shows the microplastic and sediment bottom deposit's total height and the suspension density's estimated value (Equation 2.3).

The results detailing the deposits stratigraphy and volumes are described in sections 3.2.1 to 3.2.3. The stratigraphy and volumes results are based on the analysis of 155 slices coming from the microplastic and sediment deposit's, in which 38 were made up of only microplastic, 82 of only sediments, and 35 of microplastic-sediment (Appendix 6 shows pictures of the slices). Section 3.2.4. includes calculations of microplastic and sediment particle's fall velocity in experiment sets where particles behave as individual particles and where hindered effects are likely. Finally, a comparison of these results with the research of Amy (2006) is included in section 3.2.5.

Table 3.2. Total height of the deposits and suspension density.

Tube name	Total substrate height (x10^{-3} m)	Suspension density (kg/m^3)
MP_5S_0	24	1006 (baseline)
$MP_{10}S_0$	44	1013 (baseline)
$MP_{15}S_0$	66	1021 (baseline)
MP_5S_5	36	1076
$MP_{10}S_5$	53	1084
$MP_{15}S_5$	82	1092
MP_8S_7	57	1116
$MP_{13}S_7$	74	1117
MP_0S_9	47	1140 (baseline)
MP_5S_9	59	1148
$M_{10}S_9$	95	1155
MP_7S_{12}	76	1194
MP_5S_{14}	73	1219
$MP_{10}S_{14}$	97	1227
$MP_{15}S_{14}$	120	1235
$MP_{13}S_{16}$	119	1260
MP_0S_{19}	94	1284 (baseline)
$MP_{10}S_{19}$	118	1299
MP_5S_{24}	113	1364
MP_0S_{29}	109	1429 (baseline)
MP_5S_{29}	129	1437
$MP_{10}S_{29}$	150	1445
MP_7S_{32}	147	1484
MP_5S_{34}	143	1511
MP_0S_{39}	145	1577 (baseline)
MP_5S_{44}	175	1659

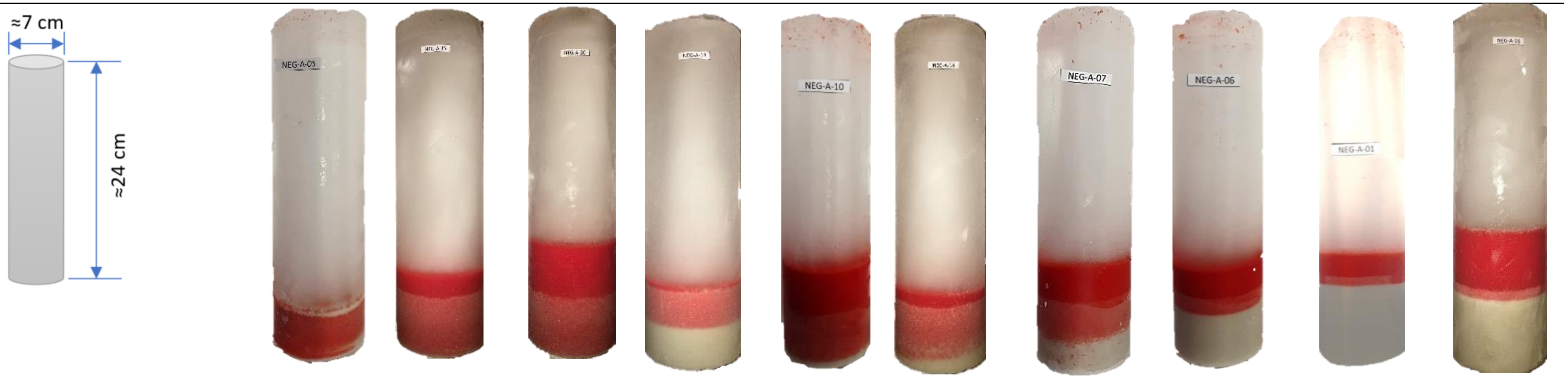

Name	**MP_5S_5**	**$MP_{10}S_5$**	**$MP_{15}S_5$**	**MP_8S_7**	**$MP_{13}S_7$**	**MP_5S_9**	**$MP_{10}S_9$**	**MP_7S_{12}**	**MP_5S_{14}**	**$MP_{10}S_{14}$**
Suspension density (kg/m^3)	**1075**	**1084**	**1092**	**1116**	**1117**	**1148**	**1155**	**1194**	**1219**	**1227**

Name	**$MP_{15}S_{14}$**	**$MP_{13}S_{16}$**	**$MP_{10}S_{19}$**	**MP_5S_{24}**	**MP_5S_{29}**	**$MP_{10}S_{29}$**	**MP_7S_{32}**	**MP_5S_{34}**	**MP_5S_{43}**
Suspension density (kg/m^3)	**1235**	**1260**	**1299**	**1364**	**1437**	**1445**	**1484**	**1511**	**1659**

***Figure continue in the next page**

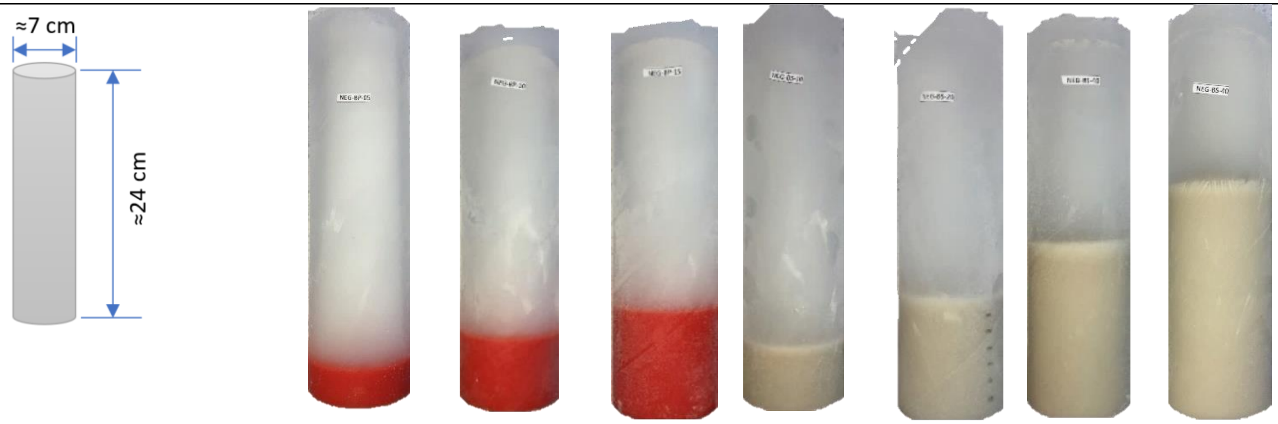

NAME	$MP_{5}\,S_{0}$	$MP_{10}\,S_{0}$	$MP_{15}\,S_{0}$	$MP_{0}\,S_{9}$	$MP_{0}\,S_{19}$	$MP_{0}\,S_{29}$	$MP_{0}\,S_{39}$
Suspension density (kg/m^3)	**1006**	**1013**	**1021**	**1140**	**1284**	**1429**	**1577**

Figure 3-3: Images showing the final structure of deposits and substrates formed within the settling tube experiments after the settling process. The first 19 settling tubes contain different volumes of microplastic-sediment ordered with respect to the suspension density. In each image, the orange layer depicts the microplastic deposit whilst the white layer depicts the sediment deposit. The last seven settling tubes correspond to the microplastic and sediment baseline runs (see Table 3.1).

3.2.1. Grain size distribution baseline settling tubes.

Figure 3-4 shows an example of the particle size distribution of pure microplastic and sediment grain size deposits from a baseline experimental run. The vertical axis of the plots corresponds to a unitary height (z), expressed as the relation between the slice thickness (h) and the total height (H_T) of the deposit, where z is equal to 1 at the top of the deposit and z is equal to 0 at the bottom.

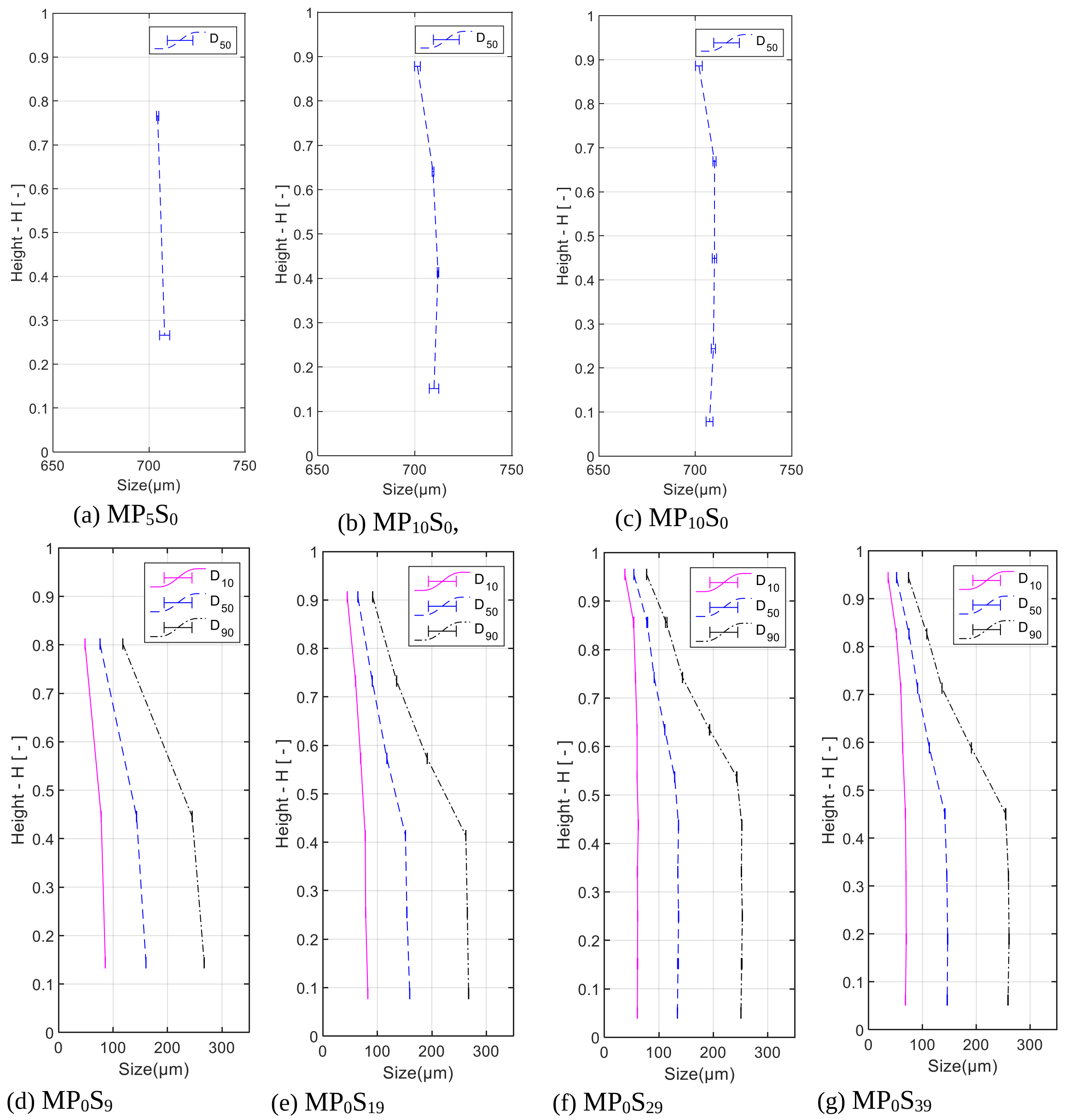

Figure 3-4. Characteristic particle sizes of the stratigraphy generated in the baseline runs. (a) -(c) Shows the distribution of the microplastic baseline characteristic diameters (D50) as a function of the normalised deposit height. The microplastic content in the plots is 5% (a),10% (b) and 15%(c). (d)-(g) Shows the distribution of the sediment baseline characteristic diameters (D10, D50, and D90) as a function of the normalized deposit height. The content of sediment in the plots is 9% (d), 19%(e), 28%(f) and 38% (g).

The microplastic baseline experiments (MP_5S_0, $MP_{10}S_0$, $MP_{15}S_0$) formed an ungraded deposit independently of the amount of the initial volume of plastic in the settling tubes with D_{50}=708±3.5 µm. The microplastic cubes were observed to align next to each other, reducing the gaps between the particles. The total height (H_T) of the deposits in these three tubes is 23.5 mm (MP_5S_0), 43.7 mm ($MP_{10}S_0$), and 65.9 mm (MP_0S_{38}), resulting in a linear relation with microplastic volume percentages.

The sediment baseline experiments (MP_0S_9, MP_0S_{19}, MP_0S_{29}, MP_0S_{39}) have two deposition patterns that may be described as an ungraded deposit at the bottom and a graded deposit at the top (Figure 3-4). The ungraded deposit was formed of medium-larger sized particles (D_{50}= 144±9.6 µm) occurring between the bottom of the tube z = 0 until z = 0.4-0.55 (mm/mm). The graded deposit was formed of the finest particles (D_{50}=61.5±11µm) and occurred between z = 0.4-0.55 (mm/mm) to z = 1.0 (mm/mm). The deposits heights (H_T) in these tubes are 35.7 mm (MP_0S_9), 73.2 mm (MP_0S_{19}), 108.9 mm (MP_0S_{29}) and 145.5 mm (MP_0S_{39}), follow a linear relation with the sediment volume percentage.

3.2.2. Comparison results with Amy (2006) research

To validate the methods used in this research, results from experiments MP_0S_9, MP_0S_{19}, and MP_0S_{29}, were compared with experiments "Run 1", "Run D1", and "Run 12" from the study of Amy (2006) (Figure 3-5). Amy's (2006) settling tubes contained 1%-2% more sediment; however, these percentages are within the volumetric differences provided by the range of sediment densities (±4%) and thus it is deemed to be an equivocal comparison.

The comparison (Figure 3-5) shows differences in particle sizes but similarities in the depositional patterns. The difference in sizes may be explained as Amy (2006) used smaller particle sizes (250 µm) of glass spheres in comparison with this study (350 µm). However, the similarities between the two studies in the larger-medium ungraded and finest graded deposits corroborate the experimental methods' reproducibility in size distribution.

The different methodology deployed also explains some of the difference between the almost straight graded curve profiles of this research and the slightly irregular curve in Amy (2006). Whereas Amy cut the frozen cores lengthwise along their axis and then extracted samples along the centre line, presenting more data sets, in this research, the frozen core was cut into slices with bigger samples, showing more average results (Section 2.4.).

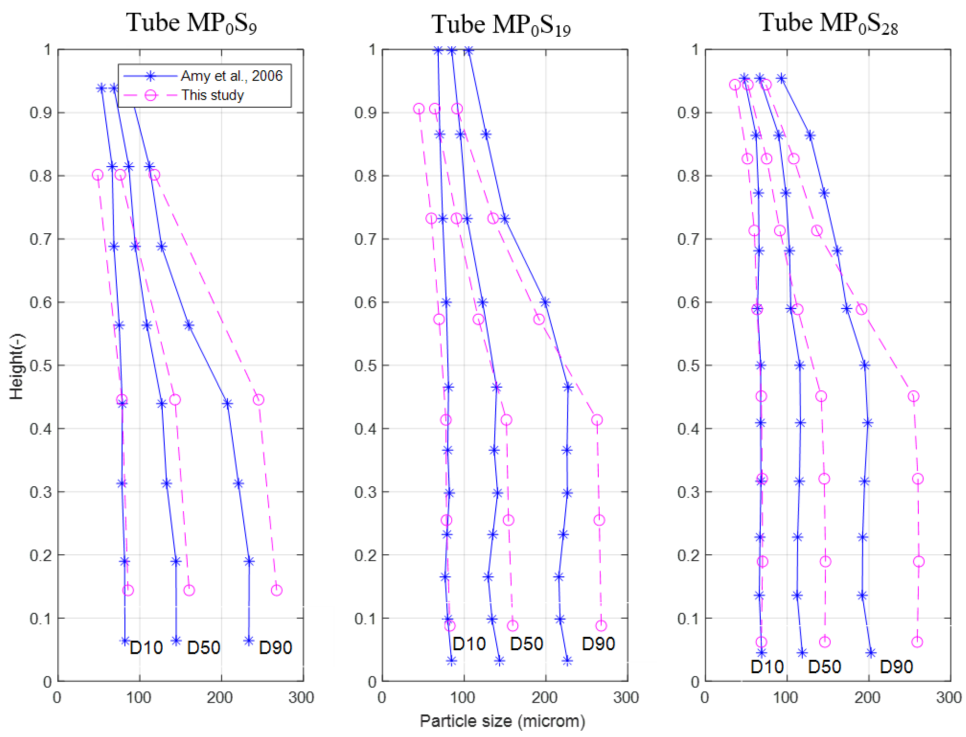

Figure 3-5. Comparison between the results of the sediment baseline with the experimental tubes of Amy. L. (2006). The pink dashed lines show the D10, D50 and D90 of the deposits in this study (Tubes MP0S9, MP0S19 and MP0S29). The solid blue lines represent the same characteristic diameters for experiments "Run 1", "Run D1", and "Run 12" in Amy (2006).

3.2.3. Grain size and volume distribution of microplastic-sediment settling tubes.

Grain size distributions and deposit characteristics of the settling experiments involving mixtures of sediment and microplastics are shown in Figure 3-6. Figure 3-6-a shows the characteristic's diameter size distribution of the total deposit whilst Figure 3-6- b-c show the grain size distribution for sediment and microplastic deposits, respectively. The vertical axes in these plots corresponds to a unitary height (H) expressed as the relation between the height (z) and the maximum thickness (h) of the deposit where z equals 1 at the top of the deposit, and z equals 0 at the bottom. Figure 3-6 is organised from the lowest (Tube MP_5S_5, ρ_{sus} =1076kg/m^3) to highest (MP_5S_{34}, ρ_{sus} =1511 kg/m^3) initial suspension density and numbered with roman symbols.

The tubes with initial suspensions density lower than 1117 kg/cm^3 (*Figure 3-6*, tubes i. to v.) form the greatest deposit heights. Microplastic (Figure 3-6, tubes i. to v.) forms an ungraded deposit with the smallest microplastic at the top (D_{50}=705±18 µm) and the largest microplastic at the bottom (D_{50}=772±49 µm). Whereas sediment (Figure 3-6, tubes i. to v.) forms a slightly graded substrate with the finest particle at the top (D_{50}=68±21 µm) and the largest particles at the bottom (D_{50}=152±10 µm).

Tubes with suspension density from 1117 kg/cm^3 to 1511 kg/cm^3 (*Figure 3-6*, tubes vi. to xvi.) form medium-lower height substrates. The microplastic substrates form a slightly ungraded deposit with an average D_{50}= 698±49 µm at the top and a D_{50}= 748±74 µm at the bottom. The sediment substrates are characterised by two grain size distributions: ungraded at the bottom and graded at the top. The ungraded deposit is formed with the medium-largest (D_{50}= 153±6 µm), from the bottom up the unitary heights 0.2-0.5 mm/mm. The graded substrate is formed with the finest (D_{50}= 47±34 µm) particles, from unitary heights of 0.2-0.5 mm/mm to the top. The graded substrate unitary heights increase as a function of the suspension density, with greater heights observed with greater suspension density.

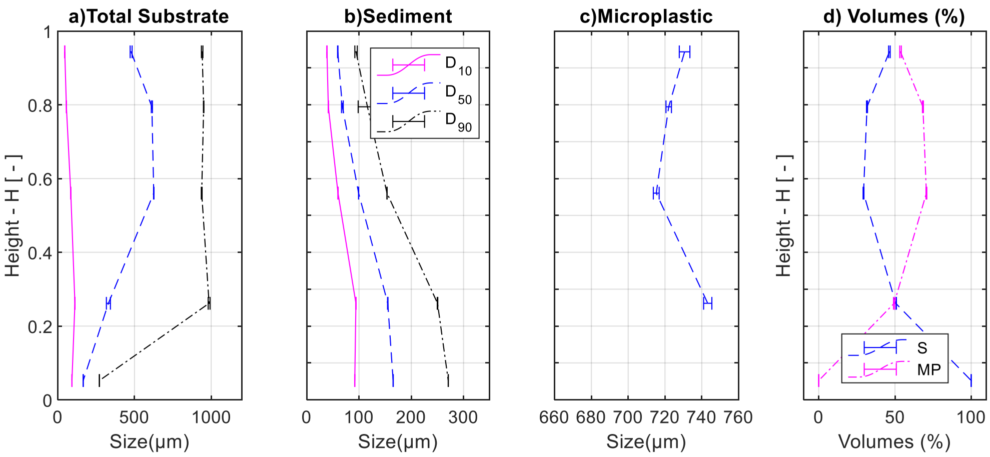

i) MP5S5, ρ_{sus} =1076 kg/m^3

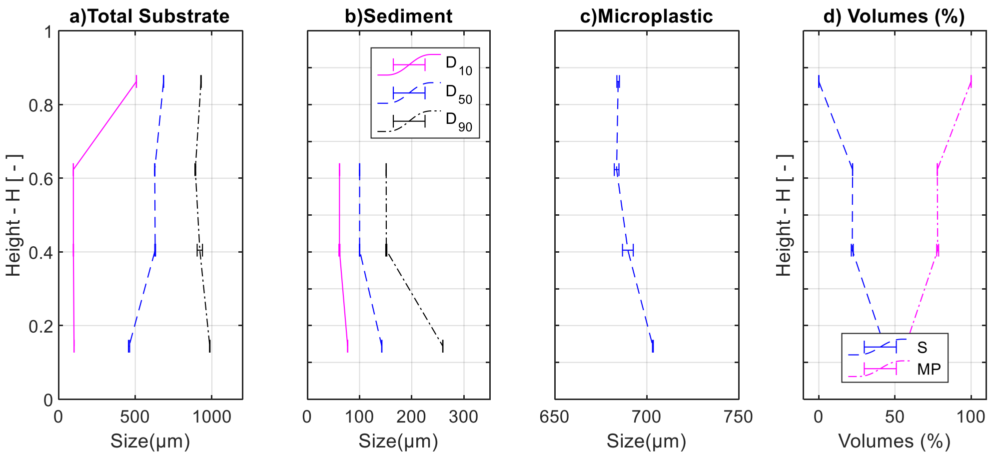

ii) MP10S5 ρ_{sus} = 1084 kg/m^3

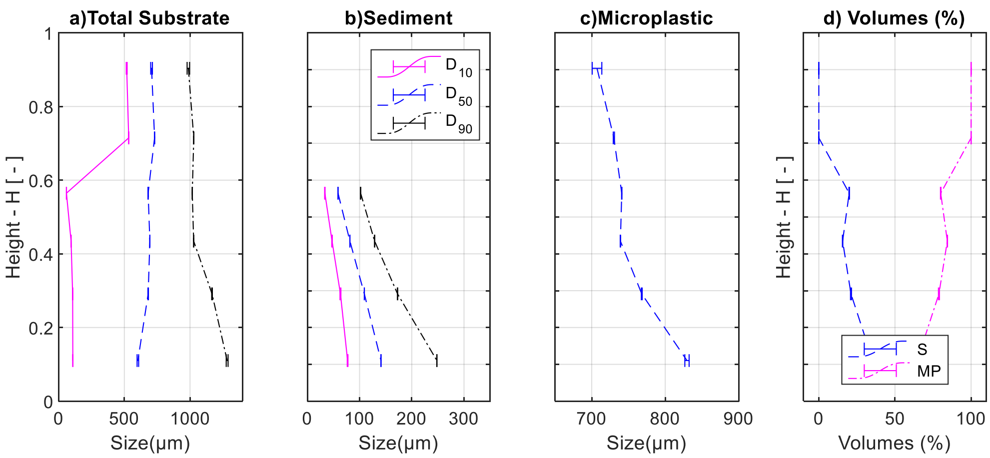

iii) MP15S5 ρ_{sus} = 1092 kg/m^3

*Figure continues on next page

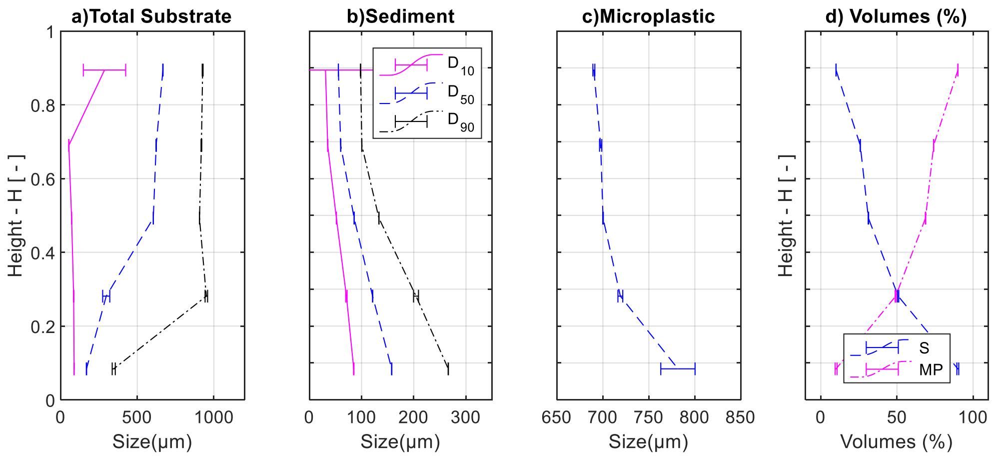

iv) MP_8S_7 ρ_{sus} =1116 kg/m^3

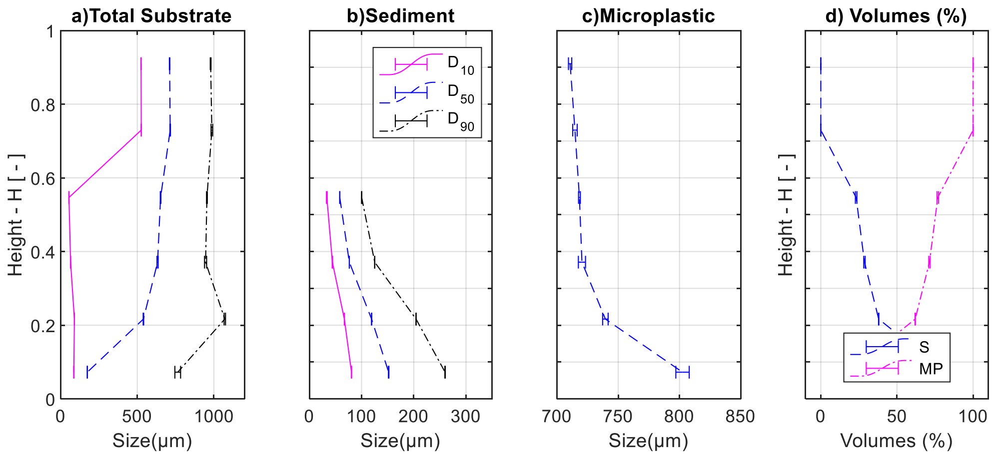

v) $MP_{13}S_7$ ρ_{sus} = 1117 kg/m^3

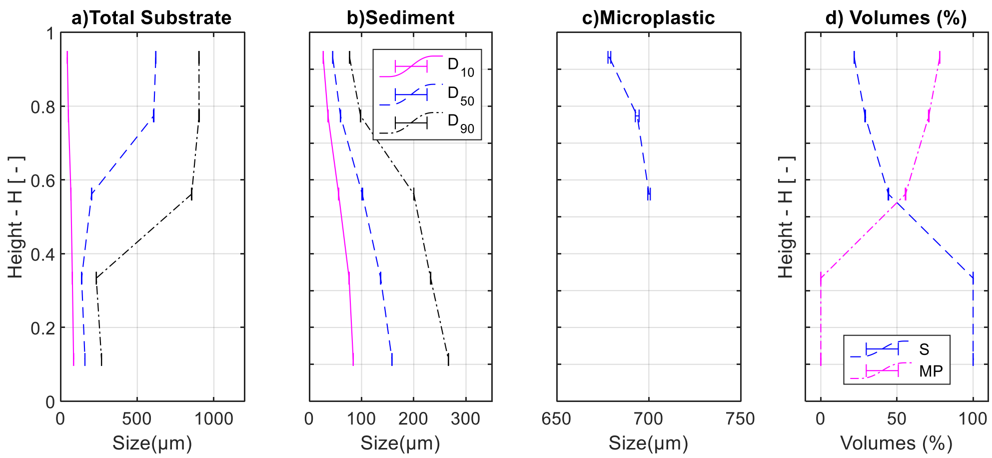

vi) MP_5S_9 ρ_{sus} = 1148 kg/m^3

***Figure continues on next page**

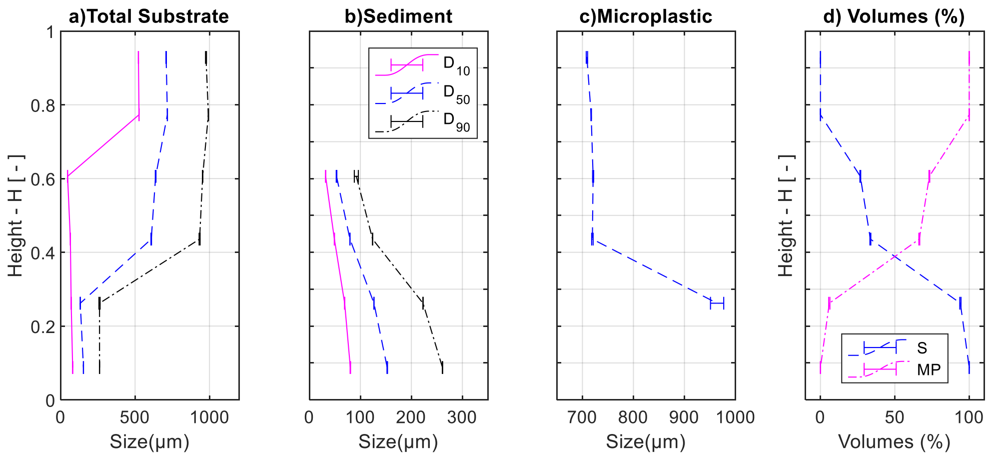

vii) MP$_{10}$S$_9$ ρ_{sus} = 1155 kg/m^3

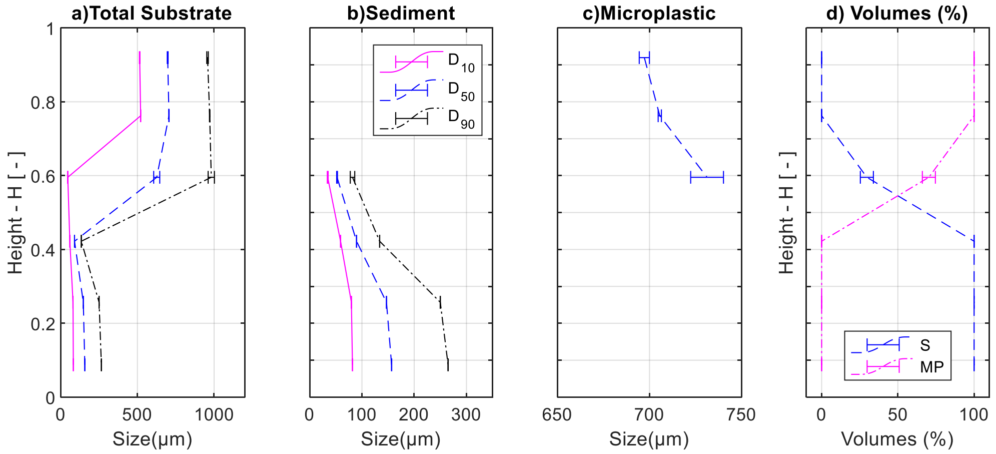

viii) MP$_7$S$_{12}$ ρ_{sus} = 1199 kg/m^3

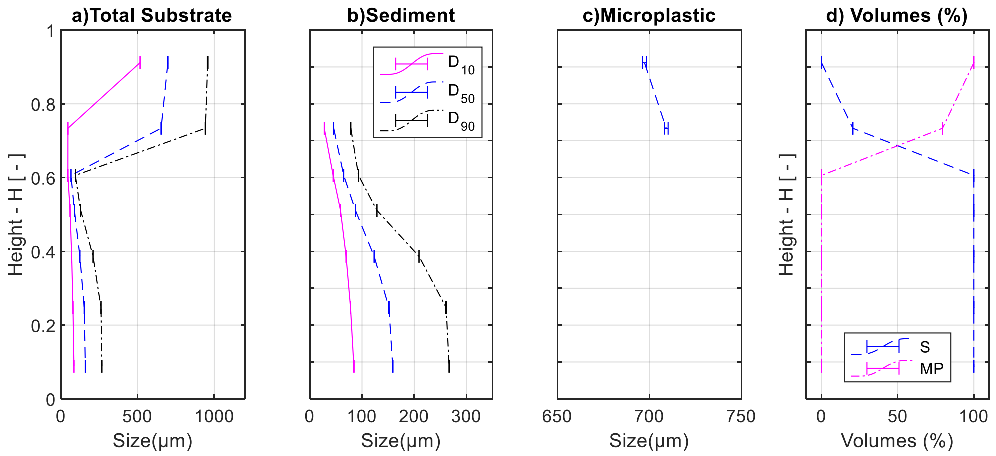

ix) MP$_5$S$_{14}$ ρ_{sus} =1219 kg/m^3

*****Figure continues on next page

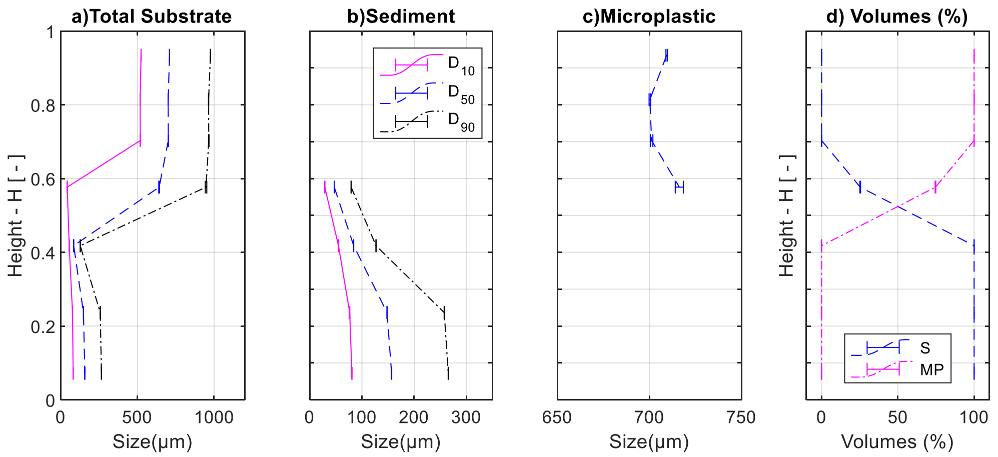

x) MP$_{10}$S$_{14}$ ρ_{sus} =1240kg/m^3

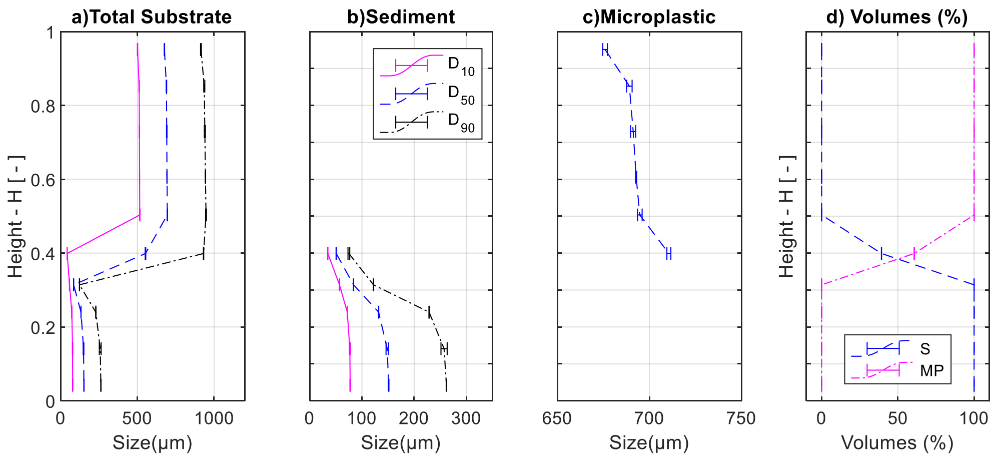

xi) MP$_{15}$S$_{14}$ ρ_{sus} = 1248 kg/m^3

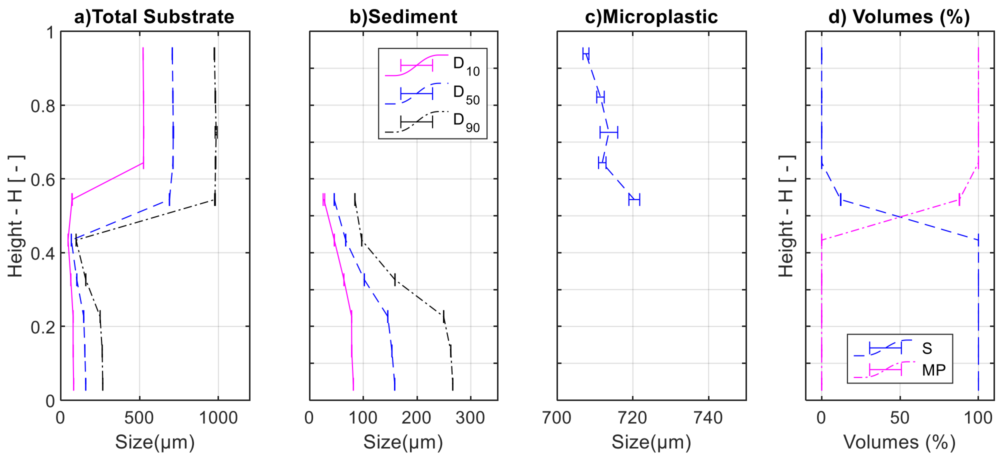

xii) MP$_{13}$S$_{16}$ ρ_{sus} = 1260kg/m^3

*Figure continues on next page

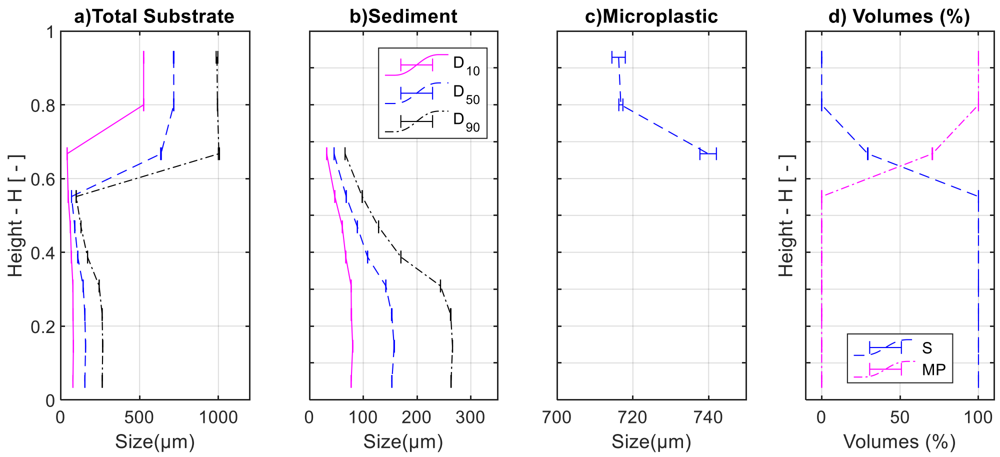

xiii) $\mathbf{MP_{10}S_{19}}$ $\boldsymbol{\rho_{sus}}$ **=1299 kg/m³**

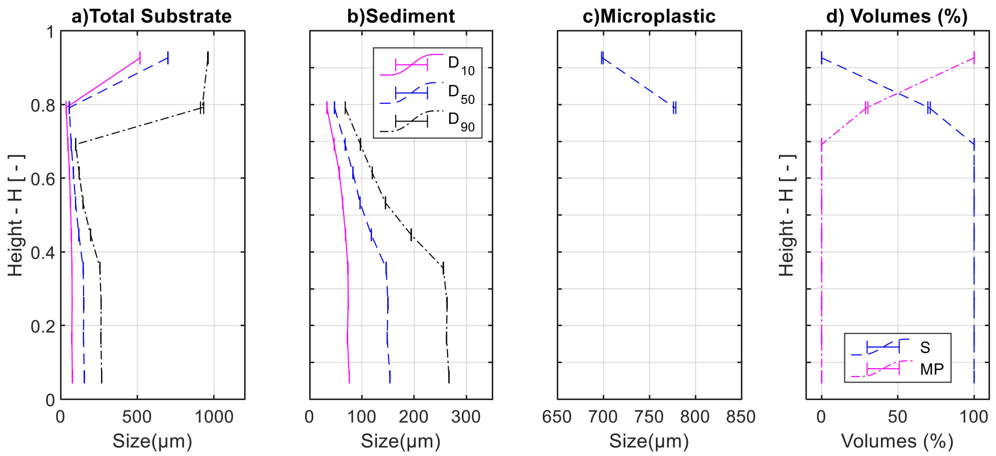

xiv) $\mathbf{MP_{5}S_{24}}$ $\boldsymbol{\rho_{sus}}$ **= 1364 kg/m³**

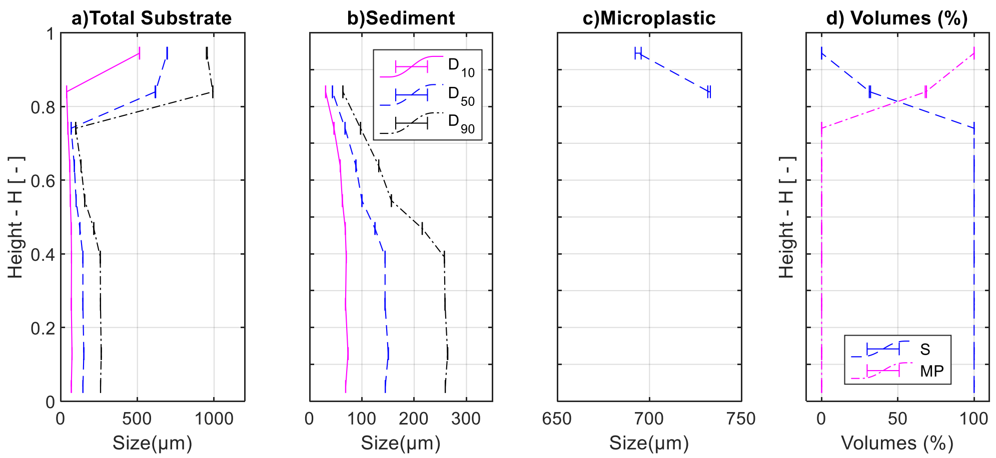

xv) $\mathbf{MP_{5}S_{29}}$ $\boldsymbol{\rho_{sus}}$ **=1437 kg/m³**

*Figure continues next page

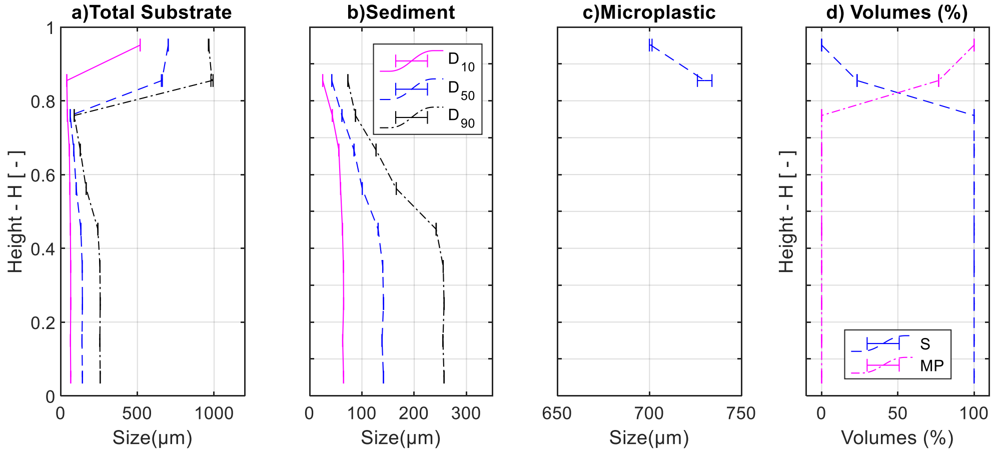

xvi) MP5S34 ρ_{sus} =1511 kg/m³

Figure 3-6. Size distribution identified in the settling tubes with different volumes of microplastic and sediment. Plot (a) shows the distribution of the characteristic diameters of the total deposit. Plots (b) and (c) show the distribution of the characteristic diameters of the microplastic and sediment deposits as separate grain size distribution. Plot (d) shows the distribution of the volumes between microplastic and sediment in the deposit. The plots (a) to (d) are shown for each settling tube, organized from the lower suspension density to the highest, numbered with roman symbols.

The trends of the settling tubes particles size (Figure 3-6) can be summarised in the following four aspects. The sediment's smallest particles (D_{10}) formed a slightly graded substrate in all the tubes. The sediment D_{50} and D_{90} followed the trend of ungraded deposits with suspension density lower than 1117 kg/cm^3 and ungraded-graded deposits with suspension density higher than 1117 kg/cm^3. The unitary heights of the limit between the graded-ungraded substrates increase with greater suspension density. The microplastic deposits were characterised to form slightly ungraded deposits.

3.2.4. Volume distribution settling tubes.

The distribution of the volume of microplastics deposited within each mixed substrate across the 35 slices is shown in Figure 3-7. It can be seen that these deposits represent medium to high microplastic volumes (43% to 82%), with a secondary group displaying lower volumes (2%-25%). The distributions of these volumes versus the substrate heights are shown in Figure 3-6-d. The largest mixture deposits were formed in the settling tubes with suspension densities lower than 1116 kg/m^3. The lower percentages (2%-25%) were allocated in settling tubes between 1116 kg/m^3 to 1155 suspension densities. A detailed analysis of the mixtures substrates is presented in Section 3.2.5.

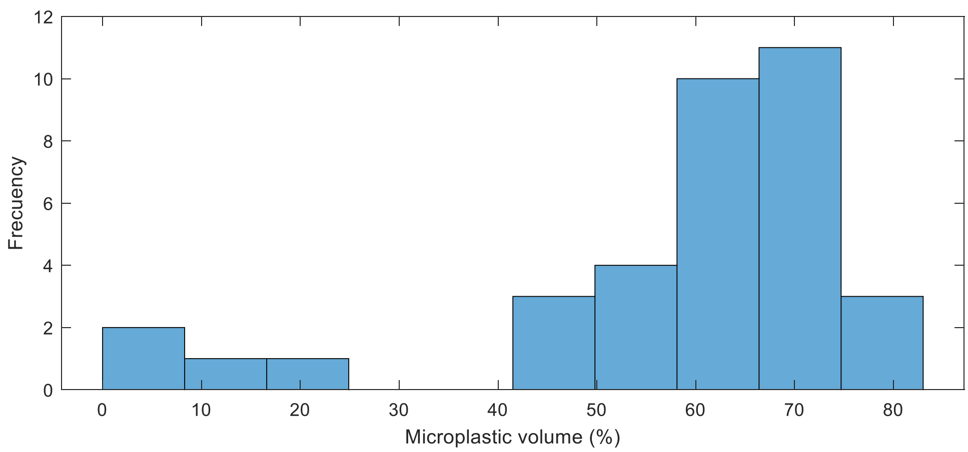

Figure 3-7. Experimental results of the measured volume in the observed deposited substrates.

3.2.5. Substrates definition

Four substrates are defined based on the colour configuration formed in the settling tubes (Figure 3-2) and the results of the size and volume distribution between the deposits (Figure 3-4). The first layer is the microplastic substrate (MP), composed of 100% plastic (dark orange layer, *Figure* 3-3), and the second one is the sediment substrate (S) (white layer, *Figure* 3-3), composed of 100% of sediment particles. The mixed layer composed of both microplastic and sediment (light orange layer, *Figure* 3-3) is separated into two substrates based on the volume distribution (Figure 3-7). The layer with medium to higher microplastic volumes (43% to 82%) is classified as a mixture of high microplastic content (HMP-S). The layer with lower volumes (2% -25%) is classified as a mixture of low microplastic content and sediment (LMP-S). From now on, the four substrates are described as follows:

i) Microplastic dominated (MP)

ii) Mixture: high microplastic content and low sediment content (HMP-S)

iii) Mixture: low microplastic content and high sediment content (LMP-S)

iv) Sediment dominated (S)

Table 3.3 shows the height of each substrate in millimetres and its unitary height estimated with the total deposit height. Based on these values, four diagrams were created to understand the spatial distribution with respect to the volumetric content of microplastic and sediment (*Figure 3-8*). The spatial distribution diagrams were created using natural neighbours interpolations methods based on the measured heights (mm) of MP, HMP-S, and S substrates. In the legends of the diagrams (Figure 3-8), the dark colours represent the largest height values and light colours the lowest height values. The four diagrams are described as follows:

- Diagram A: shows the substrates in each settling tube (dimensional with respect to the total height, Table 3.3 column # 2-4-6-8).
- Diagram B: shows the spatial distribution of the microplastic substrate heights (MP) (Table 3.3 column # 1).
- Diagram C: shows the spatial distribution of the heights of high microplastic content and low sediment content substrate (HMP-S). The grey highlighted area indicates the location of low microplastic content and high sediment content substrate (LMP-S). The suspension density values are summarised with grey lines every 50 kg/cm^3. (Table 3.3 -column # 3-5).
- Diagram D: shows the spatial distribution of the sediment substrate height (S) (Table 3.3-column # 8).

Table 3.3. Height of the microplastic (MP), mixture HMP-S, mixture LMP-S and sediment (S) substrates measured in each settling tube.

Heights	Height microplastic substrate		Height Mixture HMP-S		Height Mixture LMP-S		Height Sediment		Total height
Column	**1**	**2**	**3**	**4**	**5**	**6**	**7**	**8**	**9**
Tube name	**h_{MP} (mm)**	**h_{MP}/H_T (%)**	**h_{HMP-S} (mm)**	**h_{HMP-S}/H_T (%)**	**h_{LMP-S} (mm)**	**h_{LMP-S}/H_T (%)**	**h_S (mm)**	**h_S/H_T (%)**	**H_T (mm)**
MP_5S_{14}	15.10	21%	6.1	8%			51.67	71%	72.8
MP_5S_{24}	21.90	19%	2.2	2%			88.40	79%	112.5
MP_5S_{33}	19.20	13%	3.1	2%			120.70	84%	143.0
MP_5S_{42}	19.30	11%	3.1	2%			152.20	87%	174.6
MP_5S_5			30.9	86%			5.00	14%	35.9
MP_7S_{12}	22.07	29%	13.1	17%			41.10	54%	76.3
$M_{10}S_9$	26.35	28%	26.8	28%	25.38	27%	16.00	17%	94.6
$MP_{10}S_{19}$	42.07	36%	2.7	2%			72.77	62%	117.6
$MP_{10}S_{28}$	41.70	28%	3.1	2%			105.10	70%	149.9
$MP_{13}S_7$	31.00	42%	34.7	47%	1.90	3%	6.00	8%	73.6
$MP_{13}S_{16}$	55.00	46%	4.5	4%			59.75	50%	119.3
MP_7S_{31}	28.00	19%	3.1	2%			115.70	79%	146.8
MP_5S_9	2.98	5%	24.7	42%	21.35	36%	10.15	17%	59.1
MP_8S_7	9.03	16%	37.6	66%	2.00	1%	8.48	15%	57.1
$MP_{10}S_5$	11.22	21%	40.3	75%			1.88	4%	53.4
$MP_{10}S_{14}$	39.90	41%	6.6	7%			50.38	52%	96.9
$MP_{15}S_{14}$	62.55	52%	7.7	6%			49.98	42%	120.2
$MP_{15}S_5$	38.38	47%	41.5	50%			2.40	3%	82.3
MP_5S_{28}	20.13	16%	2.1	2%			106.30	83%	128.6
MP_5S_0	23.50	100%						0%	23.5
$MP_{10}S_0$	43.50	100%						0%	43.5
$MP_{15}S_0$	65.90	100%						0%	65.9
MP_0S_9							47.00	100%	47.0
MP_0S_{19}							94.00	100%	94.0
MP_0S_{28}							108.90	100%	108.9
MP_0S_{38}							145.00	100%	145.0

From these four diagrams and the heights shown in Table 3.3, the four substrates are described as follows:

a) Microplastic substrates (Figure 3-8, Diagram B)

The microplastic substrate (MP) was formed at the top of the deposits, and a height between 3 mm and 63 mm, representing 5%-52% of the total deposit. The microplastic substrate layer was identified in all the experiments except MP_5S_5; the microplastic was mixed with the sediment in this tube as there were.

The lower microplastic heights are located in runs MP_5S_9 (2.98 mm). The maximum height was formed in run $MP_{15}V_{14}$ (62 mm) and the baseline case $MP_{15}S_0$ (65.9 mm).

- The behaviour of the heights (Figure 3-8, Diagram B) is divided into two groups :
- Below $\Phi_S<0.15$: the heights increases as a function of the microplastic-sediment volumes.
- Above $\Phi_S>0.15$: the heights increase as a function of the sediment volume.

b) HMP-S substrates (Figure 3-8, Diagram C)

The high microplastic and sediment content (HMP-S) was observed below the MP substrate in all the settling tubes. The HMP-S layer has heights between 2.1 to 44 mm, representing 2% to 86% of the total height. The highest values were measured in tubes with 5% sediment volumes (MP_5S_5, $MP_{10}S_5$, $MP_{15}S_5$), and lower values were measured in tubes with more than 28% of sediment volumes.

The behaviour of this substrate is divided into two groups (Figure 3-8, Diagram C):

Below $\Phi_S<0.10$, the height of the substrate increases as a function of the microplastic-sediment volumes.

Above $\Phi_S>0.10$, the height of the substrate decreases as V_S increases, regardless of the amount of microplastic.

c) LMP-S substrate (grey highlight area in Figure 3-8, Diagram C)

The mixture of low microplastic and sediment content (LMP-S) was formed above the HMP-S in experimental runs: $MP_{10}S_9$, $MP_{13}S_9$, MP_5S_9, and MP_8S_7, between sediment volumes 7% to 9% (grey highlight area in Figure 3-8, Diagram C). The LMP-S layer has heights between 2 mm to 25.4 mm, representing 3% to 36% of the total deposit (H_T). The largest size was formed in Φs =0.09 and the minimum in Φs =0.07.

a) **Sediment substrate** (Figure 3-8, Diagram D)

The sediment substrate (S) was formed at the bottom of the settling tube. The layer has heights between 2 mm to 152 mm, representing between 3% to 87% of the total deposit. The sediment layers' thickness grows as sediment content increases (Figure 3-8, Diagram D), with heights between 2 mm and 150 mm. As an exception in the MP5S5, a top layer was formed with a height of 3 mm with the finest particles.

Finally, Table 3.4 summarises the characteristic of heights, volumes, and grain size distribution of the four substrates already described.

Table 3.4. Characteristic of heights, volumes, and size distributions of the microplastic (MP), mixture HMP-S, mixture LMP-S and sediment (S) substrates in the settling tube.

<table>
<tr><th colspan="2">Substrate name</th><th>Microplastic substrate

(MP)</th><th>Mixture of high microplastic and sediment content

(HMP-S)</th><th>Mixture of low microplastic and sediment content

(LMP-S)</th><th>Sediment

(S)</th></tr>
<tr><td colspan="2">Created in the settling tubes</td><td>All

(Except MP_5S_5)</td><td>All</td><td>$MP_{10}S_9$, $MP_{13}S_9$, MP_5S_9, MP_8S_7</td><td>All</td></tr>
<tr><td colspan="2">Microplastic content</td><td>100%</td><td>43-82%</td><td>2% -25%.</td><td>0%</td></tr>
<tr><td colspan="2">Heights (mm)</td><td>0-63 mm</td><td>2 mm - 44 mm</td><td>2mm-25 mm</td><td>2 mm – 152 mm</td></tr>
<tr><td colspan="2">Unitary Heights (%)</td><td>0% - 50%</td><td>2%-86%</td><td>3%-36%</td><td>1% -87%</td></tr>
<tr><td rowspan="4">Behaviour heights versus Vs</td><td>Φs: 0.05-0.10</td><td rowspan="2">Increase as

Φ_{MP}-Φ_S increase.</td><td>Increase as

Φ_{MP} decrease.</td><td>Decrease as

Φ_S increase.</td><td rowspan="4">Increase as Φs increases</td></tr>
<tr><td>Φs: 0.10-0.15</td><td rowspan="3">Decreases as the Φ_S increases.</td><td rowspan="3">-</td></tr>
<tr><td>Φs: 0.15- 0.45</td><td rowspan="2">Increase as Φ_{MP} increase</td></tr>
<tr><td>Φs: 0.20-0.45</td></tr>
<tr><td colspan="2">Grain size distribution</td><td>Ungraded</td><td>Sediment: Partially graded
Microplastic: Ungraded</td><td>Sediment: Partially graded
Microplastic: Ungraded</td><td>Graded at the top -ungraded bottom</td></tr>
</table>

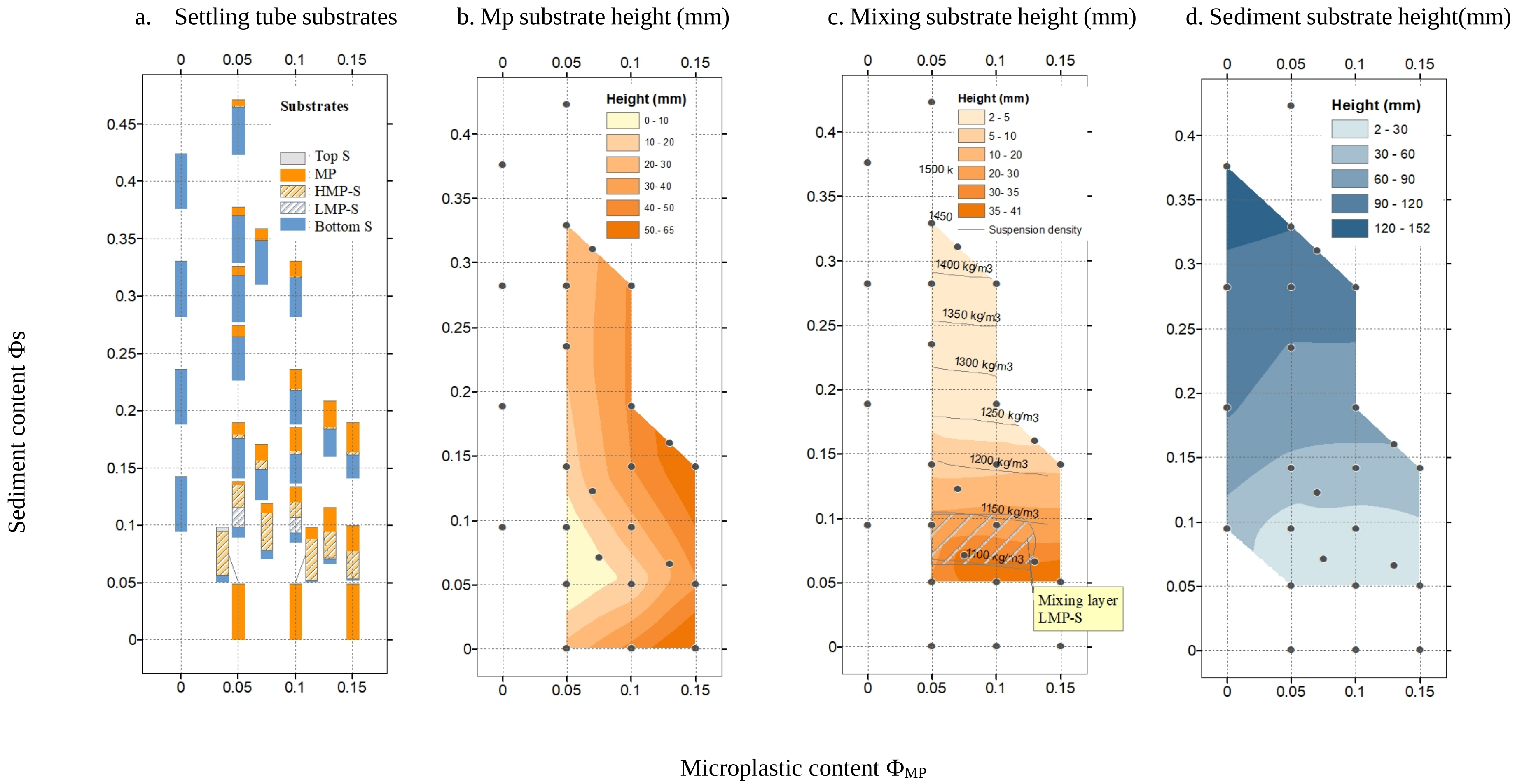

Figure 3-8. Results of the microplastic and sediment settling experiments as a function of volumetric concentrations of each material. A) Substrate distribution in each settling tube (dimensional as a function of the total deposit). B) Height variation of the microplastic substrate (mm). C) Height variation of the high microplastic content substrate (mm). Location of the low microplastic content substrate and variation of the suspension density (grey lines show). D) height variation of the sediment substrate (mm).

3.2.6. Sediment and microplastics fall velocities.

The fall velocity of an individual particle is estimated using the relationship proposed by Ferguson and Church (2004) (Equation 2-1, Section 2.1). Applying this equation for sediment, using diameters (D10, D50, D90) and the parameters C_1=18- C_2 = 0.4 (recommended for perfect spheres), and for microplastics using microplastic D50 with the parameters C_1=24 -C_2 =1.2 (recommended for irregular shapes), it was found that the fall velocity of sediment varies between 2.0 mm/s (D10) to 30.17 mm/s (D90), whilst the microplastic fall velocity remains constant at 15.5 mm/s (D50). The microplastic and sediment fall velocities shows that both materials have a similar fall velocity, as although the microplastic has a lower density it has a bigger size than the sediment.

From the videos captured (Methods, Section 2.3.) during the settling experiments through the transparent bottles, as it was expected due the particle interaction effects the fall velocity behaviour of the microplastic cloud decreases as the volume of sediment increases. From the 22 video frames extracted (Appendix 5), it is estimated that the microplastic cloud fall velocity is 6.44 mm/s for MP_5S_5, 4.09 mm/s for MP_5S_9, 2.45 mm/s for MP_5S_{14} and 0.37mm/s MP_5S_{44} (Figure 3-9). The measured velocities decrease as the volumes of sediment increase. Microplastic and sediment were observed in the lowest concentration transparent bottle (MP5S5) to form a mixed substrate composed of the two materials. In MP_5S_{14} and MP_5S_9, as the volume of the sediment increases, changes in the microplastic cloud velocities occur due to observed horizontal flow created by the settling sediment particles. After all the microplastic was deposited, the fine particles of sediment continued settling through the free spaces between the microplastic. In the transparent bottle with the highest sediment volume (MP_5S_{44}), the sediment particles appear as almost as floating grains, and the microplastic was observed to behave positively buoyant.

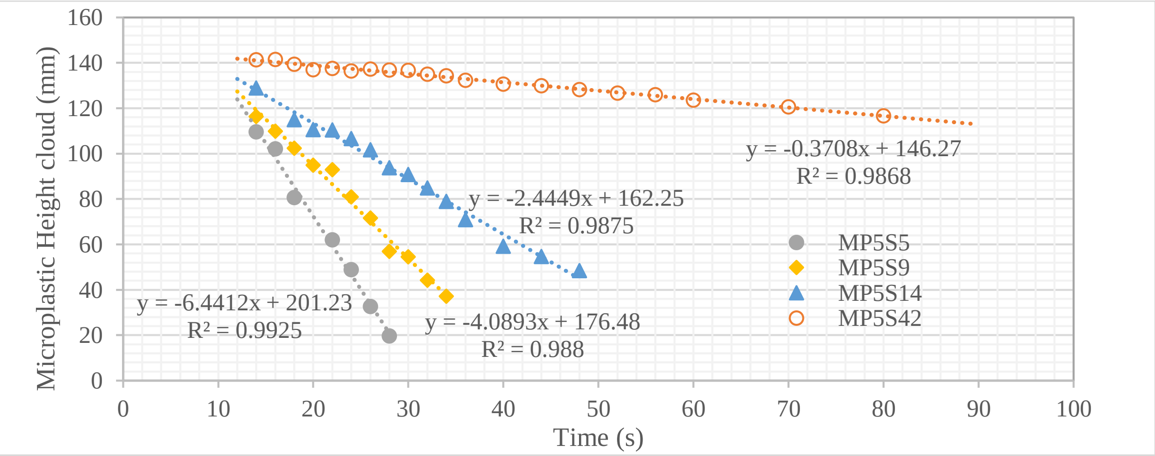

Figure 3-9. Height of the microplastic cloud in time in four experimental transparent bottles: MP_5S_5, MP_5S_9, MP_5S_{14} and MP_5S_{44}. The fit equation slope represents the microplastic cloud's fall velocity of each experimental tube.

Using the approach of Davis and Gecol (1994) (Equation 2-3 and 2-4) to estimate the hindered fall velocity for the microplastics and sediment characteristics diameters (Table 3.5). It can be seen that a threshold condition between suspension densities 1155 kg/m^3 to 1194 kg/m^3 exists, where the negatively buoyant microplastic behaviour starts to display positively buoyant tendencies. The same trend is determined for the smallest and intermediate sediment particles. For suspension density higher than 1092 kg/m^3, sediment particles with a D_{10} presented rising velocities, and for suspension densities higher than 1364 kg/m^3, sediment particles with a D_{50} presented rising velocities. The hindered fall velocity results are used in the discussion as a reference to analyse the settling regimes defined in the experimental tubes.

Table 3.5. Hindered fall velocity estimations for each experimental (Davis and Gecol, 1994)

Name	Suspension density (kg/m^3)	Sediment hindered fall velocity (mm/s)			Microplastics hindered fall velocity (mm/s)
		D10	**D50**	**D90**	**D50**
MP_5S_5	1076	-0.80	-8.02	-16.57	-4.20
$MP_{10}S_5$	1084	-0.27	-5.61	-13.22	-3.24
$MP_{15}S_5$	1092	0.04	-3.85	-10.30	-2.45
MP_8S_7	1116	-0.08	-5.02	-12.78	-1.75
$MP_{13}S_7$	1117	0.17	-3.42	-9.97	-1.37
MP_5S_9	1148	0.04	-4.78	-12.91	-0.25
$M_{10}S_9$	1155	0.28	-3.25	-10.15	-0.30
MP_7S_{12}	1194	0.49	-2.57	-9.64	1.41
MP_5S_{14}	1219	0.63	-2.12	-9.30	2.55
$MP_{10}S_{14}$	1227	0.62	-1.35	-7.17	1.73
$MP_{15}S_{14}$	1235	0.55	-0.83	-5.36	1.14
$MP_{13}S_{16}$	1260	0.62	-0.61	-5.19	1.70
$MP_{10}S_{19}$	1299	0.72	-0.28	-4.94	2.53
MP_5S_{24}	1364	0.89	0.26	-4.52	3.90
MP_5S_{29}	1437	0.82	0.57	-3.29	3.62
$MP_{10}S_{29}$	1445	0.60	0.42	-2.36	2.36
MP_7S_{32}	1484	0.65	0.58	-2.23	2.75
MP_5S_{34}	1511	0.68	0.68	-2.15	3.01
MP_5S_{44}	1659	0.40	0.53	-0.92	1.77

3.2.7. Relation suspension density versus the height of the substrate of the high microplastic-sediment mixture (HMPS)

From the analysis of the spatial distribution of the substrate HMP-S and the contour lines of the suspension density (Figure 3-8, Diagram C), a trend was observed between the two variables (Figure 3-10). Where suspension density was lower than 1250 kg/m^3, the heights of the HMP-S substrate increased as the suspension density decreased. However, where suspension density is higher than 1250 kg/m^3, the height of the HMP-S does not change significantly, regardless of suspension density. The rising and sinking velocities limits (Davis and Gecol, 1994) of the microplastic and sediment are also highlighted in Figure 3-10. The highest substrates are formed where the D_{50} microplastic and D_{50} sediment have sink velocities. The intermediate-lower substrates are formed when the microplastic rise and sediment sinks. Finally, the lowest heights are formed when the microplastic – sediment has risen velocities. The relation between the height of the HMP-S substrates versus the suspension density and the behaviour of the fall velocities confirmed the hypothesis that the microplastic and sediment volumetric content controls the stratigraphy characteristics of the deposit.

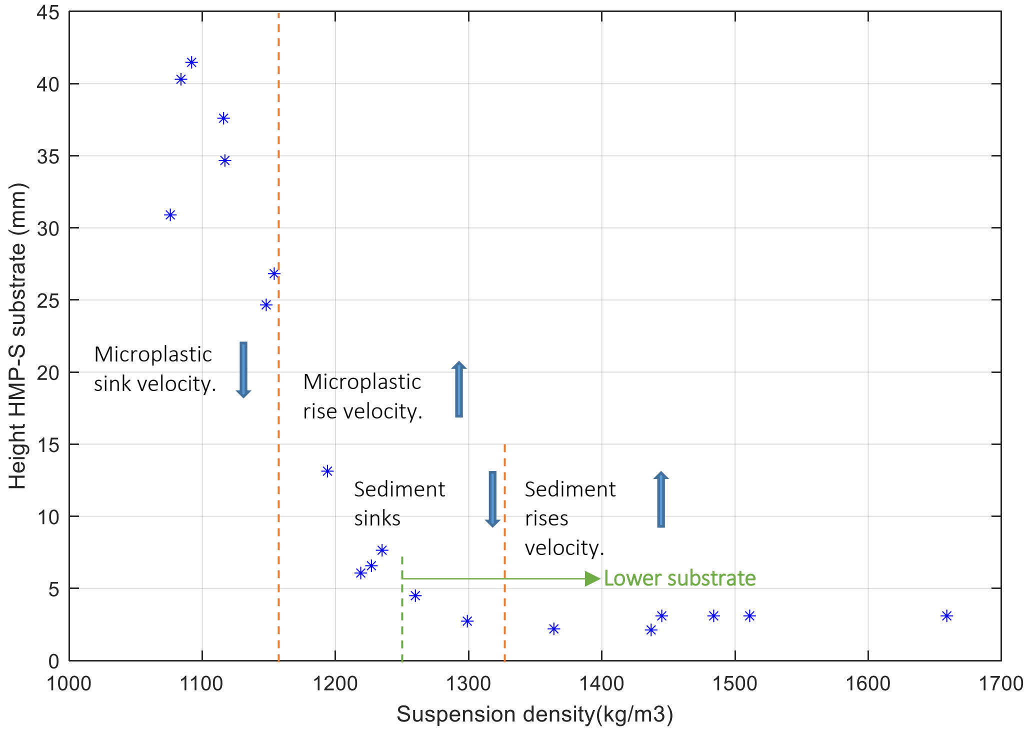

Figure 3-10. Height of the mixed substrates HMP-S as a function of the suspension density.

3.3. Discussion

3.3.1. Substrate formation, stratigraphy, and definition of settling regimes.

The substrate formation for this experimental work can be split into three settling regimes. The classification of each regime is based on the substrates definition (Section 3.2.5.), the relation of the suspension density with the height of the HMP-S substrate (Figure 3-10), the grain size distribution results (Section 2.2.3), the fall velocities values (Table 3.5), and settling velocity observations (Section 3.2.6). The definition of the settling regime is also based on prior work into concentrations of settling fluxes (Druit, 1995; Amy et al., 2006; Dorrell and Hogg, 2010; Guo et al., 2015;) and the gravitational forces balances in the suspension (Phillips and Smith, 1971; Lick, 2009). The names selected are based on the concentrations represented by the suspension density, similar to the research of Druit (1995). From now on, the three settling regimes are defined as lower, intermediate, and high suspended concentrations.

a) Lower suspended concentrations (ρ_{sus}<1100 kg/m^3)

The first settling regime is defined in suspension densities lower than 1100 kg/m^3. In this regime, the microplastic and sediment particles settle in a free settling regime (Druit, 1995; Amy et al., 2006; Guo et al., 2015). The highest HMP-S substrate is formed because both materials have similar fall velocities (w_{sS} =2.0 mm/s -30.17 mm/s, w_{sMp} = 15.5 mm/s) (Figure 3-11). The low suspended concentration regime forms a partially ungraded deposit with sediment and microplastic, with higher sediment particles deposited at the bottom and the finest sizes deposited on the top. In tubes $MP_{10}S_5$ and $MP_{15}S_5$, the excess microplastic was deposited at the top of the mixture substrate. In tube MP_5S_5, the equal volumetric content formed a sediment deposit with the smallest particles at the top, a mixed deposited at the middle and a sediment deposit with the largest particles at the bottom.

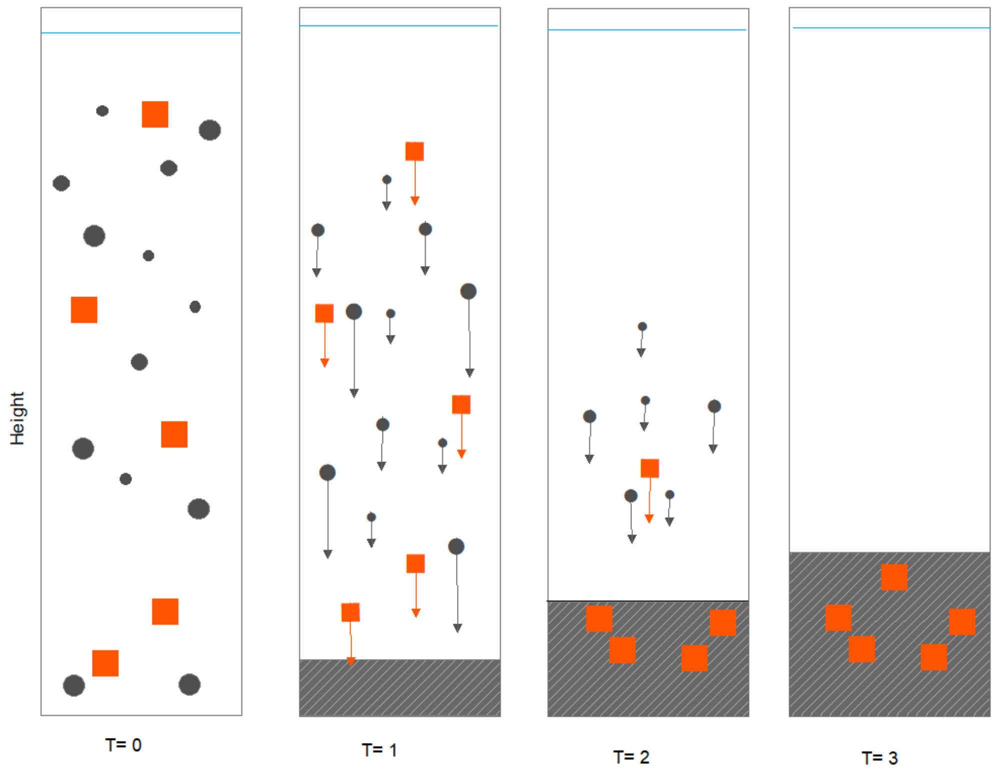

Figure 3-11. Diagram of the microplastic and sediment low suspended concentrations settling process. In the diagrams, the orange square represents the microplastic particles, grey spheres represent the sediment, and the straight line indicates the particles fall velocity direction..

b) Intermediate suspended concentrations (1100 kg/m^3<ρ_{sus}<1250 kg/m^3)

The next regime occurs between suspension densities of 1100 kg/m^3 and 1250 kg/m^3 (Figure 3-12). In this regime, the microplastic fall velocity decreases as the sediment concentration increase as a result of the particle interactions inside the settling tubes (Kynch, 1952; Richardson and Zaki, 1954; Druit, 1995; Amy et al., 2006; Guo et al., 2015). The velocities may change due to the recirculating flow created by the settling sediment particles, which influence the balances between gravitational forces and interflows of the microplastic particles tubes (Druit, 1995; Amy et al., 2006; Lick et al., 2009; Guo et al., 2015). As the suspension density increases, the interflows are stronger and drive the observed reduction of the HMP-S heights, explaining the linear relation of the height of HMP-S substrates between suspension densities 1100 kg/m^3 to 1250 kg/m^3 in Figure 3-10. At higher concentrations, the strength of the return flow is so strong that the microplastic particles in the first few seconds of the settling process are observed to float (positively buoyant high-density microplastic) on the top of the sediment substrate until the flows calm down. An intensive network of return flow has been explained as an effective way to separate lighter particles and see them separated at the top of the mixture (Richardson and Zaki, 1954; Phillips and Smiths,1971).

The LMP-S substrate is formed when the interflows are not strong enough to influence all microplastic particles in suspension, resulting in some particles becoming trapped in the sediment substrate. Explaining why the LMP-S height is lower in the higher sediment concentration runs (Vs=10%) and higher in the lower sediment concentration runs (Vs=7%). The LMP-S substrate is characterised by a transition where the microplastic particles sink or rise before deposition.

In the intermediate concentration, as the density of the suspension grows, mixing layers are formed in the higher depths with the finest-medium sediments (D_{50}=80-100µm). As the suspension density increases, there is an evolution between ungraded sediment deposits to graded sediment deposits.

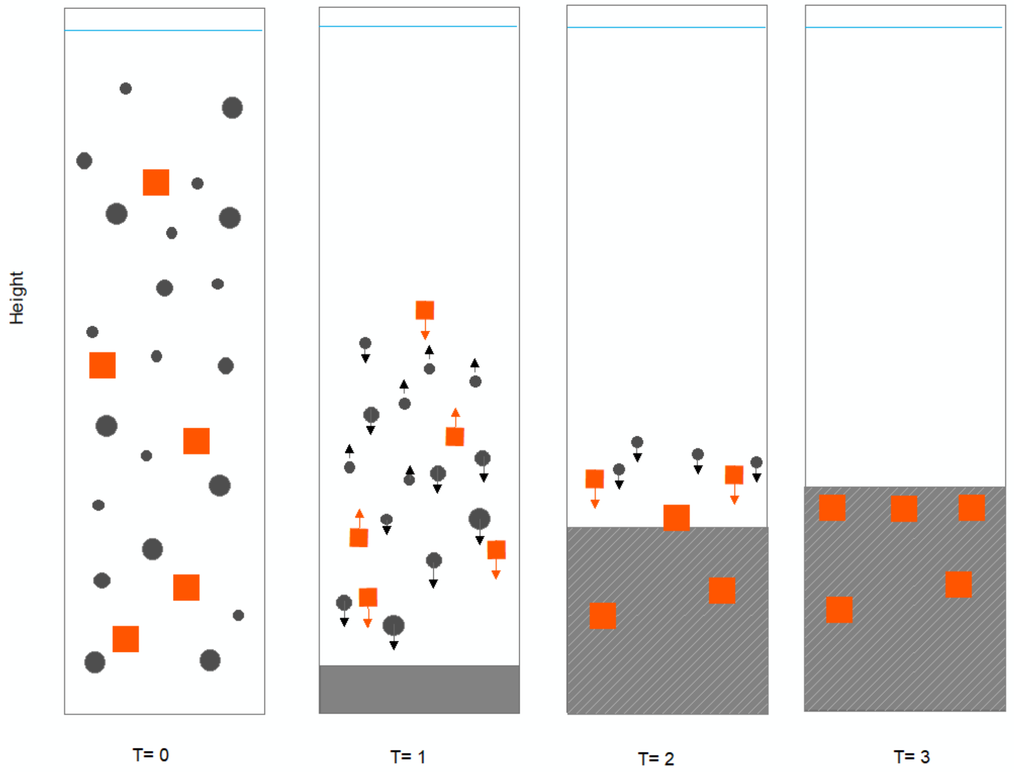

Figure 3-12. Diagram of the microplastic and sediment intermediate suspended concentrations settling process. In the diagrams, the orange square represents the microplastic particles, grey spheres represent the sediment, and the straight line indicates the particles fall or rising velocities directions.

c) High suspended concentrations (ρ_{sus}>1250 kg/m^3)

The high suspended concentrations regime is defined in suspension densities from 1250 kg/m^3 to 1659 kg/m^3 (Figure 3-13). Sediment particles are described as almost floating grains, allowing microplastic particles to move to the surface (positively buoyancy microplastic) due to their lower density than sediment, forming the lower heights of the HMP-S substrates. The floating substrates of microplastic and sediment settle slowly until a mixed layer is formed with the finest sediments (D_{50}=65 µm), forming a relatively constant thickness because content of microplastics was always distributed at the top surface. The sediment deposit is formed with an ungraded deposit at the bottom and a graded deposit at the top, and the stratigraphy characteristics of these high concentrations (Amy et al., 2006; Dorrell and Hogg, 2010).

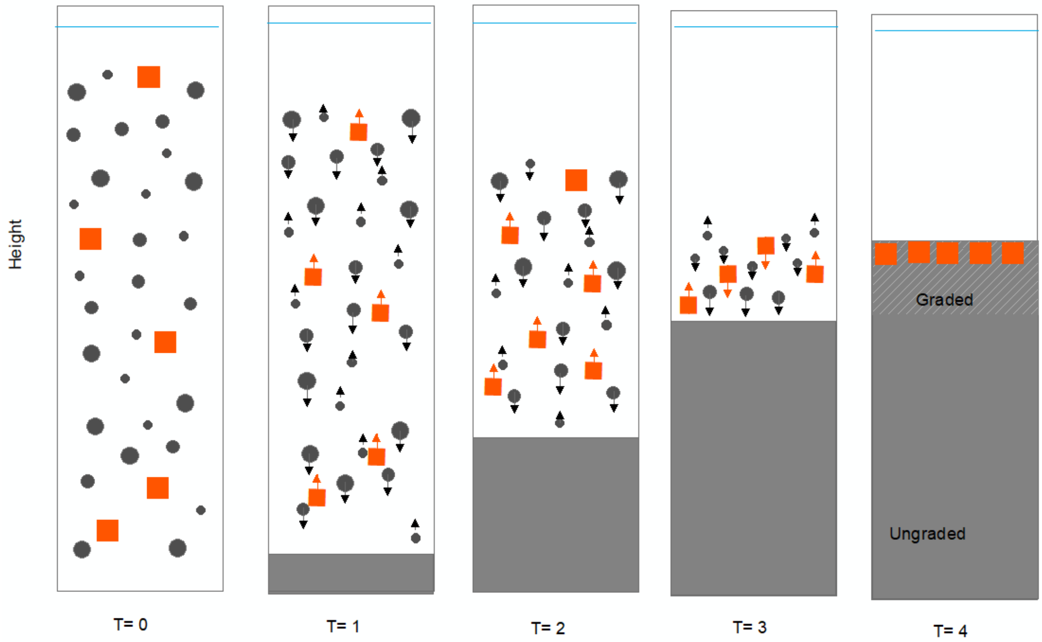

Figure 3-13. Diagram of the microplastic and sediment high suspended concentrations settling process. In the diagrams, the orange square represents the microplastic particles, grey spheres represent the sediment, the straight line indicates the particles fall or rising velocities directions.

Finally, a final diagram of these settling regimes is summarised in *Figure* 3-14

Settling process of suspended concentrations of microplastic and sediment		
Low suspended concentrations **Suspended density lower than** $\rho_{sus} < 1110$ kg/cm^3	**Intermediate suspended concentrations** **Suspended density between** $\boldsymbol{\rho_{sus}}$**=1110 kg/cm**^{3} **to** $\boldsymbol{\rho_{sus}}$ **=1250 kg/cm**^{3}	**High suspended concentrations** **Suspended density higher** $\boldsymbol{\rho_{sus}}$**>1250 kg/cm**^{3}
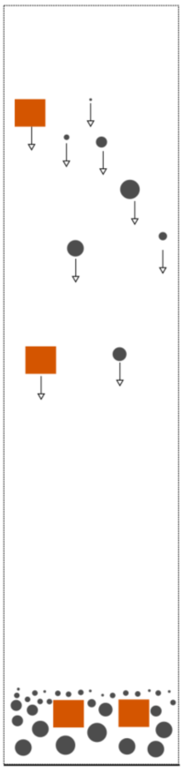	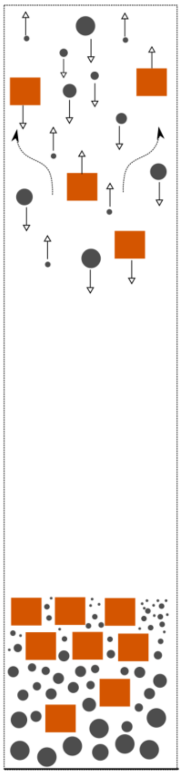	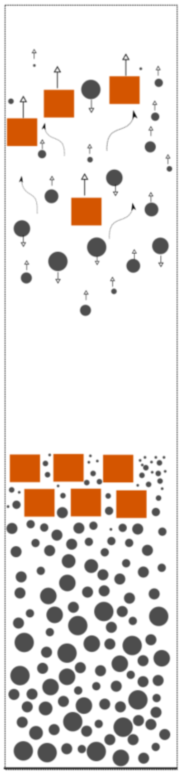
Particles fall as individual particles and form a partially ungraded mixing layer of microplastic–sediment (HMP-S). The excess microplastic volumes are deposited at the top of the deposit.	The interflows surrounding the sediment particles start to slow down the deposition of the microplastic and result in the reduction of the HMP-S height. MP particles sink or rise before deposition. The LMP-S substrate is formed in the lower concentrations when the interflows are not strong enough to influence all the microplastic particles	Sediment's fall velocity is significantly reduced. Microplastic rise to the top of the substrate between the suspended sediment particles and forms the smallest mixing substrates (HMP-S). The height of the HMP-S is almost constant as sediment and microplastic increase.

Figure 3-14. Description and diagrams of the settling regimes described in this research, low, intermediate, and high concentrations settling regimes of microplastics and sediment mixtures. In the diagrams, the orange square represents the microplastic particles, grey spheres represent the sediment, the straight line the fall of the particles, and the irregular lines represent the interflows.

3.3.2. Interpretation of the results

The results explained that the deposition height of the nylon particle in the sediment depended on the physical characteristics of the particle (density, shape and size) and the concentrations in the suspension. From the three regimes defined above, it is inferred that in calm water the definition of the deposition height of the microplastic particles in the sediment bed is defined by the suspended particle concentration. The same microplastic particle can be deposited in the top substrate layers in higher suspended concentrations, or can be deposited deeper in the substrate in lower suspended concentrations. In intermediate suspended concentrations, microplastic typically settles in the middle. The depositional pattern in function of the suspension density helps explains why it is common for researchers to find the same plastic-type deposited in different levels of the substrate regardless of the depth of sampling (Martin et al., 2017; Hurley et al., 2018; Dikareva and Simon, 2019; Fan et al., 2019; Jiang et al., 2019; Chouchene et al., 2021; Lin et al., 2021; Saarni et al., 2021).

The experimental work evidences the physics conditions why the microplastic particles can be stored in the sediment bed in calm water. Limiting the mobilisation by the river flows thus impacts transport potential and enhances long-term storage. The microplastic accumulation in the river sediment bed has implications in estimating the amount of microplastic transported to Oceans from the river environment.

Researchers are constantly changing the depth or area of sampling in the field to study microplastic pollution in sediments as there is a lack of an official, accepted methodology (Correia et al., 2019). The results in descriptions of microplastic deposition in rivers without any clear understanding of the behaviour of the spatial distribution patterns (Martin et al., 2017; Hurley et al., 2018; Dikareva and Simon, 2019; Fan et al., 2019; Jiang et al., 2019; Chouchene et al., 2021; Lin et al., 2021; Saarni et al., 2021). The findings from this research help to explain that one of the parameters that control the horizontal deposition patterns is the suspended concentrations of microplastic and sediment loads. Further, it suggested that a unified sample method is needed to predict the horizontal depositional pattern of the microplastic.

The calculated values of fall velocities under different regimes (Section 3.2.6) of free settling (Equation 2-1, Ferguson and Church, 2004), hindered (Equation 2-3 and 2-4, Davis and Gecol, 1994), and microplastic cloud (Section 3.2.6, laboratory measured) help to explain the influences of the particle-particle interactions occurring within the suspension. An individual microplastic particle's free settling velocity is calculated to be 15.5 mm/s (Ferguson and Church, 2004). Conversely, the fall velocity of the microplastic cloud (Tube Mp_5S_5) was 6.44 mm/s, showing a reduction of 60% between free settling velocities. The hindered velocity in tube Mp_5S_5 was 4.20 mm/s, suggesting a reduction of 73% from the free settling velocity. The graded deposit observed in tube Mp_5S_5 was in a free settling regime. However, the hindered and microplastic cloud velocities indicated a significant reduction (60%-73%) of the microplastic fall velocity. Demonstrating an important reduction of the materials' fall velocities affecting the deposit grain size distribution and definition of the substrates.

The Davis and Gecol (1994) calculations refer to only the fall velocity value representing the settling process. However, one of the main observations of the transparent bottles is that microplastic particles in the intermediate and high concentrations change their buoyant stages during the settling process. In intermediate concentrations, some particles can rise in the first seconds influenced by interflows and then settle after the interflows dissipation. In the high concentration, all the microplastics were observed to rise to the top layer and slowly settle. The heights of the final depositional substrates depend on this process.

3.4. Conclusion

The work detailed in this chapter discussed the deposition process of negatively buoyant microplastic and sediment mixtures in riverbeds in calm water. The experiments were composed of 26 settling tubes with different volumes of Nylon pellets (ρ_{MP} = 1150 kg/m^3 , D_{50}=686±2.4μm), sediments (ρ_s = 2500 kg/m^3 , D_{50}=105±0.2μ) and freshwater. The settling tubes formed four types of substrates: microplastic (100% MP), a mixture of the high content of microplastic (43%-82%, HMP-S), a mixture of low content of microplastic(43%-82%, LMP-S), and a sediment substrate (100% S). The formation of the substrate types, their heights, and typical grain sizes is shown to depend on the sediment, microplastic, and freshwater volumes. The suspension density (ρ_{sus}) reported is representative of the initial volumes and is shown to be a parameter that relates the density of the materials with the volumetric contents, describing the suspended concentration in the settling tube.

The suspension density is found to be the dominant parameter that governs microplastic particle settling behaviour in the deposition process and, thus, the heights of a substrate (MP, HMP-S, LMP-S, and S). In low concentrations (ρ_{sus}<1110 kg/cm^3) particles fall as individual particles and form the highest mixing layer of microplastic–sediment (HMP-S). In intermediate concentrations (1110 kg/cm^3 ρ_{sus}<1250 kg/cm^3), reverse buoyancy and interflows increases rate at which the bed is built, reducing the HMP-S height and the formation of the LMP-S when the some microplastic particles sink or rise. Finally, in higher concentrations (ρ_{sus}>1250 kg/cm^3) microplastic particles rise to the top rapidly of the substrate forming the smallest mixing substrates (HMP-S).

From the strong positive buoyant of the microplastic at higher concentrations, microplastic particles are deposited in top layers in higher suspended concentrations. In lower suspended concentrations, the microplastic particle is deposited deeper in the sediment bed. Concluding that the deposition depth in mixtures of sediment and negatively buoyant microplastics in calm waters depends on the plastic-sediments properties (density, size, geometry) and the number of particles in the suspension.

The next thesis chapter aims to advance the experimental work detail here but with microplastic buoyancy with respect to the fluid density. Future work that complements these findings should focus on studying the behaviour of the deposition of microplastic particles with other sediment ranges, considering more complex processes such as aggregations between plastics and sediments. The phenomenon has the ability to change microplastic settling velocity and should influences deposit structure but is currently unquantified.

Chapter 4 . The experimental settling process of microplastic and sediment mixtures: positive-neutrally buoyant and constant suspension density

Chapter three demonstrated that the substrate formed in the experimental tubes with negative buoyancy microplastic particles and sediments is defined by the particle interaction in the suspension. The suspension density (ρ_{sus}, Equation 2-7) were determined as the physical parameter that classified if the suspension is in a free or hindered settling regime. The regimes defined the microplastic deposition height in the sediment bed, substrates formation and particle size distribution. Therefore, Chapter 4 was designed to study the regime's behaviour with positive and neutrally microplastics to complete the range of plastic density found in the environment, and extend the results in the free settling regime.

Chapter four consists of 26 experimental tubes: eight variable suspension densities and 18 with fixed suspension density (Figure 2-2). The variable suspension density consisted of eight experimental tubes designed to study the substrate formed with positive and neutral microplastics in a free and hindered regime. The 18 settling tubes with fixed suspension density extended the results in only free settling regime, to extend the study of sediment and microplastic deposits formed with more common suspended concentrations.

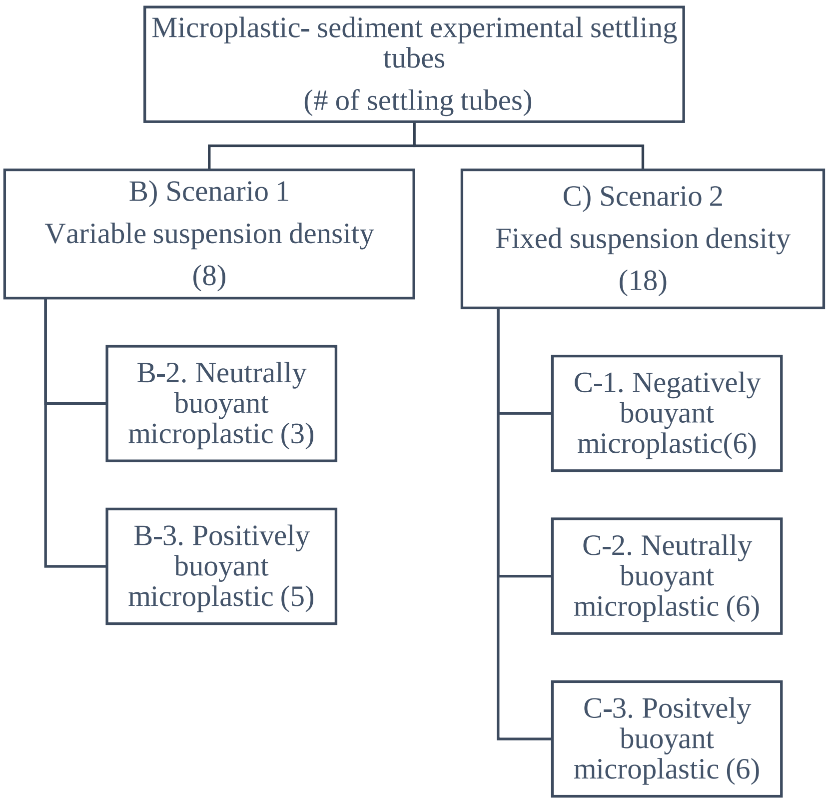

Figure 4-1. Set of experiments settlings tubes included in this chapter thesis.

Hence, Chapter four presented the results, discussion, and conclusion of the second part of the experimental work of the microplastic and sediments settling process. The chapter starts with a summary introduction of the methods and details of the diameters, volumetric content and densities of the experimental materials (Section 4.1). The experimental tubes' results are divided into variable and fixed suspension densities. The results of the particle size distribution and volumetric content of the eight settling tubes with variable suspension density are presented in Section 4.2. Based on the results, a discussion and conclusion of these settling tubes is presented to define the free settling and hindered regimes of the positively and neutrally buoyant microplastics. Therefore, the result of the stratigraphy formed in the settling tubes with fixed suspension density is presented, followed by a discussion and conclusions (Section 4.3). Finally, the chapter ends with the definition of the settling regimes for the experimental conditions and interpretations of the results in the field (Section 4.4 and 4.5).

4.1. Introduction

The experimental conditions in this chapter were designed following the results of Chapter 3, where the suspension density (ρ_{sus}, Equation 2-7) were determined as the physical parameter that defines the particle size distribution and substrate stratigraphy of the mixtures of negatively buoyant microplastic and sediment. The experiments completed the range of plastics densities found in the environment (neutrally and positively buoyant) and extended the results in the free settling regime, ending in 26 settling experimental tubes. The experiments use one plastic-type and salinity solutions to recreate scenarios of positively, negatively, and neutrally buoyant microplastics to represent the range of plastics that are polluting the rivers.

Table 4.1 , Table 4.2 and Figure 4-2 detail the different concentrations of microplastic (Φ_{Mp}), sediment (Φ_S), and fluid (Φ_f) added to the settling tubes. The microplastic was the same plastic used in Chapter 3, orange nylon pellets with a density of 1150 kg/cm^3 and an average equivalent diameter of D_{50}=686±2.4µm. The sediment is formed by a mixture of 5 different types of glass spheres, with equivalents diameters of D_{10}=73±0.05 µm, D_{50}=105±0.2µm, and D_{90}=211±0.5µm, and a density between 2400-2600 kg/m^3. The saline solutions to recreate different plastic buoyant conditions, which have a density between 1002.6 kg/m^3 and 1195.6 kg/m^3, were created by diluting a specific amount of salt in water (Table 2-4).

The eight tubes with variable suspension density were designed to define the free or hindered settling regimes for positively and neutrally buoyant microplastic particles. The initial volumetric concentrations were selected based on the settling regimes defined in Chapter 3, where settling tubes with suspension densities lower than 1110 kg/cm^3 were defined in a free settling regime and higher values were defined with intermediate and higher hindered effects. Therefore, the volumetric conditions of these eight tubes were selected to cover a low, intermediate and higher suspension density, as is listed in Table 4.1. The tubes contained a fixed fluid density of 1195.6 kg/m^3 for the positively buoyant and 1120.2 kg/m^3 for the neutrally buoyant microplastic, sediment volumetric concentration (Φ_S) from 0.05 to 0.43 and microplastic concentrations (Φ_{Mp}) from 0.05 to 0.13.

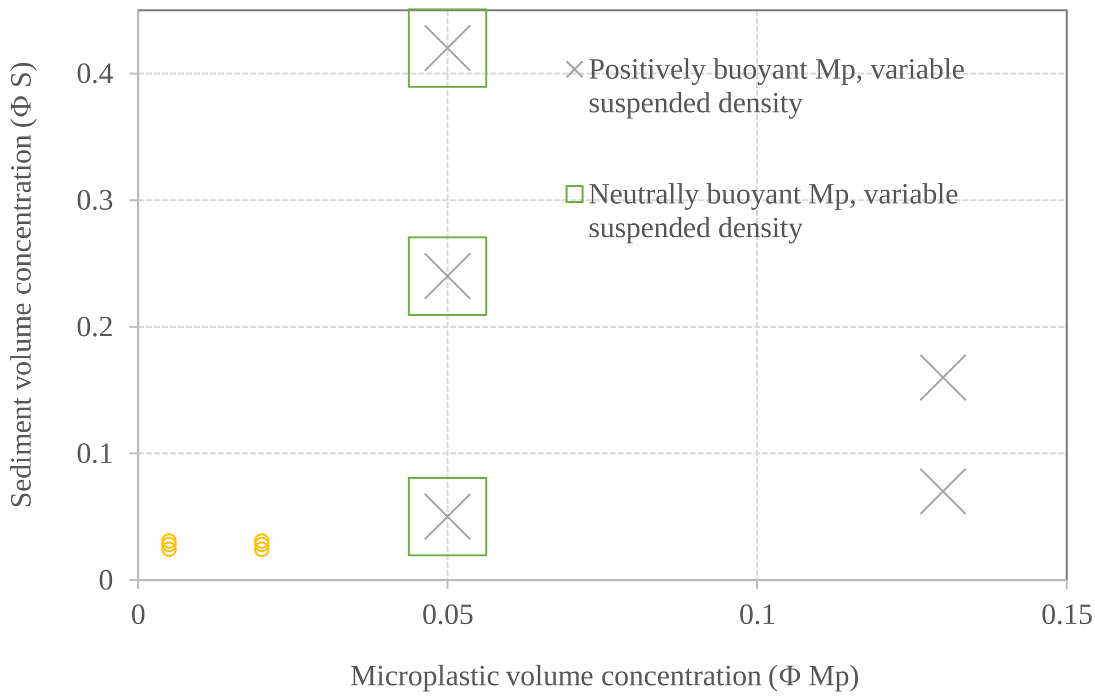

Figure 4-2. Volumes of microplastic and sediment added to the 26 experimental tubes. Grey "X" corresponds to the five positively buoyant microplastic settling tubes, green squares to the three neutrally buoyant microplastic settling tubes with variable suspension density, and the yellow circles are the 18 experimental tube scenarios with a fixed suspension density.

Table 4.1. Name, sediment, microplastic and fluid volumes of 8 settling tubes, variable suspension density, with fixed fluids densities.

Name	**Volumetric concentration Φ**			**Fixed Fluid density (kg/m^3)**	**Suspension density (kg/m^3)**
	Microplastic	**Sediment**	**Fluid**		
Positively buoyant microplastic					
$+MP_5S_{24}$	0.05	0.24	0.71	1195.6	1504
$+MP_5S_{43}$	0.05	0.43	0.51	1195.6	1739
$+MP_5S_5$	0.05	0.05	0.91	1195.6	1270
$+MP_{13}S_7$	0.13	0.07	0.81	1195.6	1290
$+MP_{13}S_{16}$	0.13	0.16	0.71	1195.6	1407
Neutrally buoyant microplastic					
$\approx MP_5S_{24}$	0.05	0.24	0.71	1120.2	1451
$\approx MP_5S_{43}$	0.05	0.43	0.51	1120.2	1701
$\approx MP_5S_5$	0.05	0.05	0.91	1120.2	1201

A further 18 tubes were designed to consider solely the free settling regime, expanding the results to different plastic densities and concentrations more representative of riverine environments. Crucially each experiment has the same value of initial suspension densities: ρ_{sus} =1227 kg/m^3 for positively buoyant, ρ_{sus} =1152 kg/m^3 for neutrally buoyant and ρ_{sus} =1052 kg/m^3 for negatively buoyant microplastic. The volumetric conditions were selected to cover three sediment volumetric concentration (Φ_S = 0.024, 0.028 and 0.031) and two microplastic concentrations (Φ_{Mp} = 0.02 and 0.05). The fluid density varies from 1186.8 kg/m^3 to 1195.2 kg/m^3 for the positively buoyant microplastics, from 1108.2 kg/m^3 to 1117.8 kg/m^3 for the neutrally buoyant microplastic and from 1002.6 kg/m^3 to 1014.6 kg/m^3 to negatively buoyant microplastic.

Table 4.2. Name, sediment, microplastic and fluid volumes of 18 settling tube, fixed initial suspension density.

Name	Volumetric concentration Φ			Fluid density (kg/m^3)	Suspension density (kg/m^3)
	Microplastic Φ_{Mp}	Sediment Φ_S	Fluid Φ_f		
Positively buoyant microplastic					
$+MP_{2.0}S_{2.4}$	0.02	0.024	0.955	1195.9	1227
$+MP_{2.0}S_{2.8}$	0.02	0.028	0.952	1191.1	1227
$+MP_{2.0}S_{3.1}$	0.02	0.031	0.949	1187.4	1227
$+MP_{0.5}S_{2.4}$	0.005	0.024	0.970	1195.2	1227
$+MP_{0.5}S_{2.8}$	0.005	0.028	0.967	1190.4	1227
$+MP_{0.5}S_{3.1}$	0.005	0.031	0.964	1186.8	1227
Neutrally buoyant microplastic					
$\approx MP_{2}S_{2.4}$	0.02	0.024	0.955	1117.3	1152
$\approx MP_{2}S_{2.8}$	0.02	0.028	0.952	1112.1	1152
$\approx MP_{2}S_{3.1}$	0.02	0.031	0.949	1108.2	1152
$\approx MP_{0.5}S_{2.4}$	0.005	0.024	0.970	1117.8	1152
$\approx MP_{0.5}S_{2.8}$	0.005	0.028	0.967	1112.7	1152
$\approx MP_{0.5}S_{3.1}$	0.005	0.031	0.964	1108.8	1152
Negatively buoyant microplastic					
$MP_{2}\ S_{2.4}$	0.02	0.024	0.955	1012.5	1052
$MP_{2}S_{2.8}$	0.02	0.028	0.952	1006.8	1052
$MP_{2}S_{3.1}$	0.02	0.031	0.949	1002.6	1052
$MP_{0.5}S_{2.4}$	0.005	0.024	0.970	1014.6	1052
$MP_{0.5}S_{2.8}$	0.005	0.028	0.967	1009.1	1052
$MP_{0.5}S_{3.1}$	0.005	0.031	0.964	1004.9	1052

4.2. Variable suspension density settling tubes, with fixed fluid density.

4.2.1. Results

Figure 4-3 shows the pictures of the 8 experimental tubes, different layers were formed with only microplastic or sediment or a mixture of microplastic-sediment, depending on the microplastic, sediment and fluid volumes. The results of each settling tube's stratigraphy, volume and size distribution are described as a function of suspension density and microplastic buoyancy.

Positively buoyant microplastic

Name	$+MP_5S_{43}$	$+MP_5S_{24}$	$+MP_{13}S_7$	$+MP_{13}S_{16}$	$+MP_5S_5$
Suspension density	1739 kg/m^3	1504 kg/m^3	1407 kg/m^3	1290 kg/m^3	1270kg/m^3
Fixed fluid density	1227 kg/m^3				
Bottom substrate	0.162 m	0.0917m	0.0615 m	0.0252 m	0.0179 m

Neutrally buoyant microplastic

Name	$\approx MP_5S_{43}$	$\approx MP_5S_{24}$	$\approx MP_5S_5$
Suspension density	1701 kg/m^3	1451 kg/m^3	1201 kg/m^3
Fixed fluid density	1120.2 kg/m^3		
Bottom substrate	0.166 m	0.107 m	0.0331 m

Figure 4-3. Substrates formed in the 8 settling experimental tubes with variable suspension density and fixed fluid density. The first row shows the results of the positively buoyant microplastics, and the second row shows the result for the neutrally buoyant microplastic. The orange particles are the microplastic, and the white bottom layer are the sediments.

I. Positively buoyant microplastic settling tubes

The first five settling tubes from Figure 4-3 shows the result of the positively buoyant microplastic scenarios with suspensions densities between 1270 kg/m^3 to 1739 kg/m^3. The microplastic formed a thick layer at the top of the fluid, and the sediment a layer at the bottom, except tube MP_5S_5, which included a mixture layer with 1.04% of microplastic. The height of the bottom deposit varies between 0.179 m to 0.162 m.

The sediment particle size distribution of the five experiments with suspension densities between 1270 and 1739 kg/m^3 is presented in *Figure 4-4*. Tubes with higher suspended concentration (ρ_{sus}>1400 kg/m^3) formed an ungraded substrate from the bottom to unitary heights 0.5-0.6 (m/m), with an equivalent average D_{50} = 152.1 µm. From unitary heights 0.5-0.6 (m/m) to the top of this sediment core, a graded substrate was formed with sediment particles between D_{50} =108.3 µm and D_{50} =52.8 µm. Tubes +$MP_{13}S_7$ and + MP_5S_5, with lower suspension density (ρ_{sus}<1270 kg/m^3), formed a graded substrate with the biggest particles deposited at the bottom (D_{50}=160.6µm) and the smallest at the top (D_{50}=66.1µm).

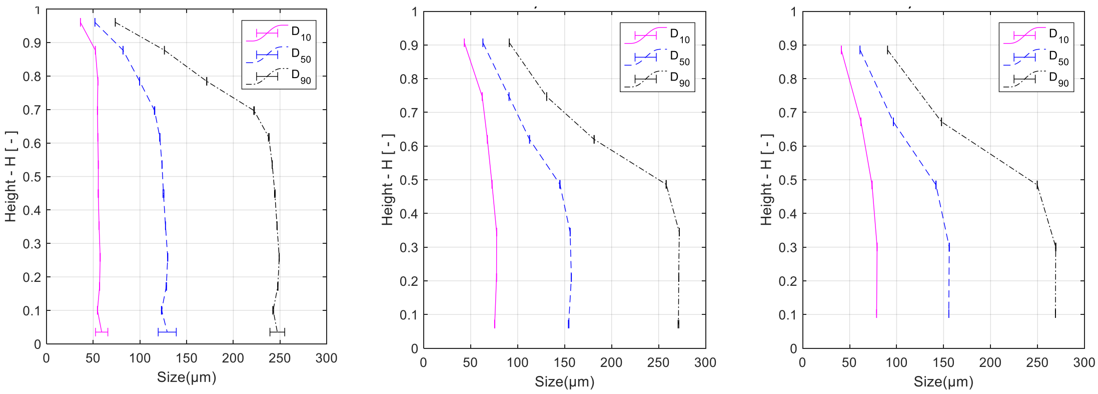

a) Mp_5S_{43}, 1739 kg/m^3 b) Mp_5S_{24}, 1504 kg/m^3 c) $Mp_{13}S_{16}$, 1407 kg/m^3

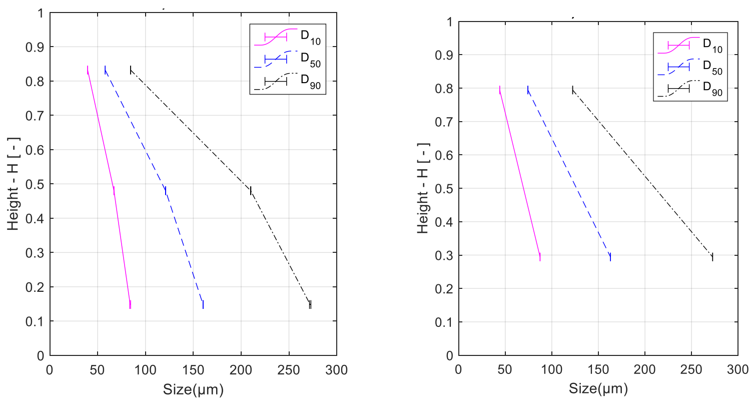

d) MpS_7, 1290 kg/m^3 e) Mp_5S_5, 1270 kg/m^3

Figure 4-4. Sediment particle size distribution of the five experimental settling tubes in the scenario with suspension densities between 1270 to 1739 kg/m^3, with positively buoyant microplastic particles. The plots show the sediment core's characteristic diameters of D10, D50, and D90.

The mixture layer formed at the sediment top layer of tube $+MP_5S_5$ (ρ_{sus}=1270 kg/m^3) (Figure 4-5), has a volume content of 1.04% microplastic, with an average microplastic size of D50 =640.01 µm. In addition, one microplastic particle was found to be deposited at the top sample of the tube $+MP_{13}S_7$ (ρ_{sus}=1290 kg/m^3).

Figure 4-5. Microplastic experimental tube MP_5S_5 (positively buoyant) top view sediment substrates with a microplastic volume content of 1.04%. Orange particles are microplastic deposited in the core.

II. Neutrally microplastic settling tubes

The second row of *Figure 4-3* shows the neutrally buoyant microplastic experimental scenarios with suspension densities between 1201 kg/m^3 and 1701 kg/m^3. Two microplastic layers were formed, one at the top of the fluid and a second above the sediment, with an average height of 0.0152 m. A sediment layer was formed at the bottom of the tubes MP_5S_{42}, MP_5S_{24}, and tube MP_5S_5, was formed of a mixed layer. The sediment-microplastic bottom deposit has a height between0.151 m to 0.197 m.

The sediment-microplastics particle size and volume distribution of the three neutrally buoyant experiments with variable suspension densities are shown in Figure 4-6. The settling tubes $\approx MP_5S_{43}$ and $\approx MP_5S_{24}$ formed an ungraded sediment substrate from the bottom to unitary heights 0.35-0.5 (m/m), with an equivalent diameter of D_{50} = 132.0 µm. From unitary heights of 0.35-0.5 (m/m) to the top, a graded sediment substrate was formed with particles between D_{50} =132.0 µm to D_{50} =52.9 µm. Tube $\approx MP_5S_5$, with the lower suspension density (ρ_{sus}=1201 kg/m^3), formed a graded substrate with the biggest particles deposited at the bottom (D_{50}=160.6µm) and the smallest at the top (D_{50}=89.7 µm). The settling tube $\approx MP_5S_5$ formed a mixed substrate with microplastic contents of 2.24% at the top and 0.15% at the bottom.

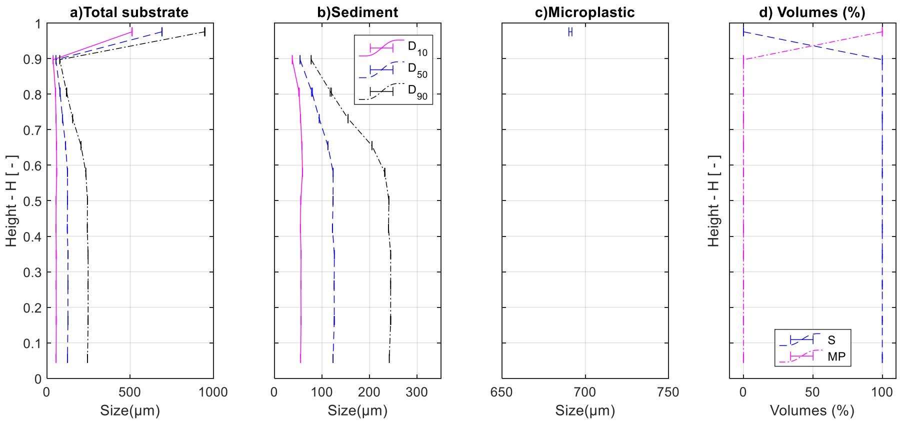

≈ MP_5S_{42}, ρ_{sus}= 1701 kg/m^3

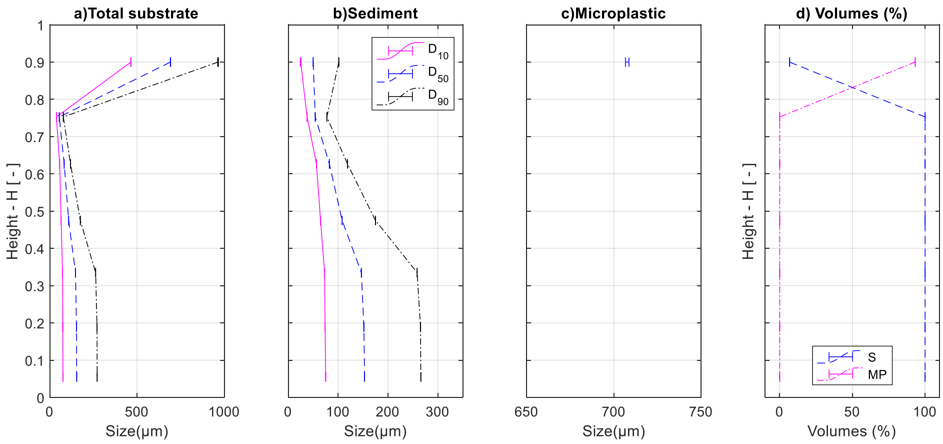

≈ MP_5S_{24}, ρ_{sus}= 1451 kg/m^3

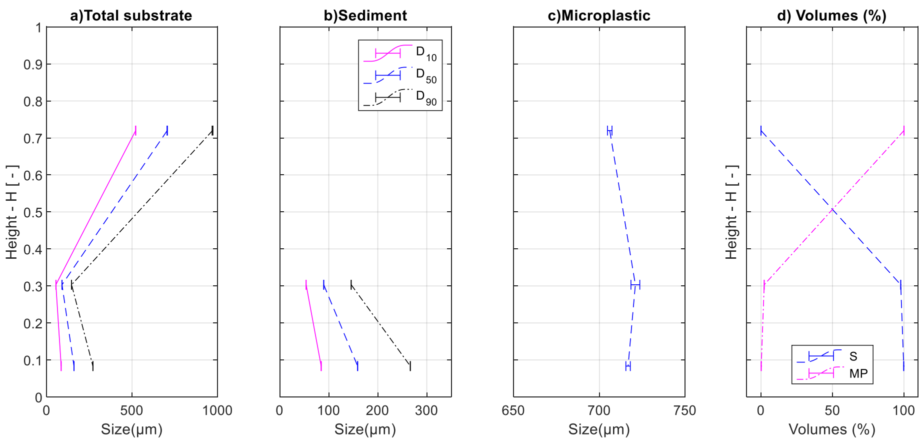

≈ MP_5S_5, ρ_{sus}= 1201 kg/m^3

Figure 4-6. Sediment and microplastic particle size and volume distribution of the three experimental settling tubes, scenario with suspension densities between 1201 and 1701 kg/m^3, with neutrally buoyant microplastic particles.

4.2.2. Discussion

The depositional structure formed in the settling tubes can be explained by the function of the particle interaction in the suspension. The settling regimes (free settling or hindered) are defined if a positively and neutrally bouyant microplastic can be deposit or not in the sediment substrate. The regime delimitation is based on the particle size distribution and the value of the suspension density. For a better undestanding of the settling regimes a numerical fall velocity analysis using the modified Davis and Gecol model (DG) by Cuthbertson (2008) it is included.

III. Fall velocity analysis

The particles fall velocity was estimated for all the settling tubes, considering all hindered effects such as return flow, increased viscosity, and buoyancy of the bimodal mixture (Cuthbertson et al., 2008). The velocity (W_s) was estimated using the contents of the microplastic, sediment, and fluid density for each settling tube, with the modified Davis and Gecol model (DG), with the correction proposed by Cuthbertson (2008) (Equation 2-3 to 2-6). The model needs a base fall velocity for a free settling particle, which was determined using Ferguson and Church (2004) (Equation 2.1.). The equation was applied in the range of size distribution selected for the clean material and studied in detail with the equivalent diameters. As this research has scenarios of rising, and sinking particles, it is considered a (+) positive base fall velocity (w_s) when the fluid density has a higher value than the density of the plastic ($\rho_f > \rho_{MP}$) and a (-) negative when the fluid density has a lower value than the density of the plastic ($\rho_f < \rho_{MP}$).

The modified Davis and Gecol model (DG) is shown in Figure 4-7 and Table 4.3 for the experimental tubes in the range of the characteristic diameters (D_{50} for microplastic and D_{10}, D_{50} and D_{90} for sediment). The velocity changes as a function of the suspension density and particle size distribution. In Figure 4-7, blue lines represent the sediment fall velocity; the dashed lines are settling tubes without microplastic particles in the sediment core(ρ_{sus}<1270 kg/m^3), the dash lines are the settling tubes that do not trap microplastics, showing the strong dependence on the settling fall velocities to trap microplastic particles.

The sediment DG fall velocity in the higher suspension densities (ρ_{sus}>1700 kg/m^3) shows values lower than -1x10^{-3}m/s regardless of size distribution, representing the effects of high particle interaction (Druit, 1995; Amy et al., 2006). The higher rising microplastic velocity (2.98-3.0x10^{-3}m/s) explains how the particles rise through the almost suspended sediment particles and can not get trapped in the sediment core.

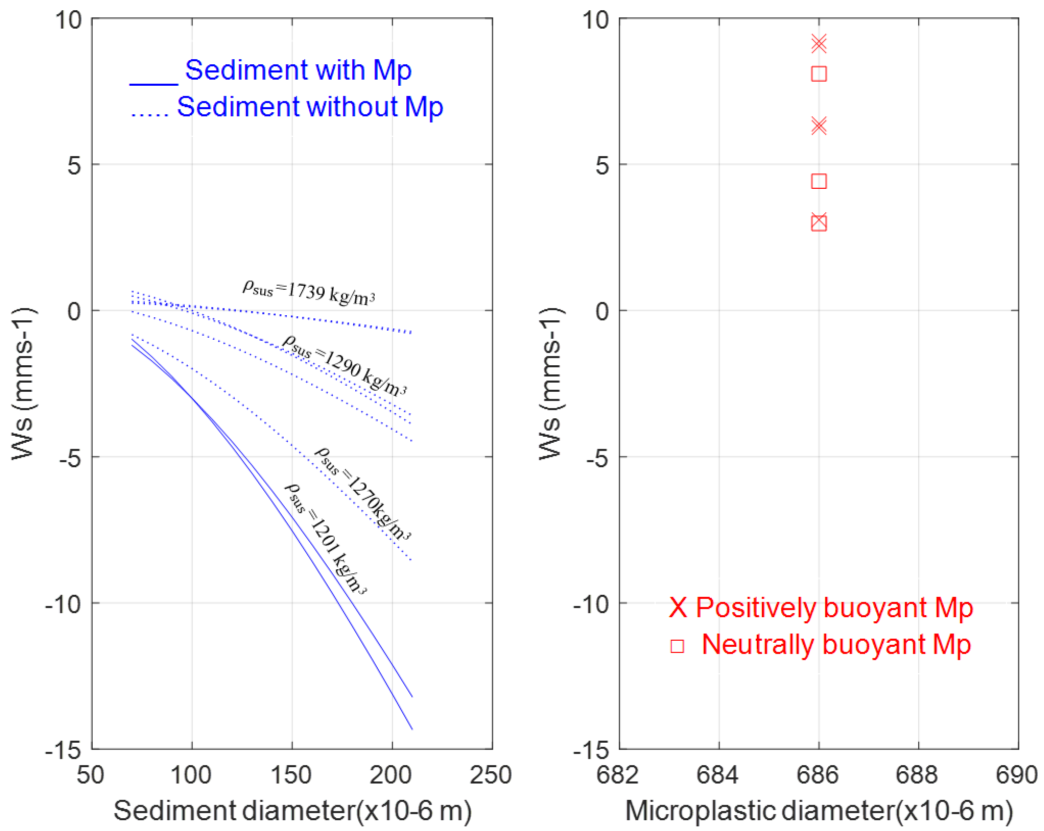

Figure 4-7. Estimated initial velocities for the 8 experimental settling tubes with variable suspension density, with fixed fluid densities. The continuous blue lines are the values for the sediment cores with microplastic, and the blue point line is the sediment cores without microplastics. The red "X" represents the positively buoyant microplastic, the squares represent the neutrally microplastic.

In the intermediate suspended concentrations (1407 kg/m^3<ρ_{sus}<1504 kg/m^3), the balances between the rising and fall velocities explains why the microplastic cannot get trapped in the sediment core. The higher neutrally-positively buoyant microplastics rising velocities W_{sMp}=6.29x10^{-3}m/s to 9.05x10^{-3}m/s, are fast enough to be trapped in the intermediate (D_{50})-bigger (D_{90}) sediment particles falling velocities (W_{ss}= -0.14 to -8.66x10^{-3}m/s). Explaining that any microplastic that was trapped in the sediment core is because the bed is built faster than the rising microplastic.

In the case of the settling tube +$MP_{13}S_7$ (ρ_{sus}=1290 kg/m^3) the microplastic velocity (6.29 x10^{-3}m/s) rise first than the sinking sediment D_{10} (-0.93x10^{-3}m/s) and D_{50} (-5.20x10^{-3}m/s). However, the D_{90} sediment settle faster (-8.66x10^{-3}m/s) than the rising microplastic, explaining the possible reason why this settling tube trapped 1 particle in the sediment core.

Table 4.3. Summary of the results for modified Davis and Gecol model for the 8 experimental settling tubes with variable suspension density (S: Sediment, Mp: microplastics).

Settling tube	**Fluid density (kg/m³)**	**Suspension density (kg/m³)**	**Hindered velocity (mm/s)** W_{SS} (1x10⁻³m/s) *D₁₀*	*D₅₀* s	*D₉₀*	W_{sMp} *D₅₀* (1x10⁻³m/s)	**Delta W_s =** W_{sMp} (D_{50})+ W_{SS} (D_{50})	**Volume MP in the mixture substrate %**
≈MP_5S_5	1120.2	1201	-1.16	-7.90	-14.45	4.42	-3.49	2.40
+MP_5S_5	1195.6	1270	-1.35	-7.85	-13.33	9.21	1.35	1.04
+$MP_{13}S_7$	1195.6	1290	-0.93	-5.20	-8.66	6.26	1.05	1 particle
+$MP_{13}S_{16}$	1195.6	1407	-0.10	-1.85	-4.51	6.38	4.53	0.00
≈MP_5S_{24}	1120.2	1451	0.60	-0.14	-3.94	8.09	7.96	0.00
+MP_5S_{24}	1195.6	1504	0.44	-0.34	-3.63	9.05	8.71	0.00
≈MP_5S_{43}	1120.2	1701	0.30	0.37	-0.80	2.98	3.34	0.00
+MP_5S_{43}	1195.6	1739	0.25	0.28	-0.74	3.10	3.38	0.00

For the lower suspension densities (ρ_{sus}>1270 kg/m^3), the sediment settles at the highest velocities (-1.16x10^{-3}m/s to -14.45x10^{-3}m/s), with a significantly difference between the characteristic equivalent diameters, explaining the creation of the graded substrate from Figure 4-4 and Figure 4-6 (free settling). The rising positively buoyant microplastics velocities (4.42x10^{-3}m/s and 9.21x10^{-3}m/s) are not fast enough than the sinking sediment, and get trapped in the sediment bed.

IV. Stratigraphy

Figure 4-8 and Figure 4-9 presented a diagram of the substrate's formation for the low and highest suspended concentrations settling tubes with positively and neutrally buoyant microplastics. The diagrams are based in the initial hindered velocities estimated (Davis and Gecol, 1994; Cuthbertson et al, 2008, Table 4.3), particles size, particle density and fluid density.

In the highest suspended concentration settling tubes with positively buoyant microplastics (ρ_{sus}>1407 kg/m^3; tubes +MP_5S_{43}, MP_5S_{24} and $MP_{13}S_{16}$; 29%< Φ_{S+Mp}<47%), the sediment substrate forms an ungraded substrate from the bottom to unitary heights 0.5-0.6 (m/m) (dimensionless of the depth of bed) and graded substrate at the top of the sediment core (*Figure 4-3*). At the beginning of the settling process all particles are distributed all over the water column (Time=0, Figure 4-8). The hindered effects slowdown or accelerates the particle velocities in the suspension (Time=1 and 2, Figure 4-8).

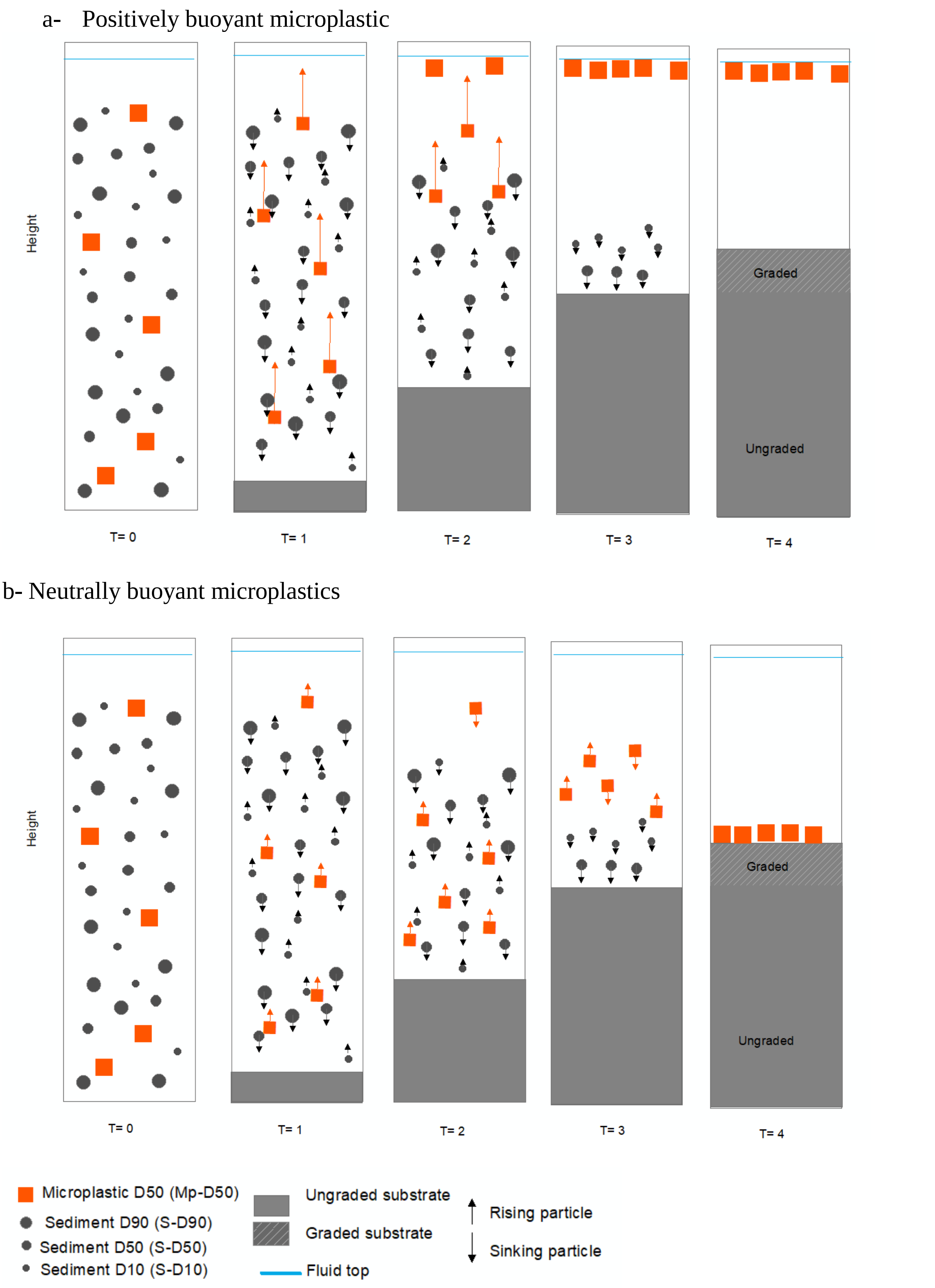

Figure 4-8. Schematic diagram of the formation of the sediment and microplastic substrates with hindered effects. The direction and magnitude of the arrows are based in the estimations of the hindered velocities by the modified Davis and Gecol model (Cuthbertson et al, 2008).

The sediment ungraded substrate is formed by the rising or sinking smallest- intermediate sediment particles characteristic diameters (D_{10} - D_{50}, Table 4.3) and the larger sinking sediment particles (D_{90}, Table 4.3). The graded substrates are formed in further steps (Time=3 and 4, Figure 4-8-a) with the remaining smallest-medium sediment particles. In this time step the hindered effects begin to dissipate, the remaining sediments settle because the fluid density is lower than the sediment. The initial suspension density conditions dictate the initial dynamics of the particles (hindered velocities, Table 4.3), and the final sedimentation is government by the fluid density (ρ_S=2500 kg/m^3> ρ_f=1195.6 kg/m^3). From the beginning to the end of experiments (Time=1 and 4, Figure 4-8-a) the positively buoyant microplastic rise faster through the sediment matrix and creates a top layer, and no positively buoyant microplastics can get trapped in the sediment core.

In the highest suspensions densities suspensions with neutrally microplastics (ρ_{sus}>1451 kg/m^3; tubes MP_5S_{43}, MP_5S_{24} ; 29%<Φ_{S+Mp}<47%), the sediments substrate formed a ungraded substrate at the bottom to dimensionless depth 0.35-0.5 (mm/mm) and graded substrates at the top of the sediment deposit (*Figure 4-6*). As it has been explained in the previous paragraph the hindered effects create the sediment ungraded substrates (Time=1 and 2, Figure 4-8-b) at the bottom, the graded substrates are formed in further steps (Time=3 and 4, Figure 4-8-b) with the remaining smallest-intermedium sediment particles. In the experiments the neutrally buoyant microplastics upwards through the sediment matrix, which cannot get trapped in the sediment core (Time=1 to 3, Figure 4-8-b). When the sediment bed is built, the microplastics sink above the sediment, because the fluid density is lower than the microplastic (ρ_{Mp}=1150 kg/m^3> ρ_f=1120.2 kg/m^3). The initial suspension density conditions dictate the initial dynamics of the particles (hindered velocities, Table 4.3), and the final sedimentation is government by the fluid density.

In the lower suspension density settling tubes (ρ_{sus}<1270 kg/m^3; tubes $+MP_5S_5$, $\approx MP_5S_5$; Φ_{S+Mp}=10%), the tubes formed graded substrates (*Figure 4-6* and *Figure 4-3*). In time step cero all the particles are in suspension (Figure 4-9). In time steps one to four (Figure 4-9) heavier particles fall first, followed by the medium and finally, the lighter ones, corresponding to a free settling regime (Richardson and Zaki, 1954; Druit, 1995; Amy et al., 2006; Guo et al., 2015). The falling sediments builds a deposit by trapping the rising microplastic (hindered velocities, Table 4.3) forming substrates with 1.04% to 2.4% microplastic content. The remaining positive buoyant microplastic rise (Figure 4-9-b) to the top of the fluid (ρ_{Mp}= 1050 kg/m^3< ρ_f=1195.6 kg/m^3). In the last steps (Time=4, Figure 4-9-a) the remaining neutrally buoyant microplastic can sink above the sediment substrate because its density is higher than the fluid (ρ_{Mp}=1150 kg/m^3> ρ_f=1120.2 kg/m^3).

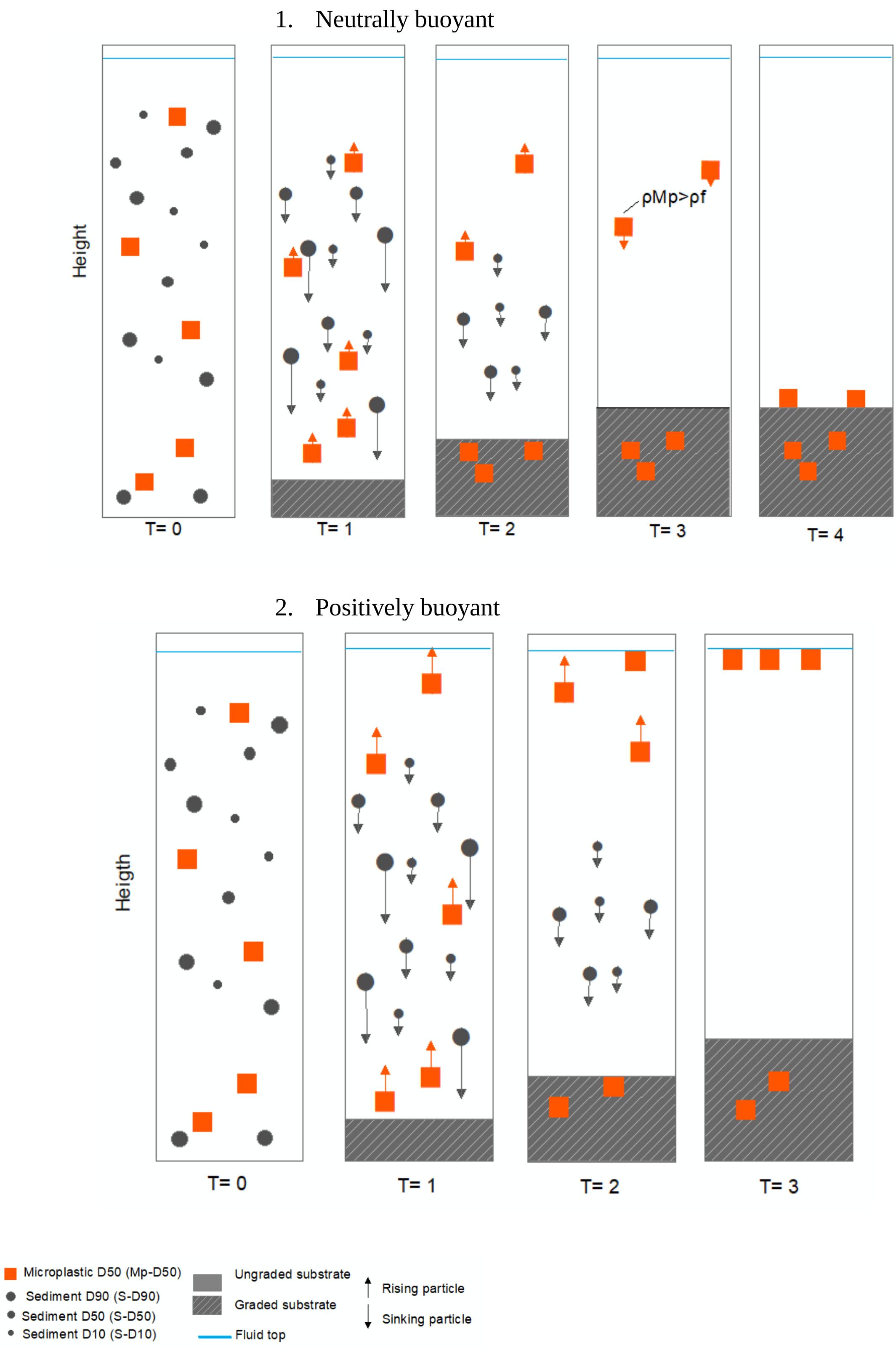

Figure 4-9. Schematic diagram of the formation of the sediment and microplastic substrates free settling. The direction and magnitude of the arrows are based in the estimations of the hindered velocities by the modified Davis and Gecol model (Cuthbertson et al, 2008).

The threshold were sediments-microplastics formed mixed substrates can be approximated between suspensions densities 1270 kg/m^3- 1290 kg/m^3. Here the lowest percentage of microplastics was trapped (1.04%) in tube +Mp_5S_5 (ρ_{sus} = 1270 kg/m^3) and one particle was trapped in the tube +$Mp_{13}S_7$ (ρ_{sus} = 1290 kg/m^3), highlighting a transition process where a difference of 10 kg/m^3 in the suspension density promotes the highest particle interactions, affecting the magnitudes of the initial velocities.

Analysing the settling tubes with variable suspension density determined that tubes with higher hindered effects cannot trap microplastic in the sediment core. The particle interaction in the suspension accelerates the rising velocities of the neutrally and positive microplastics, and decelerates the sediment fall velocities (Davis and Gecol, 1994; Cuthbertson et al, 2008). The microplastic's rising velocities are fastest than the sediment falls velocities, the sediment bed is built first and no microplastic is trapped suspensions (Figure 4-8). Opposite, the settling tubes in a free settling regime can trap microplastic in the sediment core. The particle interaction is not strong enough, and particles fall in a free settling. The sediment falls faster than the rising neutral-positive microplastics, trapping the microplastic particles in the sediment bed (Davis and Gecol, 1994; Cuthbertson et al, 2008).

The initial suspension density fractionates the microplastics regardless the fluid density, so its dynamics are essentially equivalent until all sediment deposited. The first eight settling tubes with variable suspension density defines the characterisation of hindered and free-settling suspension effects for neutrally and positively buoyant microplastics. The microplastics trapped in the sediment bed are expected to be a product of suspended concentrations in a free settling regime. For this reason, the second part of this experimental tubes focus on the additional effects of the sediment-microplastics substrates formation with lower concentrations in a free settling regime, representing more realistic suspended concentrations found in the environment.

Fixed suspension densities characterise the next 18 settling tubes for each buoyant condition. Designed to consider solely the free settling regime, expanding the results to different plastic densities and concentrations more representative of riverine environments. The fixed suspension densities scenario has three target suspension densities: 1052 kg/m^3, 1152 kg/m^{3}and 1227 kg/m^3:

- Six tubes with negatively buoyant microplastic, constant suspension density 1052 kg/m^3.
- Six tubes with neutrally buoyant microplastic, constant suspension density 1152 kg/m^3.
- Six tubes with positively buoyant microplastic, constant suspension density 1227 kg/m^3.

The results and discussion of this 18 settling tubes are presented in the following section 4.3.

4.3. Fixed suspension density

4.3.1. Results

Figure 4-10, shows the pictures of the 18 experimental tubes. Layers were formed with only microplastic or sediment or a mixture of microplastic-sediment. The results of each settling tube's stratigraphy and volume is described as a function of suspension density and microplastic buoyancy. Appendix 7 includes the estimations of the volumes analysis of the 18 settling tubes.

The particle size distribution was not analysed in this set of experiments. As demonstrated in Chapter 3 and Section 4.2. the settling tubes with a volumetric content lower than 10% are in a free settling regime, forming a graded substrate. Therefore, these settling tubes have lower volumetric content than 5.1% to secure a graded particle size distribution and focus the results on the microplastic volumetric content trapped in the sediment bed.

Positively buoyant microplastic

Name	$+MP_{2.0}S_{2.4}$	$+MP_{2.0}S_{2.8}$	$+MP_{2.0}S_{3.1}$	$+MP_{0.5}S_{2.4}$	$+MP_{0.5}S_{2.8}$	$+MP_{0.5}S_{3.1}$
Height of the bottom substrate	0.010 m	0.011 m	0.0104 m	0.0092 m	0.0113 m	0.0121 m

Neutrally buoyant microplastic

Name	$\approx MP_{2.0}S_{2.4}$	$\approx MP_{2.0}S_{2.8}$	$\approx MP_{2.0}S_{3.1}$	$\approx MP_{0.5}S_{2.4}$	$\approx MP_{0.5}S_{2.8}$	$\approx MP_{0.5}S_{3.1}$
Height of the bottom substrate	0.010 m	0.0173 m	0.0182 m	0.0104 m	0.0118 m	0.0132 m

Suspension density = 1152 kg/m^3

**Figure continues in the next page*

Negatively buoyant microplastic

Name	$MP_{2.0}S_{2.4}$	$MP_{2.0}S_{2.8}$	$MP_{2.0}S_{3.1}$	$MP_{0.5}S_{2.4}$	$MP_{0.5}S_{2.8}$	$MP_{0.5}S_{3.1}$
Height of the bottom substrate	0.0165 m	0.0220 m	0.0167 m	0.0109 m	0.0180 m	0.0135 m
Suspension density = 1052 kg/m^3						

Figure 4-10. Substrates formed in the 18 settling experimental tubes, with constant suspension density and variable fluid densities. The first rows show the results of the buoyant microplastics, the second rows for the neutrally microplastics and third row for the negatively buoyant microplastics. The orange particles are the microplastic, and the bottom white ones are the sediments.

I. Positively buoyant microplastic settling tubes

The first row (Figure 4-10) shows the positively buoyant microplastic experimental tubes with a fixed suspension density ρ_{sus}= 1227 kg/m^3. A top finer layer of microplastic was formed in all tubes at the top of the fluid, and a sediment-microplastic mixture layer was formed at the bottom, with a height between 0.0100 m to 0.0121 m.

The microplastics and volume distribution of the settling tubes with a constant suspension density (ρ_{sus}=1227 kg/m^3) is shown in Figure 4-11. The six settling tubes trap positively buoyant microplastic in the sediment core, the higher content of microplastics the higher percentages get trapped. Tubes with initial microplastic volumes 0.5% (+$MP_{0.5}S_{2.4}$, +$MP_{0.5}S_{2.8}$, +$MP_{0.5}S_{2.8}$) form mixtures layers with microplastic contents between 2.77±0.69% to 8.08±7.62%. Tubes with 2% initial microplastic volume ($MP_{0.5}S_{2.4}$, +$MP_{0.5}S_{2.8}$, and +$MP_{0.5}S_{2.}$) formed a mixed substrate with more microplastic volumes between 4.00±1.07% to 22.18±4.72%.

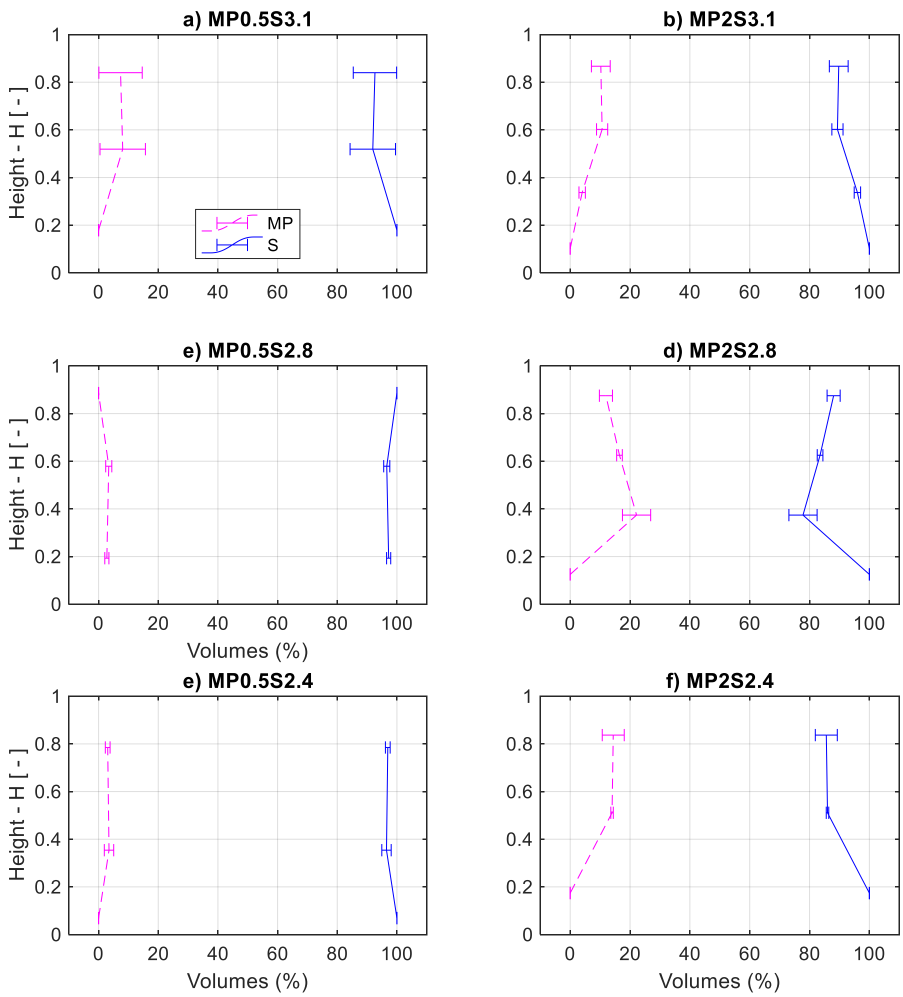

Figure 4-11. Microplastic and sediment volume distribution in the substrate within in the positively buoyant microplastic settling experiments with constant suspension density (ρ_{sus}= 1227 kg/m³). The dashed line represents the microplastic, and the continuous line is the sediment.

II. Neutrally microplastic settling tubes

The second row Figure 4-10, shows the neutrally buoyant microplastic experimental tubes with a suspension density ρ_{sus}= 1152 kg/m^3. A thin layer of only microplastic was formed at the top of the fluid and above the sediment core. The bottom core formed mixtures of sediment and microplastic with a height between 0.0100 m to 0.0182 m.

The volume distribution of the neutrally buoyant microplastic with a constant suspension density (1152 kg/m^3) is shown in Figure 4-12. Tubes with 0.5% initial microplastics volumes (≈ $MP_{0.5}S_{2.4}$, ≈ $MP_{0.5}S_{2.8}$, and ≈ $MP_{0.5}S_{3.1}$), contain microplastic percentages between 11.33±3.46% and 21.8±14.4%, with the highest value between unitary heights, 0.4-0.6 mm/mm. Tubes with 2% initial microplastic volumes (≈ $MP_2S_{2.4}$, ≈ $MP_2S_{2.8}$, and ≈ $MP_2S_{2.4}$) formed layers with microplastic content between 6.11±1.29% and 20.6%±7.05%, with the highest values measured at the top layer. Tubes with a lower amount of sediment (2.4%) (≈ $MP_{0.5}S_{2.4}$ and ≈ $MP_2S_{2.4}$) did not form a microplastic layer at the top of the sediment core. The microplastic was not well distributed; it was observed to be accumulated in the middle, with differences around up to 14.4% compared with the extremes sides of the sample.

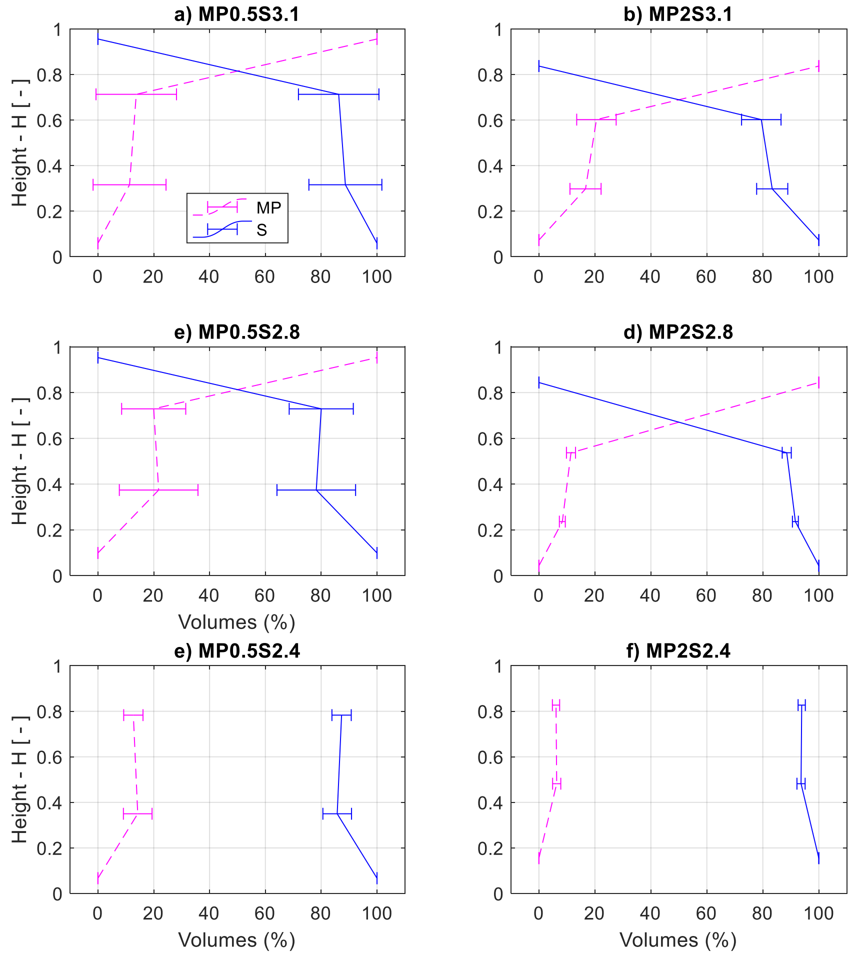

Figure 4-12. Microplastic and sediment volume distribution in the substrate formed in the neutrally buoyant microplastic settling experiment tubes with a constant suspension density (ρ_{sus}= 1152kg/m^3). The dashed line represents the microplastic, and the continuous line is the sediment.

III. Negatively buoyant microplastic

The final row in Figure 4-10, shows the negatively buoyant microplastic experimental tubes with a suspension density ρ_{sus}= 1052 kg/m^3. The deposit was formed of different layers of only microplastic, sediment, or mixtures, with heights between 0.0109 m to 0.022 m.

Figure 4-13, shows the volume distribution of the negatively buoyant microplastic with constant suspension density (1052 kg/m^3). The stratigraphy can be described as only a sediment layer deposited at the bottom, microplastic layers at the top (except tube $MP_2S_{2.8}$) and a mixture layer deposited in the middle of the core. The lowest microplastic concentration ($MP_{0.5}S_{2.4}$, $MP_{0.5}S_{2.8}$, $MP_{0.5}S_{3.1}$) creates the lowest mixture layers with contents between 9.81±1.04% to 23.2±26.9% of microplastic. Tubes with higher microplastic content ($MP_2S_{2.4}$, $MP_2S_{2.8}$, $MP_2S_{3.1}$) create mixture layers with higher microplastic volumes, between 23.2±2.1% to 52.7±0.8%. The microplastic was observed to accumulate in the middle, with 26.9% more microplastic than on the extreme sides.

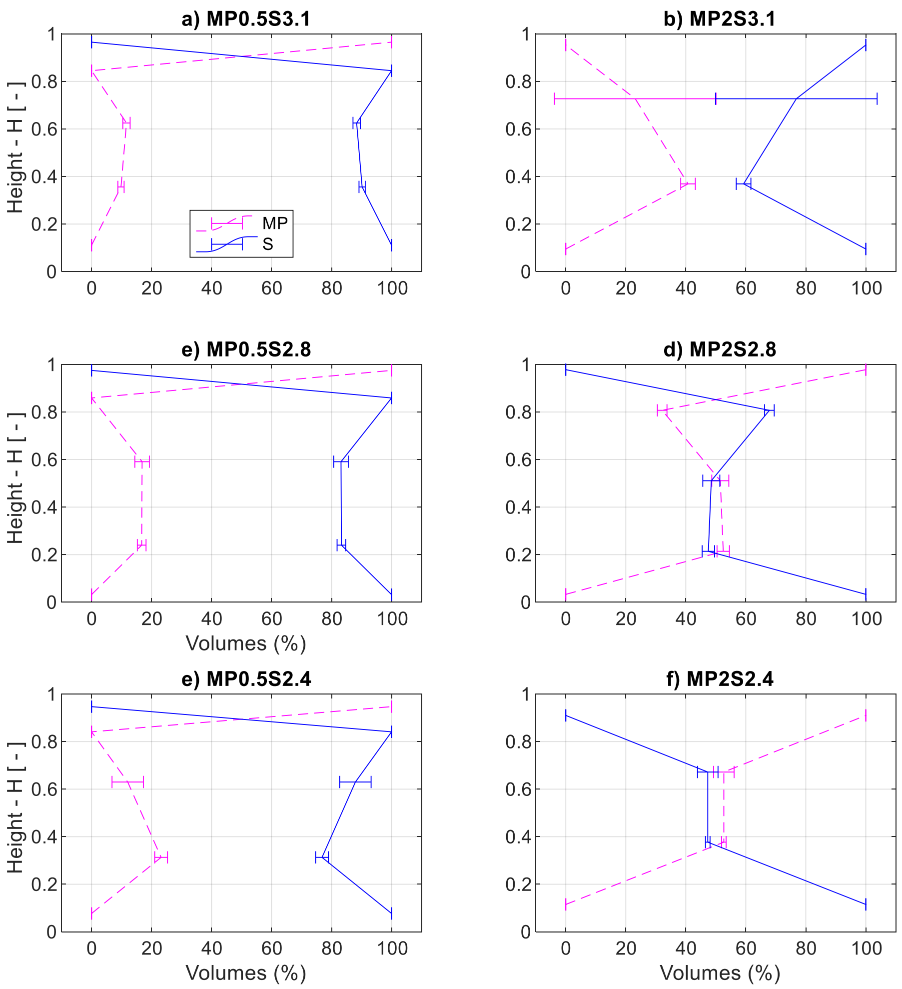

Figure 4-13. Microplastic and sediment volume distribution in the substrate formed in the negatively buoyant microplastic settling experiment with a constant suspension density (ρ_{sus} = 1052 kg/m^3).

Finally, Figure 4-14 summarises a diagram of the stratigraphy formed in the 18 tubes with a constant suspension density. The presence of microplastic particles in the sediment substrate can be observed regardless of its density at different depths. The negatively buoyant microplastics have the highest amounts of microplastics (10.72±1.42% to 52.2±2.28%), followed by the neutrally (6.23±1.24 to 20.9±11.0) and positively buoyant microplastics (3.09±0.86 to 16.9±5.17).

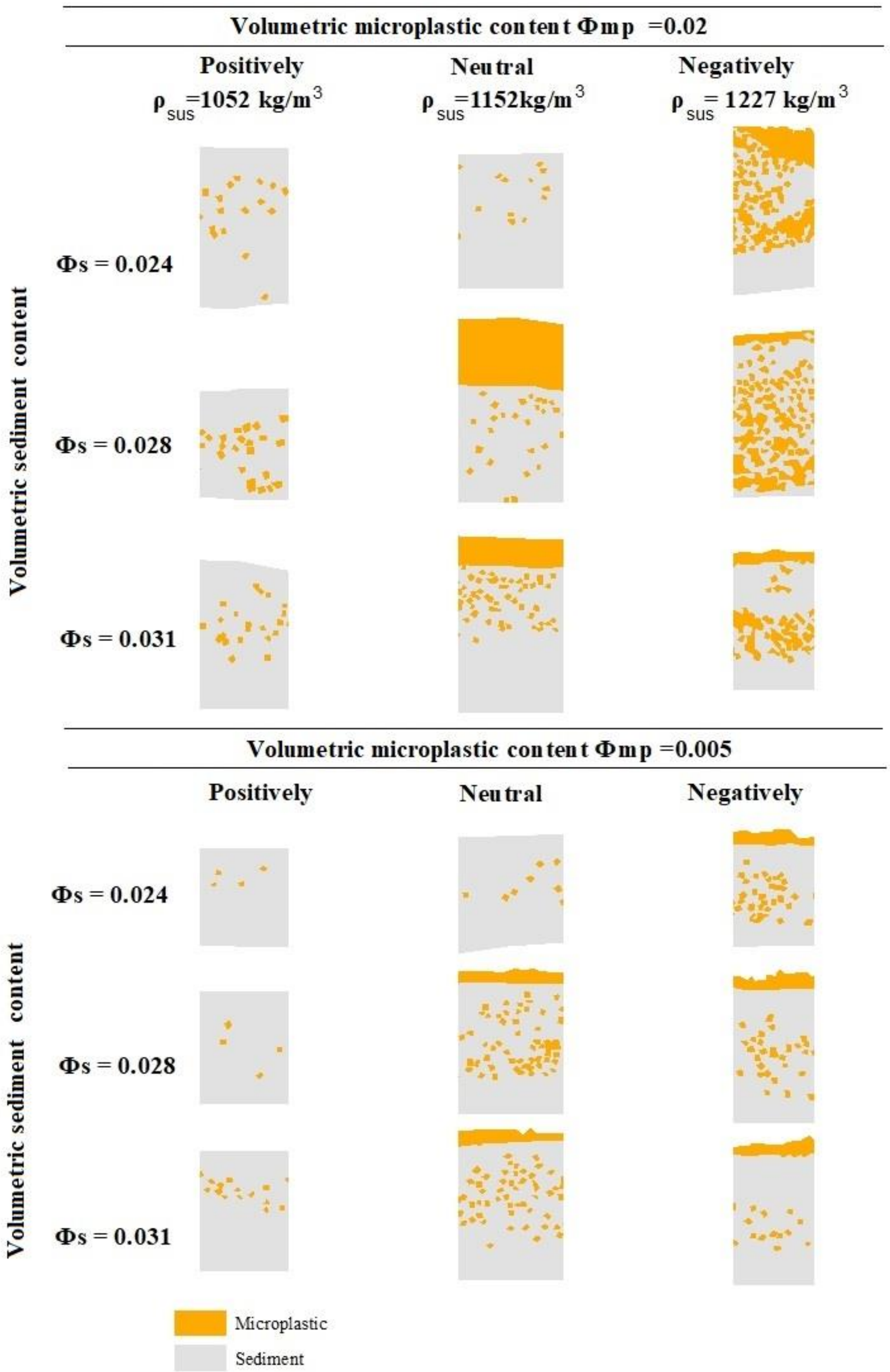

Figure 4-14. Schematic diagram of the stratigraphy formed in the 18 tubes with positively, neutrally, and negatively buoyant plastics with constant suspension density.

4.3.2. Discussion

The depositional structure formed in the settling tubes can be explained by the function of the particle interaction in the suspension. All the sediments cores contains microplastics, suggesting the suspended concentrations were in a free settling, as it was discussed and explained in Seccion 4.2.2. For a better undestanding the modified Davis and Gecol model (DG) by Cuthbertson (2008) was also included for this settling tubes analysis.

I. Fall velocity analysis

The particles fall velocity was estimated for all the settling tubes, with the modified Davis and Gecol model (DG), with the correction proposed by Cuthbertson (2008) (equation 2-3 to 2-6). The base fall velocity for a free settling particle was determined using Ferguson and Church (2004) (equation 2.1.). The equation was applied to sediments and microplastics equivalent diameters. A (+) positive base fall velocity (w_s) describes rising and a (-) negative sinking fall velocities.

The modified Davis and Gecol model (DG) is shown in *Figure 4-15* tubes in the range of the characteristic diameters (D_{50} for microplastic and D_{10}, D_{50} and D_{90} for sediment), blue lines represent the sediment fall velocity and the red symbols represents the microplastics.

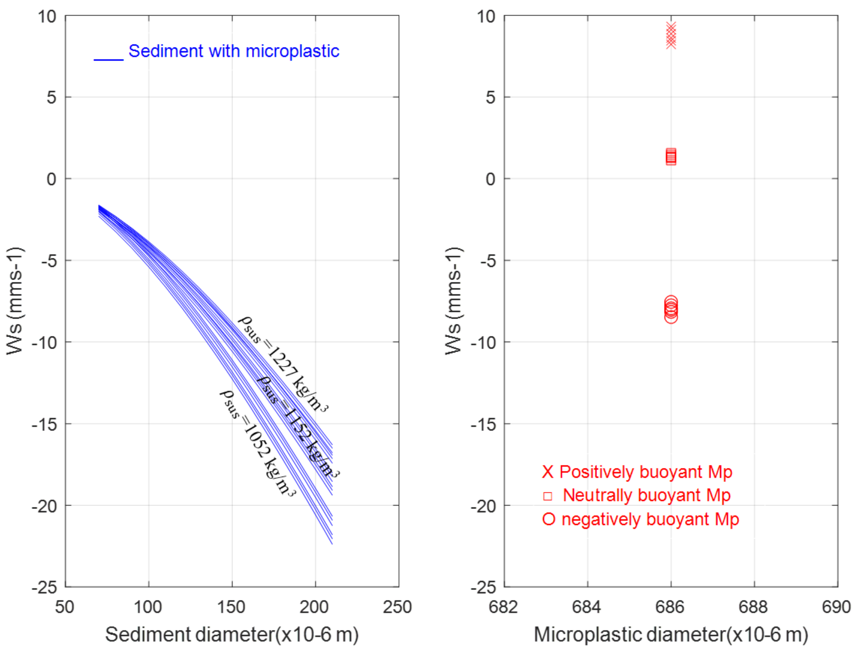

Figure 4-15. Estimated settling velocities for the 18 experimental settling tubes with constant suspension density and variable fluid density. The continuous blue lines are the values for the sediment cores. The red "X" represents the positively buoyant. microplastic, the squares represent the neutrally microplastic, and the "O" represent the negatively buoyant.

Table 4.4. shows the rising-settling velocities for the modified Davis and Gecol model (DG) in the range of the characteristic diameters. To relate fall velocity to the microplastic percentages deposits and suspension density, the differences between sediment and microplastics D_{50} fall velocities were included in the analysis, described as $\Delta W_s = W_{sMp}\ (D_{50}) + W_{sS}\ (D_{50})$.

Table 4.4. Summary of the results for the 18 experimental tubes with constant suspension density and variable fluid density (S: Sediment, Mp: microplastics).

Settling tube	**Fluid density (kg/m³)**	**Suspension density (kg/m³)**	**Hindered velocity (x10⁻³m/s)**				**Delta W_s = W_{sMp} (D_{50})+ W_{sS} (D_{50})**	**Volume MP in the mixture substrate %**
			W_{sS}			W_{sMp}		
			D_{10}	***D_{50}***	***D_{90}***	***D_{50}***		
$MP_{0.5}S_{2.4}$	1014.6	1052	-2.58	-14.1	-22.6	-8.47	-22.60	17.6
$MP_{0.5}S_{2.8}$	1009.1	1052	-2.42	-13.6	-22.2	-8.16	-21.80	16.8
$MP_{0.5}S_{3.1}$	1004.9	1052	-2.30	-13.3	-22.0	-7.94	-21.23	10.7
$MP_{2.0}S_{2.4}$	1012.5	1052	-2.23	-12.9	-21.4	-8.03	-20.97	52.2
$MP_{2.0}S_{2.8}$	1006.8	1052	-2.07	-12.5	-21.1	-7.75	-20.22	45.4
$MP_{2.0}S_{3.1}$	1002.6	1052	-1.96	-12.1	-20.8	-7.55	-19.67	31.9
$\approx MP_{0.5}S_{2.4}$	1117.8	1152	-2.26	-12.2	-19.5	1.30	-10.90	13.5
$\approx MP_{2.0}S_{2.4}$	1117.3	1152	-2.13	-11.6	-18.7	1.12	-10.49	6.23
$\approx MP_{0.5}S_{2.8}$	1112.7	1152	-2.12	-11.8	-19.2	1.46	-10.32	20.9
$\approx MP_{2.0}S_{2.8}$	1112.1	1152	-1.99	-11.2	-18.4	1.26	-9.93	9.92
$\approx MP_{0.5}S_{3.1}$	1108.8	1152	-2.01	-11.5	-19.0	1.56	-9.91	12.5
$\approx MP_{2.0}S_{3.1}$	1108.2	1152	-1.89	-10.9	-18.2	1.35	-9.53	18.6
$+MP_{2.0}S_{2.4}$	1195.9	1227	-2.07	-10.8	-16.9	8.23	-2.54	14.2
$+MP_{0.5}S_{2.4}$	1195.2	1227	-2.05	-11.0	-17.6	8.87	-2.09	3.27
$+MP_{2.0}S_{2.8}$	1191.1	1227	-1.94	-10.4	-16.6	8.45	-1.93	16.9
$+MP_{2.0}S_{3.1}$	1187.4	1227	-1.85	-10.1	-16.4	8.62	-1.48	8.30
$+MP_{0.5}S_{2.8}$	1190.4	1227	-1.92	-10.6	-17.3	9.12	-1.45	3.1
$+MP_{0.5}S_{3.1}$	1186.8	1227	-1.83	-10.3	-17.1	9.32	-0.98	7.72

The modified Davis and Gecol model (DG) predicted the initial rising and sinking velocities of the particles in the settling tubes. From this results schematics diagrams were made to explain the build bed in the settling tubes (Figure 4-16).

The sediment fall velocities settles in a free settling regime, with a significant difference between the velocities of the characteristic equivalent diameters (-1.96×10^{-3} m/s to -22.6×10^{-3} m/s.). Potentially explaining the creation of a graded substrate, where the particle interaction in the suspension is not strong enough, the heaviest particle falls first, followed by the medium and lowest (Druit, 1995; Amy et al., 2006).

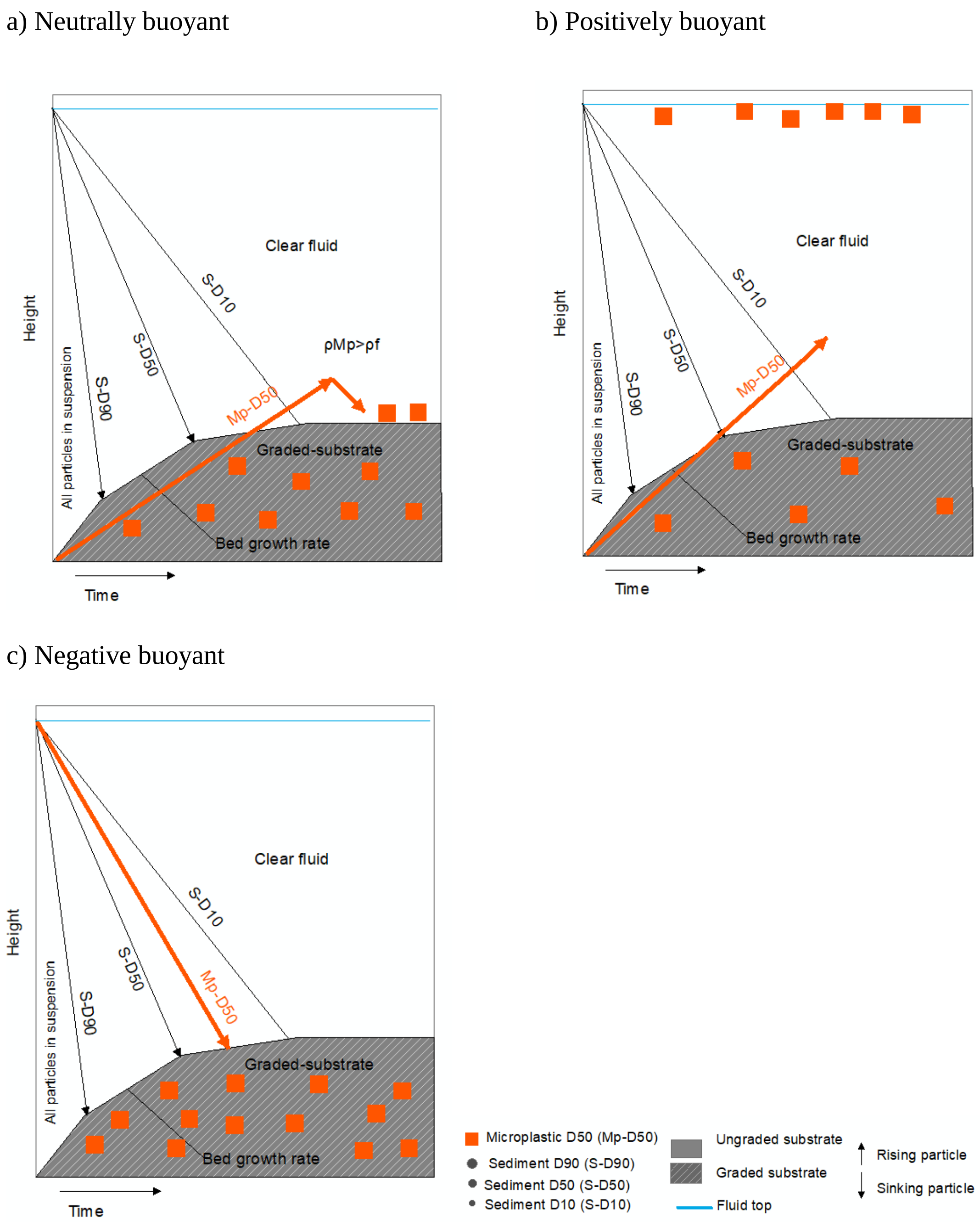

Figure 4-16. Schematic diagram of the formation of the sediment and microplastic substrates free settling. The direction and magnitude of the arrows are based in the estimations of the hindered velocities by the modified Davis and Gecol model (Cuthbertson et al, 2008).

For the neutrally microplastic (Figure 4-16-a), the lower rising velocities (1.12-1.56x10^{-3} m/s) are not faster than the falling sediment (-1.89x10^{-3} m/s to -19.5x10^{-3} m/s) and get trapped in the sediment core. The falling sediment particles build the bed and trap the neutrally microplastics, forming mixed substrates with microplastic contents from 0.15% to 22%. The relatively constant rising speeds can explain the unclear pattern of the neutrally microplastic particles in the sediment core (Figure 4-14) and why the microplastics were observed to be trapped in the middle and top of the deposits. When the sediment bed is built, the microplastics sink above the sediment. The initial suspension density conditions dictate the initial dynamics of the particles (Table 4.4), and the final sedimentation is government by the fluid density ($\rho_{Mp}>\rho_f$).

In the case of positively buoyant microplastics (Figure 4-16-b), the sinking sediment (1.83 x10^{-3} m/s to-17.6 x10^{-3} m/s) build the bed fast enough to trap the rising microplastics (+8.2 to +9.3 mm/s). The falling sediment particles trap the positively buoyant microplastics and form mixed substrates with microplastic contents from 3.1% to 14.2%. Higher amounts of microplastic and sediment promotes a greater concentration of plastic trapped in the half of the deposit.

The negatively buoyant microplastic, the particles settle at -7.5 to -8.5x10^{-3} m/s, sharing fall velocities with the sediment particles (-1.96 to -22.65x10^{-3} m/s) (Figure 4-16-c). Creating mixed substrates with microplastic contents from 9.81±1.04% to 52.7±0.8%. Explaining the formation of the mixture's substrates, the accumulation of more microplastics in the middle of the sediment core, and why as the settling tubes contain more microplastics and sediment, more microplastics can be deposited in the sediment core. The sediment armours all the microplastic in the bed, a phenomenon important for the long-term storage of the microplastic in the river bed. The top microplastic layer measured above the sediment (Figure 4-10), corresponded to the final sedimentation of the microplastics particles government by the fluid density.

The modified DG shows how sensitive the fall velocity is to the initial volumetric contents. Explaining the diverse stratigraphy (Figure 4-14) and the microplastic volumes trapped in the sediment in the settling tubes. The higher rising velocities of the positively buoyant microplastics, promotes less microplastics storages, in compared with the intermediate rising velocities of the neutrally buoyant microplastics. The negative buoyant microplastics stored higher amounts of microplastics, because they settle at similar fall velocities.

The substrates formed are a consequence of the initial suspension density, fluid density and particle density. The initial substrates formation dynamics are essentially equivalent until all the sediment is deposited. The positive buoyant microplastic not stored in the river bed rises to the top of the fluid. The microplastics top layer over the bed is formed after all the sediments are deposits, with the microplastics that were not stored in the bed and have a higher density than the fluid. The negatively buoyant microplastic initial deposit is formed by initial suspension conditions. The suspension density is so light that it fractionates the microplastic regardless of the fluid density.

4.4. Substrate formation, stratigraphy, and definition of settling regimes

From the stratigraphy and fall velocities analysis presented in Sections 4.2. and 4.3. the definition of the settling regimes can be described as a function of the suspension density. The definition of the settling regime is also based on prior work into concentrations of settling fluxes (Druit, 1995; Amy et al., 2006; Dorrell and Hogg, 2010; Guo et al., 2015), the fall velocity analysis and the gravitational forces balances in the suspension (Phillips and Smith, 1971; Cuthbertson et al.; 2008; Lick, 2009). The names selected are based on the suspension density, summarised in Figure 4-17 and described as:

Low suspended concentrations: Suspended concentrations with suspended density lower than 1270 kg/m^3

The microplastics and sediment particles are in the free settling regimes (Druit, 1995; Amy et al., 2006), where the interaction of the particles in the suspension is not strong enough, and heavier particles fall first, followed by the medium and finally the small ones. The plastic particles can be deposited or trapped in the sediment core, forming mixtures of microplastics and sediment. The stratigraphy formed depends on the volume, size distribution, and plastic density. The neutrally-positively microplastic get trapped in the sediment core, because the sediment fall velocities are faster than the rising microplastic. The negatively buoyant microplastics created mixtures of substrates because both particles can settle at similar fall velocities.

High suspended concentrations: Suspended concentrations with suspended density higher than 1270 kg/cm^3

The sediment substrate formed ungraded substrate at the bottom and graded substrates at the top of the sediment core influenced particles interaction in the suspension. The hindered effects of the particle's interaction in the suspension slows the sediment deposition and accelerates the rising velocities of the microplastics (Davis and Gecol, 1994; Cuthbertson et al, 2008). As an result, the sediment fall velocity is not sufficiently fast to trap the rising microplastics. The positively buoyant microplastics rise to the fluid top.. The neutrally microplastics can rise or float, then sink in the sediment in the later stages of the settling process when the particle's interactions process are dissipated.

<table>
<tr><td colspan="2">Settling process of suspended concentrations of microplastic and sediment</td></tr>
<tr><td>Low suspended concentrations
Suspended density lower than 1270 kg/cm^3
ρ_{sus} <1270 kg/cm^3</td><td>High suspended concentrations
Suspended density higher than 1270 kg/cm^3
ρ_{sus}>1270 kg/cm^3</td></tr>
<tr><td>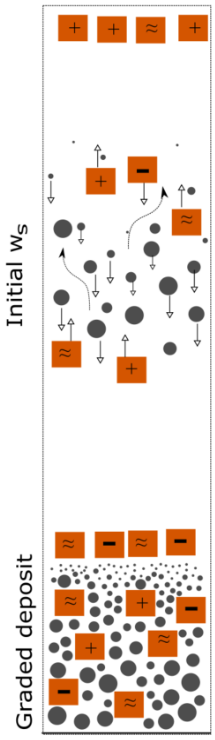
</td><td>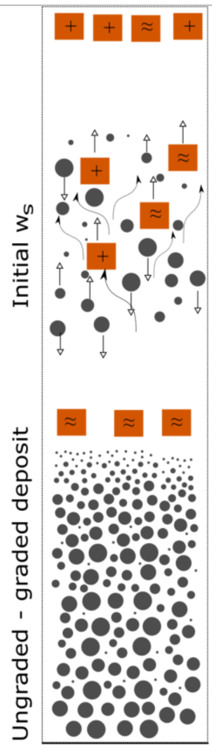
</td></tr>
<tr><td>Sediment particles fall in a free settling regime.

Microplastic particles can form mixtures of microplastics and sediment.

The sediment falls velocities built the deposit more quickly than rising microplastics, thus the neutrally-positively buoyant microplastics can get trapped in the sediment.

The negatively buoyant microplastics form mixed substrates because both particles can settle at similar velocities.

The positively microplastic not storages in the bed rise to the top of the fluid.

Depending on the fluid density, the neutrally buoyant microplastics can sink to the top of the sediment deposited. ρ_{Mp}>ρ_f.

The stratigraphy formed depends on the volume, size distribution, fluid density and plastic density.</td><td>The particle's interaction in the suspension slows down the sediment deposition and accelerates the rising velocities of the neutrally-positively buoyant microplastics.

The sediment deposition rate is not fast enough to trap the rising neutrally or positively buoyant microplastics.

The neutrally-positively buoyant microplastics rise to the top of the fluid across the sediment and form suspended microplastic layer.

Depending on the fluid density, the neutrally.

buoyant microplastics can sink to the top of the sediment deposited. ρ_{Mp}>$\rho_{f.}$

The stratigraphy formed depends on the volume, size distribution, fluid density and plastic density.</td></tr>
</table>

Figure 4-17. Settling regimes of neutrally, negatively and positively microplastic particles in function of the suspended density.

4.5. Interpretation of the results in the field and research question

From settling regimes, it can be explained one of the physical parameters that controls the vertical distribution in calm water of the microplastic pollution in sedimentary deposits is the concentration of particles in the suspension. It is inferred that in hindered settling regime the neutrally and positively buoyant microplastics cannot get trapped in the sediment layers. The neutrally microplastic can be found deposited above the sediment, because they were positive buoyant in the initial suspension and then they are negative buoyant in the ambient fluid after sediment deposit. In a free settling regime, positively, negatively, and neutrally microplastic particles can be found in the sediment bed. The microplastic deposition in the settling tubes in function of the suspension density agrees with the observations of mixtures of positively, neutrally, and negatively buoyant plastics deposited in the real -world sediment beds regardless of the sampling depth (Mao et al.; 2021; Zhou et al., 2021).

Studies of microplastic pollution in sediments lack consistent methods for sampling in the field (Correia et al., 2019). Results typically describe the microplastic deposition in rivers without unclear behaviour of the spatial distribution patterns (Martin et al., 2017; Hurley et al., 2018; Dikareva and Simon, 2019; Fan et al., 2019; Jiang et al., 2019; Chouchene et al., 2021; Lin et al., 2021; Saarni et al., 2021). The settling tubes stratigraphy results of this research helps to clarify that one of the parameters to control the deposition of microplastic particles in rivers is the suspension density. A parameter defined by the volumetric concentrations, size, and density of the materials,

The results presented in this chapter thesis confirms that also the positively and neutrally buoyant microplastics particles can be storaged in the sediment bed. As it was mention in Chapter 3, this limits the mobilisation by the river flows thus impacts transport potential and enhances long-term storage. The microplastic storages in the sediment bed has implications in estimating the amount of microplastic transported to Oceans from the river environment.

The dynamics of a suspended mixture of microplastic and sediment depends on whether particles are affected by free settling or hindered settling , and have a strong dependence on the physical characteristics of the materials. A practical rule to determine whether the microplastic particle was government by a free settling or hindered settling effects, for the wide range of microplastic densities, shapes, sizes, and aggregation processes is to include the study of the particle size distribution in the sediment samples. From the experimental results, the sediment and microplastic particle size distribution (graded-ungraded) define the settling regime and can be used to study the depositional process of microplastic pollution.

4.1. Conclusions

The experimental settling process of microplastic and sediment mixtures: positive-neutrally buoyant and constant suspension density chapter studies settling dynamics and depositional processes of microplastic in the sediment bed in calm water. Experiment comprised 26 settling tubes with positively, neutrally and negatively buoyant microplastic to cover the plastic range found in the environment. Different volumes of nylon pellets (ρ_{MP} = 1150 kg/m^3, D_{50}=686±2.4µm), sediments (ρ_s = 2500 kg/m^3, D_{50}=105±0.2µ) and saline solutions (1002.6 kg/m^3$< \rho_f <$1195.6 kg/m^3) were added to each experimental tube. The settling tubes formed sediment substrates with and without microplastics. The threshold was determined as a function of both the initial suspension and final fluid density. The physics characteristics of the materials defined if the suspended particles are in a free settling or hindered settling effects.

Settling tubes with suspended density lower than 1270 kg/m^3 were defined in suspended concentrations in a free settling regime, where negatively, positively and neutrally buoyant microplastic was deposited in the sediment substrate. Particles in the suspension fall or rise as individual particles. Denser-bigger particles fall first following the medium, smallest and lighter-bigger particles rise first following the medium, smallest. Under the experimental conditions the sediment fall velocity was higher than rising microplastics velocity. Thus, the neutrally-positively buoyant microplastics got trapped in the sediment. Negatively buoyant microplastics form mixed substrates because both particles can settle at similar velocities.

Settling tubes with suspended concentrations higher than 1270 kg/m^3 were defined as sediment suspensions affectedby hindered settling. Here, microplastics were not trapped inside the deposit. The particle's interaction in the suspension slows the deposition and accelerates the rising velocities of the microplastics. The bed growth rate is not fast enough to trap rising buoyant microplastics. Microplastics rise to the top of the fluid across the sediment and form a suspended microplastic layer. Depending on the fluid density the microplastics can sink at the top of the sediment in the later stages of the settling process when the particle sediment is deposited.

The deposition of a microplastic particle in calm water in the sediment bed is a function of the plastic density, size distribution and volumetric contents in the suspension. Depending on these physical parameters, the same microplastic particle can be deposited in different depths in a free settling regime or cannot be deposited in the sediment core with hindered effects. The microplastic depositional in function of the plastic characteristic and volumetric content in the suspension helps to explain why it is common for researchers to find heterogeneous mixtures of neutrally, positively, and negatively buoyant plastics deposited in the sediment beds. In conclusion microplastic particle deposition in calm waters depends on the plastic-sediments properties (density, size, geometry), fluid density and the number of particles in the suspension.

The results of these experimental tubes follow the findings of the studies with different suspended concentrations (Druit, 1995; Amy et al., 2006; Guo et al., 2015) and the hindered fall velocities model developed by Davis and Gecol (1994), which integrate the results of Batchelor (1982), Batchelor and Wen (1982), and Richardson-Zaki (1954). Highlighting the interaction of the particles influences the settling process of the mixtures of microplastics and sediment, return flow, increased viscosity, and buoyancy of a bimodal mixture in suspension.

Upcoming studies complementing this research should emphasise revising the depositional processes with other sediments ranges, considering more complex procedures such as aggregations between plastics and sediments. Parameters able to change the settling particle velocity, with effects in the stratigraphy.

The results highlight the importance of considering the microplastic storages in the river bed in calm water, and the estimation of the possible mobilisation of microplastics when the river floods these areas. Presenting the final aim developed in Chapter 5, where a numerical model of a river was run considering the storage of microplastics in the river bed.

Chapter 5 . Transport and deposition of microplastic particles in a braided river: Hydro-morphodynamical numerical model using the software Delft3D’

The experimental work explained in the last three chapters concluded that the interaction of the particles in the suspension govern the deposition depth of the microplastic in the river bed, promoting high storage of the microplastic and restricting the transport of the particles for the river flow. It is important to incorporate this effect in numerical models of microplastic transport and deposition in rivers. For this reason, Chapter 5 developed a numerical model that simulated the storage of microplastics in a braided river bed.

The main objective of the numerical model is to recreates the microplastic-sediment interactions in the river bed to study the spatial and temporal distribution patterns, morphological changes, and load balances of plastic debris in rivers. The research questions posed to achieve the main objective of this research are:

- What are the morphology changes in a riverbed with microplastic?
- How much plastic is stored in a river system?
- How does the interaction between the sediment and microplastics influence plastic fluxes' transport and deposition patterns?

The chapter begins with an introduction to the scope of some numerical modelling of the transport and sedimentation of microplastics particles in the rivers. Basic concepts of a braided river are introduced to justify the case scenario, following by a descriptions of predictive predictors parameters for particle transport. The method section detailed the adaptation to the study case, transports predictors selected, initial software conditions and scenarios. The results section separates the outcomes from the numerical model in three topics: microplastic loads temporal and their spatial distribution, morphology evolution and hydraulics characteristics. The discussion section details analysis of the microplastic fluxes and balances, effects of the microplastic loads in the river forms and patterns of the microplastic fluxes in the braided river. The chapter ends relating the results with field samples, reviewing the research questions and an analysing the method advantages and limitations.

5.1. Introduction

Riverbed are sites of storage, transports, and transfers of microplastics particles as a result of the river flow together with sediment particles. The temporal and spatial microplastic distribution in the river bed is controlled by meteorology, hydrology, hydraulics, and sediments properties of the river system, such as wind, tides, velocity profiles and shear stress (Kim et al., 2015; Horton et al., 2017; Liedermann et al., 2018; Emmerik et al., 2019; Eo et al., 2019; He et al., 2021; Kumar et al., 2021; Markus et al. 2022; Rolf et al., 2022; Russell et al. 2022). The accumulation and migration of plastics is also controlled by topography, bedforms, flood areas, and vegetation of the river system (He et al.,2020; Russell et al., 2022; Liro et al., 2020).

The highly microplastic heterogeneous transport and deposition processes (Kumar et al., 2021) has been recreated by numerical models, incorporating hydrodynamics, mass balance, and statistical theories (Uzum et al., 2021). Depending on the study, models include the influences of tides, wind flows, bathymetry, sources, and aggregation processes (Uzum et al. 2021). However, there are relatively few numerical models that integrates the study of sediment and microplastic particles interacting in the river bed (Drummond et al, 2022; Shiravania et al, 2023). Numerical models have been considered the dynamic of the microplastics with a static river bed without considering the effects of the plastic storage in the bed. The study of sediment and microplastic particles interacting in the river bed is an important effect to be consider, given that the presence of the plastics increased the average diameter of the materials in the bed; an increase in critical shear stress may be needed for erosion ([b]Waldschläger and Schüttrumpf, 2019; Ockelford et al., 2020), impacting the formation of bedforms (Russell et al., 2022). Also, the settling experimental results (Chapters 2, 3 and 4) explained that the microplastic particle forms mixed substrate with the sediment, limiting the availability to be transported.

Studying the dynamics between the microplastic and sediment in the river bed enables understanding of more realistic spatial and temporal distribution patterns, morphology changes, and load balances of plastic debris in rivers than models with a static bed, with more accurate estimations of the dynamics of microplastic fluxes to interpret the environmental impacts. Therefore, a hydro-morphodynamic numerical model was created to simulate a microplastic-sediment interactive layer in the river bed. The model recreated the sedimentation, erosion, resuspension, and transportation of microplastics together with sediment particles, simulating a more real dynamic in the river bed.

The study case is a braided river based on the River South Saskatchewan (Canada) created by Schuurman (2015). It is selected because it has been measured in the field a braided river accumulates more plastics than a linear channel (Liro et al., 2022), effects of more areas with sediments bars, herbaceous vegetation and wood jams, and the active migrating of the bed forms can act as a sink and fragmentation of the plastics (Nyberg et al., 2023). Further the model has been used as a base study in other research (Baar et al., 2019; Kleinhans et al., 2019; Zhang et al., 2020), providing an already hydraulic and morphologically calibrated model, which simplified the methods and times to develop the objectives of this chapter (see more details Appendix 8). In addition, it is a geomorphology pattern that can be found in one of the most plastic polluted rivers in the world, Ganges river, Padma River (Lebreton et al.; 2017).

A braided river is formed by a network of channels that divide and rejoin between sediment bars (Figure 5-1)(Schuurman and Kleinhans, 2015). Braided rivers are wide and shallow, associated with transporting large volumes of sediment (Charlton, 2008); it is highly dynamic and constantly changes its morphology. The main channels are wider and deeper and contain higher average flows; secondary channels cross the sediment bars, are less wide and shallow, and only transport flow at determined rates. The sediment bar heads can efficiently trap slowly settling particles such as microplastics, with recirculation flows, whilst the sediment bar tails can incorporate microplastic in the river flow (Ghinassi, 2023).

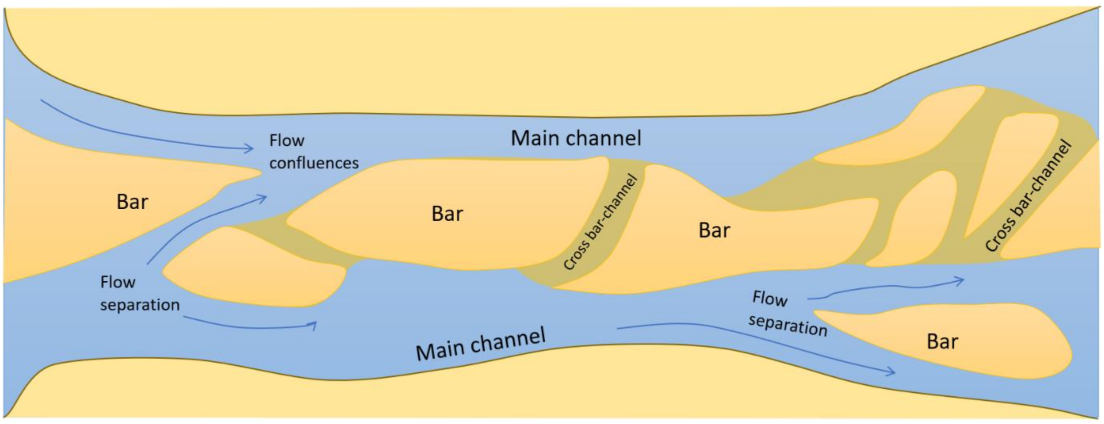

Figure 5-1. Braided riverbed morphology. Formed by a network of channels that divide and rejoin between sediment bars (Best, 1987, Charlton, 2008; Schuurman and Kleinhans, 2015).

Braided river velocity and shear stress profiles depend on the geometry of the channels, which influences the erosion and deposition of the sediment particles. The maximum velocity and shear stress are located at the centre in the straight channels. In sinuous channels, the curvature affects the formation of secondary flows and modifies the transverse distributions of mean velocities and fluid shear stresses (Church et al., 2012; Pradhan et al., 2018; Khanarmuei et al., 2020). In general, upward flow of the secondary flow promotes sediment transport (Yang et al., 2012), resulting in erosion at the outer bank and deposition at the inner bank (Bathurst et al., 1979).

Flow confluences and separation zones have a significant impact on the morphodynamics in braided river. The hydrodynamic of a confluence is divided into the main and tributary flow, maximum velocity and shear stress zone, and the flow deflection and separation zone (Best, 1987). Each zone depends on the tributary flow ratio, confluence angle (ϴ), bed discordance, and upstream planform (Bilal et al., 2020). Confluences promotes greater turbulence with the formation of vortices and helical secondary circulations. The flow separation is an area of lower pressure and flow recirculation (Bilal et al., 2020) and explains sediment bars formation.

The complex interaction between the river flow and sediment particles in a braided river can be recreated with a hydro-morphodynamical model, as these types of models can simulates the evolution of bedform shape in time by the erosion, deposition and transportation of the suspended or deposited particles. The balance between deposition and erosion rates formulates material exchange between the bed (suspended or bedload). The mass-balance equilibrium is created as a function of the flow velocity components, secondary flows, particle settling velocity effects, shear stress and particle transport predictors (Deltares, 2020).

To proceed further, a hydro-morphodynamical numerical model was selected as the method that simulates river dynamics capable of answering the research questions. The following section explain the concepts of fluid dynamics for particle transport and the basic notions needed to explain the numerical model methods (Section 5.2.) and results (Sections 5.3.).

5.1.1. Fluid dynamics for particle transport and deposition

Viscous and inertial forces in the river flow control of the transport and deposition of particles in the river bed (Dingman, 2008). The viscous force is a frictional force that comes due to the motion of the fluid in the river bed, and the inertial force (Dingman, 2008). In rivers the inertial force may be associated with gravitational acceleration of a flow down a slope. The Reynolds number (Re) is a parameter that relates the viscous and inertial forces and classifies the river flow as laminar or turbulent (Equation 5-1).

$$R_e = \frac{VL}{v} \tag{5-1}$$

In which V is the velocity, L is a characteristic length that depends on the channel geometry, and v = kinematic viscosity of the liquid. The flow is laminar if the viscous force dominates and the liquid particles move in smooth paths. The turbulent flow occurs if the internal force dominates and the fluid particles move in irregular directions (Chaudhry, 2008).

The bed shear stress (τ_b), in a one-dimensional channel with a steady and uniform flow, the shear stress is defined as (Garcia, 2008):

$$\tau_b = \rho_f \; g \; H \; S \tag{5-2}$$

ρ_f = fluid density, g = gravitational acceleration, H is the flow depth, and S is the slope.

For boundary turbulent flow the shield stress is divided in viscous and turbulences (Pope, 2000).

The shear velocity (u_*) provides a measure of the flow turbulence and its ability to entrain and suspend sediment particles, it is described as (Chaudhry, 2008) :

$$u_* = \sqrt{\tau_b/\rho_f} \tag{5-3}$$

Similarly. the velocity profile results from the balance of viscosity and turbulence in the river flow (Dingman, 2008). The river flow's velocity distribution (U) varies along the channel's depth and width. Figure 5-2 shows a river section's typical velocity and shear stress profiles.

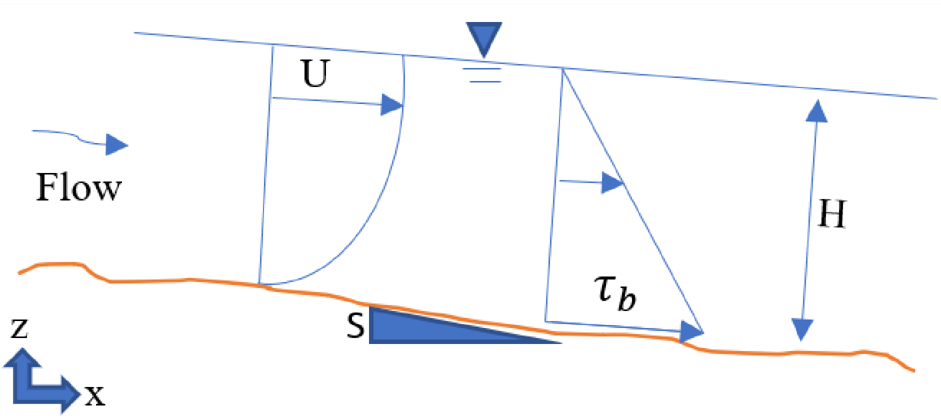

Figure 5-2. One-dimensional open channel fluid forces responsible for the transport and deposition of particles in rivers environments in one-dimensional channel, steady and uniform flow (Chaudhry, 2008; Dingman, 2008).

II. Threshold condition for particle transport

The incipient motion is defined as the moment when a particle begins to move. Given that river particles have different sizes, shapes, and densities the incipient motion is difficult to determine. Researchers have historically defined the critical condition of movement as the function of the dimensionless shear stress (τ) (Shields, 1936; Yalin and Karahan, 1979; Parker, 2005). Shields (1936) generates a diagram of the incipient motion based on the critical shear stress (τ_c^*) and the shear Reynolds number (Re*) defined as :

$$\tau_c^* = \frac{\tau}{\rho g R D_i^*} \tag{5-4}$$

$$Re^* = \frac{u_* D_i^*}{v} \tag{5-5}$$

Where τ_c^*= bed shear stress for initiation of motion ; $u_* = \sqrt{\tau/\rho}$, shear velocity; D_i^* = sediment particle size; $g =$ acceleration of gravity ; $R = (\rho_s - \rho)/\rho$, the submerged specific gravity of the sediment; ρ_s= sediment density; ρ= water density and v= kinematic viscosity.

The incipient motion is still poorly understood due to inherent laborious definition of the threshold. For example, in the work Parkers (2005), Yalin and Karahan (1979) and Shields (1936). The value of the shear stress for incipient motion differ significantly (Figure 5-3.;Shields, 1936; Yalin and Karahan, 1979; Parker, 2005).

Recently, critical shear stresses in microplastic and sediment mixtures have been measured by [b]Waldschläger and Schüttrumpf (2019). They found that the plastic initiation of the motion has different values depending on the physical properties and sediment size where it was deposited. The authors mentioned the importance of considering the hiding effect of plastic in sediment ([b]Waldschläger and Schüttrumpf, 2019). The study included 15 types of microplastic particles, in a combination of 4 negative buoyant polymer (PS, PA, PVC, PET) with densities between 1008-1368 kg, 5 types of shapes (pellet, fragment, sphere, and fiber) and equivalent diameters between 750 µm to 5040 µm. The sediment mixtures used in the research were a medium sand, coarse sand, fine gravel and mixed sediment with equivalent diameters between 450 µm to 3000 µm.

The results of this study are shown in Figure 5-3. The microplastic data do not fit to any of the three relations of incipient motion. [b]Waldschläger and Schüttrumpf (2019) study with 15 microplastics represents the diverse condition found in field samples, and demonstrates the complexity of the definition of critical shear stress in comparison with the sediment shear stress threshold. Highlighting that in rivers the threshold critical shear stress for microplastic particles it is not uniform, its specific transport depends on the plastic shape, density, size and type of sediment, which demonstrates the necessity of having specific diagrams for plastic particles deposited in different sediment size particles.

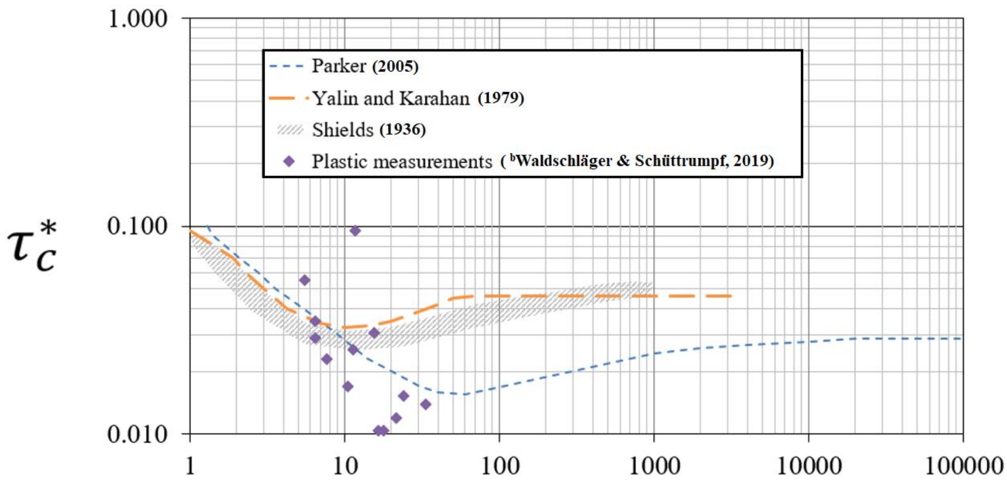

Figure 5-3. Diagrams of incipient motion and microplastic particles in different sediments beds and density (Shields, 1936; Yalin and Karahan, 1979; Parker, 2005; [b]Waldschläger and Schüttrumpf, 2019).

Another correlation that estimates the particle shear stress is made by Soulsby and Whitehouse (1997), this equation imposes that the shear stress cannot surpass a value of 0.30 because this exceeds the grains weight force in the top layer of the bed:

$$\tau_c^* = \frac{0.3}{1+1.2D_d} + 0.055[1 - \exp(-0.020D_d)] \tag{5-6}$$

$$D_d = \left[\frac{g\left(\frac{\rho_s}{\rho_f}-1\right)}{v^2}\right]^{1/3} \tag{5-7}$$

Where τ_c^*= bed shear stress for initiation of motion ; D_d= dimensional grain size; g = acceleration of gravity ; ρ_s= sediment density;ρ_f = fluid density and v= kinematic viscosity

III. Predictors for particles transport and deposition models

Fluid dynamics forces and particle physical characteristics define the type of movement during the transport as suspended load or bedload. Suspended load describes particles carried within the water column, and the bedload is particles transported near the bed (van Rijn, 1990; Bridge, 2013), Figure 5-4. Suspended load consists of particles suspended by turbulent eddies and transported downstream (Charlton, 2008). Bedload can be moved along the bed by saltation following, a shallow trajectory, or interaction with the bed by rolling and sliding (Charlton, 2008). The total load can be described as the volume of particles a river transports in suspended sediment and bed load for a given period. The estimation of these loads is carried out through predictors, these are equations that have been proposed as a result of investigations of the transporting sediment loads. Two predictors were used in this investigation: Partheniades-Krone (1965) and Engelund-Hansen (1967).

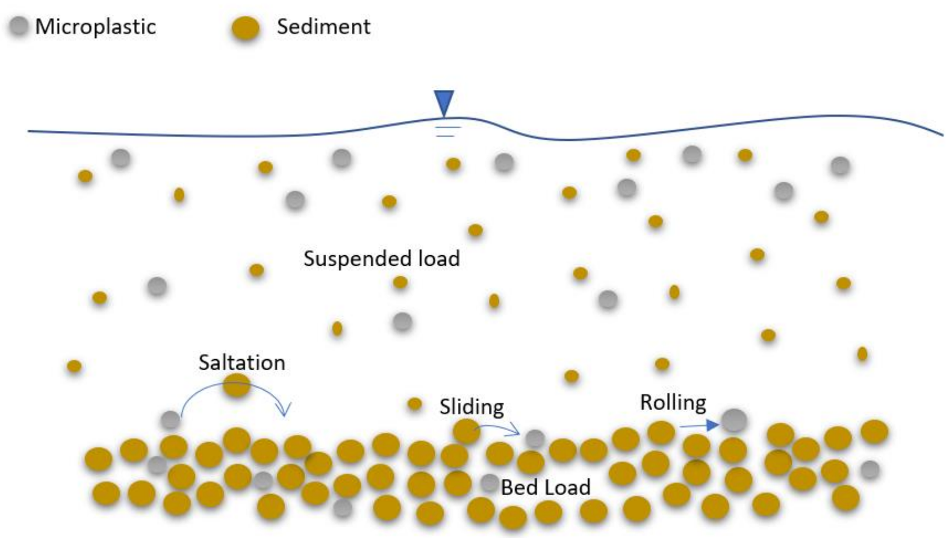

Figure 5-4. Sediment and microplastic forms of transport in rivers.

A predictor for suspended sediment transport is the formulation of Partheniades-Krone (1965) for cohesive sediment, which is divided into erosion and deposition fluxes:

$$\text{Erosion flux, } \mathrm{E} = \mathrm{M}\ \mathrm{S}(\tau_b, \tau_{ce}^*) \qquad \left({}^{\mathrm{kg}}\!/_{\mathrm{m^2 s}}\right) \tag{5-8}$$

$$\mathrm{S}(\tau_b, \tau_{ce}^*) = \begin{cases} \left(\frac{\tau_b}{\tau_{ce}^*} - 1\right), \text{when } \tau_b > \tau_{ce}^* \\ 0, \text{when } \tau_b \le \tau_{ce}^* \end{cases} \tag{5-9}$$

$$\text{Deposition flux, De} = \mathrm{w_s}\ \mathrm{C_b}\ \mathrm{S}(\tau_b, \tau_{cd}^*) \ \left({}^{\mathrm{kg}}\!/_{\mathrm{m^2 s}}\right) \tag{5-10}$$

$$\mathrm{S}(\tau_b, \tau_{cd}^*) = \begin{cases} \left(1 - \frac{\tau_b}{\tau_{cd}^*}\right), \text{when } \tau_b < \tau_{cd}^* \\ 0, \text{when } \tau_b \ge \tau_{cd}^* \end{cases} \tag{5-11}$$

Where E is the erosion flux, De is the deposition flux, M is the erosion parameter, τ_b bed shear stress, τ_{cd}^* critical deposition shear stress, τ_{ce}^* critical erosion shear stress, w_s fall velocity. The Partheniades-Krone (1965) predictor defines the suspended sediment transport in function of the bed shear stress (τ_b) and critical shear stress τ_{ce}^*. When the bed shear stress is higher than critical erosion shear stress, the erosion flux is estimated as the erosion parameter (M) multiplied by the erosion function (S). The particle deposition is estimated when the bed shear stress (τ_b) is lower than the critical deposition shear stress (τ_{cd}^*). The deposition flux is estimated in the function of the particles' fall velocity ($\mathrm{w_s}$), the average sediment concentration ($\mathrm{C_b}$) and the deposition function (S).

A predictor for total transport (T_T) is the relation of Engelund-Hansen (1967):

$$\mathrm{T_T} = \frac{0.05\alpha q^5}{\sqrt{g} C^3 \Delta^2 D_{50}} \tag{5-12}$$

Where, q in the magnitude of flow velocity, Δ *is* the relative density($(\rho_S - \rho_w)/\ \rho_w$), C is Chezy friction coefficient estimated roughness formulations such as Colebrook-White (1937), α is the calibration coefficient.

5.2. Methods

The numerical model selected to simulate the transport and deposition of microplastic particles is Delft3D, given its established hydrodynamics, sediment transport, morphology, and water quality for fluvial, estuarine, and coastal environments numerical model (Deltares, 2020). The sediment transport tools of Delft3D offer multiphase sediment transport (normally non-cohesive and cohesive sediment), bed load transport, influences of waves surfaces and hindered settling (Deltares, 2020). The model uses the Navier-Stokes equation to resolve the unsteady flow, and converge to one solution based in the initial conditions (Deltares, 2020).

The following section describes the software tools, scenarios, and initial conditions to run the numerical models used to answer the current research questions (model setup).

5.2.1. Software methods

Based on a detailed review of the software user manual and the objectives of this research, three methods were selected as possible ways to model microplastic pollution: treat the microplastics as a separate non-cohesive, cohesive particle simulation, or use a particle tracking tool. The non-cohesive or cohesive particle simulation is part of the multiphase sediment transport method. Particle tracking is part of the water quality package to trace instantaneous or continuous pollutant release.

Each method's capacity, advantages, and limitations were examined using six parameters (Table 5.1): inflow of the microplastic load, settling velocity, erosion-sedimentation-resuspension between the microplastic and sediment, and depositional layers. The six parameters selected were based on the formulations of the software and inputs of physic characteristic:

- Inflow of microplastic load: the microplastic must enter the river as a suspended load to represent a pollutant.
- Erosion-sediment-resuspension approach: the method needs to estimate the erosion and deposition of microplastic particles.
- Settling velocity approach: the method needs to estimate the fall velocity in a free settling regime to represent the deposition of the plastic.
- Hindered settling velocity: the method needs to adjust the fall velocity as a result of the particle interaction in the suspension (main conclusion of the experimental settling tubes Chapters 2,3 and 4)
- Microplastics and sediment interaction in the river bed: the method should be able to deposit, erode, and resuspend the microplastics together with the sediment particles, creating mixed substrates.
- Depositional layers: the method needs to model the substrates as depositional layers that evolve with time.

Table 5.1. Capacity, advantages, and limitations of the three methods evaluated to model microplastic pollution using the software Delft 3D (Deltares, 2020).

Parameter	Single-phase model	Multiphase model	Particle tracking model
Can the tool model a microplastic load enter into the flow conditions?	No, this tool is designed for only bed load transport, limiting the model of a suspended microplastic flow.	Yes, the tool is appropriate to model suspended concentrations. Is it possible to add an entering microplastic flow.	Yes, the tool allows two options: instantaneous or continuous release (typical representation of a pollutant in a river)
The settling velocity approach is adequate to model the microplastic?	Yes, it is estimated by the software with Van Rijn (1993) or Engelund Hansen. (Only bed load)	Yes, it is user input. The settling velocity can be estimated using appropriate equations for the microplastic.	Yes, it is user input. The settling velocity can be estimated using appropriate equations for the microplastic.
Is it possible to model the hindered (particle interactions) effect in the settling velocity?	Yes, estimated by the software using the relation of Richard and Zaki (1953)	Yes, estimated by the software using the relation of Richard and Zaki (1953)	Yes, it is user input. The hindered effects can be estimated using appropriate equations or parameters for the microplastic.
Sediment/Erosion/ resuspension approach	Sediment transport relations estimate the concentrations in the bed Van Rijn (1993) is by default, there are 12 options available.	The fluxes between the water phase and the bed are calculated with Partheniades-Krone (1965) formulations (Equation 5-8 to 5-11)	All particles get an equal settling velocity in the vertical. When the shear stress is below the critical value, particles hitting the bottom settle into the sediment layer. All particles return to suspension when the bottom shear stress exceeds a critical value.
Can the tool the interaction of the sediment and microplastic in the sediment bed?	Yes, it is possible to have the sediment and microplastic modelling the river morphology.	Yes, it is possible to have the sediment and microplastic modelling the river morphology.	No, this tool only models the transport and deposition of the particles based on hydraulics and static bathymetry.
Is it possible to study depositional layers of microplastics in the sediment bed?	Yes, the software allows adding layers to study the stratigraphy deposit in the bed.	Yes, the software allows adding layers to study the stratigraphy deposit in the bed.	No, this tool only models the particles' transport and deposition based on hydraulics and static bathymetry.

Therefore, after analysing each criterion for the three methods, the method of treating the microplastics using as a multiphase sediment was chosen. The tool is appropriate to simulated a microplastic suspended concentration dynamic, and the settling velocity can be adapted to a plastic particle. Allowing the plastic fraction to interact with the morphodynamical model, and the interaction between the sediment-plastic in the bed and the deposition strata can be studied. Effectively the microplastic takes on the role of a 'cohesive' phase in a standard implementation of Delft3D. The method is simply the tool that allows implementing the transport and deposition equations for suspended particles with some adaptations to model the microplastics, as explained below.

The method of multhiphase particles meets all the requirements for formulating the plastic particles (Table 5.1). The cohesive particle formulation allows the modelling of a suspended microplastic fraction entering the river system. The concentrations can be estimated as proportional to the availability of the sediments and microplastic fractions (Figure 5-5). The microplastic load fluxes between the water phase and the bed are calculated with the Partheniades-Krone formulation (1965) (Equation 5-8 to 5-11); this formulation can represent the erosion-sedimentation and resuspension of a suspended particle, representing the dynamics of a plastic particle.

All particles have a settling velocity in the vertical; when the shear stress is below a critical value, particles settle in the sediment layer. When the shear stress exceeds a critical value, particles return to suspension (Deltares, 2020). The settling velocity is a user input and can be estimated for the plastic. The hindered effects can be added as reference density (kg/m^3) using the formulation of Richardson and Zaki (1954). Finally, microplastics can be approximated using plastic physics characteristics, switching off cohesive processes in the standard model.

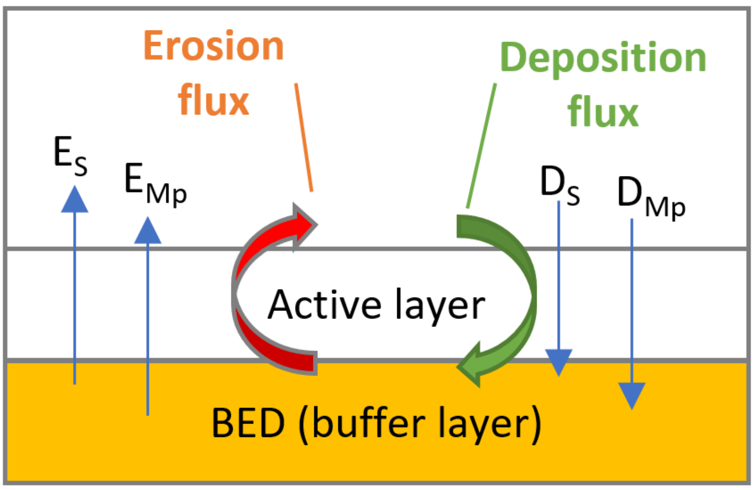

Figure 5-5. Schematic interaction of multiphase sediment and microplastic fraction in the bed (Adapted from van Weerdenburg and van Maren, 2022; Deltares, 2020)

The single-phase method (Table 5.1) was not considered because it is designed for only bed load, and a suspended microplastic load cannot be added, which rules out its use . In this study, the microplastic load must be included as a separate suspended load fraction to represent the microplastic pollutant. In addition, it has been tested that the predictors for river bed load transport can have significant estimations and develop contrasting morphologies (Baar et al., 2019), adding extra calibration tests to the models.

The particle tracking method is created for pollutants; however, it only models the particle transport and deposition based on hydraulics and static bathymetry, limiting the interaction of the sediment and microplastic particles in the bed (Table 5.1). Therefore using particle tracking, the main objective of this study could not be achieved.

5.2.2. Scenarios

Based on the software tools analysed and the objectives of this research, three main scenarios are modelled (Figure 5-6) and described:

A) Morphodynamic braided river model without plastic. The model is used as a baseline to compare the morphologic changes with the plastic scenario.
B) Morphodynamic model with plastic. The model studied the interaction between the sediment microplastic in the bed (active strata) of the particles using a multiphase particle fraction with plastic physical characteristics. The scenario was created using the initial conditional of the baseline (scenario A) with addition of a suspended microplastic load of 1000 particles per cubic meter.
C) Morphodynamic model with plastic. Modelled the same conditions as scenario B, with a suspended microplastic load of 3000 particles per cubic meter.

Figure 5-6 details a diagram of the scenarios designed to explain the transport and deposition patterns of microplastic pollution in the sediment bed.

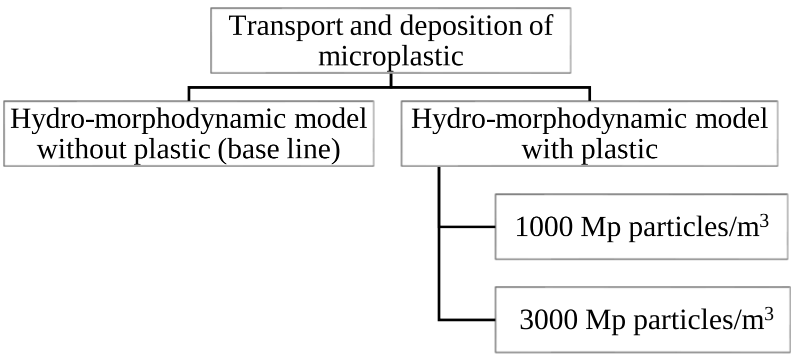

Figure 5-6. Diagram of the three models run for this research: hydrodynamic-morphology model (Baseline), hydrodynamic-morphology model with a load of 1000 Mp/m^3, hydrodynamic-morphology model with a load of 3000 Mp/m^3.

5.2.3. Model setup

The case study for this research was a braided river based on the River South Saskatchewan, Canada. Schuurman et al. (2015) created the model to study the response to disturbances in sand braided rivers, and the original inputs were adapted to achieve the objectives of this research. From the original model, to obtain detailed results the grid was refined to a mesh of 62x1202 rectangles. The initial width was reduced to half, to save computational time due to the increment of the number of grid cells, ending in a width of 2500 m. The river discharge by Schuurman et al. (2015) is an upstream boundary with partitioned ten inflow sections with a discharge of 2000 m^3/s, ending in a total discharge of 20 000 m^3/s. The sediment bed characteristics were modified to match the sediment used in the settling experiments (Chapters 2,3, and 4), representing a natural sediment with D_{50}=105 µm. Figure 5-7 shows the initial bathymetry of the braided river, described as a linear channel with a constant slope of 0.0093%. The initial water level was a constant level of 5 m in all the grid.

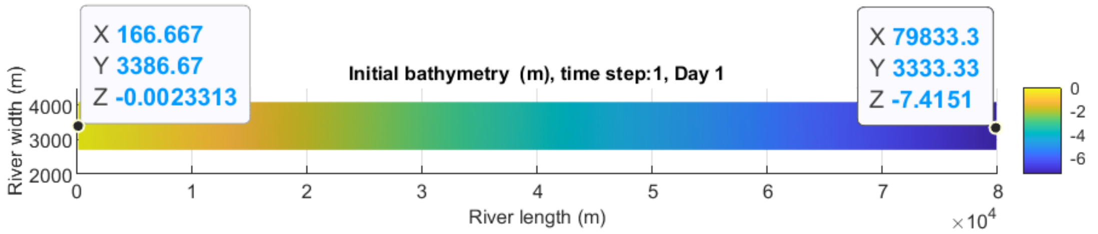

Figure 5-7. Initial bathymetry of the braided river model.

To model the microplastics, a second particle load was added with a diameter of D=686 µm and a density of 1150 kg/m^3 (the same as the plastic used in the experimental work). The fall velocity for a free settling particle was determined using Ferguson and Church (2004) (Equation 2.1.), estimated as 15.5 mm/s. The critical erosion of this fraction was estimated using the Soulsby and Whitehouse (1997) relation (Equation 5-6), calculated as 0.055 N/m^2. The suspended concentrations were estimated based on 1000 and 3000 nylon pellets per one cubic meter of water flow, counted as 1.94×10^{-4} kg/m^3 (1000 Mp) and 5.83×10^{-4} kg/m^3 (3000 Mp). The microplastic load was added as a constant suspended concentration entering the river discharge at the upstream boundary of the model.

The suspension density estimated for the scenario with 1000 particles per cubic meter is 1000.000025 kg/m^3, and for the 3000 particles per cubic meter is 1000.000076 kg/m^3. Based on the experimental work results (Chapters 3 and 4), the particles' interaction in the suspension can be described in free settling regimes. The suspension density estimation was made using the volumetric contents and density of the plastic and water. The fluid density used in the numerical model is 1000 kg/m^3 (default), and the plastic density is 1150 kg/m^3.

The computer software was run in 2D dimensional with results in the depth averages. The particle load predictors to resolve the particles dynamic are the relation of Engelund-Hansen (1967) for the sediment and Partheniades-Krone (1965) for the microplastic.

A realistic erosion parameter was needed to represent the microplastic eroding in the bed. Partheniades-Krone (1965) impliment this parameter (Equation 5-8, 'parameter M') in the estimation of the erosion flux, it represent represent the microplastic erosion rate in $kg/m^2/s$ in the sediment bed. In the literature, there is a lack of this erosion parameter for the specific microplastic particle selected. For this reason, the parameter was approximated by creating models with three different values: 0.0001 $kg/m^2/s$, 0.001 $kg/m^2/s$, and 0.01 $kg/m^2/s$, and selecting the one that gives similar morphology to the baseline braided river.

The results are shown in Figure 5-8, and three different morphologies can be observed. The model with an erosion parameter of 0.1 $kg/m^2/s$ creates a sinuous channel. The model with 0.001 $kg/m^2/s$ never converged because the erosion parameter was too high, and all the sediment microplastic was eroded. Finally, the intermediate erosion parameter (0.01 $kg/m^2/s$) was selected as an end satisfactory value because it created a braided river morphology similar to the control model (Schuurman, 2015). Ballent (2013) determined this parameter in laboratory conditions for plastic HD pellets with a density of 1055±36 kg/m^3, obtaining a value of 0.014$kg/m^2/s$, similar to the value selected and validating the results of the tests.

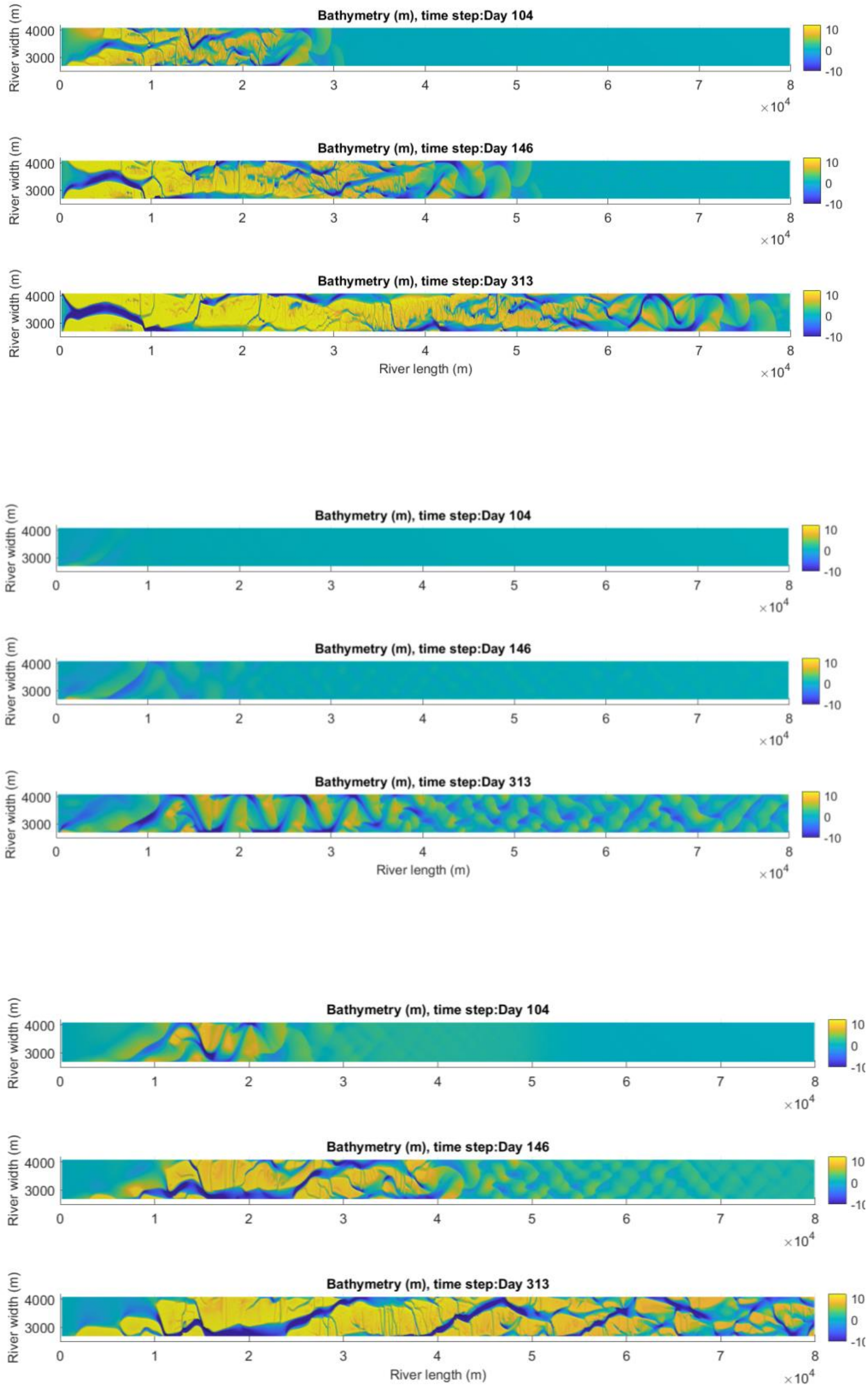

A) Erosion parameter 0.1 $kg/m^2/s$.

B) Erosion parameter 0.001 $kg/m^2/s$

C)Erosion parameter 0.01 $kg/m^2/s$

Figure 5-8. Bathymetry results for the three runs to select the erosion parameter (Equation 5-8, 'parameter M') that best represents the research's objectives. In each model, three-time steps are shown, in which A) model represents a morphology of a sinuous channel (0.1 kg/m^2/s), B) model never converges (0.001 kg/m^2/s), and C) model represents a morphology of a braided river (0.01 kg/m^2/s).

All the models were run with the hydraulic flow period of 31 days and a morphological scale factor of 25, initial conditions established by Schuurman (2015). The morphological scale factor accelerates the changes in the morphology on the basis that the morphological developments occur over a timescale that is longer than the flow changes (Deltares, 2020). A technique used to accelerate the effects of hydrodynamic flow in the bed-level changes. The time scale factor multiplies the erosion and deposition fluxes from the bed at each time step (Deltares, 2020). The changes in mass are translated into a bed level based on the dry sediment fraction densities. Therefore, the time period in this study case represents a run of 775 morphodynamic days.

After running the models, it was decided to select 42 morphodynamic days as a study period, starting on day 188 and ending on day 229. The 42 days period was chosen because it was observed to be in an approximate morphodynamic equilibrium of a braided river a similar approach was taken by Schuurman (2015) and Baar (2019). Based in the initial conditions this type of models compute one equilibrium morphology (Baar et al., 2019).

Figure 5-9 shows nine type steps of the baseline model and highlights the time step for day 188 as the beginning of the period selected for the analysis. It can be observed that from time steps days 52 to 146, the morphology is formed from upstream to downstream, until it is completed for all the numerical grid in time step 167. In time step 188 day there is an active braided river channel in the grid. After time step 229, the hydraulics conditions continue eroding and depositing the bed to the point that the model forms unrealistically morphology, with deeper channels (Days 313 to 729).

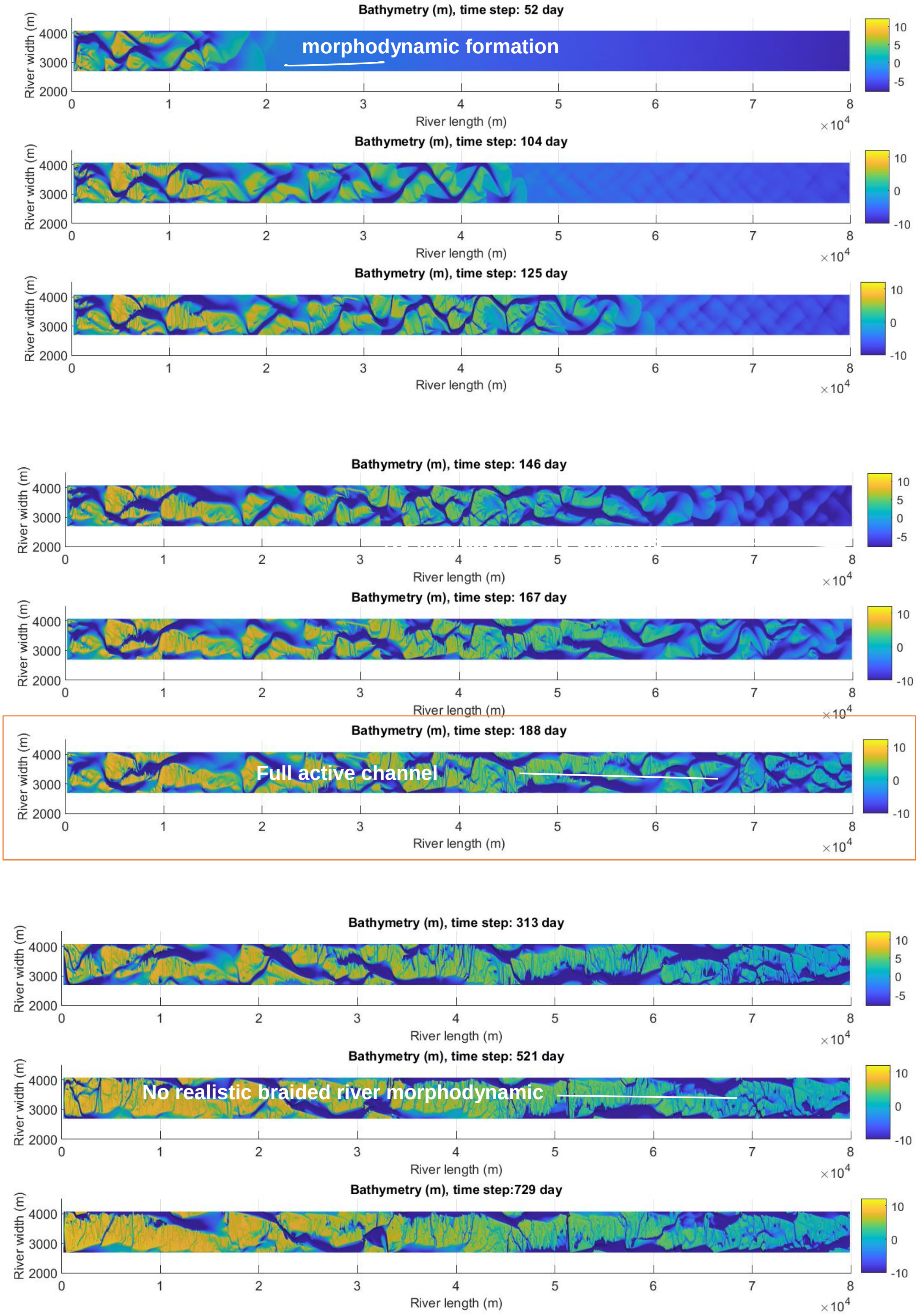

Figure 5-9. Baseline bathymetry results of nine-time steps.

5.3. Results

The result section is divided into four parts. The first two describe the temporal and spatial distribution of the microplastic loads of the scenario with 1000 Mp/m^3 and 3000 Mp/m^3. The following section compares the baseline morphology with the bathymetry formed in the rivers with microplastic. The fourth one compares the hydraulic parameters versus the microplastic loads. To better understand the results, all microplastic loads were transferred from kilograms (kg/m^3 – kg/m^2) to a number of particles (Mp/m^3 - Mp/m^2). The suspended (kg/m^3) and deposition load (kg/m^2) were divided into the mass of 1 nylon pellet estimated at 1.94E-7 kg. The mass was calculated based on the plastic density (1150 kg/m^3) and the equivalent diameter (686 µm).

5.3.1. Temporal distribution microplastic load

Figure 5-10 (Scenario 1000 Mp/m^3) and Figure 5-11 (Scenario 3000 Mp/m^3) shows the temporal distribution of the suspended (a) and deposited (b) microplastic loads, described as:

The decreasing microplastic suspended graph, which represents the load entering the model (Figure 5-10-a and Figure 5-11-a) and the rate at which it is stored in the sediment bed. The model showed that the river with a microplastic load of 3000 Mp/m^3 transported greater and faster downstream than the river with 1000 Mp/m^3. The faster transport of a higher suspended load can be demonstrated by studying the location of 99% of the suspended load. For the braided river with 1000 Mp/m^3, the load was measured until 40.8 km on day 188 and until 46.7 km on day 229, travelling 5.9 km in 42 days; and for the braided river with 3000 Mp/m^3, it was measured at 46.9 km on day 188 and 54.18 km on day 229, travelling 7.28 km in 42 days.

In terms of the behaviour of the suspended microplastic load (Figure 5-10-a and Figure 5-11-a), is noted that in the first 10 km, the graph shows different peak loads and does not show a constant pattern between the time steps. After the 15 km, a curve with a similar trend for the three-time steps is observed. The peaks in the curves at the beginning of the model, can be interpreted that there is a more robust load in resuspension; this can be followed clearly in the increasing graph of day 229 in the first 10 km (Figure 5-11-a).

In Figure 5-10-b and Figure 5-11-b represents the microplastic load deposition in the sediment bed per m^2. Its tendency to decrease explains how the suspended microplastic load is deposited and stored in the sediment bed. The scenarios also show that the higher the amount of microplastics in the river, the greater and faster is deposit. The 99% of the load in the river, with 1000 Mp/m^3, is deposited at 39.9 km on day 188 and 46.3 km on day 229, travelling 6.4 km in 42 days. For the braided river with 3000 Mp/m^3, 99% of microplastic is deposited at 45.72 km on day 188 and 52.45 km on day 229, travelling 6.7 km. Similar to the suspended load, this effect described how a continuous microplastic load in the catchment impacts the deposition rate downstream. The curves of the microplastic deposition have a similar trend for the three-time steps, describing a higher deposition rate in the sediment bed at the beginning of the model and a more constant deposit after 30 km.

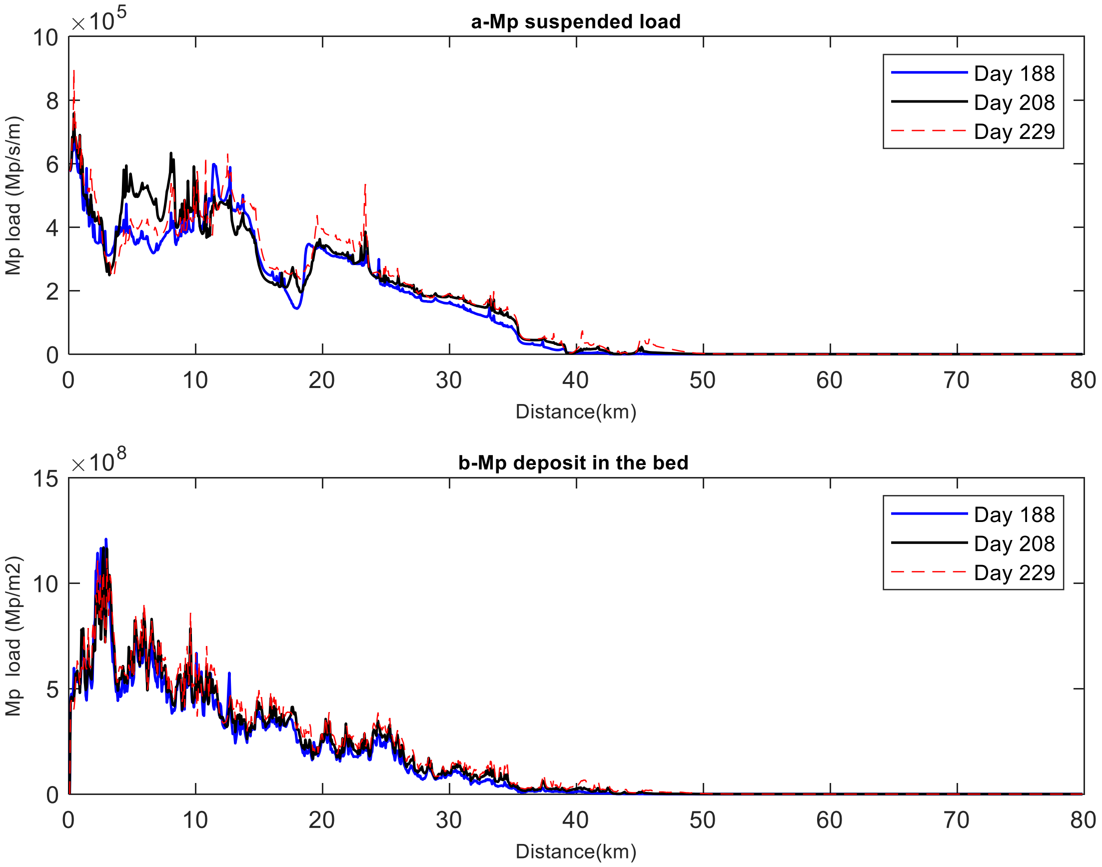

Figure 5-10. a) Width average temporal distribution of suspended load of microplastic flux. b) Width average amount of microplastic stored in the sediment bed. Scenario of the braided river with microplastic load of 1000 Mp/m^3.

Finally, as time passes, the microplastic moves downstream, an effect of the suspension, deposition, and resuspension of plastic in the system. The total microplastic load over 42 days sets microplastic fluxes balances for the study period. In the river with 1000 Mp/m^3 entry the system, 84.08 billion particles enter the braided river. Of this 100% of the load was deposited in the river bed. A total of 2,980 billion particles were in suspension, estimating a resuspension of 35 times more than the total load. A total of 310.17 billion particles get inside the braided river with 3000 Mp/m^3 entering the system. Of this 100% of the load was deposited in the river bed, and 35 835 billion particles were in suspension, estimating a resuspension of 116 times more than the total load.

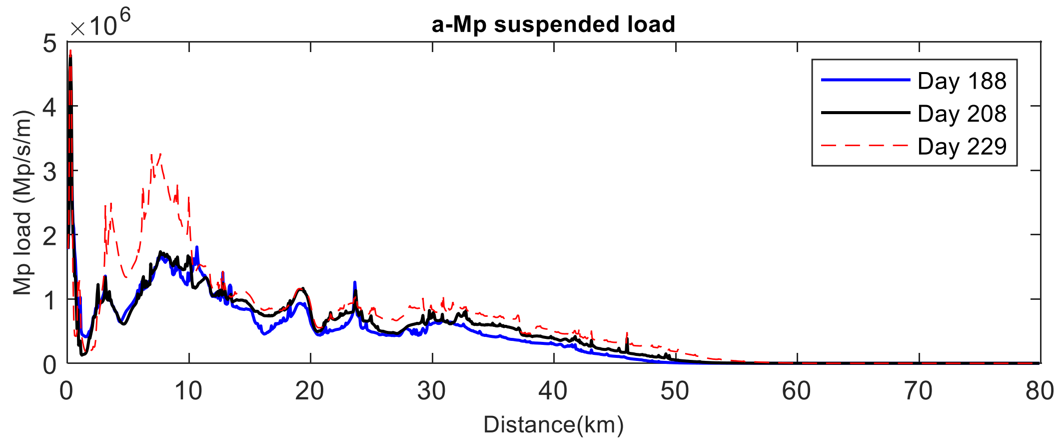

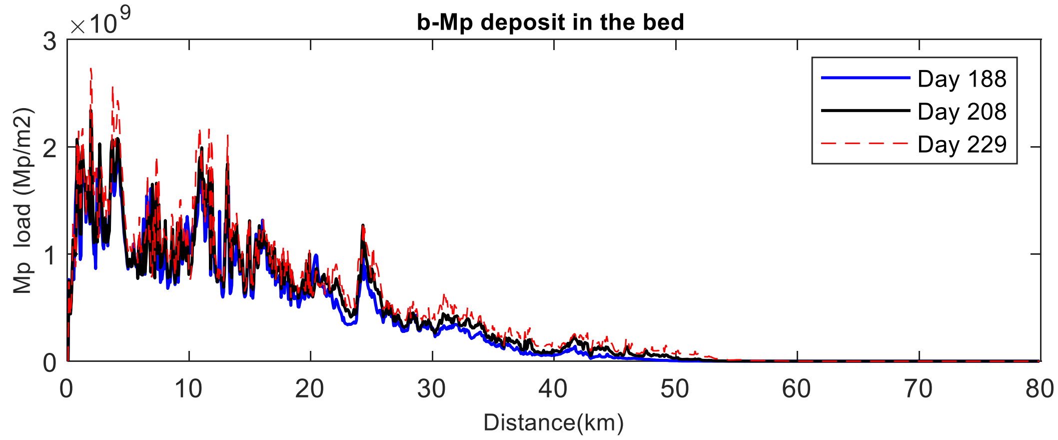

Figure 5-11. a) Width average temporal distribution of suspended load of microplastic flux. b) Width average amount of microplastic stored in the sediment bed. Scenario of the braided river with microplastic load of 3000 Mp/m^3.

5.3.2. Spatial distribution microplastic load

The microplastic deposition spatial distribution for the braided river with 1000 particles/m^3 inflows is shown in Figure 5-12-a. Based on the results of the microplastic load (Figure 5-10 and Figure 5-11), only the first 40 km of the model is included in the analysis due to 99% of the load being in this area. Cross sections with the bed elevation were included every 5 km to help understand the spatial deposition (Figure 5-12-b Figure 5-13).

It is highlighted that the highest accumulation of particles is at the beginning of the model (first 5 km) as an effect of the particle's deposition of the non-buoyant microplastic described in the previous section (Figure 5-11-b). Based on the model bed elevation and the distribution of the deposited microplastic, two specific patterns can be described: top of bars and channels. For descriptive purposes of the results, the bars are considered areas with unitary elevations from 1-0.9 (Figure 5-12-b Figure 5-13-b) and the channels with elevations higher than 0.9 m. The unitary limit criterion between the bars and the channels was defined based on the morphology modelled, according to the initial conditions.

- On the top of bars: In the first 15 km, a uniform distributed load between $2x10^7$-$1.5x10^7$ particles/m^2 is deposited on the river bars. After 15 km, the microplastic loads started to decrease, and low loads were deposited on the sediment bars. The decreasing deposits of microplastics are noticed clearly in the cross sections 25 km and 35 km for all times steps, where the highest values depths showed no microplastic loads deposited in the bed. See for example, section 40 km, where no microplastic is deposited from 0 to 1500 m, Figure 5-12-b .
- Channels: The microplastic load is distributed in all the channels. Most of microplastic is deposited on the lateral slopes, and the lowest is in the deeper part, where the load decreases as the elevation of the channel decreases. In some cases, a peak load (microplastic hot spot) is formed in one of the lateral banks of the channels. For example, in the 10 km cross sections, the deep channel allocated in the station 1500 m presents a hot spot in the left bank, where it accumulates six time microplastic 6 compared to the right bank (Figure 5-12-b Figure 5-13) . In the 5 km cross-section, the deep channel allocated in the station 2200 m presents a hot spot in the left bank.

A) Spatial distribution of the microplastic load deposited in the riverbed.

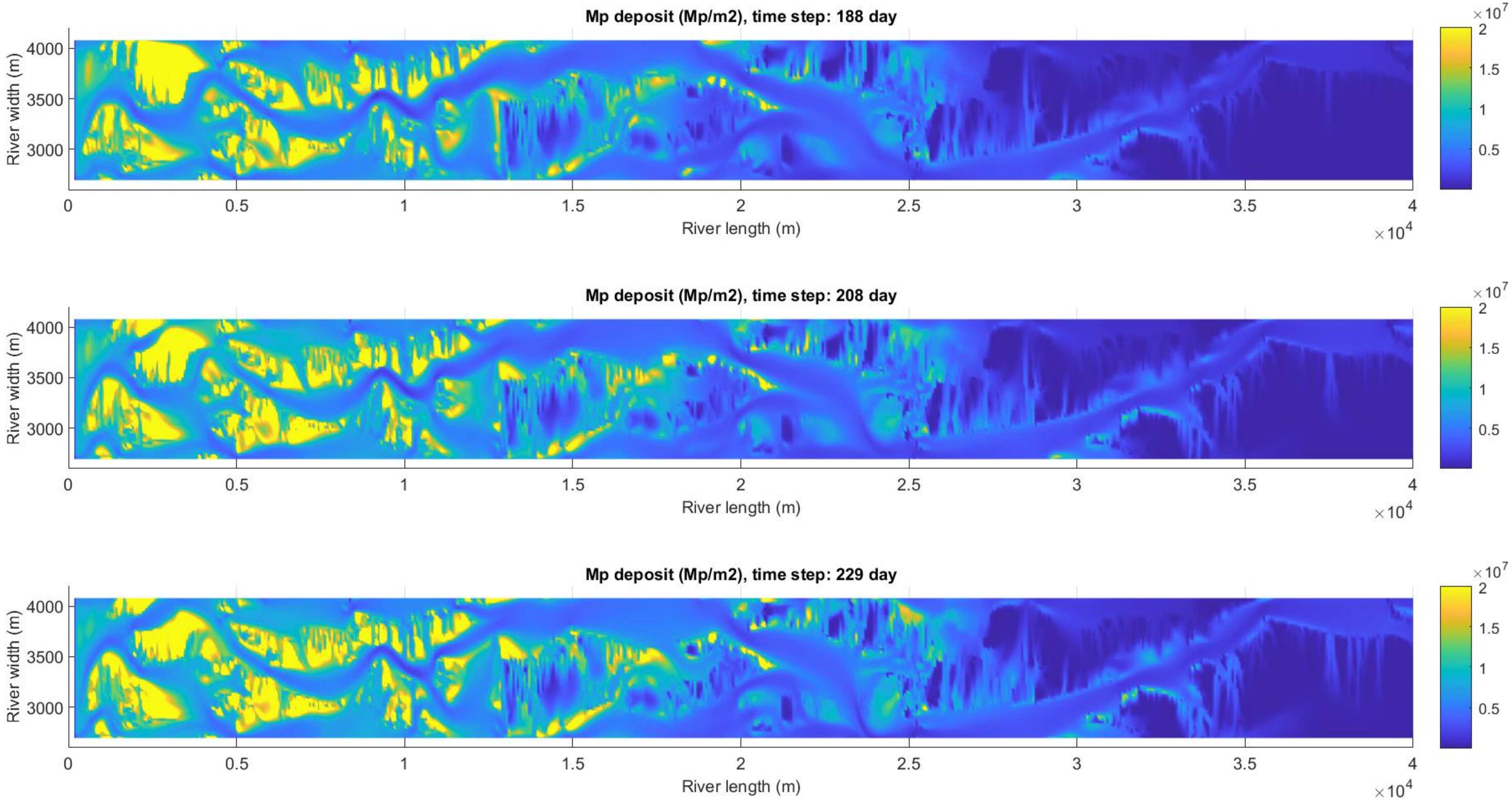

*Figure continues in the next page

B) Cross sections distribution of the microplastic load deposited in the riverbed.

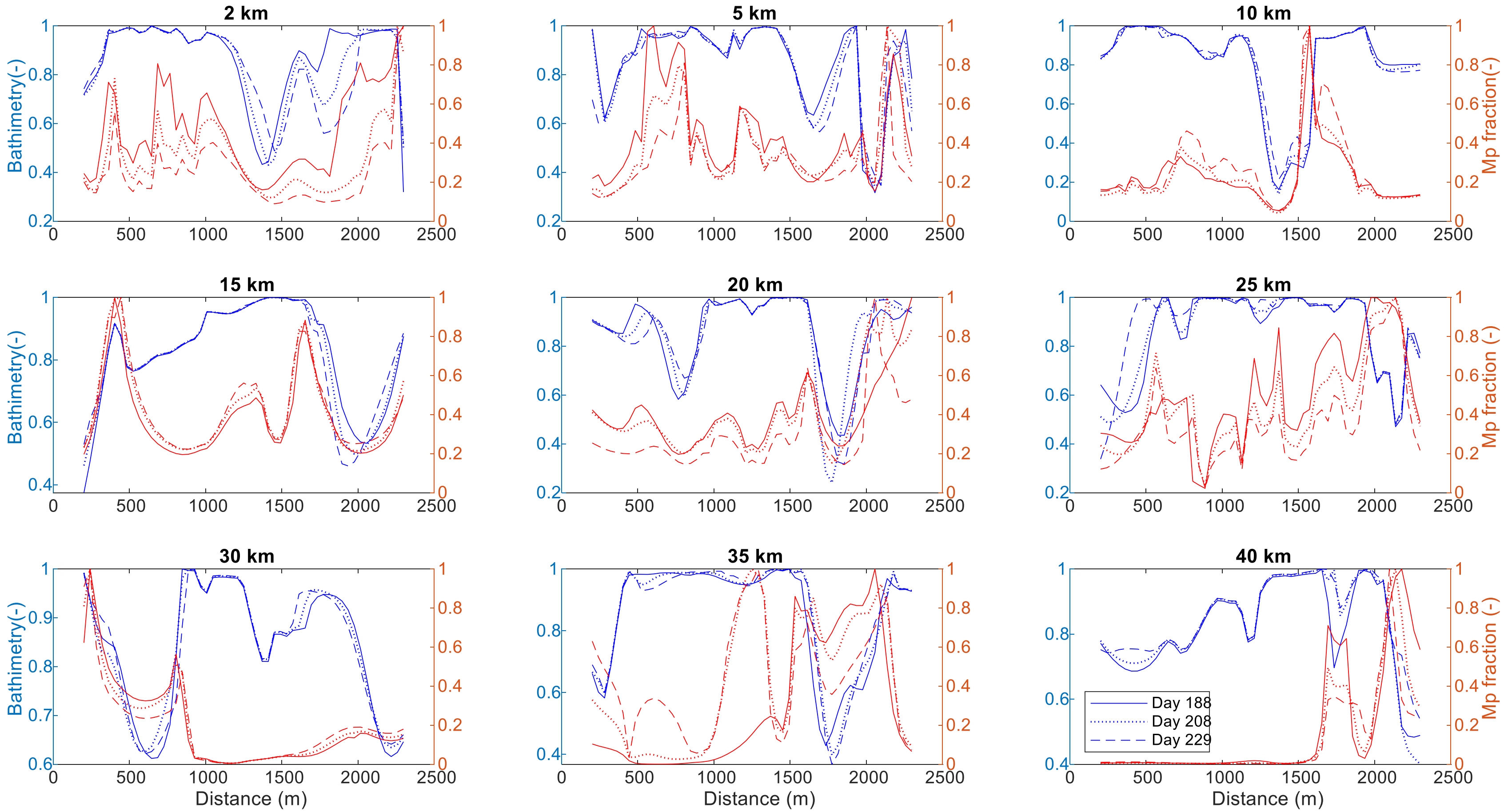

Figure 5-12. Spatial distribution of the deposition of the microplastic load in a braided river, with a microplastic load of 1000 particles/m^3, time steps day 188, 208 and 222. A) Spatial distribution. B) Cross section distribution.

The results the spatial deposition of the scenario with 3000 particles/m^3 showed the highest accumulation of particles at the beginning of the model (0 km to 20 km; Figure 5-13-a). The microplastic loads are deposited all over the braided river with the following differences between the highest elevations and channels:

- On the top of bars: The microplastic is deposited following the patterns of the bathymetry with some peaks until km 35; after this, the microplastic reduces its presence in the highest elevations of the model. The peaks are founded in a 15 km cross-section between 500 m to 1000 m, 30 km cross-section between 500 to 1000 m, and 25 km cross-section between 1500 m to 2000 m (Figure 5-13-b).
- Channels: The microplastic load is distributed in all the channels. The highest amount of microplastic is deposited in the lateral areas of the channels and the lowest in the deep elevations, where the load decreases as the elevation of the channel decreases. For example, in a 10 km cross-section, medium channel station 2200 m, Figure 5-13-b. In some of the channels, a higher amount of microplastic is deposited in one of the lateral banks; this is noticed in the 15 km cross-section, station 1750 m in the right channel bank, and the 30 km cross-section station 1600 m left bank, Figure 5-13-b.

A) Spatial distribution of the microplastic load deposited in the riverbed.

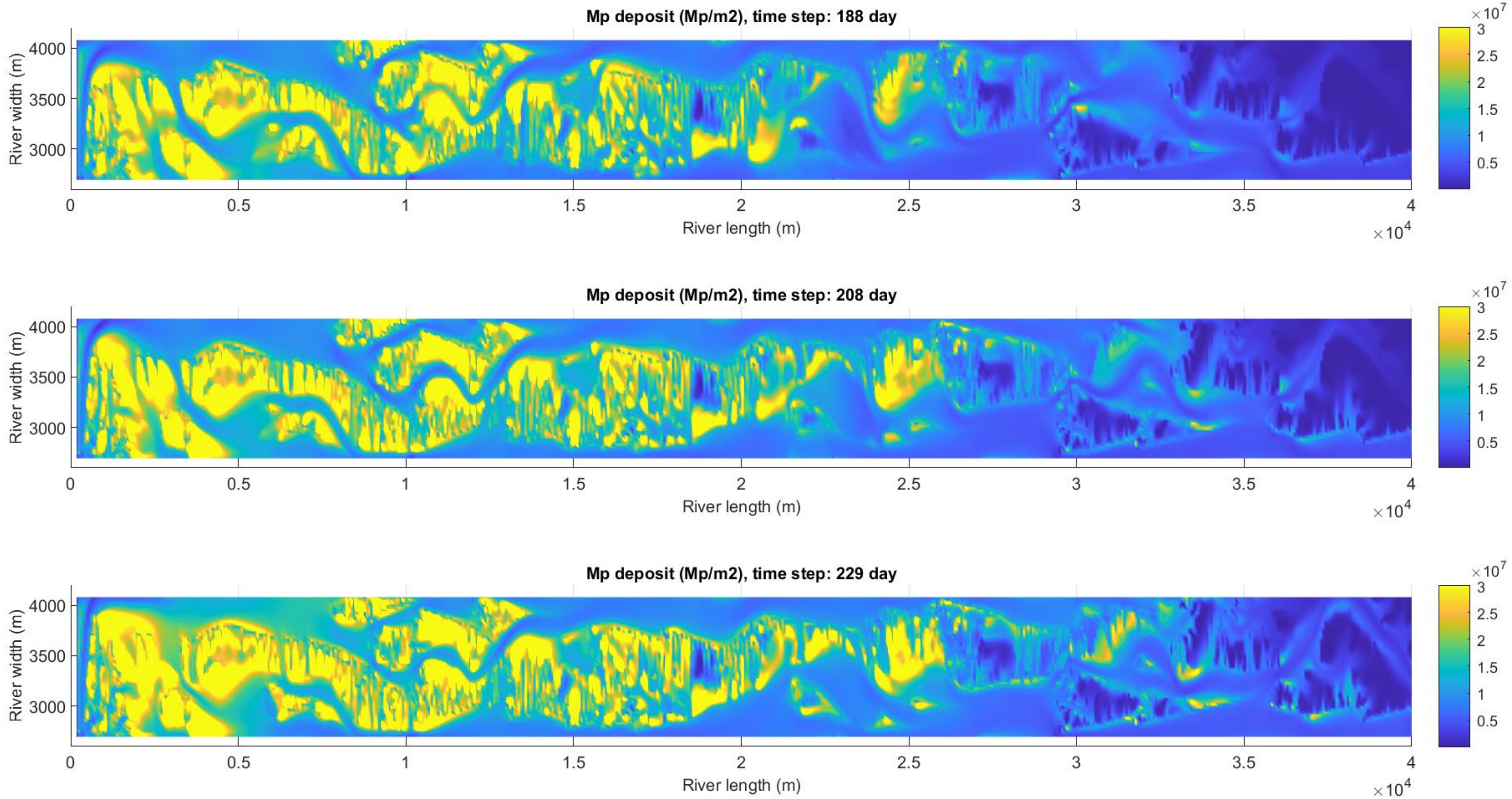

**Figure continues in the next page*

B) Cross sections distribution of the microplastic load deposited in the river bed.

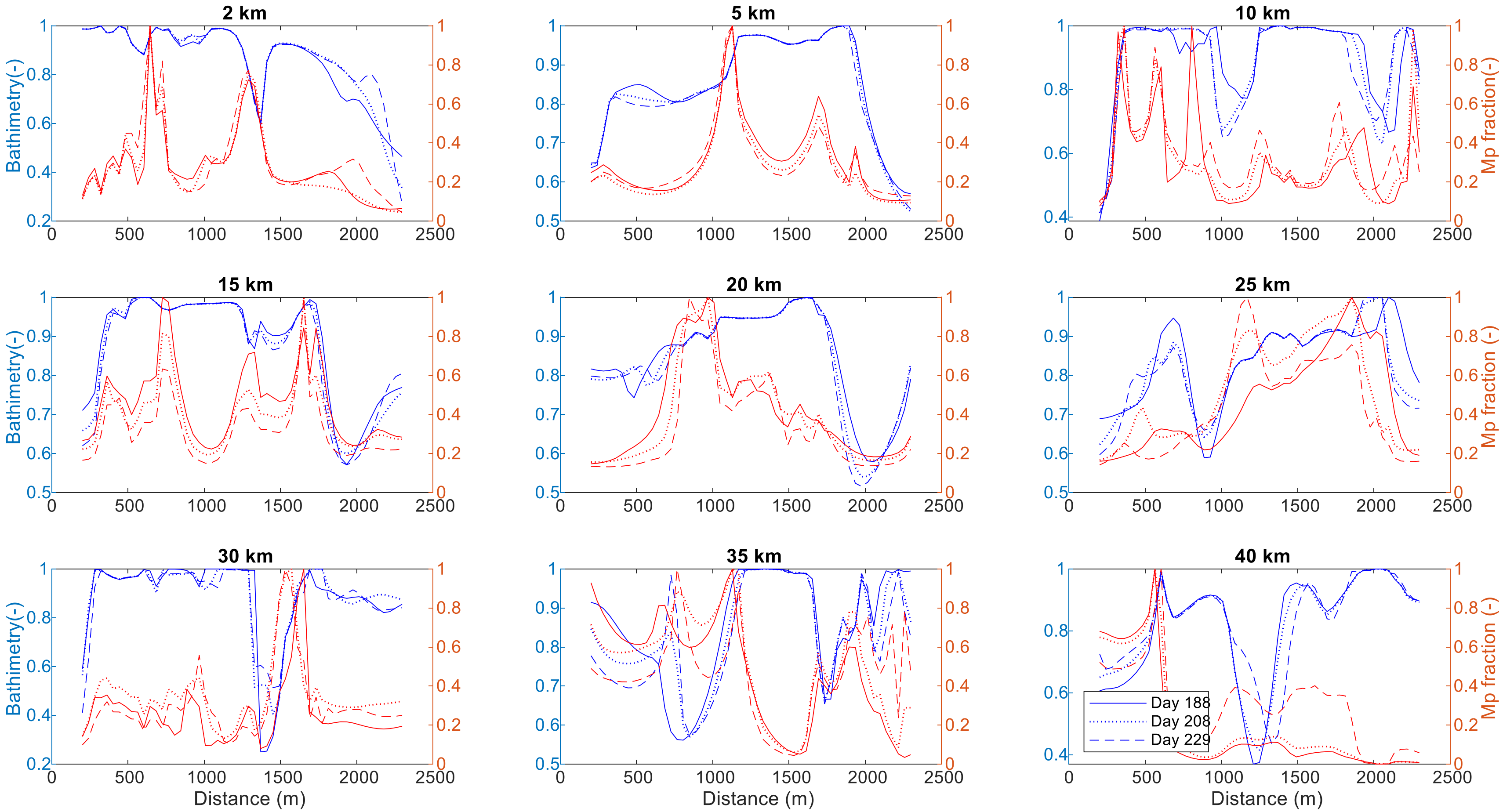

Figure 5-13. Spatial distribution of the deposition of the microplastic load in a braided river, with a microplastic load of 3000 particles/m^3, time steps day 188 , 208 and 222 . A) Spatial distribution. B) Cross section distribution.

The spatial distribution of the suspended microplastic loads is shown in Figure 5-14 for the braided river with 1000 particles/m^3. It can be observed how the microplastics are only being transported in the channels. In the first 15 km, all the channels transport microplastic; the more deep the channel, the higher the suspended load. Between 15 and 25 km, the microplastic load accumulated more in the deep channel (main channel), and less microplastic was transported in the secondary channels. After 25 km, most microplastics are transported in the main channel. However, when comparing the three-time steps, it is noticed that the load is also transported through the cross bars channels as time passes (Figure 5-14-b).

The spatial distribution of the suspended microplastic loads for the braided river 3000 particles/m^3 is shown in Figure 5-15. It can be observed how the microplastics are only being transported in the channels, with the higher concentration in the deeper depths. The highest suspended load is observed to travel in the main channels and then enter the secondary channels as time passes.

A) Spatial distribution of the microplastic suspended load.

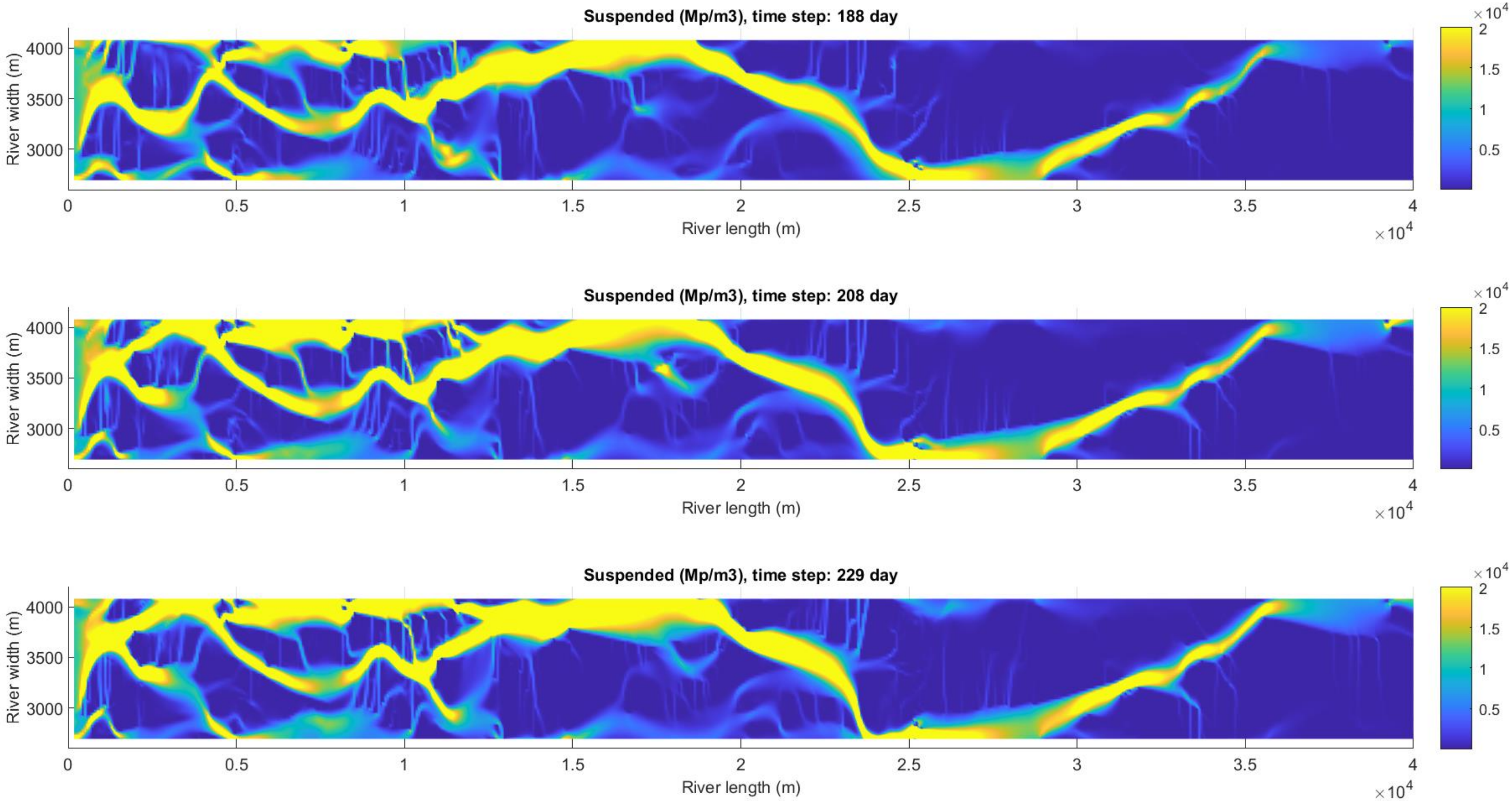

**Figure continues in the next page*

B) Cross sections distribution of the microplastic suspended load

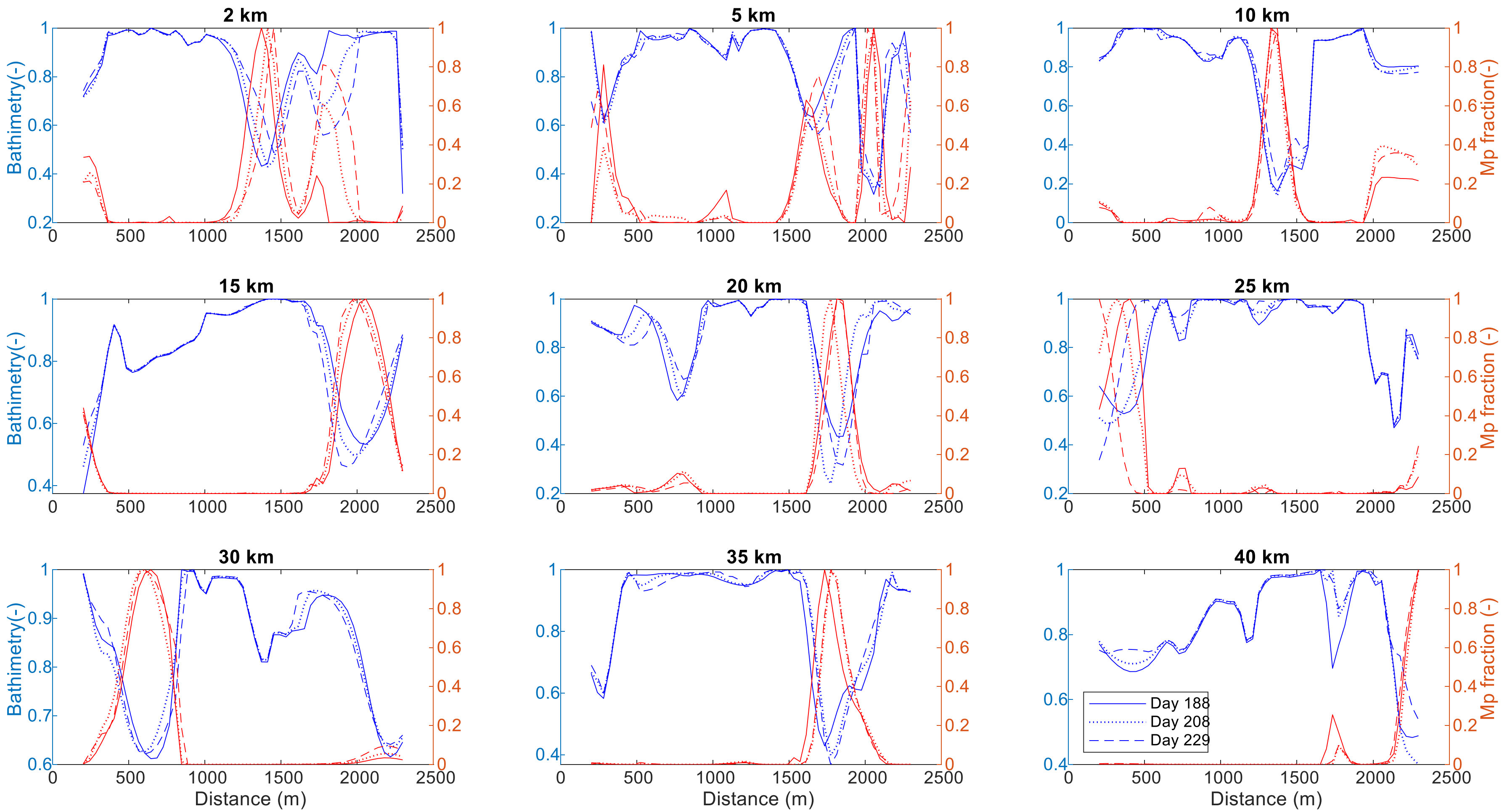

Figure 5-14. Spatial distribution of the microplastic suspended load in a braided river, with a microplastic initial load of 1000 particles/m³, time steps day 188, 208 and 222. A) Spatial distribution. B) Cross section distribution.

A) Spatial distribution of the microplastic suspended load

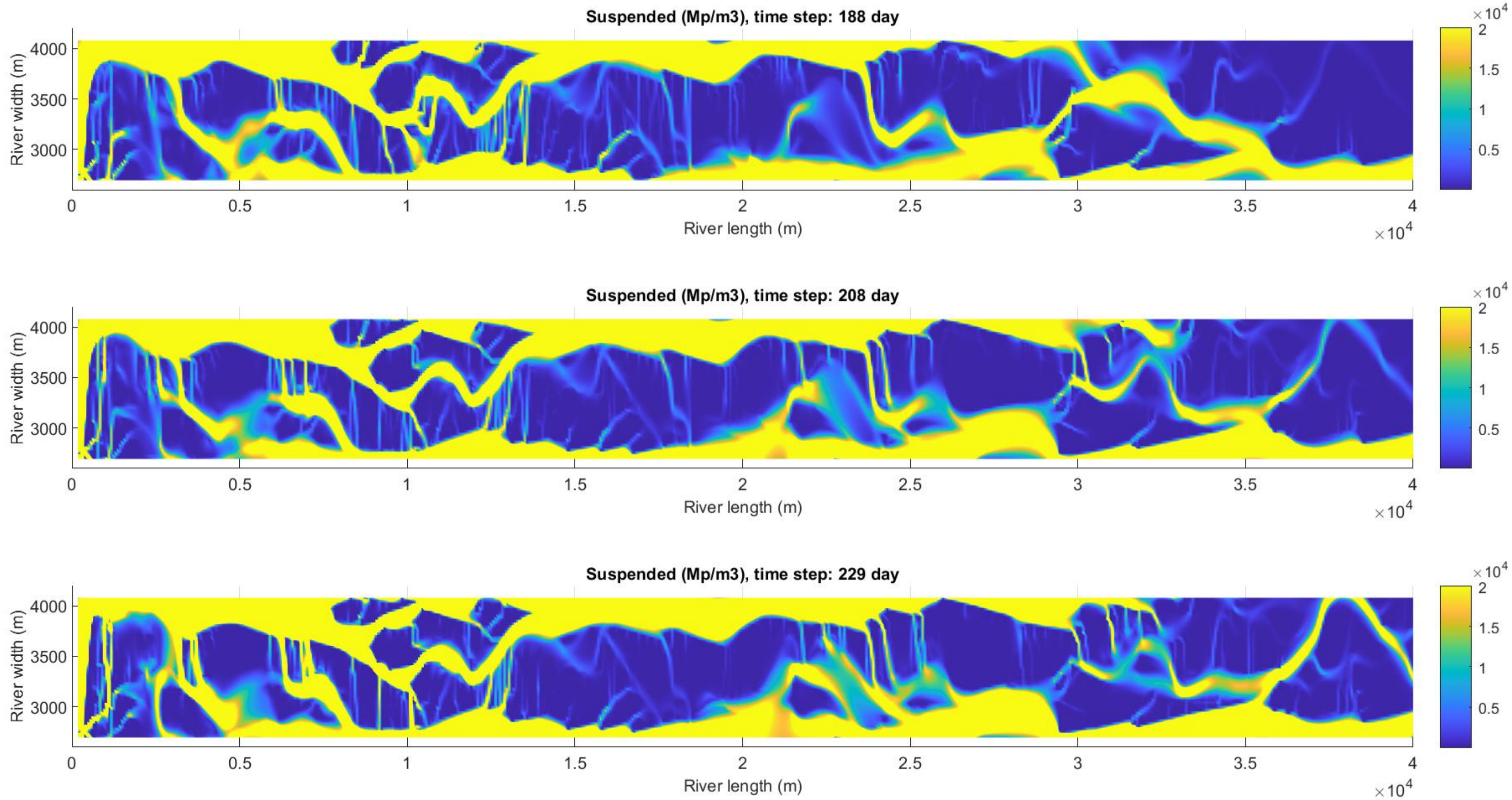

*Figure continues in the next page

B) Cross sections distribution of the microplastic suspended load.

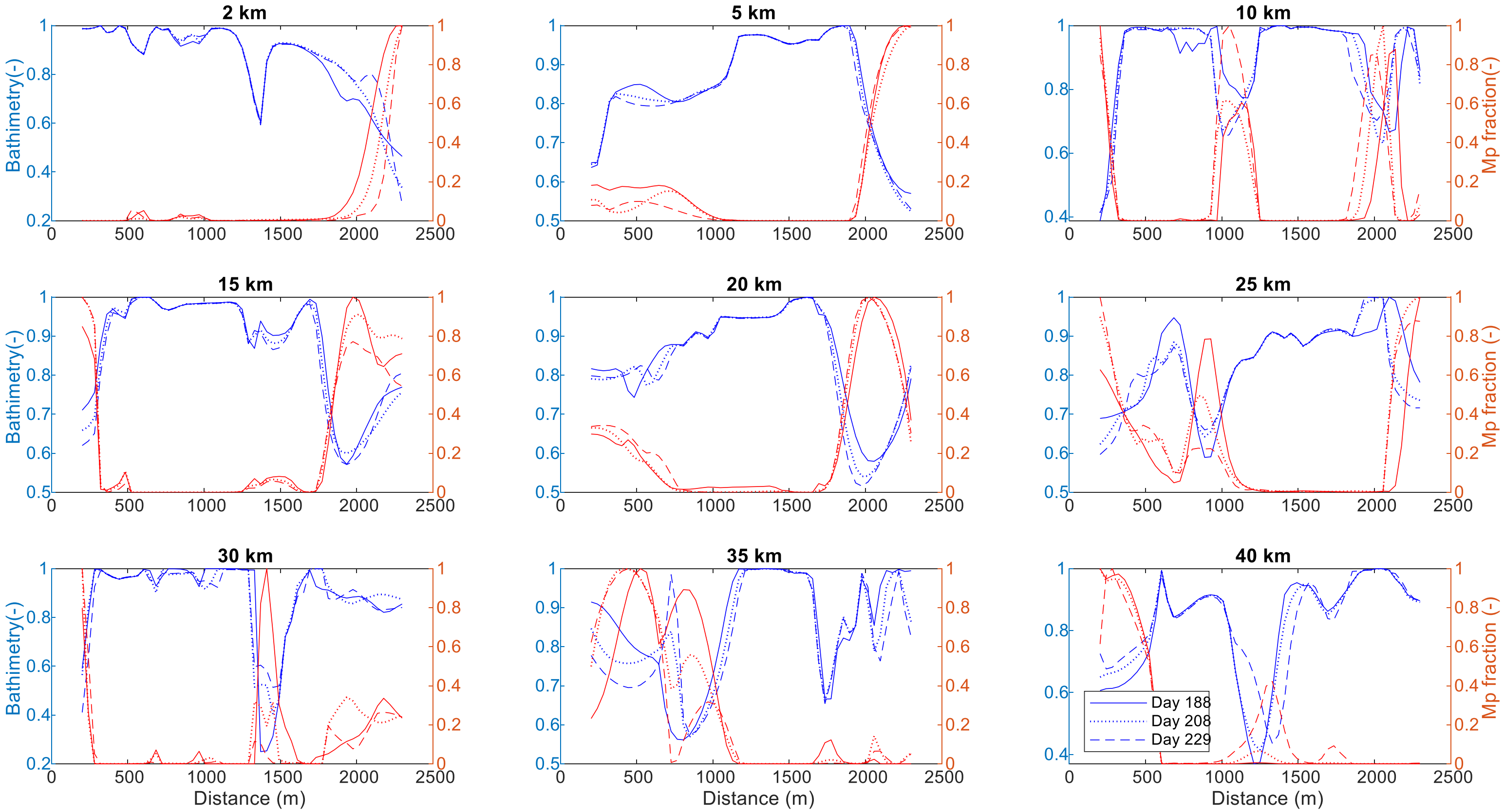

Figure 5-15. Spatial distribution of the suspended microplastic load in a braided river, with a microplastic load of 3000 particles/m^3*, time steps day 188, 208 and 222. A) Spatial distribution. B) Cross section distribution.*

5.3.3. Morphology differences

Figure 5-16 shows the bathymetry of the braided river without plastic, with a load of 1000 Mp/m^3 and 3000 Mp/m^3. The model's initial conditions resulted in three different river morphologies, showing that the erosion and deposition capacity of the river flow is affected by the initial plastic load and creating changes in the bed forms.

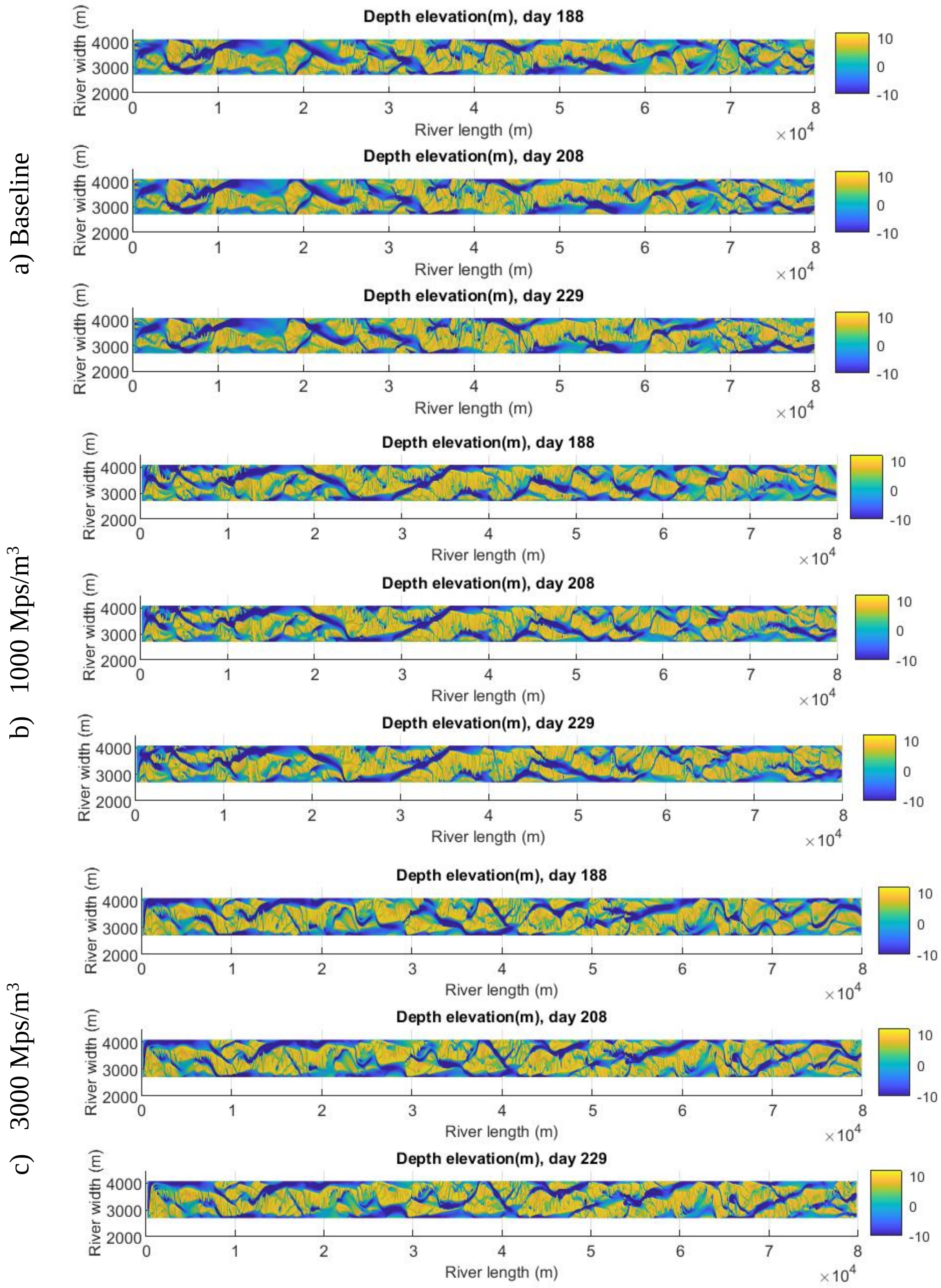

Figure 5-16. Final bathymetry results of the scenarios: a) Hydrodynamical-morphology model without plastic (baseline). b) Hydrodynamical-morphology model with a plastic load of 1000 particles/m^3 c) Hydrodynamical-morphology model with a plastic load of 1000 particles/m^3.

In the scenario without plastic, two wide channels are formed in the initial 5 km, with a middle sediment bar of 600 m of width. The main channel is formed between 2000 m to 3000 m with a width of 1000 m and a depth of 10 m; a secondary channel is created from 300 m to 1100 m, with a width of 800 m and a depth of 5 m. The river with 1000 particles/m^3 of plastic, in the first 2.5 km, creates the same two channels and bars with different sizes. The main channel has similar width, around 1000 m, but increases its depth from 10m to 20m. The secondary channel keeps its width and increases its depth in the double. The braided river, with 3000 Mp particles/m^3, completely changed the initial bed form; a central channel is formed at the left of the river, with a depth of 15 m and a width of 7000 m; in this case, two secondary channels are created with a width of 300 m and depth between 7.4 m, the bar extended it width to 1750 m.

Downstream the models had three different morphologies, a product of the initial conditions described in Section 5.2.3. and the presence or not of the microplastic. The high amount of microplastic deposited at the beginning of the model results in deeper channels and larger bars. Histograms of the depths were compared to associate the differences between the three scenarios in the first 40 km of river. Comparing the results with and without plastic, it can be noticed how the effects of the microplastic load changed the bed elevations distribution (*Figure* 5-17).

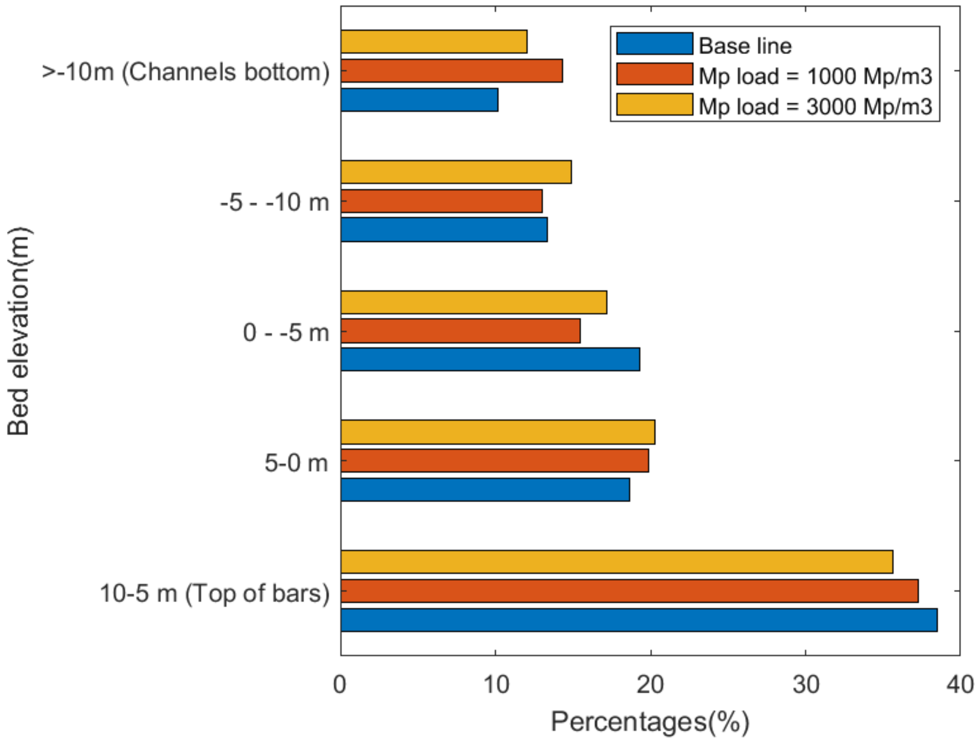

Figure 5-17. Bed elevation distribution for the baseline and scenarios with plastic.

5.1.1 Hydraulics relation versus microplastic load

The results of the velocity and shear stress values versus deposition of the microplastic are shown in *Figure 5-18.* The maximum velocity in the model is around 3.5 m/s, and the maximum shear stress is 40N/m^2. Both scenarios show realistic results where higher amounts of microplastic are deposited with lower velocity and shear stress. An exponential decay curve shows the best fit to the point cloud. Both scenarios result in a decay factor of -0.9 for velocity and -0.12 for shear stress, showing the same fitting trend.

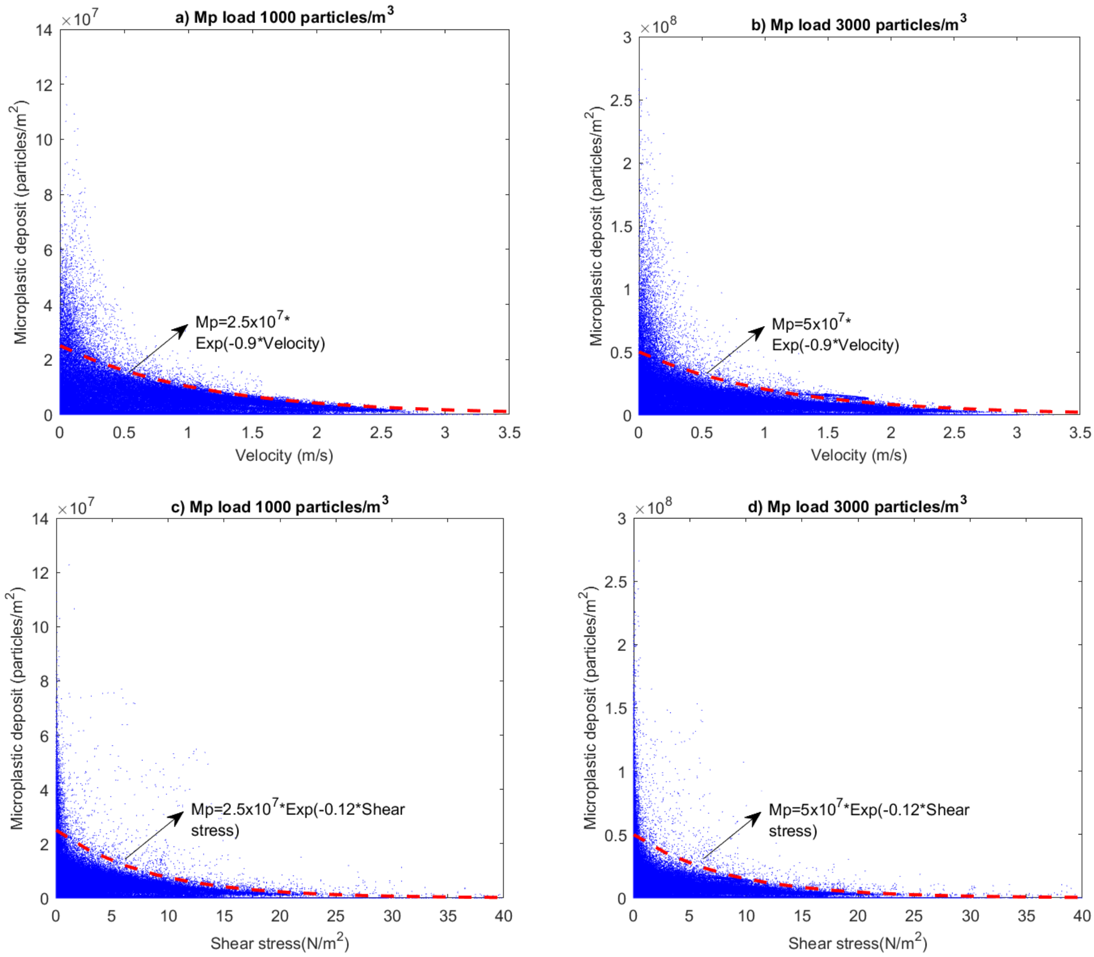

Figure 5-18. Relations between microplastic deposits in the bed versus velocity and shear stress distributions. A) Velocity distribution and C) Shear stress versus microplastic deposited in the bed for the 1000 Mp/m^3 load scenario. B) Velocity distribution and D) Shear stress versus microplastic deposited in the bed for the 3000 Mp/m^2 load scenario.

Figure 5-19, presents the spatial distribution water depth for the day 188. For the two scenarios the riverbed was complete submerged in water, with a minimum water elevation of 0.05m. The top of bars was submerged with water elevation from 0.05 m to 7.0 m. The channels register water elevations from 7.0 m deep. The greater depths (>20 m) are noted in the channel pools.

a) Scenario with 1000 Mp/m^3

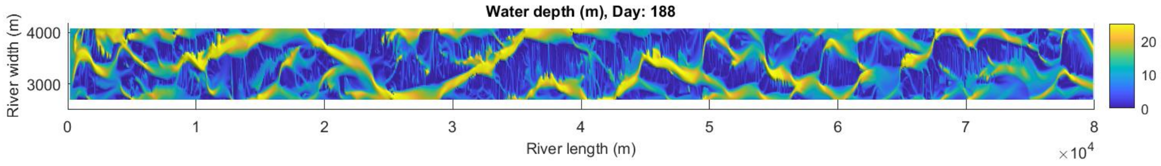

b) Scenario with 3000 Mp/m^3

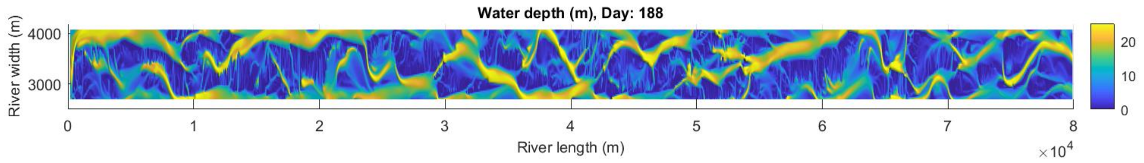

Figure 5-19. Water depth spatial distribution for the day 188. Scenario with a) 1000 Mp/m^3 and b) 3000 Mp/$m^{3.}$ The yellow areas are deeper depths, and the blue areas are the shallow depths.

5.4. Discussion

5.4.1. Microplastics fluxes balance

The erosion-depositional numerical model with plastic pollution defined the sediment bed as a source of storage of non-buoyant microplastic near the upstream boundary, with slow transport downstream. The non-buoyant plastic pollutants that enter the braided river in suspension, are deposited in the riverbed, and are resuspended. The microplastic, on average, travel with a speed of 140m/day for the model with 1000 m^3/s and 173 m/day for the 3000 m^3/s, travelling between 6-7 km in 42 days in average flow conditions. The model predicted that microplastic fluxes travel faster as more microplastic is in the system (higher concentration).

The transport of particles in suspension, the high deposition of the plastic near the sources, and the slow transport downstream have been found in studies of microplastic pollution. Koutnik et al. (2021) analysed the microplastic field concentrations reported by 196 studies from 49 countries. They described that the concentration of microplastic in rivers is higher than on the coast, reflecting the increased capacity of storage of microplastic loads in the river system. Corcoran et al. (2015), based on the field study of sedimentary layers in a lake, found that microplastic was deposited in the deepest region for less than 38 years. Nizzetto et al. (2016) created a mathematical numerical model of the Thames River. They mentioned that non-buoyant microplastics larger than 0.2 mm are contained in the sediment and resuspended in high flows. The Brisbane River (Australia) was modelled by He et al. (2020) with a three-dimensional particle transport numerical modelling; the high-density plastics accumulate close to the source points, high velocity promotes the transport of the sinking microplastics in the bed, and described a slow dispersal and transport of the microplastics in the river. Ballent et al. (2013), in their numerical models of plastic pollution in Nazaré Canyon (Portugal)also mentioned an essential accumulation of plastics near the release points. Agreement with the observations here.

The results have implications for the estimations of how much plastic enters the oceans from the river system per year, reinforcing that system wide mobilisation of plastics in rivers is limited (Emmerik et al., 2022; He et al., 2020; Koutnik et al.,2021). It is key to consider the hydraulics, hydrology, interactions in the bed, and concentrations of plastic, to evaluate the high storage capacity of the plastic near the sources and it transports speed.

5.4.2. Morphology changes

The high deposition of microplastic in the sediment bed at the beginning of the model generated changes in the morphology of the braided river, influenced by the exchanges of the sediment-microplastic loads in the river strata. Experimental tests suggest that the presence of the plastics increased the average diameter of the materials in the bed and that a higher critical shear stress is needed to erode the bed ([b]Waldschläger and Schüttrumpf, 2019; Ockelford et al., 2020,). The estimation of this effect is indirectly calculated with the erosion parameter and the shear stress in the formulation of Partheniades-Krone (Partheniades, 1965). Allowing the model to recreate the effects of the plastic in the sediment bed as demonstrated in Section 5.2.1, where a high erosion parameter promoted higher sediment erosion rates and lower values promoted less erosion.

The high amount of particles deposited at the beginning of the model impacts the formation of the river bed. In the model with 1000 particles/m^3, the plastic slowed down the erosion rates in the sediment bars and river banks, resulting in deeper channels. In the braided river with 3000 particles/m^3, a large amount of plastic deposited in the bed was such that the model could not create a braided river planform. Instead, a single channel was formed to the left of the grid.

Figure 5-20, shows the classification of the bed elevation into four categories (0.9, 0.8 and 0.6) to highlight the changes in morphology between the scenarios. Yellow represented the top of the bars, green the deeper elevations of the bars, blue higher elevations of the channels and white the deeper. The green areas can be classified as crossbar channels or the top elevation of the channels (banks). The percentages of this area are included in Figure 5-20 to compare the scenarios. It is estimated that the braided river with plastic increased the top of bars areas from 43% (without plastic) to 46-47% (with plastic), and the intermediate elevations increased from 19% (without plastic) to 20%-25% (with plastic). The channels decreased from 38% (without plastic) to 34% -28% (with plastic). Confirming that the model recreated reasonable results in the morphology changes where plastics promote higher critical shear stress to erode the bed ([b]Waldschläger and Schüttrumpf, 2019; Ockelford et al., 2020), extending the areas of the bars and promoting deeper channels.

Russell et al. (2022), used flume experiments to demonstrate that interaction between microplastics and sediment in the bed depends on the density of the particles and gravity. In tests the erosion of the outer side of the dune (stross side) increased by the presence of the plastic. The internal deposition side (lee side) was slower, so dune is overlain by migration of dunes, forming heterogeneous deposits in the sediment bed (Russell et al. 2022). The same effect is observed on a bigger scale in the numerical models, where high plastic deposition fills the shallower channels (Figure 5-20), forming plastic deposits and affecting the lateral evolution of the channel morphology.

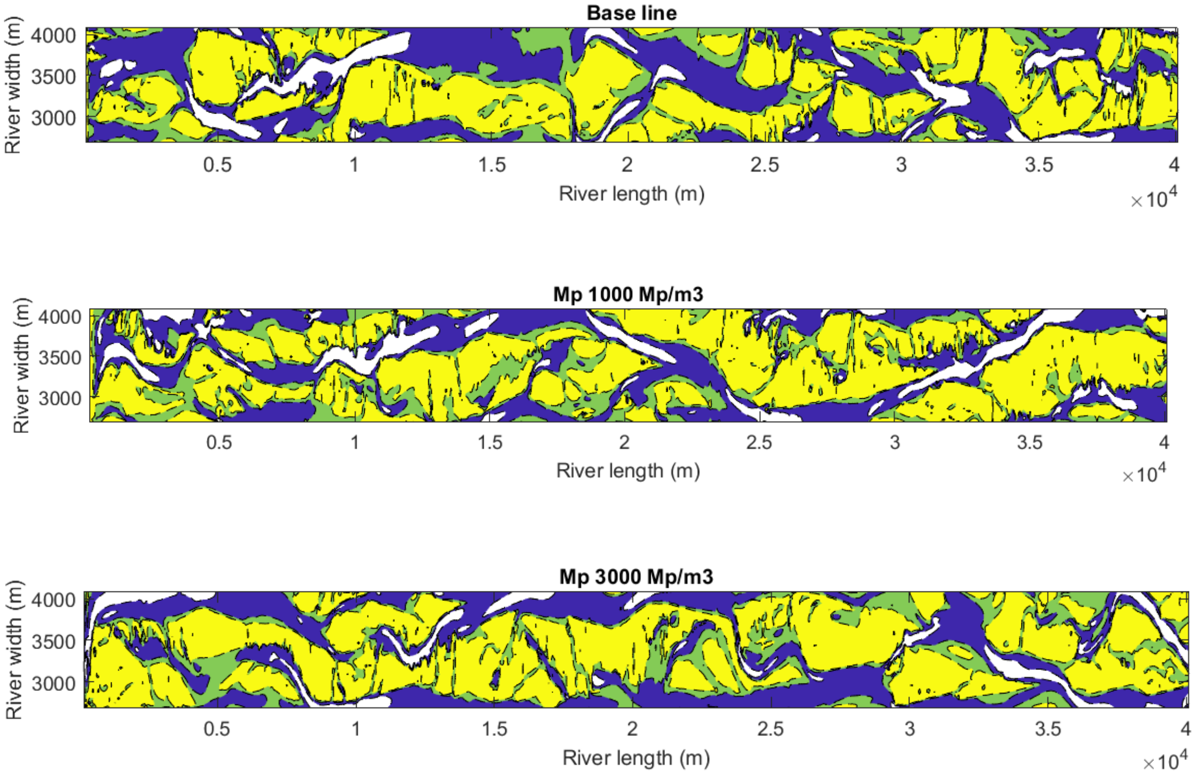

Unitary normalised depths (-)		Description	Elevation distribution (%) Baseline	Braided river with microplastic 1000 Mp/m^3	3000 Mp/m^3
	1.0-0.9	Top of bars elevations	43%	46%	47%
	0.9-0.8	Intermediate elevations	19%	20%	25%
	0.8-0.6	Channel elevations.	38%	34%	28%
	0.6-0.0	Deeper channel elevations			

Figure 5-20. Spatial distribution and percentages of the unitary bed elevation of the scenario without plastic (baseline) and scenarios with plastic. The yellow represents the top of the bars, the green channels banks or crossbar channels, the blue intermediate channel elevations and the white deeper channels elevations.

5.4.3. Patterns of deposition and transport

From the study of the spatial distributions of the suspended load, it was noticed that the microplastic is transported only in the channels (Figure 5-14 and Figure 5-15); it was determined that most of the microplastic load for days 188 to 229 is transported in the main and secondary channels. Deposits and resuspension take place in this area. Explaining that most of the microplastic deposit on the bars is a consequence of previous time steps, before day 188. To study this effect, the evolution in the time of the bed elevation, suspended and deposited microplastic load was plotted for the cross-section 2.5 km (scenario 1000 Mp/m^3) for the days 4, 10, 52, 104, 188, 208, 229 and 313 (Figure 5-21). The three diagrams were plotted in unitary normalized depths to observe them on the same scale and facilitate the comparison of the variables.

The evolution of these cross-sections showed a suspended load travelling across the model's width from day 0 to 10 (Figure 5-21-b). On day 10 the method started to create a channel in distance axis 1500 m until day 313 (Figure 5-21-a). A second channel is formed from day 52 to day 313 in distance axis 1000 m (Figure 5-21-a). Comparing the suspended load with the bed elevation, it is noticed how the microplastic fluxes started to concentrate in the second two channels from day 52 to 313 (Figure 5-21-b), as the last channel is filled. The deposited microplastic load is all over the 2.5 km cross-section from day 52 to 313 and can be concentrated in the main channels or on the bars (Figure 5-21-c). Explaining how the model recreated the depositional processes of the mixed layer of plastic and sediment during all the running. The effect of depositional layers could be studied in more detail with the software by adding vertical layers to the bed, but this was not the focus of this study.

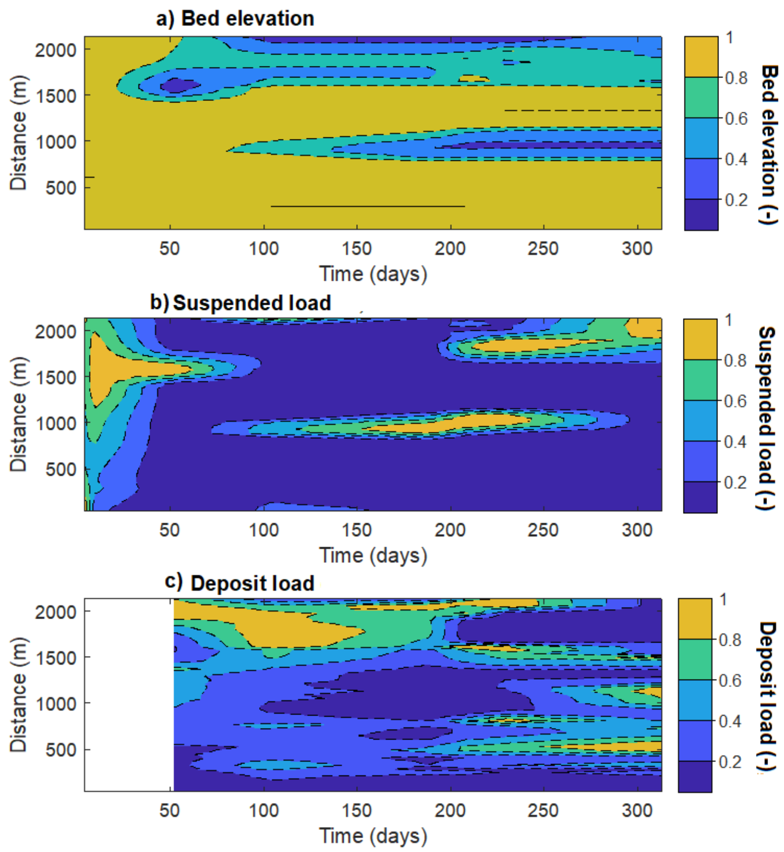

Figure 5-21. Unitary normalized depths (a), suspended microplastic load and (b) and deposited microplastic load evolution in time for the kilometer 2.5km. Scenario with 1000 Mp/m^3.

To study the microplastic deposited, it was decided to investigate the differences microplastic evolution of the channel since the spatial distribution analysis showed that a percentage of microplastic deposition in the first kilometres of the rivers corresponded with the previous time steps (Figure 5-21). Thus, total deposited microplastic load was subtracted for day 229 minus day 188. Positive and negative values, represented erosion and deposition rates (Figure 5-22).

The analysis (Figure 5-22) shows that the microplastic is deposited on the bars and river banks. The highest amounts are deposited in the inner curve of the bank main channel, areas recognised as deposition zones with lower velocities (Bathurst et al., 1979; Yang et al., 2012). Mani et al., 2016, described higher retention of microplastic particles in the right bank of the Rhine river delta, in the lowest flow velocity, where sedimentation rates increased. The lowest amount was deposited in the deeper areas of the channels, areas with higher velocities. The same pattern has been found in field samples by Rezende-Gerolin (2020), who described that lowest microplastic concentrations in the Amazon river are near the erosive areas, especially in the thalweg.

The higher suspended load travels in the braided river's main channel (Figure 5.22) and then enters the crossbar channels; consequently, microplastic loads are higher in the main channel than in the secondary. In terms of spatial distribution, the highly suspended microplastic load can be found in the thalweg of the main channel, which has been recognised as the area with higher velocities and more extended transport of microplastics (He et al., 2020).

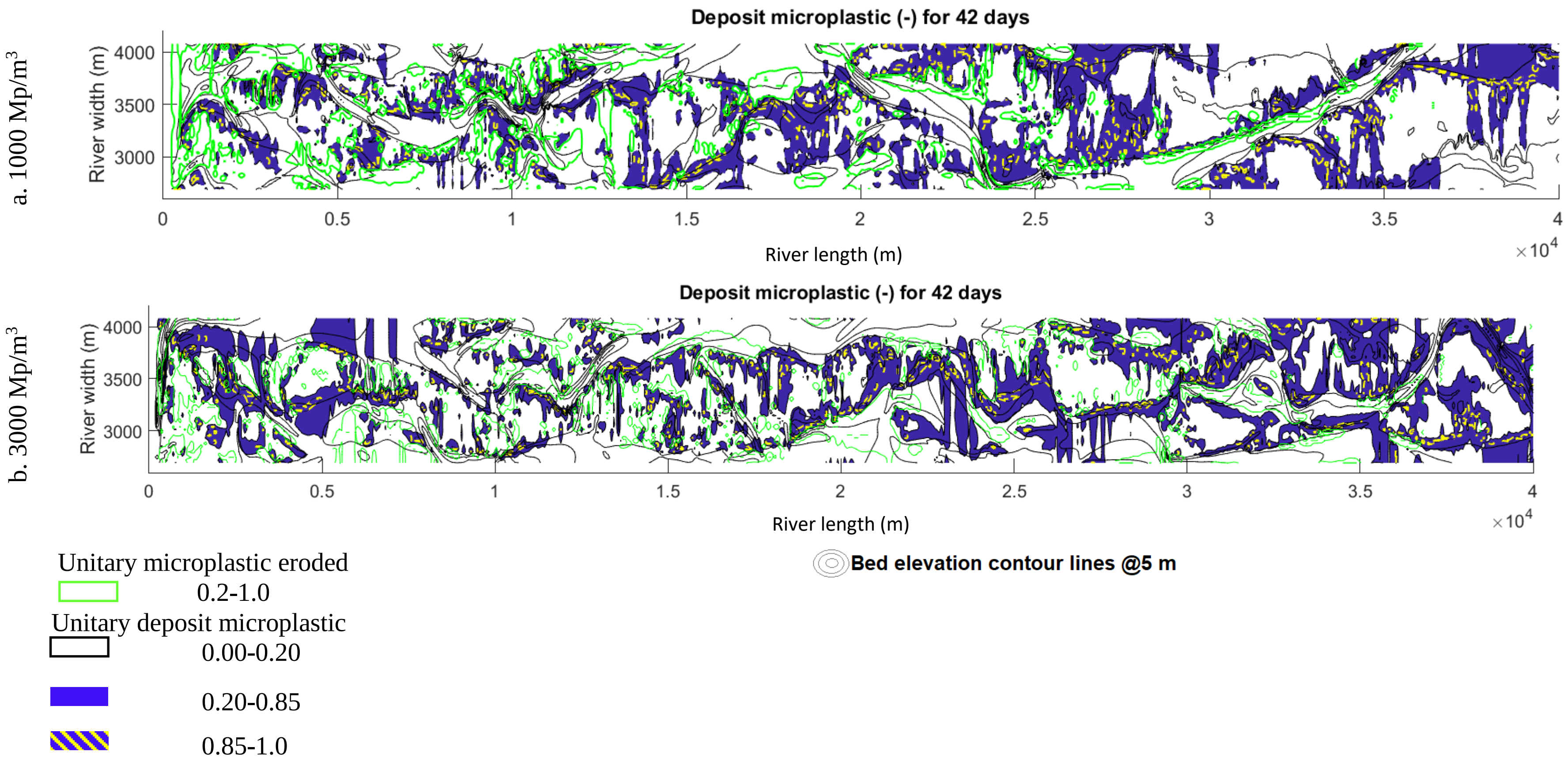

Figure 5-22. Total microplastic deposit and erode for 42 days. The green areas represent the microplastic eroded, the white areas the lower microplastics deposits, the blue areas the medium microplastic deposits, and the blue-yellow dashed areas the higher microplastics deposits. The dark grey lines are the river bed elevation every 5 m of the river.

a. 1000 Mp/m^3

b. 3000 Mp/m^3

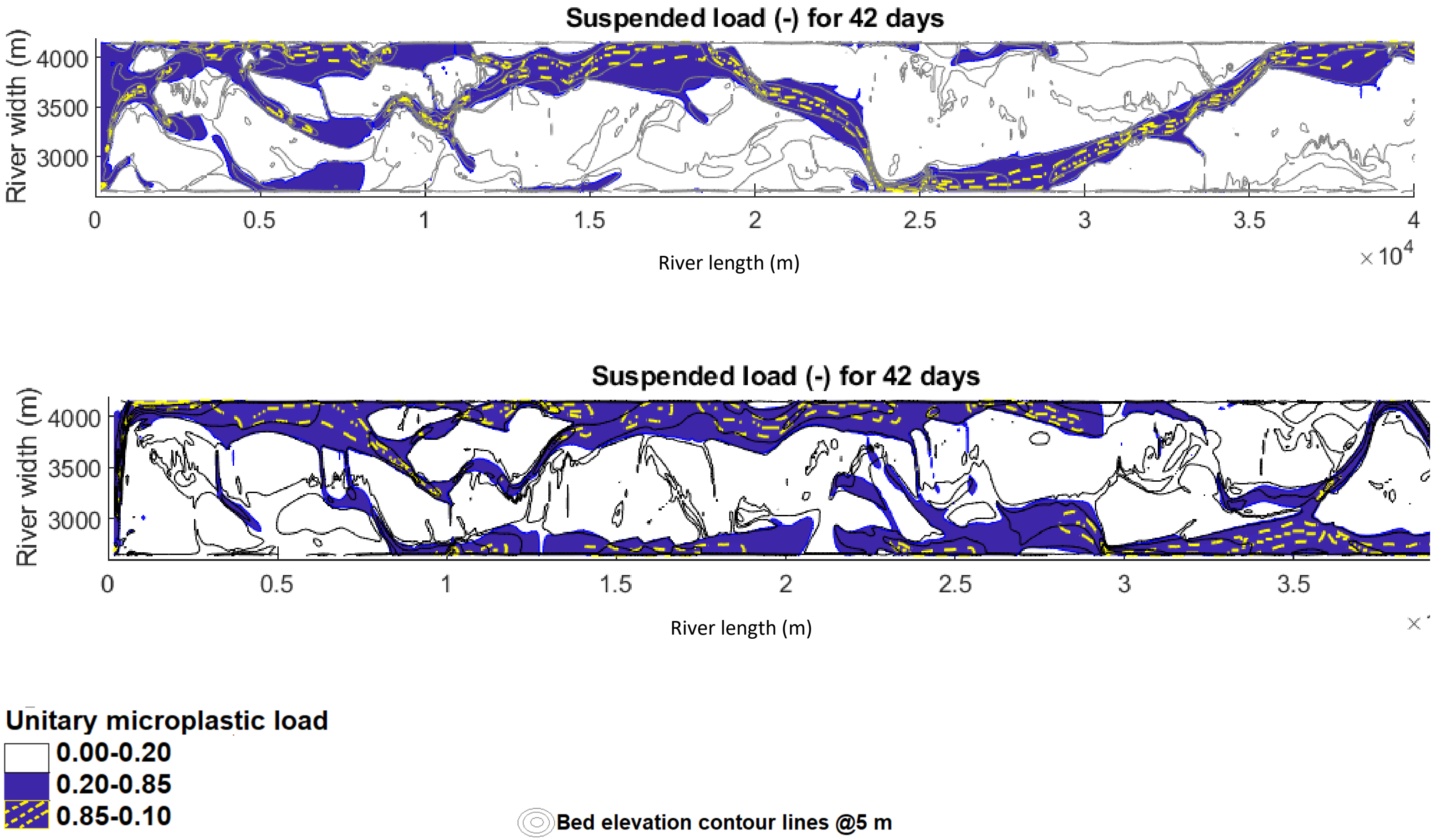

Figure 5-23. Microplastic suspended load for the study period. The white areas transport the lower suspended load, the blue areas the medium suspended load and the blue-yellow dashed areas the highest suspended loads. The dark grey lines are the river bed elevation every 5 m of the river.

5.4.4. Interpretation of the results and review of research question answers

The numerical morphodynamical model for particle transport predicts the interaction between the microplastic and sediment in the riverbed.

The artificial braided river simulation computed a riverbed, where the sediment bed acts as a source of storage of non-buoyant microplastic near the releasing points (Ballent et al. 2013, Nizzetto et al. 2016; He et al. 2021), with slow transport downstream. The non-buoyant plastic pollutants enter the braided river in suspension, are deposited in the river bed, and may become resuspended. The plastic deposited forms layers of mixed sediment that overlap, storing the plastic and reducing the volume available to be transported. The model predicts that microplastic fluxes travel faster as there is more microplastic in the system due to the higher concentration.

The total plastic load that river transport is probably one of the most critical parameters to determine to estimate the amount of plastic pollution that contaminates the oceans. New methodologies to estimate the plastic pollution of a catchment, including details of plastic sources (care products, laundry textiles, and others) and future scenarios, are being develop (Nizzetto et al., 2016; Siegfried et al., 2017; Lebreton et al., 2017; van Wijnen et al., 2019). However, understanding the distribution of the concentration of plastic pollution in rivers was demonstrated to work as a more accurate estimation of the total load of plastic than river transport. Results that suggest not all plastic from the river system is transferred to the ocean, particularly macroplastics that can have larger sizes and weights. The increased amount of microplastics deposited near the sources helps to detect industrial emissions, becoming an indicator of plastic pollution bases (Schecer et al., 2020).

The artificial river was created to interpret the repercussions of the microplastic particles and sediments interacting in the river bed and evaluate the impact on the transport downstream of the microplastic particles. In the timescale of the numerical model (42 days), the 100% microplastic load was deposited with a constant flow condition of 20 000 m^3/s. Rivers have a natural temporal variation in discharge, it is expected that in extreme events, the re-exhumed and flushed through the system increase, and in low flows, the re-exhumed decrease. Emphasises the importance of incorporating the hydrological cycle to study the microplastic dynamic fluctuations transport and deposition to estimate a more precise value of the microplastic flows balances.

The high deposition of microplastic in the sediment bed at the beginning of the model generated significant changes in the morphology of the braided river, influenced by the exchanges of the sediment-microplastic loads in the river bed. The presence of the plastics increased the higher critical shear stress needed to erode the bed ([b]Waldschläger and Schüttrumpf, 2019; Ockelford et al., 2020); increasing the capacity of the river flow to erode the bars and banks channels, resulting in deeper channels. Similar effects have been measured by the effect of vegetation and cohesive sediments (Weisscher et al, 2019).

The highest amounts of microplastics are deposited in the inner curve of the bank channel, areas recognised as deposition zones with lower velocities and accumulation of plastics (He et al., 2021, Kumar et al., 2021). The higher suspended load travels in the main channel of the braided river and then enters the secondary channels. The highly suspended microplastic load is transported in the thalweg of the main channel, which has higher velocities enhance transport microplastics (He et al., 2021)

The model explains that the effects on the microplastic spatial distribution are related to the hydrodynamic conditions, sediment particle size, and flows (Yang et al., 2021). Researchers do not have specific methods to allocate the samples in the field along the river banks, describing the microplastic deposits with a highly heterogeneous lack of consistency (Lenaker, et al., 2019; Kumar et al., 2021). The spatial distribution highlights microplastics can be deposited everywhere, but hots spots are presented as extended areas, with effect of retention in depositional layers. Thus, the best way to find a depositional pattern is to use cross-sectional sampling. Samples in the river banks, sides, and depth, reduces uncertainty (Haberstroh et al., 2020). From the suspended distribution, it is suggested that the water samples should be related to the velocity profiles of the river flow.

5.4.5. Model advantages and limitations

The most important advantage of the multiphase sediment transport model is the capacity to recreate a riverbed where a microplastic load and sediment particles exchange materials from the bottom computational layer to the bed and vice versa (Delft, 2022). The model simulated the changes in the erosion rates as a consequence of the microplastic in the sediment bed. The model assumed that the erosion rate is proportional to the availability of the sediment fraction considered in the top-most layer of the bed stratigraphy, making the model useful to consider the microplastic storages in the river bed.

The limitations of the multiphase sediment transport mode used, include the estimation of the erosion parameters, the deficiency of bed load transport and the lack of inclusion of microplastic aggregation processes. Further work, is recommended for proper estimates of erosion parameters for the specific microplastic and sediment mixtures in controlled laboratory conditions. In Section 5.2, Figure 5-8, this is a key parameter that shapes the morphology of the river and, depending on the value, will generate wrong result. However, the variety of microplastic density -shapes, and sediment size generates a range of erosion parameters scenarios limiting the method's access. The formulation of Partheniades-Krone (Partheniades, 1965) is based on the deposition and resuspension process and does not include estimations of bed load transport. The bed load transport can be significant in denser and larger microplastics, as it has been observed in flume experiments with microplastics and sediment (Russell et al., 2022). Finally, aggregation cannot be integrated when using this method (Hann et al., 2019; Leiser et al., 2020, Shiravania et al., 2023).

The study case is an artificial river that created bed forms of the river bed based in function of the river flow, particles physics characteristics (density, size, erosion parameter) and predictors of transport and deposition. Based on the initial conditions as it was indicated the numerical model converge to one solution. The results presented in the numerical model refers it specific study case to achieve the main objective to recreate a more realistic model that includes the interaction of the microplastic and sediment in the river bed.

5.5. Conclusion

The research transport and deposition of microplastic particles in a braided river: Hydro-morphodynamical numerical model using the software Delft3D', recreated a numerical model with the dynamics of deposition, erosion, resuspension, and transportation of negative buoyant microplastics in a braided river. The model estimated a riverbed where the sediments and microplastic particles interact as a function of the river flow. The study included three scenarios, one braided river without microplastic as baseline case and two scenarios with low (1000 Mp/m^3) and high (3000 Mp/m^3) suspended microplastic load. The scenarios were used to predict the morphodynamic changes in the river due to the presence of the plastic and study the temporal and spatial distribution of the suspended and deposited microplastic load.

The artificial braided river simulated a sediment bed that acts as a source of storage of microplastic near the release point, limiting the availability to be resuspended and transported downstream. The high deposition of microplastic increases the capacity of the river flow to erode the bars and banks channels, resulting in deeper channels and increased river bars. The highest amounts of microplastics were deposited in the inner curve of the main channel in the banks, and the highly suspended microplastic load is transported in the thalweg of the main channel.

The hydro-morphodynamical numerical model with microplastic presents a method to estimate the spatial and temporal distribution concentration of plastic pollution in rivers. The spatial distribution of the artificial river explains that microplastics can be deposited and storages everywhere, with localised extended hots spots areas. Therefore, it is recommended that for the study of the microplastic spatial distribution in the field, the sediment samples must be sampled cross-sectionally in the river bed, and water samples should be related to the velocity profiles of the river flow.

Finally, the method can be used to study the spatial distribution of plastic near releasing points when the relevant parameters are the depositional process and detention of hotspots of negative buoyant microplastic. For more accurate results, better estimates of the erosion parameter for the specific microplastics and sediments must be considered. It is recommended test the software with depositional layers hindered effects and compare it with laboratory conditions, useful for studying the stratigraphy of the microplastic and sediments in the riverbed.

Chapter 6 . Conclusions

Summary of the thesis and the main objective

The dynamics of microplastics particles in rivers: experimental settling processes and numerical models of the transport and deposition research focused on try to understand the physical parameters that govern the dynamics of deposition and transport of microplastic particles in fluvial systems through laboratory experiments and numerical models. The experimental work was conducted to understand the settling process of suspended microplastic and sediment mixtures, using settling tubes with nylon pellets. The particle interactions in the suspension defined the height and composition of substrate formed between the nylon pellets and the sediment after the settling process. A numerical model of an artificial braided river was chosen to complement the results of the experiments. The model was used to quantify the dynamics of a nylon suspended microplastic load, focusing on recreating the interaction of the microplastic and sediment in the riverbed. Based on three scenarios, it was possible to understand the transport, deposition and resuspension of suspended nylon microplastic load in a braided river. Integrating the work and numerical studies enhances understanding of microplastic's vertical, spatial and temporal distributions patterns in fluvial environments.

Composition thesis: experimental work and numerical model

- **Description objective 1: Experimental work**

The experimental work consisted of 52 experimental settling tubes with positively, neutrally, and negatively buoyant suspended microplastic-sediment mixtures. The microplastic selected to run all the experiments were negatively buoyant microplastic Nylon pellets (ρ_{MP} = 1150 kg/m^3, D_{50}=686±2.4μm) and sediments (ρ_s = 2500 kg/m^3, D_{50}=105±0.2μ). The neutrally and positively buoyancy microplastic conditions were created with saline solutions of variable densities. Each settling tube contained different volumes of microplastic, sediment, and fluid.

By studying the stratigraphy formed after the settling process, it was determined that the formation of the substrate types, their heights, and typical grain sizes depended on the sediment, microplastic, and fluid density volumes in the suspension. The suspension density described the representative of this physic characteristic (ρ_{sus}), a parameter that relates the density of the materials with the volumetric contents and can be related with the particle interaction behaviour in the deposition process.

The particle interaction behaviour was described as a free or hindered regime. In a free regime, the particle's interaction in the suspension is not strong enough, and particles fall (negatively buoyancy) or rise (positively buoyancy) as individual particles. At the beginning of the regime, all the particles are in suspension and mixed all over the settling tube. Denser-bigger particles fall first following the medium, smallest and lighter-bigger particles rise first following the medium, smallest, defining a graded stratigraphy. Opposite, at the beginning of the hindered regime, the particle's interaction in the suspension accelerates the rising velocities of the neutrally-positively buoyant particles. It reduces the fall velocity of the negative particles. When the movement and arrangement of the particles reach the final phase, the rising negatively buoyant particles can be deposited at the top of the substrate, this means the initial suspension density conditions dictate the initial dynamics of the particles and the final sedimentation is government by the fluid density. In the settling regimes the range of reduction or acceleration of the particles velocity strongly depends on the number of particles in the suspension and its physics characteristic.

In the experimental work, the threshold condition between the free and hindered regime is defined in the function of the suspension densities:

In suspension densities lower than ρ_{sus}<1270 kg/cm^{3,} the particle's interaction in the suspension is not strong enough, and particles fall (negatively microplastic) or rise (positively microplastic) as individual particles. Denser-bigger particles fall first following the smallest medium, and lighter-bigger particles rise first following the smallest medium. In the experimental conditions, the sediment fall velocity was higher than rising microplastics, and the neutrally-positively buoyant microplastics got trapped in the sediment. The negatively buoyant microplastics form mixed substrates because both particles can settle at similar velocities.

In the negatively buoyant microplastic settling tubes in suspended concentrations between 1110 kg/cm^3 to ρ_{sus}<1270 kg/cm^3 were classified in a transition zone between the free and hindered regime. It was determined that the interflows surrounding the sediment particles slow down the negatively buoyant microplastic deposition and start to affect the reduction of fall velocity microplastic. Some particles can sink (free regime), and others start to rise (hindered effects).

Settling tubes with suspended concentrations higher than 1270 kg/m^3 were defined in suspended concentrations with hindered effects; negatively, positively, and neutrally microplastics cannot get trapped inside the deposit. The particle's interaction in the suspension slows the sediment deposition, accelerates the rising velocities of the neutrally-positively buoyant microplastics, and inverts the fall velocity of the negative buoyant microplastic. The sediment fall velocity is not fast enough to trap the rising neutrally or positively buoyant microplastics. The neutrally-positively buoyant microplastics rise to the top of the fluid across the sediment and form a suspended microplastic layer. The neutrally microplastics can sink at the top of the sediment in the later stages of the settling process when the particle interactions dissipate. The negative microplastic particles rise to the top of the substrate forming the smallest mixing substrates.

Figure 6-1, summarizes the free and hindered settling regimes.

Settling process of suspended concentrations of microplastic and sediment	
Free settling regime 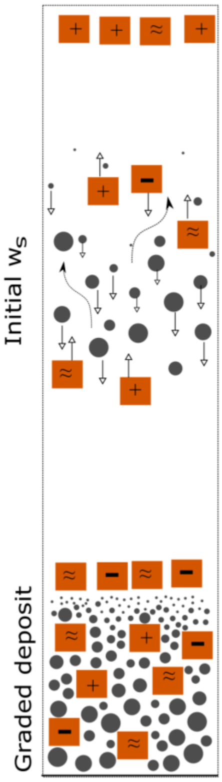	**Hindered regime** 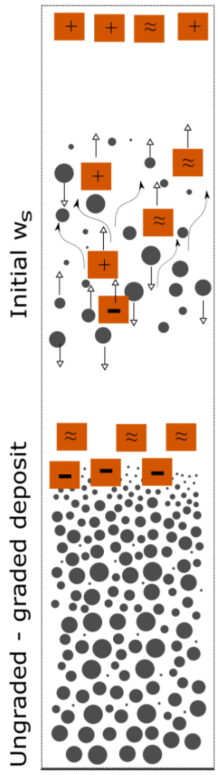
Sediment particles fall in a free-settling regime. Negatively, positively and neutrally buoyant microplastic particles can form mixtures of microplastics and sediment. The sediment fall velocities are higher than rising microplastics, and the neutrally-positively buoyant microplastics can get trapped in the sediment. The negatively buoyant microplastics form mixed substrates because both particles can settle at similar velocities. The stratigraphy formed depends on the volume, size distribution, and plastic density.	The particle's interaction in the suspension accelerated the rising velocities of the neutrally positive microplastics and reduced the fall velocity of the negatively buoyant microplastics and sediments. The sediment fall velocity is not fast enough to trap the rising neutrally, negatively, or positively buoyant microplastics. The neutrally-positively buoyant microplastics rise to the top of the fluid across the sediment and form a suspended microplastic layer. The neutrally microplastics can sink at the top of the sediment in the later stages of the settling process when the particle interactions dissipate. The negative microplastic rise to the top of the substrate between the sediment particles and forms the smallest mixing substrates.

Figure 6-1. Settling regimes of suspended concentration of microplastic and sediment. In the diagrams, the orange square represents the microplastic particles, the grey spheres represent the sediment, the straight line represents the movement of the particles, and the irregular lines represent the interflows.

From the settling tubes experimental results it is inferred that the deposition of a microplastic particle in the sediment bed is a function of the plastic density, size distribution and volumetric contents in the suspension. Depending on these physical parameters, the same nylon microplastic pellet was deposited in different depths in a free settling regime or cannot be deposited in the sediment core with hindered effects. The results help to understand that the same microplastic particles can be deposited in top layers in higher suspended concentrations, in lower suspended concentrations, the microplastic particle can be deposited deeper in the sediment bed, and in intermediate suspended concentrations, the plastic can settle at middle depths. The deposition of a microplastic particle in the sediment bed in the settling tubes helps to clarified the main goal of this research, explaining why researchers commonly found the same type of plastics deposited in sediment beds. Concluding that one of the parameters that governs the deposition depth in mixtures of sediment and microplastics in calm waters are the plastic-sediment properties (density, size, geometry) and the number of particles in the suspension.

- **Description objective 2: numerical model.**

The numerical model with plastic consisted of an artificial braided river that recreates the dynamics of sedimentation, erosion, resuspension, and transportation of microplastics together with sediment particles. The model was created to study the morphodynamical evolution of a river in the presence of microplastic, fluxes balances and patterns of transport and deposition.

The software used is Delft3D, and the method selected is the hydro-morphological flow. The study case is a braided river with a size of 2.5 km width and 80 km long, with a computational grid of 62x1202 rectangles. The river discharge was prescribed at the upstream boundary with a total of 20 000 m^3/s. The sediment bed was composed of sand (non-cohesive sediment) with D_{50}=105 µm. A second particle fraction added to the software represented the microplastics suspended load, with a diameter of D=686 µm and a density of 1150 kg/m^3.

Three scenarios were created as study cases. A morphodynamical braided river model without plastic. Used as a baseline to compare the morphology changes with the plastic scenario. Two morphodynamical models with plastic, one with a suspended microplastic load of 1000 particles per cubic meter and a second with 3000 particles per cubic meter. The microplastic load was added as an upstream boundary and constant suspended concentration.

The model recreated the dynamics of sedimentation, erosion, resuspension, and transportation of microplastics together with sediment particles. The artificial braided river computed a river bed where the sediment bed acts as a source of storage of microplastic near the release point. The non-buoyant plastic pollutant enters the braided river in suspension, are deposited in the river bed, and resuspended. The plastic was stored in the sediment bed in layers that overlap.

The model predicted that microplastic fluxes travel faster as there is more microplastic in the system due to the higher concentration.

The microplastic particles were deposited all over the riverbed of the braided river. The highest amounts were spread in all the channels and bars, in areas close to the river banks. The hotspots were identified as extended areas deposited in the inner curve of the main channel, areas recognised as deposition zones with lower velocities and accumulation of plastics (Figure 6-2). The suspended load travels in the main channel of the braided river and then enters the secondary channels. The highly suspended microplastic load is transported in the thalweg of the main channel, which has been recognised as areas with higher velocities and more extended to transport the microplastics (Figure 6-2). Finally, it was determined that the high deposition of microplastic generated changes in the bedforms of the braided river, influenced by the exchanges of the sediment-microplastic loads in the bed, increasing the capacity of the river flow to erode the bars and bank channels.

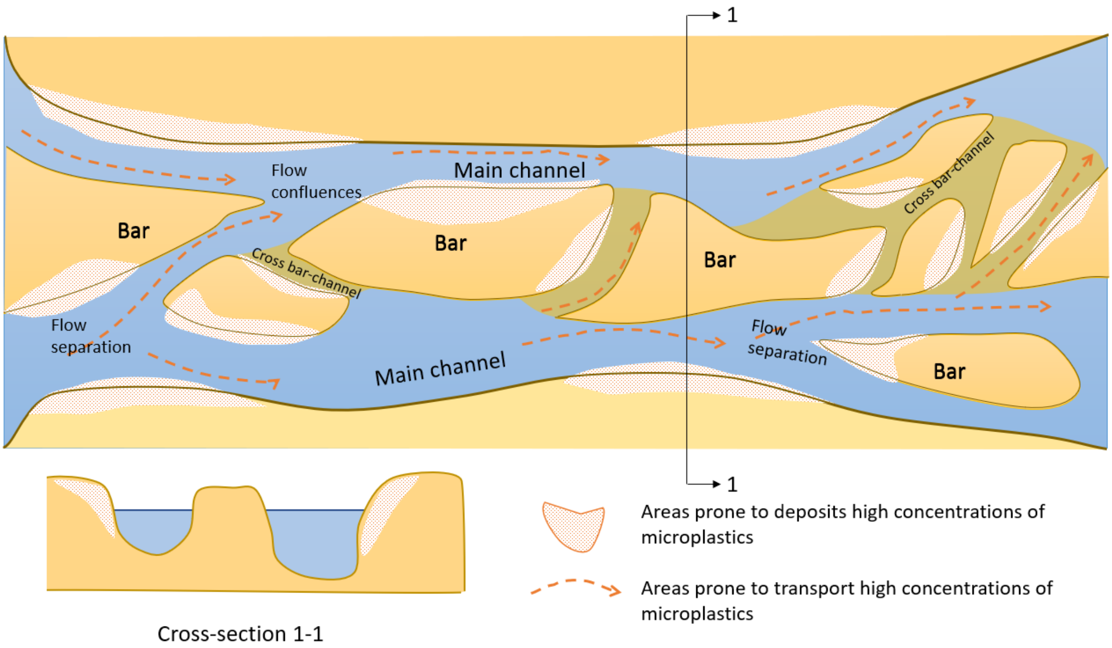

Figure 6-2. Patterns of transport and deposition of the highest concentrations of microplastics in a trenched river.

Significance of the work, recommendations, and future work

The experimental and numerical model work helps explain microplastics' spatial distribution. The settling tubes demonstrated that a negatively, positively and neutrally microplastic particle can be deposited vertically in the sediment bed. The artificial braided river explained the dynamic of the horizontal deposition, the microplastics was deposited all over the riverbed, higher deposits were described as extended areas near the riverbanks, and there was a significant effect of microplastic storages. Helping to understand the reasons for the heterogeneous dispersal distribution found in the sediments.

The results of the experimental work and numerical model help to interpret the dynamics of transport and deposition of the microplastic particles. From the experimental work results, it is inferred if a negatively bouncy microplastic enters the river system, it will be predominantly deposited and stored near the sources. The depth of deposition will be defined by the hydraulic conditions of the river flow, the concentration of the suspended load, the size, shape and density of the plastic, as well the characteristics of the sediment. In the case of positive and neutral particles will be deposited on the sediment substrate in calm water conditions when the interactions between sediment and microplastic particles are in a free regime as long as the speed of rising microplastics is not fast enough at the rate of fall of the sediment.

The numerical model suggested that the resuspension and transport of the microplastic particles will depend on the depth at which it is deposited and the erosion parameters of the river bed, which vary according to the quantity, types, sizes and shapes of microplastics deposited on the substrate. Once the particles are in suspension, their travel times will depend on physicals characteristics and the river flow's hydraulic conditions (velocities and shear forces). The hydro-morphodynamic microplastics-sediment model results have important repercussions in calculating how many microplastic particles enter the river and can reach the Ocean. Emphasizing that the quantity of plastics transported from the sources to the ocean is also controlled by the hydrology and morphology of the catchment. The possible retention effects of microplastics in sediment layers should have a significant value in the estimation, as a short term effects. In the long term, the material retained in the bed layers may be eroded and transported in extreme events.

It is recommended that field investigations of the distribution of microplastics be carried out with sediment samples cross sectionally in the riverbed, and water samples should be related to the velocity profiles of the river flow. According to the results, this will help to find patterns of microplastic concentration's horizontal spatial distribution. In the samplings that incorporate the study of the vertical arrangement of microplastics in the sediment layers, they should expect to find a heterogeneous pattern.

Upcoming laboratory experimental work should emphasise studying the depositional procedures considering more procedures such as aggregations and cohesive sediments. Parameters able to change the settling particle velocity, with effects in the stratigraphy.

The numerical models can be used to recreate study cases near releasing points, where the relevant parameters are the detention of hotspots of negative buoyant microplastic. It is recommended for more accurate results, flume experiments to determine the erosion parameter for the specific microplastics and sediments study case. It is suggested to test the software with depositional layers, hindered effects and compare it with flume conditions, to assess the effectiveness of the method predicting the stratigraphy of the microplastic and sediments in the river bed. However, it should be considered within the limitations of the method is not possible to model the bed load transport and aggregations processes.

Future work can be focused on including bed load transport, aggregations and positively-neutrally buoyant microplastic in the software methods. The bed load transport can have significant results in denser and larger microplastics, it is necessary to develop or validate existed predictors for this process. Aggregations create denser and larger particles, modifying fall velocity, changing height of deposition, transport distances and resuspension capacity. Also, it is suggested that the model can recreate the retention of positively and negatively microplastics particles in the sediment bed in a free settling regime, integrating the results of the experimental work.

The results of this study help to understand the effects of microplastics pollution in rivers. The pollutant has a high capacity for dispersion and storage in rivers. Microplastics are transported through the main channels and spread to the tributaries. They are deposited on the riverbed, banks and islands. High concentrations are transported in high velocity zones. The so-called hot spots in the sediment deposits are located near the banks, and extend into the islands, flood plains. The dynamic and the high heterogeneity that characterizes plastics explain the consequences of this pollutant. Plastics contain chemicals that deteriorate the quality of sediments and water, and several organisms have been shown to mistake this material for food and ingest it.

Finally, it is recommended to strongly focus the mitigation measures to reduce the effects of this environmental pollutant on the sources and more rational use of this material. The dynamics of microplastics particles in rivers: experimental settling processes and numerical models of the transport and deposition thesis has exemplified that as soon the pollutant enters the river, there can be a high dispersion and storage of the microplastic pollution in the rivers, impacting the water and sediments quality, life below water, in flood plain and close to the rivers.

Reference list

Abu-Hejleh, A. N., Znidarci, D., and Barnes, B. L., 1996. Consolidation characteristics of phosphatic clays. Geotechnical Engineer, 1224, 4., 295-301.

Alimi, O. S., Claveau-Mallet , D., Kurusu, R.S., Lapointe, M., Bayen, S., and Tufenkji, N. (2022) Weathering pathways and protocols for environmentally relevant microplastics and nano plastics: What are we missing ?. Journal of Hazardous Materials, 423 (A), 126955

Alosairi, Y., Al-Salem S.M., Ragum, A.Al., 2020. Three-dimensional numerical modelling of transport, fate and distribution of microplastics in the northwestern Arabian/Persian Gulf. Marine Pollution Bulletin, 161, 111723.

Amy, L. A., Talling, P. J., Edmonds, V. O., Sumner, E. J., and Lesueur, A., 2006. An experimental investigation of sand-mud suspension settling behaviour: Implications for bimodal mud contents of submarine flow deposits. Sedimentology, 53, 6., 1411–1434.

Apetogbor, K., Pereao, O., Sparks, C., Opeolu, B., 2023. Spatio-temporal distribution of microplastics in water and sediment samples of the Plankenburg river, Western Cape, South Africa/ Environmental Pollution, 323, 121303.

Baar, A.W., Albernaz, M.B., Dijk, W.M. and Kleinhans, M.G., 2019. Critical dependence of morphodynamical models of fluvial and tidal systems on empirical downslope sediment transport. Nature communications, 4303.

Ballent, A., Pando, S., Purser, A., Juliano, M.F., Thomsen, L., 2013. Modelled transport of benthic marine microplastic pollution in the Nazar´e Canyon. Biogeosciences, 10, 7957–7970.

Batchelor, G.K., 1982. Sedimentation in a dilute polydisperse system of interacting spheres: 1. General theory, Journal of Fluid Mechanics 119, 379-408.

Bathurst, J. C., Thorne, C. R. and Hey, R. D., 1979. Secondary Flow and Shear stress at river bends. Journal of the Hydraulic Division, 105, 1277-1295.

Bauer-Civiello , A., Critchell, K., Hoogenbooma, M. and Hamanna, M., 2019. Input of plastic debris in an urban tropical river system.. Marine Pollution Bulletin, 144, 235-242.

Besseling, E., Quik, J.T.K., Sun, M., Koelmans, A.A., 2017. Fate of nano- and microplastic in freshwater systems: a modelling study. Environmental Pollutant, 220, 540–548.

Best, J. L., 1987. Flow dynamics at river channel confluences: implications for sediment implications for sediment. In: Recent Developments in Fluvial Sedimentology. Tulsa: Society Paleontologist and Mineralogists, 27-35.

Bilal, A., Xie, Q., Yang, J. and Lundström, T. S., 2020. Flow and sediment behaviours and morpho-dynamics of a diffluence - confluence unit. River Research and Applications, 1-14.

Blair, C. B. and Quinn, B., 2017. Microplastic pollutants [ebook]. Amsterdam: Elsevier Science and Technology.

Blair, R. M., Waldron, S., Phoenix, V. R. and Gauchotte-Lindsay, C., 2019. Microscopy and elemental analysis characterisation of microplastics in sediment of a freshwater urban river in Scotland, UK. Environmental Science and Pollution Research, 26, 12491-12504.

Born, M.P., Brüll, C., Shaefer, D., Hilebrand, G. and Schüttumpf, H., 2023. Determination of Microplastics' Vertical Concentration Transport (Rouse) Profiles in Flumes . Environmental Science & Technology, 57, 5569-5579.

Bridge, J., 2013. Rivers and floodplains: forms, processes, and sedimentary record. Oxford: Black Well Science.

Browne, M. A., Crump, P., Niven, J.N., Teuten, E., Tonkin, A., Galloway, T. and Thompson, R., 2011. Accumulation of Microplastic on Shorelines Woldwide: Sources and Sinks. Enviromental Science and Technology, 45, 21, 9175-9179.

Camenen, B., 2007. Simple and General Formula for the Settling Velocity of Particles. Journal of Hydraulic Engineering, 133, Issue 2, 229-233.

Castañeda, R.A., Avlijas, S., Simard, M.A., Ricciardi, A., Smith, R., 2014. "Microplastic pollution in St. Lawrence River sediments". Canadian Journal of Fisheries and Aquatic Sciences, Vol. 71 No. 12, 1767–1771.

Charlton, R., 2008. Fundamentals of fluvial Geomorphology. New York: Taylor and Francis e-Library.

Chaudhry, M. H., 2008. Open-Channel Flow. Second Edition ed. New York: Springer Science Business Media.

Chouchene, K., Prata, J. C., da Costa, J., Duarte, A. C., Rocha-Santos, T. and Ksibi, M., 2021. Microplastics on Barra beach sediments in Aveiro, Portugal. Marine Pollution Bulletin, 167, 112264.

Church, M., Roy, A. G. and Biron, P. M., 2012. Gravel-Bed Rivers: processes, tools, environments. West Sussex, John Wiley and Sons.

Colebrook, C. and White, C., 1937. Experiments with fluid friction in roughened pipes. Proc. R. Soc. Lond. Ser. A Math. Physics Science., 161, 367-381.

Cook, S., Chan, H., Abolfathi, S., Bending, G.D., Schäfer, H., Pearson, J.M., 2020. Longitudinal dispersion of microplastics in aquatic flows using fluorometric techniques. Water Res. 170, e115337

Corcoran PL, Norris T, Ceccanese T, Walzak MJ, Helm PA, Marvin CH, 2015. Hidden plastics of Lake Ontario, Canada and their potential preservation in the sediment record. Environmental Pollution, 204,17-25.

Correia, J.P., da Costa, J.P., Duarte, A.C., Rocha-Santos, A.C, 2019. Methods for sampling and detection of microplastics in water and sediment: A critical review. Trac Trends in Analytical Chemistry,110,150-159.

Critchell, K., and Lambrechts, J., 2016. Modelling accumulation of marine plastics in the coastal zone; what are the dominant physical processes? Estuarine, Coastal and Shelf Science, 171, 111–122.

Davis, R.H., and Gecol, H., 1994. Hindered settling function with no empirical parameters for polydisperse suspensions. AIChE Journal 40, 570-575.

Deltares, 2020. Delft3D- Flow user Manual. Delft: Deltares.

Dikareva, N., and Simon, K. S., 2019. Microplastic pollution in streams spanning an urbanisation gradient. Environmental Pollution, 250, 292–299.

Ding, Y., Liu, H., Yang, W., 2019. Numerical prediction of the short-term trajectory of microplastic particles in Laizhou Bay. Water, 11, 2251.

Dingman, S. L., 2008. Fluvial Hydraulics. New York: Oxford University Press.

Diplas P., Kuhnle, J., Gray. D., Glysson, D. and Edwards., T., 2008. Sediment transport measurements. In Garcia, M., ed. Sedimentation Engineering. Virginia: American Society of Civil Engineers, 307–353.

Dorrell, R. M., and A. J. Hogg, 2010. Sedimentation of bidisperse suspensions, International Journal of Multiphase Flow, 36, 481 – 490.

Dorrell, R.M., Hogg, A.J.; Summer, E.J. and P.J. Talling, 2011. The structure of the deposit produced by sedimentation of polydisperse suspensions. Journal of Geophysical Research, 116, F1.

Druitt, T., 1995. Settling behaviour of some concentrated dispersions and some volcanological applications. Journal Volcanology and Geothermal Research, 65, 27–39.

Drummond, J.D., Schneidewind, U., Li, A., Hoellein, T.J., Krause, S. and Packman, A.I., 2022. Microplastic accumulation in riverbed sediment via hyporheic exchange from headwaters to mainstems. Science Advances, 8(2).

Emmerik, T., Frings, R., Schreyers, L., Hauj, R., de Lange, S., Mellink, Y., 2022. River plastic during floods: Increased mobilization, limited river-scale dispersion. EGU General Assembly 2023, Vienna, Austria, 24–28 Apr 2023, EGU23-9164.

Emmerik, T., Strady, E., Kieu-Le, T., Nguyen, L. and Gratiot, N., 2019. Seasonality of riverine macroplastic transport. Scientific Reports, 9, 13549.

Enders, K., Lenz, R., Stedmon, C.A., Nielsen, T.G., 2015. Abundance, size and polymer composition of marine microplastics ≥10 μm in the Atlantic Ocean and their modelled vertical distribution. Marine Pollution Bulletin, 100, 70–81.

Engelund, F. and Hansen, E., 1967. A monograph on Sediment Transport in Alluvial Streams. Copenhagen: Teknisk Forlag. https://repository.tudelft.nl/islandora/object/uuid%3A81101b08-04b5-4082-9121-861949c336c9. [Accessed 28 11 2022]

Eo, S., Hong S.H., Song, Y.K., Han, G.M., Shim, W.J., 2019. Spatiotemporal distribution and annual load of microplastics in the Nakdong River, South Korea. Water Research, 160, 228-237.

Erni-Cassola, G., Zadjelovic, V., Gibson, M. I. and Christie-Oleza, J. A., 2019. Distribution of plastic polymer types in the marine environment; A meta-analysis. Journal of Hazardous Materials, 369, 691-698.

Fan, Y., Zheng, K., Zhu, Z., Chen, G. and Peng, X., 2019. Distribution, sedimentary record, and persistence of microplastics in the Pearl River catchment, China. Environmental Pollution, 251, 862–870.

Fernandez, R. (2021) Image analysis code Matlab™ R2020a. University of Hull.

Ferguson, R. I. and Church, M., 2004. Simple Universal Equation for Grain Settling Velocity. Journal of Sedimentary Research, 74, 6, 933-937.

Fierro, P.J. and Nyler, E.K., 2007. The Water Encyclopedia, Hydrologic Data and Internet Resources. Boca Raton: Taylor and Francis.

Frere, L., Paul-Pont, I., Rinnert, E., Petton, S., Jaffre, J., Bihannic, I., Soudant, P., Lambert, C., Huvet, A., 2017. Influence of environmental and anthropogenic factors on the composition, concentration and spatial distribution of microplastics: a case study of the Bay of Brest, Brittany, France.. Environmental Pollution, 225, 211–222.

Fritsch, F. and Carlson R., 1980. Monotone Piecewise Cubic Interpolation. SIAM Journal on Numerical Analysis, 17, 238–246.

Garcia, M., 2008. Sediment Transport and Morphodynamics. In Garcia, M., ed. Sedimentation Engineering. Virginia: American Society of Civil Engineers, 21–163.

Gingell, D. and Parsegian, V. A., 1973. Prediction of van der waals interactions between plastics in water using the Lifshitz theory. Journal of colloid and Interface Science, 456-463.

Gou, S.; Zhang, F.; Song, X. and Wang, B., 2015. Deposited sediment settlement and consolidation mechanisms. Water Science and Engineering, 8, 4., 335-344.

Guyson International Limited-a , 2021. Blast media data sheet, Guyson Termoflash. Available online: https://s3-eu-west-1.amazonaws.com/resources.guyson.co.uk/product-downloads/Thermoflash.pdf?mtime=20200117141126. [Accessed 28-10-2020]

Guyson International Limited-b, 2021. Blast media data sheet, Guyson Honite. Available online: https://s3-eu-west-1.amazonaws.com/resources.guyson.co.uk/product-downloads/Honite.pdf?mtime=20200117140801. [Accessed 28-10-2020]

Haberstroh, C.J, Arias, M.E., Yin, Z., Wang, M.C., 2020. Effects of hydrodynamics on the cross-sectional distribution and transport of plastic in an urban coastal river. Water Environment Research. 93, 186-200.

Hann, W. P., Sanchez-Vidal, A., Canals, M., 2019. Floating microplastics and aggregate formation in the Western Mediterranean Sea. Marine Pollution Bulletin, 140, 523-535.

Hartmann, N. B., Hüffer, T., Thompson, R. C., Hassellöv, M., Verschoor, A., Daugaard, A. E., Rist, S., Karlsson, T., Brennholt, N., Cole, M., Herrling, M. P., Hess, M. C., Ivleva, N. P., Lusher, A. L. and Wagner, M., 2019. Are We Speaking the Same Language? Recommendations for a Definition and Categorization Framework for Plastic Debris. Environmental Science and Technology, 53, 3, 1039–1047.

He, B., Smith, M., Egodawatta, P., Ayoko, G.A., Rintoul, L., Goonetilleke, A., 2021. Dispersal and transport of microplastics in river sediments. Environmental Pollution, 279, 116884.

He, B., Goonetilleke, A., Ayoko, G., Rintoul, L., 2020. Abundance, distribution patterns, and identification of microplastics in Brisbane River sediments, Australia. Science of The Total Environment, 700, 134467.

Hoellein, T., Shogren, J., Tank, J. L., Risteca, P., 2019. Microplastic deposition velocity in streams follows patterns for naturally occurring allochthonous particles. Scientific Report, 3740:3749.

Horowitz, A.J., 2003. An evaluation of sediment rating curves for estimating suspended sediment concentrations for subsequent flux calculations. Hydrological Processes, 17, 3387-3409.

Horton, A. A., Svendsen, C., Williams, R. J., Spurgeon, D. J. and Lahive, E., 2017. Large microplastic particles in sediments of tributaries of the River Thames, UK—abundance, sources and methods for effective quantification. Marine Pollution Bulletin. 114, 218–226.

Hurley, R., Woodward, J., and Rothwell, J. J., 2018. Microplastic contamination of riverbeds significantly reduced by catchment-wide flooding. Nature Geoscience, 11, 4, 251–257.

International Organization for Standardization, 2017. ISO 14688-1 Geotechnical investigation and testing, Identification and classification of soil, Part 1: Identification and description. 2 ed. s.l.

Ionut, A., Grigoraş C.G., Roşu, A., Gavrilă, L., 2015. Mathematical modelling of density and viscosity od nacl aqueous solutions. Journal of Agroalimentary Processes and Technologies, 25, 1, 41-52.

Jambeck, J.R., Geyer, R., Wilcox, C., Siegler, T.R., Perryman, M., Andrady, A., Narayan, R. and Lavender, Law K.L., 2014. Plastic waste inputs from land into the ocean. Science, 347, 6223, 768-771.

Jiang, C., Yin, L., Li, Z., Wen, X., Luo, X., Hu, S., Yang, H., Long, Y., Deng, B., Huang, L. and Liu, Y., 2019. Microplastic pollution in the rivers of the Tibet Plateau. Environmental Pollution, 249, 91–98.

Kaiser, D., Estelmann A., Kpwalski, N., Glockzon. M., 2019. Sinking velocity of sub-millimeter microplastic. Marine Pollution Bulletin, 139, 214-220.

Khanarmuei, M., Akutina, Y., Dupuis, V., Eiff, O., Trevisson, M., Suara., K., Brown, R.J., 2020. Secondary currents in smooth-wall open channel flow. London: Taylor and Francis Group.

Khatmullina L. and Isachenko I., 2017. Settling velocity of microplastic particles of regular shapes. Marine Pollution Bulletin, 114, 871-880.

Kie-Le, T.C., Thuong, Q.T, Truong, T.N.S., Le, T.N.S., Tran, Q.V., Strady, E., 2023. Baseline concentration of microplastics in surface water and sediment of the northern branches of the Mekong River Delta, Vietnam. Marine Pollution Bulletin, 187, 114605.

Kim, I., Chae, D., Kim, S., Choi, S., Woo, S., 2015. Factors Influencing the Spatial Variation of Microplastics on High-Tidal Coastal Beaches in Korea. Arch Environ Contam Toxicol, 69, 299-309.

Klein, S., Worch, E. and Knepper, T., 2015. Occurrence and Spatial Distribution of Microplastics in River Shore Sediments of the Rhine-Main Area in Germany. Environmental Science and Technology 49, 6070-6076.

Kleinhans, M., Kreveld, M., Ophelders, T., Sonke, W., Speckmann, B. Verbeek, K., 2019. Computing representative networks for braided rivers. Journal of Computational Geometry, 10 , 1, 423-443.

Koutnik,V.S., Leornard, J., Alkidm, S., DePrima, F.J., Ravi, S., Hoek, E.M.V., Mohanty, S.K., 2021. Distribution of microplastics in soil and freshwater environments: Global analysis and framework for transport modelling. Environmental Pollution, 274, 116552.

Kumar, R., Sharma, P., Verma, A., Jha, P.K., Singh, P., Gupta, P., Chandra, R., Prasad, P.V.V., 2021. Effect of Physical Characteristics and Hydrodynamic Conditions on Transport and Deposition of Microplastics in Riverine Ecosystem. Water, 13, 2710.

Kynch, G.J., 1952. A theory of sedimentation. Transactions of the Faraday Society, 58 ,166–176.

Lane, E. W., 1955. The importance of fluvial morphology in hydraulic engineering. Proceedings of the American Society of Civil Engineering, 81, 745, 1–17.

Lebreton, L., van der Zwet, J., Damsteeg, J-W., Slat B., Andraby, A. and Reisser, J., 2017. River plastic emissions to the world’s oceans. Nature Communications, 8, 15611.

Leiser., R., Wu, G. M., Neu T.R., T. R. and Wendt-Potthoff, K., 2020. Biofouling, metal sorption and aggregation are related to sinking of microplastics in a stratified reservoir. Water Research, 176, 115748.

Lenaker, P.L., Baldwin, A.K., Corsi, S.R., Mason, S.A., Reneau, P.C., and Scott, J.W., 2019. Vertical Distribution of Microplastics in the Water Column and Surficial Sediment from the Milwaukee River Basin to Lake Michigan. Environmental Science and Technology, 53, 21, 12227-12237.

Lewis, D.W. and McConchie, D. M., 1994. Analytical Sedimentology. Chapman and Hall, New York.

Li, J. and Xu, Z., 2019. Compound tribo-electrostatic separation for recycling mixed plastic waste. Journal of Hazardous Materials, Issue 367, 43-49.

Lick, W., Huang, H. and Jepsen, R., 1993. Flocculation of fine-grained sediments due to differential settling. Journal Geophysical Research, 98, C6., 10279– 10288.

Liedermann, M. et al., 2018. A Methodology for Measuring Microplastic Transport in Large or Medium Rivers. Water, 10, 414.

Lin, L., Pan, X., Zhang, S., Li, D., Zhai, W., Wang, Z., Tao, J., Mi, C., Li, Q. and Crittenden, J. C., 2021. Distribution and source of microplastics in China's second largest reservoir - Danjiangkou Reservoir. Journal of Environmental Sciences, 102, 74–84.

Liro, M., Emmerik, T., Wyżga, B., Liro, J. and Mikuś, P., 2020. Macroplastic Storage and Remobilization in Rivers. Water, 12, 2055, 3-14.

Liro, M., Mikuś, P., and Wyżga, B., 2022. First insight into the macroplastic storage in a mountain river: The role of in-river vegetation cover, wood jams and channel morphology. Science of the total Environment, 838, 3, 156354.

Lu, S., Zhu, K., Song, W., Song, G., Chen, D., Hayat, T., Alharbi, N. S., Chen, C., Sun, Y., 2018. Impact of water chemistry on surface charge and aggregation of polystyrene microspheres suspensions. Science of the Total Environment, 630, 951–959.

Lwanga, E.H., van Roshum, I, Munhoz, D.R., Meng, K., Rezaei, M., Goossens, D., Bijsterbosch, J., Alexandre, N., Oosterwijk, J., Krol, M., Peters, P., Geissen, V., Ritsema, C., 2023. Microplastic appraisal of soil, water, ditch sediment and airborne dust: The case of agricultural systems. Environmental Pollution, 316, 1, 120513.

Malvern Instruments Limited, 2013. Mastersizer 3000 User Manual. Malvern Instruments Ltd.

Malvern Instruments Limited, 2015. A basic guide to particle characterization. Available online: https://www.cif.iastate.edu/sites/default/files/uploads/Other_Inst/Particle%20Size/Particle%20Characterization%20Guide.pdf [Accessed 10/03/2021].

Mani, T., Hauk, A., Walter, U., Burkhardt-Holm, 2016. Microplastics profile along the Rhine River. Scientific reports, 5, 17988.

Mao, R., Song, J., Yan, P., Ouyang. Z., Wu, R., Liu, S., Gou, X., 2021. Horizontal and vertical distribution of microplastics in the Wuliangsuhai Lake sediment, northern China. Science of the Total Environment, 754,1-6.

Mehta, A.J. and McAnally, W. H., 2008. Fine-Grained Sediment Transport. In Garcia, M., ed. Sedimentation Engineering. Virginia: American Society of Civil Engineers, 251–304.

Meijer, L.J.J., van Emmerik, T., van der Ent, R., Schmidt, C., Lebreton, L., 2021. More than 1000 rivers account for 80% of global riverine plastic emissions into the ocean. Sciences Advances, 7, 18.

Moore, C. J., Lattin, G. L. and Zellers, A. F., 2011. Quantity and type of plastic debris flowing from two urban rivers to coastal waters and beaches of Southern California. Journal of Integrated Coastal Zone Management, 11, 65-73.

Nyberg, B., Harris, P.T., Kane, I., and Maes, T., 2023. Leaving a plastic legacy: Current and future scenarios for mismanaged plastic waste in rivers. Science of The Total Environment, 869, 161821.

Nizzetto, L., Bussi, G., Futter, M.N., Butterfield, D., Whitehead, P.G., 2016. A theoretical assessment of microplastic transport in river catchments and their retention by soils and river sediments. Environmental Science Processes and Impacts, 18, 1050-1059.

Ockelford, A., Cundy, A. and Ebdon, J.E., 2020. Storm Response of Fluvial Sedimentary Microplastics. Sciences Report 10, 1865.

Pane, V. and Schiffman, R. L., 1985. A note on settlement and consolidation. Geotecnique, 35, 1, 69-72.

Parker, G., 2005. 1D Sediment transport morphodynamics with applications to rivers and turbidity currents. Available online: <http://hydrolab.illinois.edu/people/parkerg/powerpoint_lectures.htm [Accessed 27 / 06/2021]

Partheniades, E., 1965. Erosion and Deposition of Cohesive Soils. Journal of the Hydraulics Division, 91, 105-139.

Phillips, C.R. and Smiths, T.N., 1971. Modes of settling and relative settling velocities in two-species dispersions. Industrial Engineering Chemistry Fundamental, 10 , 581–587.

Pope, B., 2000. Turbulent flows. Cambridge: Cambridge University press.

Pradhan, A., Kumar, K. K. and Sankalp, S., 2018. Variation of Velocity Distribution in Rough Meandering Channels. Advances in Civil Engineering, 2018, Article ID 1569271.

Prokić, M.D., Gavrilović, B.R., Radovanovića, T.B., Gavrić, J.P., Petrović, T.G., Despotović, S.G., Faggio, C., 2021. Studying microplastics: Lessons from evaluated literature on animal model organisms and experimental approaches. Journal of Hazardous Materials, 414, 125476.

Quik, J.T.K., de Klein, J.J.M., Koelmans, A.A., 2015. Spatially explicit fate modelling of nanomaterials in natural waters. Water Research 80, 200–208.

Rezende-Gerolin, C., Nascimento-Pupim, F., Oliveira-Sawakuchi, A., Henrique-Grohmann, C., Labuto, G., Semensatto, D., 2020. Microplastics in sediments from Amazon rivers, Brazil. Science of The Total Environment, 749, 141604.

Richardson, J.F. and Zaki, W.N., 1954. Sedimentation and fluidization: Part I. Trans. Institute Chemical Engineering, 32.

Rochman, C. M., 2015. The complex mixture, fate and toxicity of chemicals associated with plastic debris in the marine environment. In M. Bergmann, L. Gutow, and M. Klages, ed. Marine anthropogenic litter. Springer, Cham, Switzerland. 117–140.

Rolf, M., Laermanns. H., Kienzler. L., Pohl, C., Möller, J.N., Laforsh, C., Löder. M.G.J., Bogner, C., 2022. Flooding frequency and floodplain topography determine abundance of microplastics in an alluvial Rhine soil. Science of the Total Environment. 836, 155141.

Russell, C., Fernández, R., Parsons, D.R., and Gabbott, S., 2022. Plastic pollution in riverbeds fundamentally affects natural sand transport. Under review in Communications Earth and Environment. Preprint available through Research Square.

Saarni, S., Hartikainen, S., Meronen, S., Uurasjärvi, E., Kalliokoski, M. and Koistinen, A., 2021. Sediment trapping – An attempt to monitor temporal variation of microplastic flux rates in aquatic systems. Environmental Pollution, 274, 116568.

Scherer, C., Weber, A., Stock, F., Vurusic, S., Egerci, H., Kochleus, C., Arendt, N., Foeldi, C., Dierkes, G., Wagner, M., Brennholt, N., Reifferscheid, G., 2020. Comparative assessment of microplastics in water and sediment of a large European river. Science of The Total Environment, 738, 139866.

Schuurman, F., Kleinhans, M.G., Middelkoop, H., 2015. Network response to disturbances in large sand-bed braided rivers. Eartg Surface Dynamics, 4, 25-45.

Scopetani, C., Chelazzi, D., Mikola, J., Leiniö. Heikkinen, R., Cincinelli, A., Pillinen J., 2020. Olive oil-based method for the extraction, quantification and identification of microplastics in soil and compost samples. Science of The Total Environment, 733, 139338.

Shields, A., 1936. Application of similarity principles and turbulence research to bed-load movement. California: Soil Conservation Service Cooperative Laboratory, California Institute of Technology Pasadena.

Shim, W.J., Hong, S.H., Eo, S., 2018. Marine Microplastics: Abundance, Distribution, and Composition. Zeng E.Y., ed. Microplastic Contamination in Aquatic Environments. Elsevier, 1-26.

Shiravania, G., Oberrechta, D., Roscherc, L., Kernchend, S., Halbachb, M., Gerrietsb, M., Scholz-Böttcherb, B.M., Gerdtsc, G., Badewienb, T.H., and Wurptsa, A., 2023. Numerical modelling of microplastic interaction with fine sediment under estuarine conditions. Water Research, 119564.

Sibson, R., 1981. A Brief Description of Natural Neighbor Interpolation. In: Barnett, V., ed. Interpreting Multivariate Data. New York: John Wiley and Sons, 21-3.

Siegfried, M., Koelmans, A. A., Besseling, E., Kroeze, C., 2017. Export of microplastics from land to sea. A modelling approach. Water Research, 127, 249-257.

Sijs, R., Kooij, S., Holterman, H. J., Van De Zande, J., Bonn, D., 2021.. Drop size measurement techniques for sprays: Comparison of image analysis, phase Doppler particle analysis, and laser diffraction. AIP Advances, 11, 015315.

Silveira, A. V., Cella, M., Tanabe, E. H., Bertuol, D. A., 2018. Application of tribo-electrostatic separation in there cycling of plastic wastes. Process Safety and Environmental Protection, 114, 219–228.

Simon-Sánchez, L., Grelaud, M., Garcia-Orellana, J., Ziveri, P., 2019. River Deltas as hotspots of microplastic accumulation: The case study the Ebro River , NW Mediterranean. Science of the Total Environment, 687, 1186-1196.

Skaf, D. W., Punzi, V. L., Rolle, J. T., Kleinberg, K. A., 2020. Removal of micron-sized microplastic particles from simulated drinking water via alum coagulation. Chemical Engineering Journal 386, p. 123807.

Skalska, K., Ockelford, A., Ebdon, J. and Cundy. A.B., 2020. Riverine microplastics: Behaviour, spatio-temporal variability, and recommendations for standardised sampling and monitoring. Journal of Water Process Engineering, 38, 101600.

Soulsby, R.L., and R. J.S. W Whitehouse. 1997. Threshold of sediment motion in coastal environments. Proceedings Pacific Coasts and Ports, 97, Conference, 1, 149154.

Sulistyowati, L., Nurhasanah, Riani, E., Cordova, M.R., 2022. The occurrence and abundance of microplastics in surface water of the midstream and downstream of the Cisadane River, Indonesia. Chemosphere, 291, 133071.

The Royal Society, 2019. Microplastics in freshwater and soil. Available online. https://royalsociety.org/-/media/policy/projects/microplastics/microplastics-evidence-synthesis-report.pdf [Accessed 16/11/2019]

Tinke, A. P., Carnicer, A., Govoreanu, R., Scheltjens, G., Lauwerysen, L., Mertens, N., Brewster, M. E., 2008. Particle shape and orientation in laser diffraction and static image analysis size distribution analysis of micrometer sized rectangular particles. Powder Technology, 186, 2., 154–167.

Uzum, P., Farazande, S. and Guven, B., 2022. Mathematical modelling of microplastic abundance, distribution, and transport in water environments: A review. Chemosphere, 288, 132517.

Valsangkar, A. J., 1992. Principles, methods and applications of particle size analysis. Canadian Geotechnical Journal, 29, 1006.

van Rijn, L. C. van, 1993. Principles of Sediment Transport in Rivers, Estuaries and Coastal Seas. Aqua Publications, The Netherlands.

van Rijn, L. C., 1990. Principals of Morphology in Rivers, Estuaries and Coastal Seas. Amsterdam: Aqua Publications.

van Weerdenburg, R. and van Maren, B. (2022). Fine sediment transport modelling in D-Morphology or D-Water Quality? [Presentation]. Delft3D User Days 2022 (Day 2), Netherlands.

van Wijnen, J., Ragas, A. M. and Kroeze, C., 2019. Modelling global river export of microplastics to the marine environment: Sources and future trends. Science of the Total Environment, 673, 392-401.

Wagner, S. et al., 2019. Relationship between Discharge and River Plastic Concentrations in a Rural and an Urban Catchment. Environmental Science and Technology, 53, 10082-10091

Waldschläger, K., Lechthaler, S., Stauch, G., Schüttrumpf, H., 2020. The way of microplastic through the environment – Application of the source-pathway-receptor model, review. Science of the Total Environment, 713, 136584.

[a]Waldschläger, K. and Schüttrumpf, H., 2019. Effects of Particle Properties on the Settling and Rise Velocities of Microplastics in Freshwater under Laboratory Conditions. Environmental Science and Technology, 53, 4, 1958–1966.

[b]Waldschläger, K., and Schüttrumpf, H., 2019. Erosion behavior of different microplastic particles in comparison to natural sediments. Erosion Be, 53, 13219-13227.

Weisscher, S. A. H., Shimizu, Y., Kleinhans, M. G., 2019. Upstream perturbation and floodplain formation effects on chute-cutoff-dominated meandering river pattern and dynamics. Earth Surface Processes and Landforms, 44, 2156-2169.

Winterwerp, J. C. and Kranenburg, C., 2002. Fine Sediment Dynamics in the Marine Environment. 1 ed. [eBook] Elsevier Science.

Wright, S. L., R. C. Thompson, and T. S. Galloway. 2013. The physical impacts of microplastics on marine organisms: a review. Environmental Pollution, 178,483–492.

Yalin, M. S. and Karahan, E., 1979. Inception of Sediment Transport. Journal of the Hydraulics Division, 105, 11.,1433-1443.

Yang, L., Zhang, Y., Kang, S., Wang, Z., Wu, C., 2021. Microplastics in freshwater sediment: A review on methods, occurrence, and sources. Science of The Total Environment, 754, 14148.

Yang, S.-Q., Keat, S. T. and Wang, X.-K., 2012. Mechanism of secondary currents in open channel flows. Journal of Geophysical Research, 117, F04014.

Yun, G., Williams, S. and Wenbin, D., 2017. Water management of the Mekong River. Water Conservation and Management, 1(1), 10-12.

Zhang, K., Wu, S., Feng, W., Zhang, J. and Wen, 2020. Bar dynamics in a sandy braided river: Insights from sediment numerical simulations. Sedimentary Geology, 396, 105557.

Zhou Z., Zhang P., Zhang G., Wang S., Cai Y. and Wang H., 2021. Vertical microplastic distribution in sediments of Fuhe River estuary to Baiyangdian Wetland in Northern China. Chemosphere, 280, 130800.

Zhou, Y., Jing, J, Yu, R., Zhao, Y., Gou, Y., Zhang, Z., Tang, H., Zhang, H., Huang, Y., 2023. Microplastics in plateau agricultural areas: Spatial changes reveal their source and distribution characteristics. Environmental Pollution, 319, 121006.

Appendix 1: Pictures captured from the videos analysis to estimate the microplastic cloud fall velocity.

Cian lines are the measure of heights measured of the microplastic cloud. The time (T) of the frame.

T=14s	T=16s	T=18s	T=20s	T=22s	T=24s	T=26s
			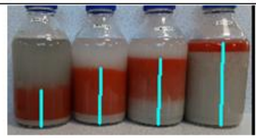	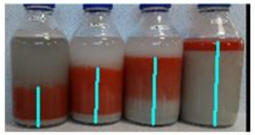		
T=28s	T=30s	T=32s	T=34s	T=36s	T=40s	T=44s
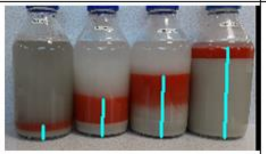	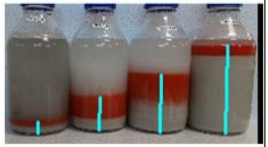	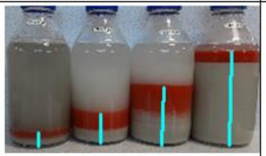	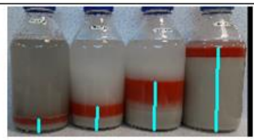	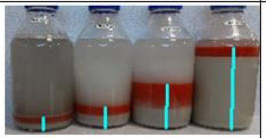		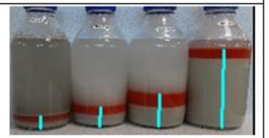
T=48s	T=52s	T=56s	T=60s	T=70s	T=80	90s
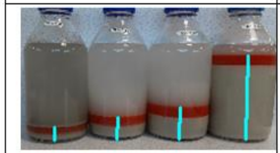	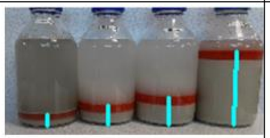			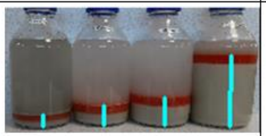	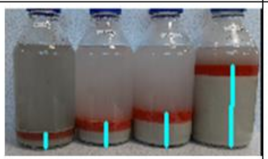	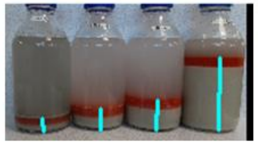

Appendix 2: Volumes of the 3 pure microplastic and sediment sample between the bins 310µm to 390 µm.

The green highlights the 5 share bins. The last column shows the summary of these share bins, with a percentage less than 0.571%. From this analysis, the division between microplastic and sediment is defined as 350 µm.

Material		Range Bin/Name	Percentage volumes Bin minimum and maximum limits 310.00µm-320.00µm **Bin 315**	320.00µm-330.00µm **Bin 325**	330.00µm-340.00µm **Bin 335**	340.00µm-350.00µm **Bin 345**	350.00µm-360.00µm **Bin 355**	360.00µm-370.00µm **Bin 365**	370.00µm-380.00µm **Bin 375**	380.00µm-390.00µm **Bin 385**	390.00µm-400.00µm **Bin 395**	**∑ Bin 335 to Bin 375 (%)**
					Sediment ←		Microplastic →					
Sediment	Sample 1	Repetition 1	0.260	0.122	0.056	0.039	0.026	0.017	0.009	0.000	0.000	0.147
		Repetition 2	0.253	0.113	0.046	0.029	0.018	0.015	0.000	0.000	0.000	0.108
		Repetition 3	0.264	0.124	0.058	0.040	0.028	0.018	0.010	0.000	0.000	0.154
	Sample 2	Repetition 1	0.360	0.282	0.212	0.152	0.099	0.053	0.018	0.000	0.000	0.534
		Repetition 2	0.363	0.286	0.216	0.156	0.102	0.055	0.019	0.000	0.000	0.548
		Repetition 3	0.371	0.293	0.224	0.162	0.107	0.058	0.020	0.000	0.000	0.571
	Sample 3	Repetition 1	0.364	0.285	0.214	0.153	0.100	0.053	0.018	0.000	0.000	0.538
		Repetition 2	0.347	0.267	0.197	0.137	0.087	0.045	0.015	0.000	0.000	0.481
		Repetition 3	0.366	0.287	0.217	0.155	0.101	0.054	0.019	0.000	0.000	0.546
Microplastic	Sample 1	Repetition 1	0.000	0.000	0.016	0.021	0.033	0.048	0.066	0.096	0.156	0.184
		Repetition 2	0.000	0.000	0.017	0.022	0.034	0.050	0.068	0.099	0.161	0.191
		Repetition 3	0.000	0.000	0.016	0.021	0.033	0.049	0.066	0.097	0.157	0.185
	Sample 2	Repetition 1	0.000	0.000	0.018	0.023	0.036	0.052	0.070	0.104	0.167	0.199
		Repetition 2	0.000	0.000	0.017	0.022	0.035	0.050	0.068	0.101	0.163	0.192
		Repetition 3	0.000	0.000	0.017	0.022	0.035	0.051	0.070	0.103	0.167	0.195
	Sample 3	Repetition 1	0.000	0.000	0.018	0.023	0.036	0.051	0.070	0.103	0.166	0.198
		Repetition 2	0.000	0.000	0.017	0.022	0.035	0.050	0.069	0.101	0.164	0.193
		Repetition 3	0.000	0.000	0.018	0.023	0.036	0.052	0.070	0.104	0.167	0.199
					Share Bins Sediment-Microplastic							

Appendix 3: Code to separate the size distribution and volumes of the microplastic and sediments

Script to plot grain size distributions from the data output by the Mastersizer

```
%Author code: Roberto Fernandez

%Modifications and updates: Lucrecia Alvarez
%   28 06 2021
%       The matrix T now is bin volumes.
%       Code read the base data from excel, a number is assigned to each experimental tube to make the estimations and plot
%       A "0" to the left of the first C_T, C_S, C_M
% 12 07 2021
%       The input is D in microns every 10 microns.
%       The phi scale is deleted.
% 20 07 2021
%       Add comments explaining the contents of the MP/Glass and clean the
%       code.
%27 07 2021
%      Add the % of the volume of microplastic in each slice
%04 11 2021
%       Estimated the average and standard deviation from the 3
%       measurements.
%       Add experimental errors bars plots
%       Add HDATABASE
%% Clean up
clearvars
clear all
close all

%% 1. Input values

% Particle size (D) – Malvern mastersizer bins in microns
% The matrix D correspond the averages value bins every 10 microm.
% Starts in 0.01 microm and % end in 2000 microm.
```

```
D = [5:10:1995]; %This matrix defines the average size of the bin from 5 to 1995.
BINST = name(D); % Reads the number of bins in matrix D

% The index where the plastic/glass will be in 350 microns. No overlap is considered.

% The bins limit between sediment and microplastic was selected based on
% the pure of microplastic and sediment samples. The samples share 5
% bins from 330 microm to 380 microm. In which 50% of the microplastic volumes share bins are above
% 355 microm and 50% of the sediment volumes share bins are above 355 microm. From this analysis it is
% decide that division between microplastic and sediment 350 microms bin.

idxM = 35; % Number of bins that divides the microplastic and sediment in the matrix

DATABASE=readmatrix('C:\Users\611577\Desktop\lu_matlab\matrix_errors.xlsx'); %Read database stored in 'matrix.xlsx'
%This matrix is composed of:
%Column 1: The number of the experimental tubes (see variable INDEX)
%Column 2 to end-2: The volume of MP or S in each bins of the matrix D
%Column end: Volume of Microplastic in each slice

HDATABASE=readmatrix('C:\Users\611577\Desktop\lu_matlab\h_errors.xlsx');
%Column 1: The number of the experimental tubes (see variable INDEX)
%Column 2: The height

INDEX = 14;
%number of the experimental tube, this number can be 1 to 28 (except
%4,9,12)
% #     Name %
% 1     MP5S14
% 2     MP5S24
% 3     MP5S33
% 4     MP5S42****
% 5     MP5S5
% 6     MP7S12
% 7     M10S9
% 8     MP10S19
% 9     MP10S28***
% 10    MP13S7
```

```
% 11    MP13S16
% 12    MP7S31****
% 13    MP5S9
% 14    MP8S7 (show a mistake in the error bar)
% 15    MP10S5
% 16    MP10S14
% 17    MP15S14
% 18    MP15S5
% 19    MP5S28
% 20    MP5S0
% 21    MP10S0
% 22    MP15S0
% 23    MP0S9
% 24    MP0S19
% 25    MP0S28
% 26    MP0S38


TN=find(DATABASE(:,1)==INDEX); % Find the numbers of the rows that match with the INDEX in the DATABASE
TN1 = DATABASE (TN,:); % Extract the information of the INDEX experimental tubes
T= TN1(:,2:end-1); % Extract the volumes in each bins to estimate the DN for each experimental tube from TN1
VMP = TN1(:,end);% Extract the volumes microplastic for the INDEX experimental tube from TN1.
VMP= VMP';
VS= 100-VMP; %Estimated the volume of sediment

HN=find(HDATABASE(:,1)==INDEX);% Find the numbers of the rows that match with the INDEX in the HDATABASE
HN1= HDATABASE(HN,:);% Extract the normalized height for the INDEX experimental tube to make the plot of DN from HN.
H= HN1(:,2);
H= H';

intM = 'pchip'; % Correspond at the method of interpolation to estimate the DN. pchip or linear


%% 2. Loop through a single deposit to compute the grain size percentiles of each layer

for r = 1:size(T,1)
```

```
% 2.1. Calculate the amount of material inside each bin
% Separate the sample between the sediment and microplastic fraction

% a) Sediment fraction

  S = T(r,1:idxM); % Volumes for each bins values
  D_S = D(1:idxM); % Bins average values

% b) Microplastic fraction
   M = T(r,idxM+1:end); % Volumes for each bins values
   D_M = D(idxM+1:end); % Bins average values

% 2.2. Compute cumulative distributions for total, sediment and microplastic samples

   C_S = cumsum(S); %Cumulative distribution for microplastic
   C_M = cumsum(M); % Cumulative distribution for microplastic
   C_T = cumsum(T(r,:)); % Cumulative distribution for total sample

%2.3.  Normalized the cumulative distribution

   % a) Normalize the total sample

   C_T = C_T./C_T(end)*100; %This equation divides each bin volume in the total sum.

% b) Normalize microplastic sample

if max(C_M)>0
   C_M = C_M./C_M(end)*100;
else
   C_M = [];
end

if max(C_S)>0

% c) Normalize sediment sample

   C_S = C_S./C_S(end)*100;
```

```
else
   C_S = [];
end

% 2.4.Remove columns with repeated zeros or 100s (This step is
% necessary so the interpolation method find the solution to estimated
% the DN.

repValsT = find(diff(C_T)~=0)+1;
repValsS = find(diff(C_S)~=0)+1;
repValsM = find(diff(C_M)~=0)+1;

% 2.5. New cumsum vectors obtained after removing columns with repeated and
% ad a 0 at the beginning of the matrix
% values
C_T = [0 C_T(repValsT)];
C_S = [0 C_S(repValsS)];
C_M = [0 C_M(repValsM)];

% 2.6. Corresponding new vectors of the D matrix

D_T =[D(min(repValsT)-1) D(repValsT)];
D_S =[D_S(min(repValsS)-1) D_S(repValsS)];
D_M =[D_M(min(repValsM)-1) D_M(repValsM)];

% 2.7. Makes the interpolation of the DN.
% The function "if" is included to assign NaNs, when there is no value to estimated.
% The number 1 is assigned as the refence value for the conditioner of
% "if"

%a) Total core

if numel(C_T) > 1
   p10T(r) = interp1(C_T, D_T, 10, intM);
   p50T(r) = interp1(C_T, D_T, 50, intM);
   p90T(r)  = interp1(C_T, D_T, 90, intM);
% Otherwsie - assign NaNs
```

```
    else
        p10T(r) = NaN;
        p50T(r) = NaN;
        p90T(r) = NaN;
    end

    % b) Sediment

    if numel(C_S) > 1
        p10S(r) = interp1(C_S, D_S, 10, intM);
        p50S(r) = interp1(C_S, D_S, 50, intM);
        p90S(r) = interp1(C_S, D_S, 90, intM);

     else
        p10S(r) = NaN;
        p50S(r) = NaN;
        p90S(r) = NaN;
    end

    % c) Microplastic

    if numel(C_M) > 1
        p10M(r) = interp1(C_M, D_M, 10, intM);
        p50M(r) = interp1(C_M, D_M, 50, intM);
        p90M(r) = interp1(C_M, D_M, 90, intM);
    % Otherwsie - assign NaNs
    else
        p10M(r) = NaN;
        p50M(r) = NaN;
        p90M(r) = NaN;
    end

end

%% 3. Plots

%  Estimations of the average values and standard deviations of the
```

```
%  D10, D50 and D90

xx = size(p50T);
rows= xx(1,2);
y = rows/3;

for i= 1:y;

    N = (1:3:rows);% Creates a matrix every 3 numbers

    %Total estimations
  Mep10T(i) = mean(p10T(N(1,i):N(1,i)+2)); %Average total plot D10
  SDp10T(i) =std(p10T(N(1,i):N(1,i)+2)); %Standard desviation total plot D50
  Mep50T(i) = mean(p50T(N(1,i):N(1,i)+2)); %Average total plot D10
  SDp50T(i) =std(p50T(N(1,i):N(1,i)+2)); %Standard desviation total plot D50
  Mep90T(i) = mean(p90T(N(1,i):N(1,i)+2)); %Average total plot D10
  SDp90T(i) =std(p90T(N(1,i):N(1,i)+2)); %Standard deviation total plot D50

     %Sediment estimations
  Mep10S(i) = mean(p10S(N(1,i):N(1,i)+2)); %Average total plot D10
  SDp10S(i) =std(p10S(N(1,i):N(1,i)+2)); %Standard desviation total plot D50
  Mep50S(i) = mean(p50S(N(1,i):N(1,i)+2)); %Average total plot D10
  SDp50S(i) =std(p50S(N(1,i):N(1,i)+2)); %Standard desviation total plot D50
  Mep90S(i) = mean(p90S(N(1,i):N(1,i)+2)); %Average total plot D10
  SDp90S(i) =std(p90S(N(1,i):N(1,i)+2)); %Standard desviation total plot D50

  %Microplastic estimations
  Mep10M(i) = mean(p10M(N(1,i):N(1,i)+2)); %Average total plot D10
  SDp10M(i) =std(p10M(N(1,i):N(1,i)+2)); %Standard desviation total plot D50
  Mep50M(i) = mean(p50M(N(1,i):N(1,i)+2)); %Average total plot D10
  SDp50M(i) =std(p50M(N(1,i):N(1,i)+2)); %Standard desviation total plot D50
  Mep90M(i) = mean(p90M(N(1,i):N(1,i)+2)); %Average total plot D10
  SDp90M(i) =std(p90M(N(1,i):N(1,i)+2)); %Standard desviation total plot D50

  %Volumes
  MeVS(i)=mean(VS(N(1,i):N(1,i)+2));  %Average volumes sediment
  SDVS(i)=std(VS(N(1,i):N(1,i)+2)); %Standard desviation sediment
```

```
 MeVMP(i)=mean(VMP(N(1,i):N(1,i)+2)); %Average volumes microplastic
 SDVMP(i)=std(VMP(N(1,i):N(1,i)+2)); %Standard desviation volumes microplastic

end

% PLOTS WITH ERROR BARS

    %Total

subplot(1,4,1)

errorbar(Mep10T,H,SDp10T,'m','horizontal');
   hold on
   errorbar(Mep50T,H,SDp50T,'b','horizontal');
   errorbar(Mep90T,H,SDp90T,'k','horizontal');
   ylim([0 1]);
   xlim([0 1200]);
   ylabel('Height - H [ - ]');
   xlabel('Size(µm)');
   title('a)Total Substrate');
   grid on

   %SEDIMENT
subplot(1,4,2)
errorbar(Mep10S,H,SDp10T,'m','horizontal');
   hold on
   errorbar(Mep50S,H,SDp50S,'b','horizontal');
   errorbar(Mep90S,H,SDp90S,'k','horizontal');
   ylim([0 1]);
   xlim([0 400]);
   %ylabel('Height - H [ - ]');
   title('b)Sediment')
   xlabel('Size(µm)')
   legend('D_{10}', 'D_{50}', 'D_{90}')
   yticklabels ({})
   grid on
```

```
subplot(1,4,3)

errorbar(Mep50M,H,SDp50M,'b','horizontal');

    ylim([0 1]);
    xlim([650 850]);
    title('c)Microplastic')
    xlabel('Size(µm)')
    yticklabels ({})
    grid on

subplot(1,4,4)

errorbar(MeVS, H, SDVS,'b--','horizontal'); hold on
errorbar(MeVMP, H, SDVMP,'m--','horizontal');
ylim([0 1])
xlim([-10 110])
title('d) Volumes (%)')
xlabel('Volumes (%)')
ylabel('Height - H [ - ]')
legend('S', 'MP', 'Location','south')
yticklabels ({})
grid on
yticklabels ({})
%

%% 3. Final matrix with a summary of Dn

DT = [(p10T)' (p50T)' (p90T)'];
DS = [(p10S)' (p50S)' (p90S)'];
DM = [(p10M)' (p50M)' (p90M)'];
 STMP=[(SDp10M)' (SDp50M)' (SDp90M)'];
STS=[(SDp10S)' (SDp50S)' (SDp90S)'];
STT=[(SDp10T)' (SDp50T)' (SDp90T)'];

DFINAL= [DT DS DM];
```

Appendix 4: Outputs of the picture analysis simulation for particle size distribution

Running	The first picture in the top to the left is the original image. The next two pictures are the conversion steps to the white-black (top right). The final picture is use for the particles size analysis (bottom left). The Middle bottom picture is the sample selected. The red crosses (bottom right picture) symbolized the particle detected.	Size distribution of the sample L= average side D= equivalent diameter estimated with a surface area of the particle	Frequency histogram of the side and equivalent diameter of the sample
Test 1	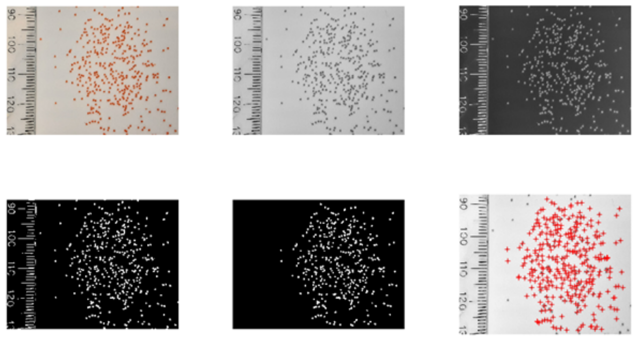	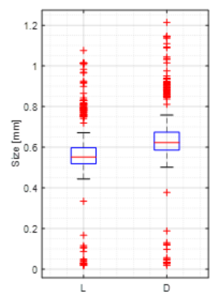	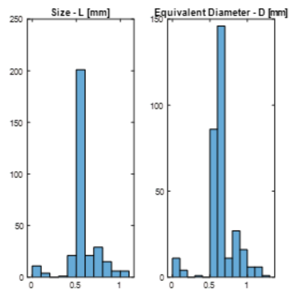
Test 2	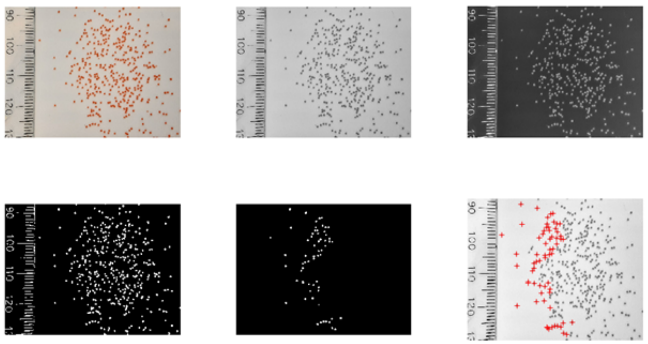	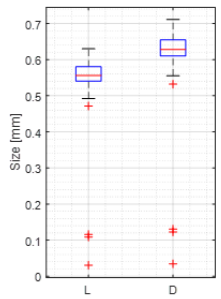	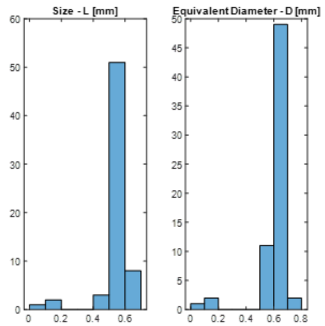

Appendix 5: Calibration curve to determine the volume errors of the image analysis, volumes distribution core lower than 0.03 m

a) Table of the volume results from the analysis of the three images using the code

Name	Sensitive used in the Code	Volume Image 1 (%)	Volume Image 2 (%)	Volume Image 3 (%)	Average Image volume (%)	Standard deviation
1	0.85	2.977	2.090	2.609	2.56	0.446
2	0.85	3.776	2.865	3.622	3.42	0.488
3	0.85	5.685	5.113	4.503	5.10	0.59
4	0.85	10.181	7.457	8.339	8.66	1.39
5	0.75	13.623	14.271	12.935	13.6	0.67
6	0.75	15.612	16.135	14.120	15.3	1.05
7	0.75	19.088	18.996	19.099	19.1	0.06
8	0.65	25.813	25.650	26.077	25.8	0.22
9	0.65	27.457	28.590	29.524	28.5	1.03
10	0.65	31.619	32.261	33.515	32.5	0.96
11	0.65	36.353	39.037	35.128	36.8	2.00
12	0.55	42.354	43.337	41.383	42.4	0.98
13	0.55	50.900	50.754	50.322	50.7	0.30

b) Code “Image Analysis”

```
%% Code to measure the surface area of mixtures of microplastics and sediment, Named: volume_microplastic_15_03_2020,
%Authors, Roberto Fernandez and Lucrecia Alvarez
clear all
close all
%1. Read the three images
```

```
%Matrix compose of all the three images
filesnames = [{'cali_12_87.jpg'} {'cali_12_88.jpg'} {'cali_12_89.jpg'}];
%Value of sensitive to calibrate the percentages of microplastic
 sensitivityvalue = 0.50
%2. Loop to read the volume of the microplastic

for j=1:3;
    %%for i=1:30;
   % 2.1. Read the image
  I= imread(filesnames{j});
    %2.2. Crop the image to take out the scale bar that is not part of theanalysis
    bw1= imcrop(I,[0 0 3088 1950]);
    %2.3. Convert the image to grey
    bw2= rgb2gray(bw1);
    %2.4. Improve the constrast.
    bw3= imadjust(bw2).
   % 2.5. binarize the image with a sensitivity (High content of microplastic   % need a low sensitivity)
     %%% sensitivityvalue = sensitive range(1,i);
bw4 = imbinarize(bw3, 'adaptive', 'Sensitivity', sensitivityvalue );%bright or dark %0.78 with less %0.60 with high
      %1 Microplastics
   %0 Sediment
       %2.6. Clean the sediment
    % a) Remove all particles that are not connected less than n  pixels ()
    bw5=bwareaopen(bw4,100); %
      %b)  Fill the spaces inside the sediment with squares of 3 pixels.
    SE = strel('sphere',3);
    bw6 = imdilate(bw5,SE);
 % 2.7. Clean the microplastic and sediment
     %a) Invert the bynary image
   bw7 = imcomplement(bw6);
   %0 Microplastic
   %1 Sediment
   % b) Remove all particles that are not connected less than n  pixels ()
```

```
 bw8=bwareaopen(bw7,100); %
 % c)  Fill the spaces inside the microplastic with squares of 3 pixels.
 SE = strel('sphere',1);
 bw9 = imdilate(bw8,SE);
 % d) Invert the bynary image
bw10 = imcomplement(bw9);
%1 Microplastic
%0 Sediment
%% 2.8. Estimate the percentages of microplastic
   sum(sum(bw10));
 per_MP=(1-sum(sum(bw10))/numel(bw10))*100 ;
 %%%%MPPER(j,i) = [per_MP];
 MPPER(j) = [per_MP];

 % 2.9. Plot the figure

 figure
 subplot(2,3,1), imshow(I);
 title ("Calibration picture");
 subplot(2,3,2), imshow(bw2);
 title ("Grey image");
 subplot(2,3,3), imshow(bw3);
 title("Contrast improve");
 subplot(2,3,4), imshow(bw6);
 title("Binary 1, Clean Sand");
 subplot(2,3,5), imshow(bw9)
 title("Binary 2, Clean MP");
 subplot(2,3,6), imshow(bw10);
  title("Final figure (black MP)");
   end
%% end
```

c) Images results of the microplastic detected in the analysis.

From the 13 samples it is only included 3 example of the three image analysed per sample. The sequences show from left to right, top to bottom: original picture, grey image, contrast improve, binary image to clean the sediment distortions, binary image to clean the microplastics distortions, final figure.

Sample (V_{Mp})	Picture 1	Picture 2	Picture 3
Sample 1 3.42%±0.49	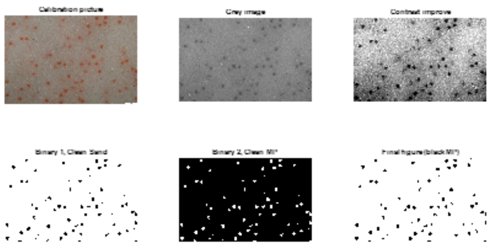	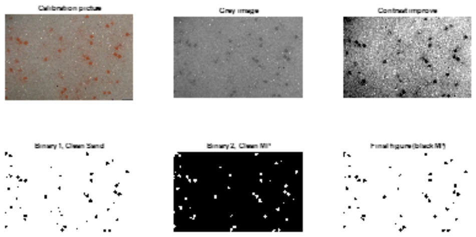	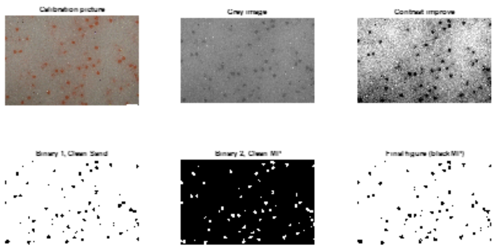
Sample 6 15.3%±1.05	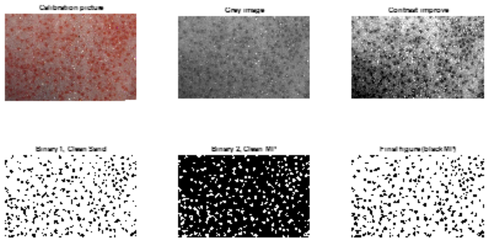	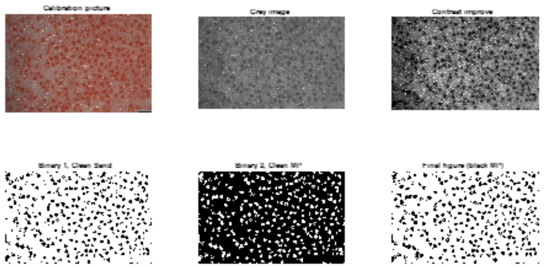	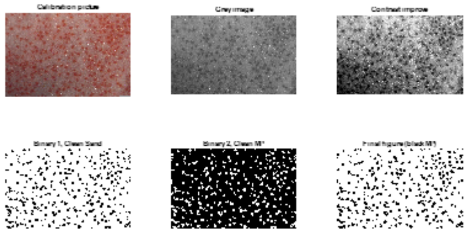
Sample 11 36.8%±2.00	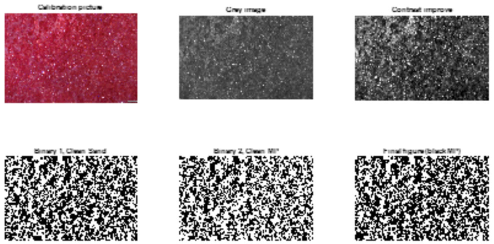	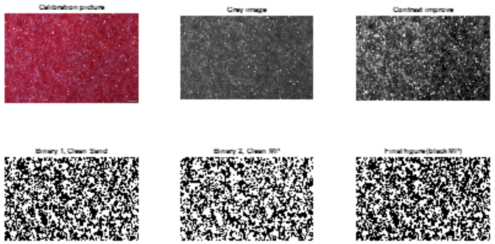	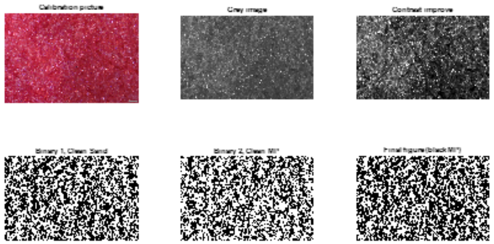

Appendix 6: Number of slices and pictures of each settling tube substrate**.**

Tube name	Total substrate height (mm)	Number of slices	Picture of the samples
MP_5S_0	24	2	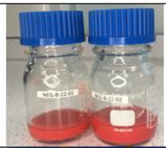
$MP_{10}S_0$	44	4	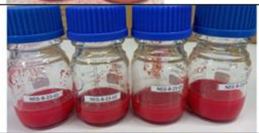
$MP_{15}S_0$	66	5	
MP_5S_5	36	5	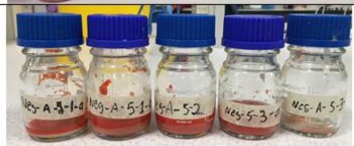
$MP_{10}S_5$	53	4	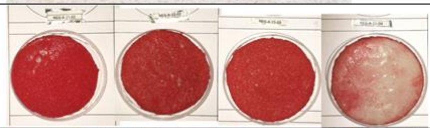
$MP_{15}S_5$	82	6	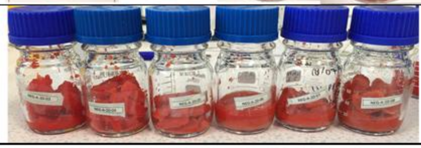

MP_8S_7	57	5	
$MP_{13}S_7$	74	6	
MP_0S_9	47	3	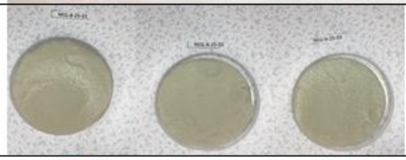
MP_5S_9	59	5	
$M_{10}S_9$	95	6	
MP_7S_{12}	76	6	

MP_5S_{14}	73	7	
$MP_{10}S_{14}$	97	7	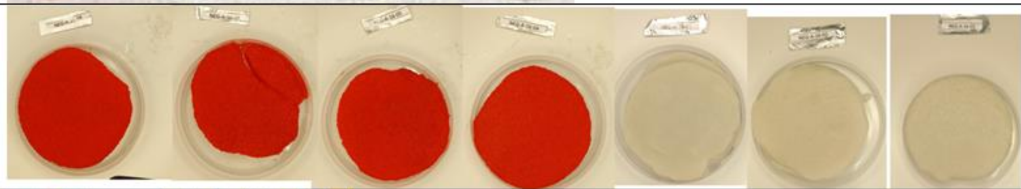
$MP_{15}S_{14}$	120	10	
$MP_{13}S_{16}$	119	10	
MP_0S_{19}	94	6	
$MP_{10}S_{19}$	118	10	

MP_5S_{24}	113	10	
MP_0S_{28}	109	8	
MP_5S_{28}	129	10	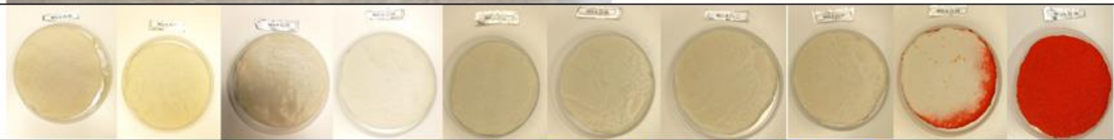
$MP_{10}S_{28}$	150	11	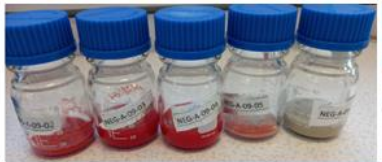 
MP_7S_{31}	147	10	 
MP_5S_{33}	143	10	

MP_0S_{38}	145	10	
MP_5S_{42}	175	12	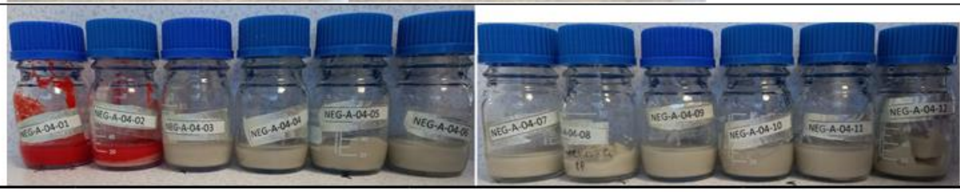

Appendix 7: Image analysis mixtures substrates fixed suspension density

a) Positive buoyant microplastics conditions

The following table show the volume results analysis of three pictures of the mixtures layers, for positive buoyant microplastics .

Tube	Layer	Volume results from the image analysis (%)			Volume corrected with the calibration curve (%)			Average volumes (%)	Desv
		Image 1	Image 2	Image 3	Image 1	Image 2	Image 3		
$MP_{2.0}S_{2.4}$	Layer 1 (Example below)	10.38	9.98	10.58	14.09	13.54	14.36	13.99	0.42
	Layer 2 (Example below)	11.12	7.70	13.00	15.10	10.42	17.66	14.39	3.67
$MP_{2.0}S_{2.8}$	Layer 1	18.04	18.56	12.34	24.54	25.26	16.76	22.18	4.72
	Layer 2	12.40	12.65	11.35	16.85	17.19	15.40	16.48	0.95
	Layer 3	10.20	9.19	7.06	13.83	12.46	9.55	11.95	2.18
$MP_{2.0}S_{3.1}$	Layer 1	2.77	2.35	3.87	3.69	3.12	5.19	4.00	1.07
	Layer 2	9.45	7.22	6.96	12.82	9.77	9.42	10.67	1.87
	Layer 3	9.86	5.26	7.57	13.37	7.09	10.25	10.24	3.14
$MP_{0.5}S_{2.4}$	Layer 1	3.89	1.63	2.35	5.22	2.14	3.12	3.49	1.57
	Layer 2	2.83	1.67	2.41	3.77	2.20	3.20	3.05	0.80
$MP_{0.5}S_{2.8}$	Layer 1	1.61	2.62	2.05	2.11	3.49	2.71	2.77	0.69
	Layer 2	2.91	1.70	3.07	3.88	2.23	4.11	3.40	1.02
$MP_{0.5}S_{3.1}$	Layer 1	12.42	2.93	2.60	16.87	3.92	3.46	8.08	7.62
	Layer 2	11.58	1.97	2.81	15.73	2.61	3.75	7.36	7.27

Volume results from the image analysis (%), Settling tube $+MP_{2.0}S_{2.4}$

		Image 1	**Image 2**	**Image 3**
Tube $MP_{2.0}S_{2.4}$	Image	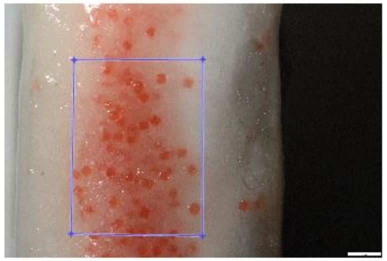	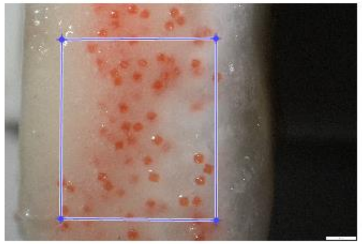	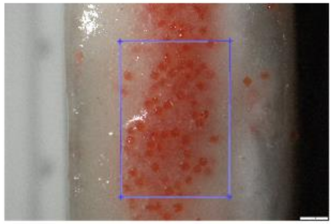
	Layer 1	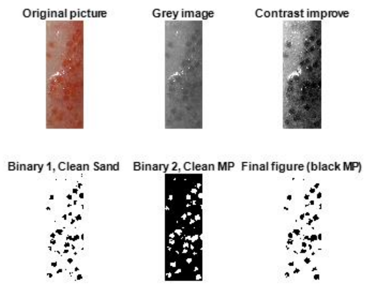	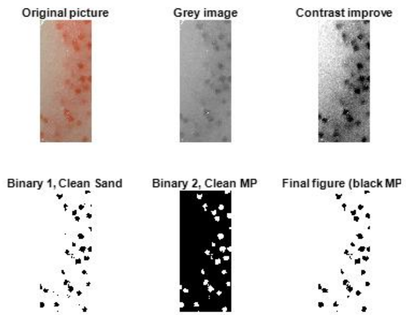	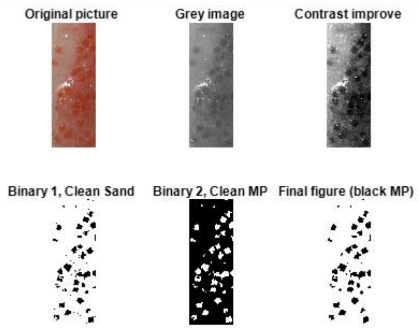
	Layer 2	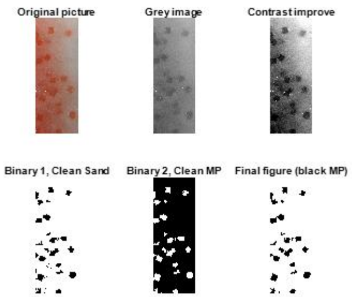	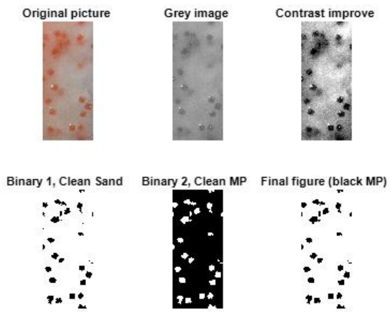	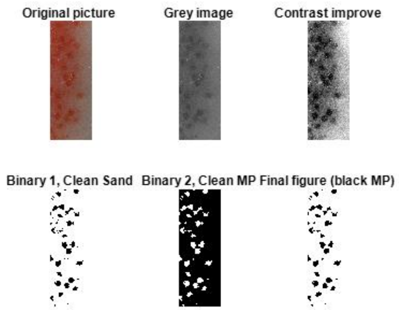

b) Neutral buoyant microplastics conditions

The following table shows the volume results analysis of three pictures of the mixtures layers, for neutral buoyant microplastics.

Neutral density microplastics									
Tube	**Layer**	**Volume results from the image analysis (%)**			**Volume corrected with the calibration curve (%)**			**Average volumes (%)**	**Desv**
		Image 1	**Image 2**	**Image 3**	**Image 1**	**Image 2**	**Image 3**		
$MP_{2.0}S_{2.4}$	Layer 1(Example below)	5.94	3.97	4.23	8.02	5.34	5.68	6.3	1.5
	Layer 2(Example below)	4.96	3.45	5.20	6.69	4.62	7.01	6.1	1.3
$MP_{2.0}S_{2.8}$	Layer 1	6.08	7.03	5.48	8.22	9.50	7.40	8.4	1.1
	Layer 2	8.34	7.34	9.70	11.29	9.93	13.16	11.5	1.6
$MP_{2.0}S_{3.1}$	Layer 1	10.13	15.17	14.00	10.29	20.63	19.03	16.6	5.6
	Layer 2	10.61	20.75	14.00	14.39	28.25	19.03	20.6	7.1
$MP_{0.5}S_{2.4}$	Layer 1	12.98	12.38	6.19	17.63	16.81	8.36	14.3	5.1
	Layer 2	11.16	10.45	6.46	15.15	14.18	8.74	12.7	3.5
$MP_{0.5}S_{2.8}$	Layer 1	12.16	8.15	27.69	16.51	11.04	37.72	21.8	14.1
	Layer 2	11.46	8.38	24.26	15.56	11.36	33.03	20.0	11.5
$MP_{0.5}S_{3.1}$	Layer 1	19.41	2.54	3.14	26.41	3.38	4.20	11.3	13.1
	Layer 2	22.29	3.29	4.78	30.34	4.40	6.44	13.7	14.4

Volume results from the image analysis (%), Settling tube neutral $MP_{2.0}S_{2.4}$

<table>
<tr><td rowspan="3">Tube $MP_{2.0}S_{2.4}$</td><td>Image</td><td>Image 1
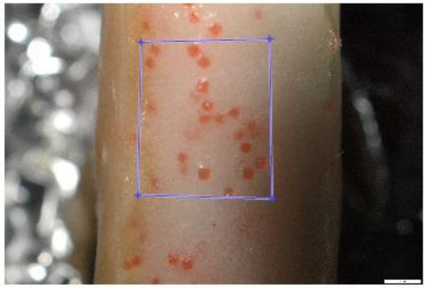</td><td>Image 2
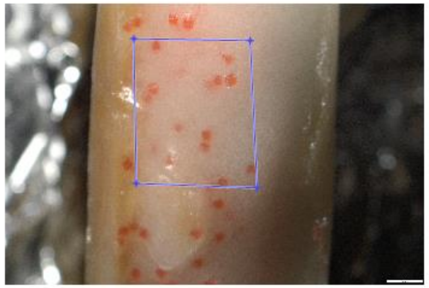</td><td>Image 3
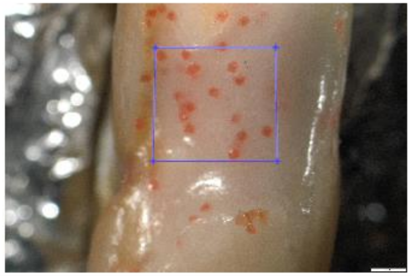</td></tr>
<tr><td>Layer 1</td><td>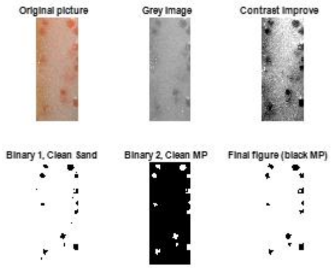</td><td>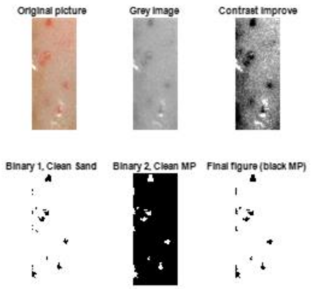</td><td>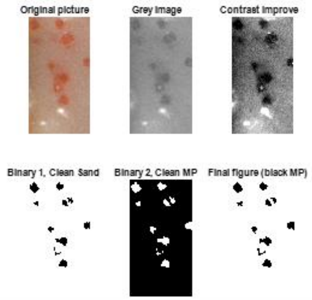</td></tr>
<tr><td>Layer 2</td><td>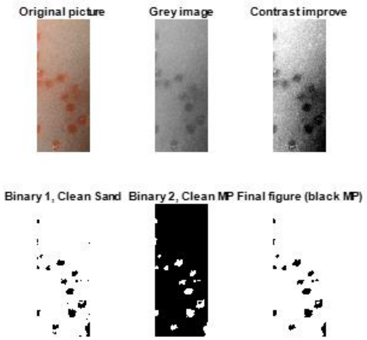</td><td>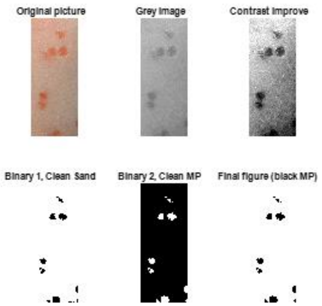</td><td>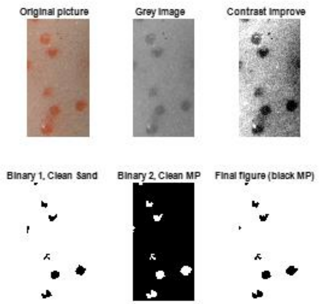</td></tr>
</table>

c) Negatively buoyant microplastics conditions

The following table shows the volume results analysis of three pictures of the mixtures layers, for negatively buoyant microplastics.

High density microplastics									
Tube	Layer	Volume results from the image analysis (%)			Volume corrected with the calibration curve (%)				Desv
		Image 1	Image 2	Image 3	Image 1	Image 2	Image 3	Average volumes (%)	
$MP_{2.0}S_{2.4}$	Layer 1	44.38	44.57	43.14	53.02	53.21	51.81	52.7	0.8
	Layer 2	39.37	46.32	43.51	48.11	54.92	52.16	51.7	3.4
$MP_{2.0}S_{2.8}$	Layer 1	42.68	42.55	46.27	51.35	51.22	54.86	52.5	2.1
	Layer 2	40.19	42.36	45.94	48.92	51.04	54.55	51.5	2.8
	Layer 3	23.32	22.59	24.88	31.75	30.76	33.88	32.1	1.6
$MP_{2.0}S_{3.1}$	Layer 1	28.64	31.17		39.02	42.47		40.7	2.4
	Layer 2	3.07	30.97		4.10	42.20		23.1	26.9
$MP_{0.5}S_{2.4}$	Layer 1	18.06	17.82	15.25	24.57	24.25	20.73	23.2	2.1
	Layer 2	4.62	12.02	10.04	6.22	16.32	13.62	12.1	5.2
$MP_{0.5}S_{2.8}$	Layer 1	11.32	13.43	12.17	15.37	18.25	16.53	16.7	1.4
	Layer 2	10.45	12.86	13.90	14.18	17.48	18.89	16.8	2.4
$MP_{0.5}S_{3.1}$	Layer 1	7.65	7.72	6.37	10.36	10.45	8.61	9.8	1.0
	Layer 2	9.39	8.76	7.63	12.73	11.87	10.33	11.6	1.2

Volume results from the image analysis (%), Settling tube negatively $MP_{2.0}S_{2.4}$

<table>
<tr><td rowspan="3">Tube $MP_{2.0}S_{2.4}$</td><td>Image</td><td>Image 1
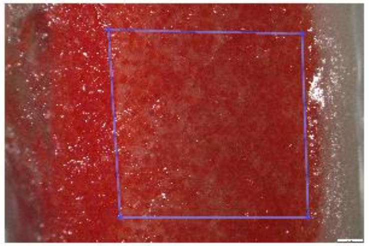</td><td>Image 2
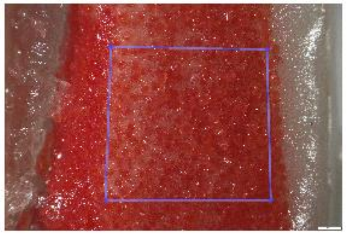</td><td>Image 3
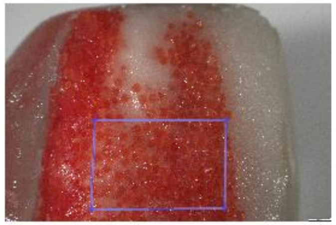</td></tr>
<tr><td>Layer 1</td><td>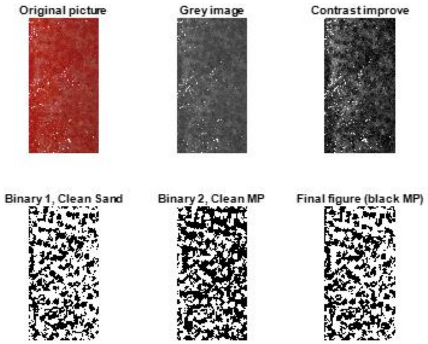
</td><td>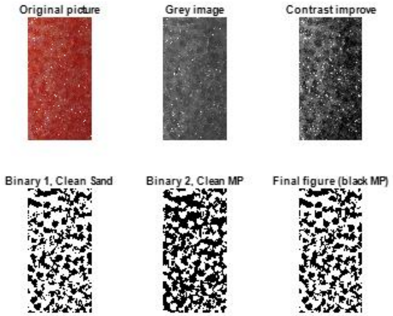
</td><td>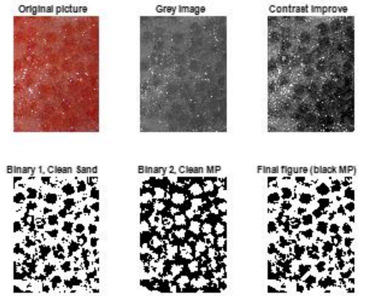
</td></tr>
<tr><td>Layer 2</td><td>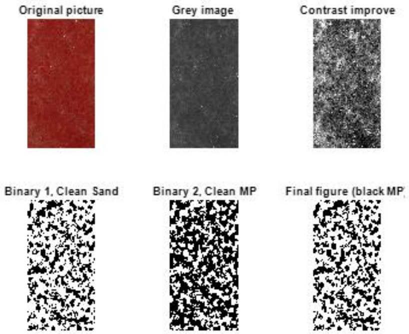
</td><td>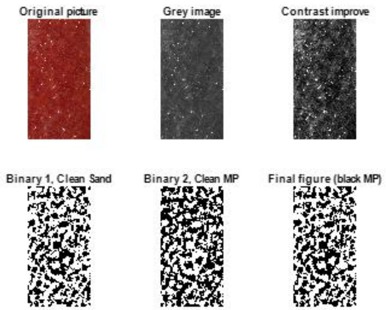
</td><td>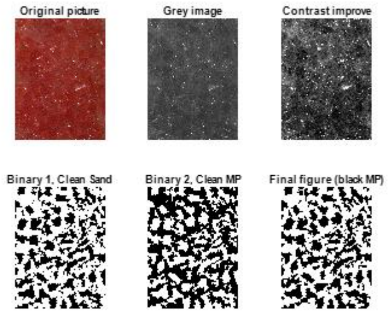
</td></tr>
</table>

Appendix 8: Study case analysis for Chapter 5

The decision of the study case for Chapter 5, was also discussed with two more options: an artificial delta and a confluence in the Mekong River. The Delta was included as an existing artificial channel with a more simple geomorphology than the braided river.The Mekong River refers to the confluence next to Phnom Penh, Cambodia. It was included as a study case with fieldwork samples of microplastic in the water and sediment from previous studies of the Energy and Environment Institute of the University of Hull. The advantages, disadvantages and time estimated to develop each model were compared in the following table. After the analysis, the Delta was discarded as it is not an ideal study case to obtain in and out total microplastic fluxes, and it was not possible to achieve one of the objectives of this study. The Mekong River was discarded as it needed extra time for hydraulics-morphological calibration and did not adjust to the time designated to develop the chapter. Finally, the best study case was the braided rivers, it is consistent with the main objectives, the estimated time is adjusted to the Ph.D. plan (5 months to develop the results), and it is an already hydraulic and morphologically calibrated model.

Channel	Braided river (complex artificial channel) (Schuurman et al., 2015)	Delta (simple artificial channel)	Mekong River
Advantage	- An already calibrated hydraulics-geomorphology model. - Average of the results in the different channels. - In and out total microplastic fluxes. - Is it possible to make a simple model, adapting the computational grid.	- An already calibrated hydraulics-geomorphology model. - Simple model	- Mekong is a polluted river (Yun et al, 2017) - Bathymetry, flows, microplastic measurements are available at the Energy and Environment Institute, University of Hull. - In and out total microplastic fluxes.

Disadvantage	Complex model	- Not possible to obtain in and out total microplastic fluxes. - Not possible to make a simple model.	- Complex model (confluences- influences of tides-river flows, winds). - Develop the model from scratch, and need calibration.
Time table (Time)	- Software skills update- Update literature review (1 week) Adjusting with the domain (2 weeks) Test fluxes scenarios (1 month) Microplastics scenarios (2 months) Analysis results (2 months) Total time ≈ five months	Software skills update-Update literature review (1 week) Adjusting the domain (2 weeks) Fluxes scenarios (1 month) Microplastics scenarios (2 months) Analysis results (2 months) Total time ≈ five months	Software skills update-Update literature review (1 week) Develop model and calibration (2 months) Fluxes scenarios (1 month) Microplastics scenarios (2 months) Analysis results (2 months) Total time ≈ seven months